Dynamic System-Wide Mass Spectrometry based Metabolomics Approach for a New Era in Drug Research

José M. Castro Pérez

Dynamic System-Wide Mass Spectrometry based Metabolomics Approach

for a New Era in Drug Research

José M. Castro Pérez

PhD thesis with summary in Dutch

October 2011

Cover: Leonardo Da Vinci Vitruvian man drawing (circa 1487)

Dynamic System-Wide Mass Spectrometry based Metabolomics Approach for a New Era in Drug Research

Proefschrift

ter verkrijging van

de graad van Doctor aan de Universiteit Leiden,

op gezag van Rector Magnificus prof.mr.P.F. van der Heijden,

volgens besluit van het College voor Promoties

te verdedigen op dinsdag 18 oktober 2011

klokke 16:15 uur

door

José M. Castro Pérez

geboren te Las Palmas de Gran Canaria, Spain

in 1971

Promotiecommisie

Promotor :	Prof. Dr. T. Hankemeier
Co-promotores:	Dr. R.J. Vreeken
	Dr. T.P. Roddy
Overige leden:	Prof. Dr. M. Danhof
	Prof. Dr. J. van der Greef
	Prof. Dr. B. van der Water
	Dr. A. Millar
	Prof. Dr. C. Fernandez-Hernandez
	Dr. D.G. Johns

Table of Contents

APPENDIX

Chapter 1

General introduction and scope

Chapter 1

General introduction and scope

The impact of metabolomics

'Whether in a cell based system or in a living organism biological end-points involve the measurement of metabolites. Thus a new 'omics' (***metabolomics***)'

Another 'omics' has emerged in the field of life sciences with the potential to provide the phenotypic link in the so-called "systems biology approach". Combination of gene expression and metabolomic data provides essential information in deciphering the basic biology. Metabolomics in the context of human biology is defined as the comprehensive measurement of all metabolites in a biological system in response to biological alteration caused by disease, dietary intervention, metabolic disorder or genetic modulation (transgenic animal models or by means of siRNA reagents) and therapeutic intervention (1, 2). In addition to improving our understanding of basic biology, the use metabolic end-points is a valuable platform to evaluate the efficacy of therapeutic intervention by small molecules, biologics, or gene therapy. Metabolic state can be characterized by assessing systems-wide metabolite concentrations at a single time point, or in a dynamic (i.e. in a multiple time point) manner. In addition, this powerful approach may be utilized to inform researchers about the metabolic state and provide vital information in the decision-making step for target identification and validation in drug research.

Metabolomics has recently been gathering momentum in terms of scientific publications. In the last 20 years, a total of 4772 journal articles (using Web of Science search engine by title 'metabolomics') have been published on the topic. And while a large number of these articles were NMR based analyses metabolomics (3-8), there has been an increase of LC/MS based metabolomics applications in the literature (9-17). Recent developments include discussions of how this technology may be applied to answering complex biological questions and its applicability to a systems biology approach as pioneered by van der Greef and his research team (18-24).

In part, in the last five years the increment number of articles in the literature is attributable to the large number of possible applications of metabolomics, including not only to human biology but also; (i) plant biology, (ii) chemical synthesis and (iii) food industry. Another reason is improvements in mass spectrometry technology which now offers improved dynamic range, and accurate mass capabilities, both of which are important for metabolomics. Examples of innovative and 'game changing' MS instruments are the Orbitrap (25-28) and QTof (29-36) type of MS analyzers both of which allow the relatively rapid and straightforward data acquisition with exquisite accurate mass data. Furthermore,

improved chromatographic separations by ultra performance liquid chromatography (UPLC) due to the use of sub 2μm particles (37) and high pressure instrumentation, permitted high resolution chromatographic separation of very challenging samples like biological fluids and tissues. In addition to this, multidimensional chromatography such as GCxGC/MS also allowed high resolution chromatographic separation (38) for analysis of extremely complex samples, for example plant extracts, where up to 200,000 metabolites can be encountered (39-47).

Complexity of the metabolome

The metabolome *per se* encompasses a large variety of endogenous components including lipids, amino acids, organic acids, nucleotides, steroids, vitamins, sugars etc… These biochemical entities possess a wide range of physicochemical properties which make each unique in both its specific analytical detection requirement and its biological role. In one metabolite class alone, for example lipids (fatty acids, phospholipids, sterols, diglycerides, triglycerides, eicosanoids etc.), there are at least 10,000 unique molecules (48) each with often specific metabolic functions such as biochemical signaling, enzyme substrate and these can serve as biomarker of disease.

The study of the metabolome can offer a phenotypic signature in the 'omic-cascade', but the real value of this analysis is in the complete coupling of transcriptome, proteome, and metabolome which may lead to a better understanding of the biochemical and patho-physiological events in living organisms.

Analytical platforms and data deconvolution

Even though technology has made great strides towards better instrumentation, the ability to have a single platform that can answer all the questions is far beyond reach. This is mainly due to the extreme diversity and large number of molecules which constitute the metabolome. Therefore, there is a need to collapse the metabolome into analyte subclasses in which certain metabolites can be analyzed by one or two analytical platforms (LC/MS and GC/MS, and/or NMR). For example, in the case of lipids it may be possible to use LC/MS as a front-line technique. This topic will be discussed in more detail throughout the thesis where the application of high resolution LC/MS for lipid profiling can play a big role in exploratory biomarkers.

Another consideration which needs particular attention is the vast amount of data which can be generated by a metabolomics analysis. Data deconvolution can be a major bottleneck. Over the years, great advancements have been made by LC/MS and GC/MS manufacturers in the creation of proprietary algorithms that allow the extraction of data in an exact mass retention time pair (EMRT) and intensity from which different types of multivariate statistical analysis (MVA) may be achieved.

Nonetheless, metabolite data must be processed, normalized and/or scaled to remove analytical/biological noise or interferences. Some of the most commonly used approaches per sample and per variable include scaling to total response, scaling to individual metabolites, scaling to unit variance, pareto scaling (most commonly used in LC/MS and GC/MS applications), and mean centering.

In metabolomics experiments, univariate methods are commonly used to detect and identify statistically significant metabolites that are up-regulated or down-regulated between different groups. These include parametric analysis for data that are assumed to be distributed, such as ANOVA (analysis of variance), t-tests, and z-tests. Multivariate data consist of the results of observations of many different variables, which in this case can be represented as metabolites, and for a number of objects, or in other words the individuals. Each one of the variables refers to classification as constituting a different dimension in the data set. Hence, an object with *n* variables may be thought of as located in a unique position in what is referred to as *n*-dimensional hyperspace. Unfortunately hyperspace complex data sets are extremely difficult to visualize, therefore multivariate analysis (MVA) is used to reduce complexity and dimensionality in the statistical data analysis. There are two types of MVA; unsupervised or supervised learning algorithms (49-54).

In the case of unsupervised modeling, the most widely used analyses are; (i) principal components analysis (PCA) and (ii) hierarchical cluster analysis (HCA). Supervised learning normally follows primary analysis by unsupervised learning. The system can be supervised when the responses of each trait and its association with each set of metabolite data is known. The desired goal is to find a model that predicts a target trait based on a selection of significant metabolites. Examples of commonly used supervised learning are; linear discrimination analysis (LDA), partial least squares discrimination analysis (PLS-DA), canonical variates analysis (CVA) and discriminant function analysis (DFA)).

Lipid profiling static and dynamic end-points

An important part of metabolomics is the study of the lipidome and this is the main focus of the research described in this thesis. These classes of molecules are an integral part of the biology of humans and animals in which lipids can mediate signal processes and can be utilized as a direct measurement of disease, genetic predisposition or mutation and drug intervention. Mass spectrometry has played a pivotal role in the analysis of lipids and other derived metabolites such as bile acids (BA). Researchers in the field of lipid profiling have shown that it is possible to obtain detailed quantitative and qualitative information on a wide range of lipids in different biological matrices and at the cellular level (55-67) as shown in Figure 1.
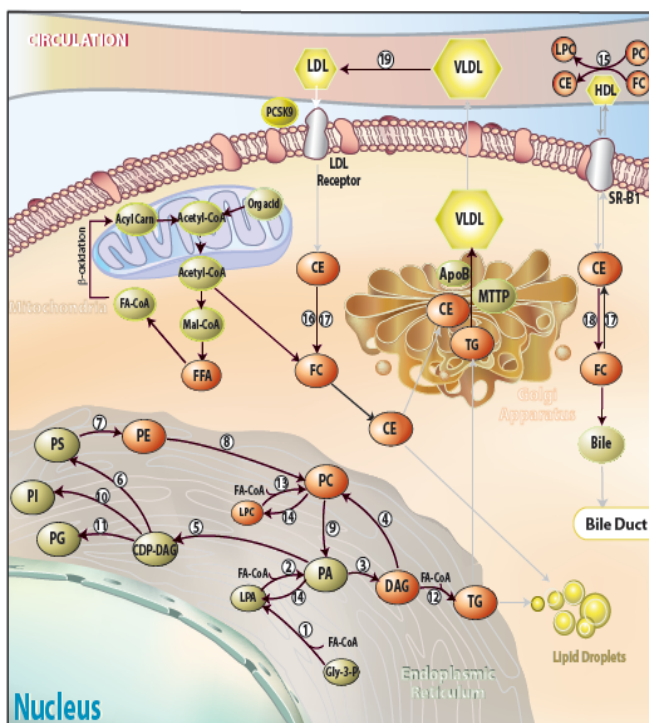
Figure 1. Biogenesis and major circulating lipids inside cells and in plasma

Abbreviations;

CE= cholesterol ester ; PC = phosphatidylcholine ; FFA = free fatty acid ; TG = triglyceride; DAG = diacylglyceride ; PS = phosphatidylserine ; PI = phosphatidylinositol ; PG = phosphatidylglycerol ; PE = phosphatidylethanolamine ; PA = phosphatidic acid ; LPC = Lyso phosphatidylcholine ; FC = free cholesterol ; LPA = Lyso phosphatidic acid ; HDL = high density lipoprotein ; LDL = low density lipoprotein ; VLDL = very low density lipoprotein ; PCSK9 = proprotein convertase subtilisin/kexin type 9; SR-B1 = scavenger receptor class B member 1; MTTP = microsomal triglyceride transfer protein

Figure created by Merck media services (copyright 2011), reprinted with permission.

Here an important aspect was the development of the analytical strategy. This included development of a novel high resolution UPLC/MS platform. This allowed a 'shotgun' approach for the analysis of lipids in plasma and tissues by which full scan MS data and high energy fragmented lipid data (MS^E) were quickly obtained (34). Another important characteristic of this investigation was the development of an ion mobility platform combined with a dual collision induced dissociation (CID) fragmentation approach using a time-of-flight mass analyzer as shown in figure 2. Time aligned parallel fragmentation (TAP) was utilized to detect and identify fatty acyl and double bond locations in phosphatidylcholines (see chapter 3).
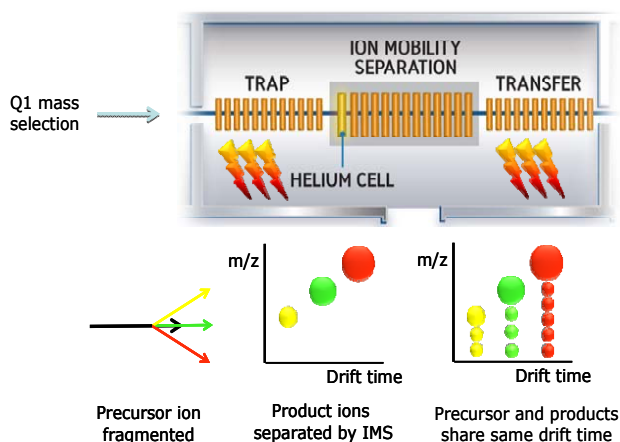
Figure 2. Schematic illustration of the time-aligned parallel (TAP) fragmentation procedure. Ions of a specific m/z ratio are selected by the quadrupole filter (Q1) and fragmented in the trap region by CID. Once fragmentation has taken place the 1st generation fragment ions enter the ion mobility drift tube and are separated by mass, collisional cross section and charge state. As the 1st generation fragment ions exit the ion mobility device, they are further subjected to CID fragmentation to generate 2nd generation fragment ions. *Figure reproduced with permission from Waters Corp.*

An important addition to mass spectrometry and the analysis of lipids has been the utilization of metabolic tracers and flux analysis. Metabolic tracers offer a direct substrate-to-product measurement and have been used in the past to study the fate of metabolism for specific metabolites in certain 'targeted' metabolic pathways such as in the case of BA biotransformations and the investigation of the turnover rate of BAs in humans (68, 69). In this thesis, this approach was utilized in a multifaceted way (i) to measure the reconjugation step of BAs *in-vitro* and *in-vivo* following silencing of the Slc27a5 gene and (ii) the possibility of utilizing the tracer approach as a biomarker for target engagement in the inhibition of the reconjugation step for BAs re-entering the liver via the enterohepatic circulation (see chapter 7).

With respect to flux analysis, it can be defined as the 'targeted or non-targeted' measurement of metabolic synthesis rate or turnover of proteins and/or metabolites in a biological system, where one or more metabolic pathways can be investigated in a 'global' system-wide setting. This approach may be applied to 'steady state' or the response of biological perturbations such as drug intervention, nutritional alterations or challenge tests such as lipid or glucose tolerance tests and physical exercise. Multiple time points after a biological perturbation do not describe a defined static event but a dynamic phenomenon, which can be vastly up-regulated and/or down-regulated. Figure 3 describes how it is possible to measure synthesis rates by the administration either intravenously or orally of a tracer.
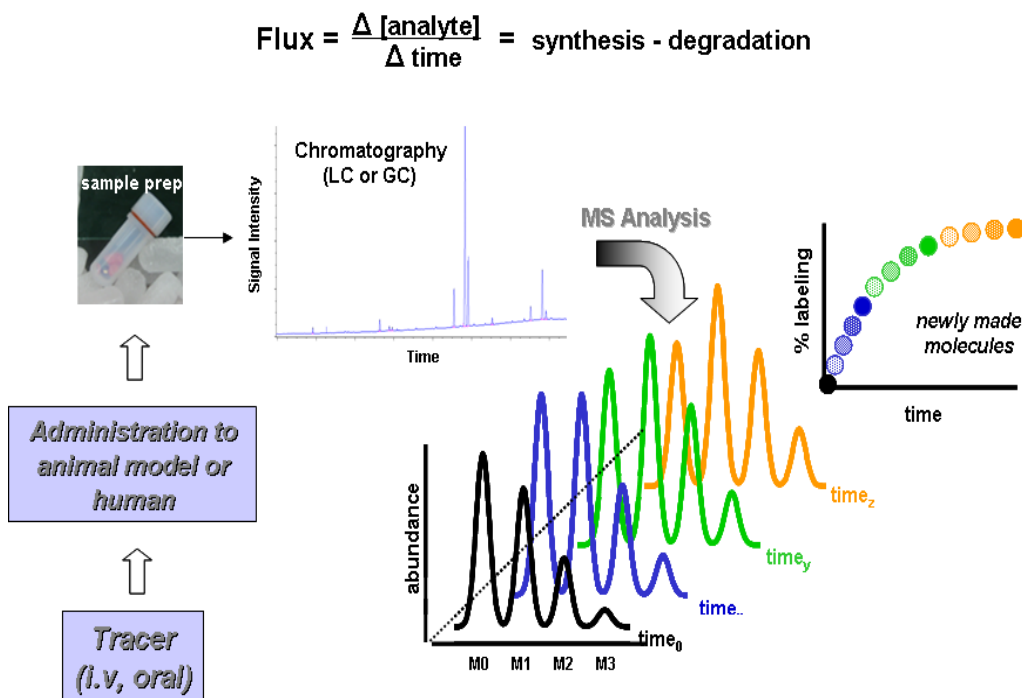
Figure 3. Metabolic flux analysis by mass spectrometry to determine the percentage labeling of newly made molecules as a means to better understand the (i) turnover rate of certain components such as proteins or metabolites and (ii) their up-regulation or down-regulation mediated by enzymatic actions in the metabolic pathway of interest

A commonly used metabolic flux tracer is 'heavy water' (D_2O) in which the deuterium present in the D_2O will be incorporated into newly synthesized molecules in cells *in-vitro* and *in-vivo* (70-74). The advantage of this approach relies on the fact that it does not change the pool size of the metabolite in question and does not lead to an unwanted biological perturbation as this flux method is inert. Subsequent mass spectral measurement of M0, M1, M2 and M3 isotopomers, i.e. containing 0, 1, 2, 3 isotopes of ^{13}C or deuterium rather than ^{12}C or hydrogen, will provide information regarding the degree of turnover during the study (see MS analysis panel of spectra in figure 3 denoting abundance (y-axis) and time (x-axis) for M0, M1, M2, and M3). As synthesis of newly made molecules increment, then M1, M2 and M3 isotopomers will correspondingly increase in abundance. Measuring the ratio of the natural background M1/M0 minus M1/M0 (or combination of M1, M2 and M3) provides information about synthesis (increment in M1/M0 ratio for newly made molecule) for the particular molecule of interest. This topic is further discussed in more detailed in chapters 8 and 9.

There is a constant flux or turnover of proteins and metabolites mediated by enzymatic action, which in turn is responsible for maintaining cell equilibrium and ultimately system homeostasis. Steady state measurements of metabolite concentrations which are intermediates in specific biochemical pathways may only provide a snapshot in time but this does measure their turnover, and their synthesis rate have to be seen in the context of a larger and more complex network of enzymes. Therefore, steady state measurements on their own may not completely reflect the underlying biochemical processes, failing to fully describe the complete phenotypic modulation. Metabolic flux analysis provides a powerful dynamic portrait of the phenotype because it captures the metabolome and its functional biology interactions mediated by enzymatic actions and in relation to the genome. Therefore, the combination of static and dynamic measurements (metabolomics and fluxomics) is expected to be a very powerful approach to enhance data interpretation in complex biological systems.

Apolipoprotein metabolism and function

Circulating lipids in the blood include; (i) fatty acids, which are mostly bound to albumin; (ii) cholesterol, which is present either in the free or esterified forms; (iii) triglycerides, which must undergo extracellular degradation so that their constituents can be absorbed by peripheral cells and (iv) phospholipids, which can be used as structural components, enzyme substrates or for signaling purposes. Cholesterol has a very important role in lipid metabolism as it is an integral component of cell membranes. It also serves as a precursor to bile acids and steroid hormones. There are two main sources of cholesterol; (i) dietary and (ii) *de-novo* synthesized (precursor being Acetyl-CoA and the rate limiting synthetic step being carried out by 3-hydroxy-3-methyl-glutaryl-CoA reductase (HMG-CoA)) (75-77). All of lipids mentioned above are transported in the blood stream by apolipoproteins. Apolipoproteins are involved in the following biological processes; (i) specific receptor binding and (ii) enzyme activation. These functions are critical to the delivery specific lipids to different sites in the body for absorption, storage or utilization depending on the specific energy requirements. Apolipoproteins are also responsible for the delivery of triglycerides to muscle tissue for their utilization as energy and transport of cholesterol for distribution throughout the body to cells. There are many different subclasses of Apolipoproteins and these are described in table 1.

Table 1. Represents the different apolipoproteins present in humans and their distribution in the different lipoproteins (chylomicrons, chylomicrons remnants, VLDL, IDL, LDL, HDL, HDL1, HDL2 and HDL3)

Apolipoprotein	Lipoprotein	Source	Diameter (nm)	Lipid (%)	Protein (%)
A1,A2,A4,B48,C1,C2,C3 and E	Chylomicrons	Intestine	90-1000	98-99	1-2
B48 and E	Chylomicron renmants	Chylomicrons	45-150	92-94	6-8
B100, C1, C2, C3	VLDL	Liver (intestine)	30-90	90-93	7-12
B100 and E	IDL	VLDL	25-35	89	11
B100	LDL	VLDL	20-25	79	21
	HDL		20-25	68	32
A1, A2,A4,C1,C2,C3 D and E	HDL1	liver, intestine,	20-25	68	33
	HDL 2	VLDL and	10-20	67	57
	HDL3	chylomicrons	5-10	43	43

Apolipoprotein B (ApoB) or otherwise referred to as non-HDL is mainly accountable for the delivery of lipids such as cholesterol and triglycerides to peripheral cells (78-80). Apolipoprotein A1 (ApoA1) or otherwise referred to as HDL is responsible for reverse cholesterol transport (RCT), a mechanism by which cholesterol is picked up from macrophages and offloaded in the liver for subsequent excretion into the feces (81-83). ApoB is secreted by the intestines as ApoB48 and by the liver as ApoB100 and both are transported to the lymph and plasma where they are assembled by a well orchestrated step involving congregation of lipids into the core (triglycerides and cholesterol esters) and outer layer (phospholipids and free cholesterol) of this Apolipoprotein. ApoB is then remodeled into cholesterol rich remnants by subsequent action of lipoprotein and hepatic lipases (LPL and HL). Thus, becoming smaller and smaller lipoprotein particles; from chylomicrons to very low density lipoprotein (VLDL), intermediate density lipoprotein (IDL) and low density lipoprotein (LDL). ApoB containing lipoprotein particles may be either taken up in the liver by LDLr receptors or in the peripheral cells of arterial walls of lipid-laden macrophages where remodeled LDL by action of lipases will become small LDL. Excess of ApoB containing particles in the arterial wall can lead to oxidation of small LDL particles (84-88). These small oxidized LDL particles can be easily taken up by cluster of differentiation 86 (CD86) and scavenger receptor A type I and II (SRA) which can ultimately cascade towards the onset of atherosclerosis. HDL is involved in RCT and other vital functions such as removal of oxidized lipids from macrophages and anti-inflammatory properties. ATP-binding cassette transporter 1 (ABCA1) is responsible for the cholesterol efflux out of the cells into ApoA1 rich and lipid poor nascent HDL. Free cholesterol in the surface of nascent HDL is esterified by action of lecithin-cholesterol acyltransferase (LCAT) (89-92). The esterification step involves hydrolysis of the phosphatidylcholine to release the fatty acyl for the esterification process. The newly made cholesterol esters (CE) move to the core of the lipoprotein to make HDL3. This newly made HDL3 particle may also pick up cholesterol from the cells via mediation of scavenger receptor class B member 1 receptors (SR-B1). This last step leads to an enlarged HDL3 particle, thus giving rise to HDL2. HDL2 can exchange lipids in a bi-directional manner with triglyceride rich lipoproteins (VLDL and LDL) modulated by cholesteryl ester transfer protein (CETP) (figure 4). This process encompasses the transfer of one molecule of cholesterol ester from HDL2 for a triglyceride molecule between triglyceride rich lipoproteins (VLDL and LDL). Finally, HDL 2 may be taken up by the liver via SR-B1 where cholesterol will be excreted in the feces or converted to bile acids. Or it may be remodeled by endothelial and hepatic lipases (HL and EL) to HDL3.
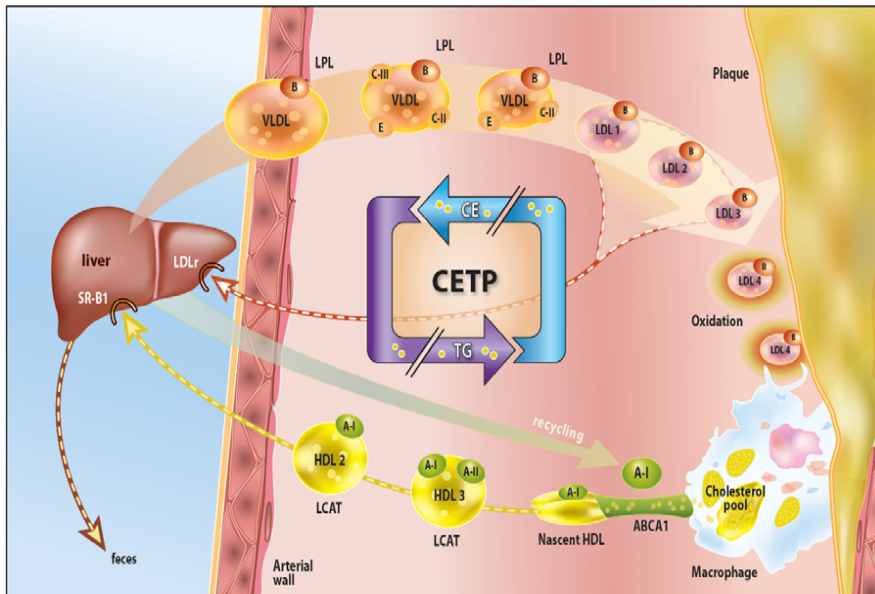
Figure 4. Cholesteryl ester transfer protein (CETP) exchanges one molecule of cholesterol ester for one molecule of triglyceride between ApoA1 containing lipoproteins and ApoB containing lipoproteins in a bi-directional fashion. Inhibition of CETP leads to increased cholesterol content and size of HDL particles. HDL promotes cholesterol efflux from the periphery arterial wall via mediation of ABCA1 to lipid poor and lipid freeapoA1. LCAT esterifies free cholesterol which is present in the outer core of HDL, and remodels discoidal HDL into spherical HDL. Then, HDL is offloaded in the liver by mediation of SR-B1 which is the last step of the reverse cholesterol transport (RCT). Where cholesterol may be excreted in the feces or converted to bile acids which are recycled and finally excreted. *Figure created by Merck media services (copyright 2011), reprinted with permission.*

Abbreviations;

LCAT = lecithin-cholesterol acyltransferase; ABCA1 = ATP-binding cassette transporter 1; SR-B1 = scavenger receptor class B member 1; LDLr = low density lipoprotein receptor; LPL =; TG = triglyceride; CE = cholesterol ester; HDL = high density lipoprotein; LDL = low density lipoprotein; VLDL = very low density lipoprotein.

Lipid analysis and its application to drug research with emphasis on atherosclerosis

Of particular interest has been the application of lipid profiling to address important questions in atherosclerosis research. Cardiovascular disease is one of the major causes of death in the western world and it is rapidly expanding to other geographies (93-96). Decreases in mortality and morbidity have been associated with reduced levels of cholesterol. Statins have been widely used to effectively manage cholesterol levels especially for patients at risk of cardiovascular disease (CVD). Other therapies, including fibrates or bile acid sequestrants have also been employed in the fight of

hypercholesterolemia. There are various added benefits of having higher levels of HDL cholesterol as clearly stated by several epidemiological studies (97, 98) which quote that increased levels of HDL cholesterol may be athero-protective. Recently, there has been a strong focus on therapies which raise 'good' cholesterol (HDL) such as niacin. A target protein which is currently being investigated, cholesteryl ester transfer protein (CETP) has the potential of being an important therapeutic target as its reversible inhibition can lead to increased levels of HDL cholesterol (99), promote RCT and reduce the atherogenic burden.

The introduction of human CETP expression in lower animal species such as mice has greatly improved the ability to study in detail lipoprotein metabolism. Studies conducted in cholesterol-fed C57BL/6 mice, resulted in a strong shift of cholesterol from HDL to LDL, resulting in reduced HDL cholesterol and increased LDL cholesterol, therefore increasing association with atherosclerosis (100). This finding correlated with expression of hCETP in apoE - /- or apoE*3-Leiden mice in which decreased HDL cholesterol levels were observed, followed by elevated VLDL, LDL, and intermediate-density lipoprotein cholesterol (101, 102). During the course of the research in this thesis, a thorough investigation of the benefits of inhibiting reversibly CETP was conducted in a pre-clinical animal model (Syrian golden hamsters). For this work, an analytical platform was developed to investigate the profiling of lipids in different lipoprotein particles in plasma by the combination of gel electrophoresis and high resolution mass spectrometry.

siRNA and shRNA knock-down (KD) animal models as a vehicle for exploratory biomarker discovery in drug research

Small interfering RNA (siRNA) is a double-stranded RNA consisting of ~ 20-25 nucleotides in length (103-106). siRNA reagents can be utilized to cause interference with the specific expression of a targeted gene. Therefore, treatment with the siRNA reagent leads to silencing of the targeted gene. The utilization of siRNA reagents in drug research has become increasingly important for either therapeutic purposes or by mean of non-permanent knock-down (KD) in preclinical animal models to investigate target identification and validation instead of using small molecules. The impact of improved biologics and especially siRNA encapsulation in lipid nano-particle (LNP) delivery vehicle has enabled the researcher with increased potency and specifically silence the expression of a targeted gene of interest to monitor the impact on the metabolome, proteome, or combination of both phenotypes, which may be characteristic of a metabolic disorder or disease. An alternative to siRNA is permanent knock-down which may be achieved by the incorporation of short hairpin RNA (shRNA) transgenes into the genome. The delivery of the shRNA to mice can be achieved in a number of ways; via viral infection, pronucleus injection or targeted insertion into the embryonic stem (ES) genome. Therefore, in this fashion a specific knock-down animal model is generated by the insertion of shRNA expression vectors in the Rosa26 locus of ES cells utilizing recombinase mediated cassette exchange (RMCE). By either siRNA or shRNA is possible to test the biological hypothesis/s without the initiation of a chemical synthesis program aimed at the pharmacological target, basically an *in vivo* model where the first proof-of-concept and mechanism of action can be studied (see chapters 5 and 6).

Ultimately, the integration of transcriptomics and metabolomics together with the use of fit-for-purpose analytics may lead to the generation of biomarkers which can be translated from rodents to the clinic. Biomarkers alone signify the most important asset in translational medicine from mice to humans, and vice versa (107, 108). Translation of biomarkers from mice to humans in certain instances can be very challenging as sometimes the animal models used may not completely reflect the full human biological state in health and disease.

Human genetics are playing an increasingly important function in target validation. Finding genetic mutations in humans with either partial loss or complete loss of function for a specific regulatory enzyme, which may be of interest for therapeutic reasons, is exceedingly valuable. Valuable clinical trait information from screening large human cohorts can enable target identification researchers to associate the traits with the gene mutation/s. Exploratory biomarkers can then be utilized in these patients to evaluate the impact of the specific genetic mutation on the metabolic state.

Therefore, involving human genetics and exploratory biomarker/s during the drug discovery process in the target validation space may prove to be a very valuable asset to move a potential new pharmacological target forward into lead identification, a process by which structural activity relationships for novel therapeutical molecules are screened against the target. Hence, the use of a multiplatform approach linking genotypic and phenotypic signatures using analytics can pave a way of the future to discover new and innovative drug therapies to treat lipid disorders. This approach may be utilized in a parallel additive therapy strategy, where multiple biological targets can be inhibited or induced to produce the desired pharmacological result.

SCOPE

The aim of the thesis was to develop metabolic analytical platforms for static and dynamic measurements that could answer biological questions for *in vitro* and *in vivo* animal models in the area of lipid research. Gene profiling together with the transcriptome and metabolome data was used in combination with the LC/MS analytical platform. In terms of the analytical platforms developed, the focus was on high resolution LC/MS but not limited, as amalgamation with other platforms such as gradient gel electrophoresis (GGE) and fast protein liquid chromatography (FPLC) were explored in more detail to investigate the lipid composition of lipoprotein particles. These analytical strategies were applied to different lipid modulating biological targets as a mean to obtaining a more detailed and characteristic phenotype description directing decisions in drug search during the drug discovery process on the basis of the analytical results obtained. Additionally, the utilization of metabolic tracers was investigated further to probe dynamic changes in the biological target and animal models in question.

In **chapter 2**, a novel 'shotgun' lipid profiling approach was discussed. This method allowed for the quantitative and qualitative measurement of a large number of lipids from a single injection and it was applied to the analysis of human volunteers with osteoarthritis. In order to further study the qualitative aspect of lipid identification, ion mobility mass spectrometry using a dual CID approach was employed in **chapter 3** to locate the position of fatty acyls and double bonds in phosphatidylcholines. In **chapter 4**, the lipid target CETP was evaluated in golden Syrian hamsters. A combination of gel electrophoresis and mass spectrometry was utilized to investigate the lipid composition of the lipoprotein particles with particular interest in HDL. Liver steatosis induced by ApoB silencing using siRNA and its possible protection from a combination siRNA therapy with fatty acid transport protein 5 (FATP5) or Slc27a5 gene was evaluated in **chapter 5**. Lipid signatures in plasma and tissues were obtained employing the analytical techniques developed in chapters 2 and 3. Further investigation of the role of Slc27a5 gene was conducted in **chapter 6** where a reduction in the levels of ApoB was observed which could potentially lead to the reduction of the atherogenic burden. In addition to this, bile acid metabolism was further investigated as this gene is also responsible for the re-conjugation of bile acids re-entering the liver from the hepatic portal vein. **Chapter 7** described in more detail the reconjugation of bile acids by the silencing of the Slc27a5 gene and how it is possible to use a metabolic tracer *in vitro* and *in vivo* to measure bile acid metabolism both quantitatively and qualitatively. The last two chapters focused on the utilization of heavy water to obtain static and dynamic lipid measurements by LC/MS. **Chapter 8**, shows how it is possible to obtain cholesterol and cholesterol ester flux data by infusion of D_2O *in vivo* using LC/MS and how the observations compared with more matured methodologies such as GC/MS. The last **chapter 9** depicts in detail the powerful combination of metabolomics together with fluxomics as a mean to enhance the identification process of lipid phenotypes by dietary perturbation utilizing high resolution LC/MS.

REFERENCES

1.   Wang, H., Tso, V. K., Slupsky, C. M., and Fedorak, R. N. *Future Oncol* **6,** 1395-406.

2.   Wang, M., Lamers, R. J., Korthout, H. A., van Nesselrooij, J. H., Witkamp, R. F., van der Heijden, R., Voshol, P. J., Havekes, L. M., Verpoorte, R., and van der Greef, J. (2005) *Phytother Res* **19,** 173-82.

3.   Beckonert, O., Coen, M., Keun, H. C., Wang, Y., Ebbels, T. M., Holmes, E., Lindon, J. C., and Nicholson, J. K. *Nat Protoc* **5,** 1019-32.

4.   Fonville, J. M., Maher, A. D., Coen, M., Holmes, E., Lindon, J. C., and Nicholson, J. K. *Anal Chem* **82,** 1811-21.

5.   Gavaghan, C. L., Li, J. V., Hadfield, S. T., Hole, S., Nicholson, J. K., Wilson, I. D., Howe, P. W., Stanley, P. D., and Holmes, E. *Phytochem Anal*.

6.   Lauridsen, M. B., Bliddal, H., Christensen, R., Danneskiold-Samsoe, B., Bennett, R., Keun, H., Lindon, J. C., Nicholson, J. K., Dorff, M. H., Jaroszewski, J. W., Hansen, S. H., and Cornett, C. *J Proteome Res* **9,** 4545-53.

7.   Legido-Quigley, C., Cloarec, O., Parker, D. A., Murphy, G. M., Holmes, E., Lindon, J. C., Nicholson, J. K., Mitry, R. R., Vilca-Melendez, H., Rela, M., Dhawan, A., and Heaton, N. (2009) *Bioanalysis* **1,** 1527-35.

8.   Nicholson, J. K., Wilson, I. D., and Lindon, J. C. *Pharmacogenomics* **12,** 103-11.

9.   Spagou, K., Wilson, I. D., Masson, P., Theodoridis, G., Raikos, N., Coen, M., Holmes, E., Lindon, J. C., Plumb, R. S., Nicholson, J. K., and Want, E. J. *Anal Chem* **83,** 382-90.

10.   Want, E. J., Coen, M., Masson, P., Keun, H. C., Pearce, J. T., Reily, M. D., Robertson, D. G., Rohde, C. M., Holmes, E., Lindon, J. C., Plumb, R. S., and Nicholson, J. K. *Anal Chem* **82,** 5282-9.

11.   Want, E. J., Wilson, I. D., Gika, H., Theodoridis, G., Plumb, R. S., Shockcor, J., Holmes, E., and Nicholson, J. K. *Nat Protoc* **5,** 1005-18.

12.   Xie, G., Plumb, R., Su, M., Xu, Z., Zhao, A., Qiu, M., Long, X., Liu, Z., and Jia, W. (2008) *J Sep Sci* **31,** 1015-26.

13.   Wilson, I. D., Plumb, R., Granger, J., Major, H., Williams, R., and Lenz, E. M. (2005) *J Chromatogr B Analyt Technol Biomed Life Sci* **817,** 67-76.

14.   Wilson, I. D., Nicholson, J. K., Castro-Perez, J., Granger, J. H., Johnson, K. A., Smith, B. W., and Plumb, R. S. (2005) *J Proteome Res* **4,** 591-8.

15.   Williams, R., Lenz, E. M., Wilson, A. J., Granger, J., Wilson, I. D., Major, H., Stumpf, C., and Plumb, R. (2006) *Mol Biosyst* **2,** 174-83.

16.   Plumb, R. S., Granger, J. H., Stumpf, C. L., Johnson, K. A., Smith, B. W., Gaulitz, S., Wilson, I. D., and Castro-Perez, J. (2005) *Analyst* **130,** 844-9.

17.   Plumb, R., Granger, J., Stumpf, C., Wilson, I. D., Evans, J. A., and Lenz, E. M. (2003) *Analyst* **128,** 819-23.

18.   Wang, J., Reijmers, T., Chen, L., Van Der Heijden, R., Wang, M., Peng, S., Hankemeier, T., Xu, G., and Van Der Greef, J. (2009) *Metabolomics* **5,** 407-418.

19.   van der Greef, J., Stroobant, P., and van der Heijden, R. (2004) *Curr Opin Chem Biol* **8,** 559-65.

20.   van der Greef, J., Hankemeier, T., and McBurney, R. N. (2006) *Pharmacogenomics* **7,** 1087-94.

21.   van der Greef, J., Martin, S., Juhasz, P., Adourian, A., Plasterer, T., Verheij, E. R., and McBurney, R. N. (2007) *J Proteome Res* **6,** 1540-59.

22.   Clish, C. B., Davidov, E., Oresic, M., Plasterer, T. N., Lavine, G., Londo, T., Meys, M., Snell, P., Stochaj, W., Adourian, A., Zhang, X., Morel, N., Neumann, E., Verheij, E., Vogels, J. T., Havekes, L. M., Afeyan, N., Regnier, F., van der Greef, J., and Naylor, S. (2004) *Omics* **8,** 3-13.

23.   Oresic, M., Clish, C. B., Davidov, E. J., Verheij, E., Vogels, J., Havekes, L. M., Neumann, E., Adourian, A., Naylor, S., van der Greef, J., and Plasterer, T. (2004) *Appl Bioinformatics* **3,** 205-17.

24.   van der Greef, J., and Leegwater, D. C. (1983) *Biomed Mass Spectrom* **10,** 1-4.

25.   Li, X., and Franke, A. A. *Anal Chem*.

26.   Lommen, A., Gerssen, A., Oosterink, J. E., Kools, H. J., Ruiz-Aracama, A., Peters, R. J., and Mol, H. G. *Metabolomics* **7,** 15-24.

27.   Weber, R. J., Southam, A. D., Sommer, U., and Viant, M. R. *Anal Chem*.

28.   Ni, S., Qian, D., Duan, J. A., Guo, J., Shang, E. X., Shu, Y., and Xue, C. *J Chromatogr B Analyt Technol Biomed Life Sci* **878,** 2741-50.

29.   Nie, H., Liu, R., Yang, Y., Bai, Y., Guan, Y., Qian, D., Wang, T., and Liu, H. *J Lipid Res* **51,** 2833-44.

30.   Kirsch, S., Muthing, J., Peter-Katalinic, J., and Bindila, L. (2009) *Biol Chem* **390,** 657-72.

31.   Castro-Perez, J., Plumb, R., Granger, J. H., Beattie, I., Joncour, K., and Wright, A. (2005) *Rapid Commun Mass Spectrom* **19,** 843-8.

32.   Foltz, D. J., Castro-Perez, J., Riley, P., Entwisle, J. R., and Baker, T. R. (2005) *J Chromatogr B Analyt Technol Biomed Life Sci* **825,** 144-51.

33.   Castro-Perez, J. M., Kamphorst, J., DeGroot, J., Lafeber, F., Goshawk, J., Yu, K., Shockcor, J. P., Vreeken, R. J., and Hankemeier, T. *J Proteome Res* **9,** 2377-89.

34.   Castro-Perez, J., Plumb, R., Liang, L., and Yang, E. (2005) *Rapid Commun Mass Spectrom* **19,** 798-804.

35.   Castro-Perez, J. M. (2007) *Drug Discov Today* **12,** 249-56.

36.   Plumb, R. S., Jones, M. D., Rainville, P., and Castro-Perez, J. M. (2007) *J Sep Sci* **30,** 2666-75.

37.   Dalluge, J., Beens, J., and Brinkman, U. A. (2003) *J Chromatogr A* **1000,** 69-108.

38.   Weckwerth, W., Loureiro, M. E., Wenzel, K., and Fiehn, O. (2004) *Proc Natl Acad Sci U S A* **101,** 7809-14.

39.   Tolstikov, V. V., Lommen, A., Nakanishi, K., Tanaka, N., and Fiehn, O. (2003) *Anal Chem* **75,** 6737-40.

40.   Schad, M., Mungur, R., Fiehn, O., and Kehr, J. (2005) *Plant Methods* **1,** 2.

41.   Scalbert, A., Brennan, L., Fiehn, O., Hankemeier, T., Kristal, B. S., van Ommen, B., Pujos-Guillot, E., Verheij, E., Wishart, D., and Wopereis, S. (2009) *Metabolomics* **5,** 435-458.

42.   Sana, T. R., Fischer, S., Wohlgemuth, G., Katrekar, A., Jung, K. H., Ronald, P. C., and Fiehn, O. *Metabolomics* **6,** 451-465.

43.   Fiehn, O., Wohlgemuth, G., Scholz, M., Kind, T., Lee do, Y., Lu, Y., Moon, S., and Nikolau, B. (2008) *Plant J* **53,** 691-704.

44.   Fiehn, O., Kopka, J., Trethewey, R. N., and Willmitzer, L. (2000) *Anal Chem* **72,** 3573-80.

45.   Fiehn, O., Kopka, J., Dormann, P., Altmann, T., Trethewey, R. N., and Willmitzer, L. (2000) *Nat Biotechnol* **18,** 1157-61.

46.   Fiehn, O., Kloska, S., and Altmann, T. (2001) *Curr Opin Biotechnol* **12,** 82-6.

47.   Fahy, E., Subramaniam, S., Murphy, R. C., Nishijima, M., Raetz, C. R., Shimizu, T., Spener, F., van Meer, G., Wakelam, M. J., and Dennis, E. A. (2009) *J Lipid Res* **50 Suppl,** S9-14.

48.   Kell, D. B., and Oliver, S. G. (2004) *Bioessays* **26,** 99-105.

49.   Goodacre, R., and Kell, D. B. (1996) *Anal Chem* **68,** 271-80.

50.   Goodacre, R., Neal, M. J., and Kell, D. B. (1996) *Zentralbl Bakteriol* **284,** 516-39.

51.   Goodacre, R., Vaidyanathan, S., Dunn, W. B., Harrigan, G. G., and Kell, D. B. (2004) *Trends Biotechnol* **22,** 245-52.

52.   Goodacre, R. (2005) *J Exp Bot* **56,** 245-54.

53.   Hall, R. D. (2006) *New Phytol* **169,** 453-68.

54.   Han, X., and Gross, R. W. (2005) *Mass Spectrom Rev* **24,** 367-412.

55.   Lagarde, M., Geloen, A., Record, M., Vance, D., and Spener, F. (2003) *Biochim Biophys Acta* **1634,** 61.

56.   Balazy, M. (2004) *Prostaglandins Other Lipid Mediat* **73,** 173-80.

57.   Lu, Y., Hong, S., Tjonahen, E., and Serhan, C. N. (2005) *J Lipid Res* **46,** 790-802.

58.   Han, X., Yang, K., Cheng, H., Fikes, K. N., and Gross, R. W. (2005) *J Lipid Res* **46,** 1548-60.

59.   Taguchi, R., Houjou, T., Nakanishi, H., Yamazaki, T., Ishida, M., Imagawa, M., and Shimizu, T. (2005) *J Chromatogr B Analyt Technol Biomed Life Sci* **823,** 26-36.

60.   Walker, J. M., Krey, J. F., Chen, J. S., Vefring, E., Jahnsen, J. A., Bradshaw, H., and Huang, S. M. (2005) *Prostaglandins Other Lipid Mediat* **77,** 35-45.

61.   Gross, R. W., Jenkins, C. M., Yang, J., Mancuso, D. J., and Han, X. (2005) *Prostaglandins Other Lipid Mediat* **77,** 52-64.

62.   Milne, S., Ivanova, P., Forrester, J., and Alex Brown, H. (2006) *Methods* **39,** 92-103.

63.   Postle, A. D., Gonzales, L. W., Bernhard, W., Clark, G. T., Godinez, M. H., Godinez, R. I., and Ballard, P. L. (2006) *J Lipid Res* **47,** 1322-31.

64.   Gross, R. W., and Han, X. (2007) *Methods Enzymol* **433,** 73-90.

65.   Tyurin, V. A., Tyurina, Y. Y., Kochanek, P. M., Hamilton, R., DeKosky, S. T., Greenberger, J. S., Bayir, H., and Kagan, V. E. (2008) *Methods Enzymol* **442,** 375-93.

66.   Goto-Inoue, N., Hayasaka, T., Zaima, N., and Setou, M. *Biochim Biophys Acta*.

67.   Stellaard, F., Sackmann, M., Berr, F., and Paumgartner, G. (1987) *Biomed Environ Mass Spectrom* **14,** 609-11.

68.   Stellaard, F., Schubert, R., and Paumgartner, G. (1983) *Biomed Mass Spectrom* **10,** 187-91.

69.   Schoeller, D. A. (1983) *Am J Clin Nutr* **38,** 999-1005.

70.   Schoeller, D. A. (1989) *Am J Clin Nutr* **50,** 1176-81; discussion 1231-5.

71.   Wong, W. W., Hachey, D. L., Feste, A., Leggitt, J., Clarke, L. L., Pond, W. G., and Klein, P. D. (1991) *J Lipid Res* **32,** 1049-56.

72.   Schoeller, D. A., and van Santen, E. (1982) *J Appl Physiol* **53,** 955-9.

73.   Schoeller, D. A., and Racette, S. B. (1990) *J Nutr* **120 Suppl 11,** 1492-5.

74.   Jo, Y., and Debose-Boyd, R. A. *Crit Rev Biochem Mol Biol* **45,** 185-98.

75.   Suh, J. W., Choi, D. J., Chang, H. J., Cho, Y. S., Youn, T. J., Chae, I. H., Kim, K. I., Kim, C. H., Kim, H. S., Oh, B. H., and Park, Y. B. *J Korean Med Sci* **25,** 16-23.

76.   Hartman, I. Z., Liu, P., Zehmer, J. K., Luby-Phelps, K., Jo, Y., Anderson, R. G., and Debose-Boyd, R. A. *J Biol Chem*.

77.   Tadin-Strapps, M., Peterson, L. B., Cumiskey, A. M., Rosa, R. L., Mendoza, V. H., Castro-Perez, J., Puig, O., Zhang, L., Strapps, W. R., Yendluri, S., Andrews, L., Pickering, V., Rice, J., Luo, L., Chen, Z., Tep, S., Ason, B., Sommers, E. P., Sachs, A. B., Bartz, S. R., Tian, J., Chin, J., Hubbard, B. K., Wong, K. K., and Mitnaul, L. J. *J Lipid Res*.

78.   Li, Y., Thapa, P., Hawke, D., Kondo, Y., Furukawa, K., Hsu, F. F., Adlercreutz, D., Weadge, J., Palcic, M. M., Wang, P. G., Levery, S. B., and Zhou, D. (2009) *J Proteome Res* **8,** 2740-51.

79.   Bossola, M., Tazza, L., Luciani, G., Tortorelli, A., and Tsimikas, S. *J Nephrol*.

80.   Shioji, K., Mannami, T., Kokubo, Y., Goto, Y., Nonogi, H., and Iwai, N. (2004) *J Hum Genet* **49,** 433-9.

81.   Bachmann, K., Patel, H., Batayneh, Z., Slama, J., White, D., Posey, J., Ekins, S., Gold, D., and Sambucetti, L. (2004) *Pharmacol Res* **50,** 237-46.

82.   Savas Erdeve, S., Simsek, E., Dallar, Y., and Biyikli, Z. *Indian J Pediatr* **77,** 1261-5.

83.   Norris, A. L., Steinberger, J., Steffen, L. M., Metzig, A. M., Schwarzenberg, S. J., and Kelly, A. S. *Obesity (Silver Spring)*.

84.   van Tits, L. J., Stienstra, R., van Lent, P. L., Netea, M. G., Joosten, L. A., and Stalenhoef, A. F. *Atherosclerosis* **214,** 345-9.

85.   Lopes-Virella, M. F., Baker, N. L., Hunt, K. J., Lachin, J., Nathan, D., and Virella, G. *Atherosclerosis* **214,** 462-7.

86.   Kuniyasu, A., Tokunaga, M., Yamamoto, T., Inoue, S., Obama, K., Kawahara, K., and Nakayama, H. *Biochim Biophys Acta* **1811,** 153-62.

87.   Lopes-Virella, M. F., Hunt, K. J., Baker, N. L., Lachin, J., Nathan, D. M., and Virella, G. *Diabetes* **60,** 582-9.

88.   Li, L., Hossain, M. A., Sadat, S., Hager, L., Liu, L., Tam, L., Schroer, S., Lu, H., Fantus, I. G., Connelly, P. W., Woo, M., and Ng, D. S. *J Biol Chem*.

89.　Hossain, M. A., Tsujita, M., Akita, N., Kobayashi, F., and Yokoyama, S. (2009) *Biochim Biophys Acta* **1791,** 1197-205.

90.　Chen, X., Burton, C., Song, X., McNamara, L., Langella, A., Cianetti, S., Chang, C. H., and Wang, J. (2009) *Int J Biol Sci* **5,** 489-99.

91.　Scarpioni, R., Paties, C., and Bergonzi, G. (2008) *Nephrol Dial Transplant* **23,** 1074; author reply 1074-5.

92.　Rayner, M., Allender, S., and Scarborough, P. (2009) *Eur J Cardiovasc Prev Rehabil* **16 Suppl 2,** S43-7.

93.　Rosamond, W., Flegal, K., Furie, K., Go, A., Greenlund, K., Haase, N., Hailpern, S. M., Ho, M., Howard, V., Kissela, B., Kittner, S., Lloyd-Jones, D., McDermott, M., Meigs, J., Moy, C., Nichol, G., O'Donnell, C., Roger, V., Sorlie, P., Steinberger, J., Thom, T., Wilson, M., and Hong, Y. (2008) *Circulation* **117,** e25-146.

94.　Menotti, A., Lanti, M., Puddu, P. E., and Kromhout, D. (2000) *Heart* **84,** 238-44.

95.　Zhang, X. H., Lu, Z. L., and Liu, L. (2008) *Heart* **94,** 1126-31.

96.　Gordon, T., Castelli, W. P., Hjortland, M. C., Kannel, W. B., and Dawber, T. R. (1977) *Am J Med* **62,** 707-14.

97.　Miller, N. E., Thelle, D. S., Forde, O. H., and Mjos, O. D. (1977) *Lancet* **1,** 965-8.

98.　Bloomfield, D., Carlson, G. L., Sapre, A., Tribble, D., McKenney, J. M., Littlejohn, T. W., 3rd, Sisk, C. M., Mitchel, Y., and Pasternak, R. C. (2009) *Am Heart J* **157,** 352-360 e2.

99.　Marotti, K. R., Castle, C. K., Boyle, T. P., Lin, A. H., Murray, R. W., and Melchior, G. W. (1993) *Nature* **364,** 73-5.

100.　Plump, A. S., Masucci-Magoulas, L., Bruce, C., Bisgaier, C. L., Breslow, J. L., and Tall, A. R. (1999) *Arterioscler Thromb Vasc Biol* **19,** 1105-10.

101.　Li, H., Reddick, R. L., and Maeda, N. (1993) *Arterioscler Thromb* **13,** 1814-21.

102.　McCaffrey, A. P., Meuse, L., Pham, T. T., Conklin, D. S., Hannon, G. J., and Kay, M. A. (2002) *Nature* **418,** 38-9.

103.　Dykxhoorn, D. M., and Lieberman, J. (2005) *Annu Rev Med* **56,** 401-23.

104.　Hannon, G. J. (2002) *Nature* **418,** 244-51.

105.　Hannon, G. J., and Rossi, J. J. (2004) *Nature* **431,** 371-8.

106.　Bakhtiar, R. (2008) *J Pharmacol Toxicol Methods* **57,** 85-91.

107.　Lee, J. W., Devanarayan, V., Barrett, Y. C., Weiner, R., Allinson, J., Fountain, S., Keller, S., Weinryb, I., Green, M., Duan, L., Rogers, J. A., Millham, R., O'Brien, P. J., Sailstad, J., Khan, M., Ray, C., and Wagner, J. A. (2006) *Pharm Res* **23,** 312-28.

Part I

LC/MS platform development

Chapter 2

Comprehensive shotgun LC-MS^{E} lipidomic analysis in osteoarthritis patients

Comprehensive shotgun LC-MS^E lipidomic analysis in osteoarthritis patients

SUMMARY

A fast and robust method for lipid profiling utilizing liquid chromatography coupled with mass spectrometry has been demonstrated and validated for the analysis of human plasma. This method allowed quantifying and identifying lipids in human plasma using parallel alternating low energy and high energy collision spectral acquisition modes. A total of 275 lipids were identified and quantified (as relative concentrations) in both positive and negative ion electrospray ionization mode. The method was validated with five non-endogenous lipids, and the linearity (r^2 better than 0.994), the intra-day and inter-day repeatability (relative standard deviation, 4-6% and 5-8%, respectively) were satisfactory. The developed lipid profiling method was successfully applied for the analysis of plasma from Osteoarthritis (OA) patients. Multivariate statistical analysis by partial least squares-discrimination analysis suggested and altered lipid metabolism associated with osteoarthritis and the release of arachidonic acid from phospholipids.

INTRODUCTION

Lipidomics can be defined as the system-wide characterization of lipids and their interaction with other biochemicals and cells. Lipidomics can be divided into two biochemical areas of equal significance; membrane functional-lipidomics and mediator functional-lipidomics, which pay particular attention to either the exhaustive and quantitative description of membrane lipid components, or the structural identification and quantification of relevant bioactive lipid species. The term "lipidome" can be defined as the comprehensive and non-exhaustive quantitative description of a set of lipid classes which may constitute a cell or bio-organism.

Lipids and their interaction with cells play a crucial role in living organisms (1-3). This is mainly due to the fact that lipids have unique and specific membrane organizing tasks as well as support properties providing cells with distinct sub-cellular membrane compartments. Lipids also extend their functionality levels to other important areas such as their specific and crucial role in cell signaling, endocrine actions and their specific function for energy production and storage. Production of lipids is very extensive by either mammalian or bacterial organisms, and their metabolic pathways are extremely capable of generating a large number of lipid classes typically in the thousands (4) which are functionally and structurally diverse each having a certain biological role. Lipids have a variety of non-polar fatty acid (FA) chains with different backbone structures and different polar head groups. The fatty acid constituents have well-defined structural characteristics, such as *cis*-double bonds in particular positions, which can act as information transporters by selective binding to specific receptors. They can penetrate membranes in their esterified form or be subjected to specific translocation across membranes to carry signals to other cells in different parts of the organism. With regards to lipid storage, such as e.g. triacylglycerols, they are relatively inert until required. In contrast to this, polar lipids have hydrophilic sites that have the capability to bind to membrane proteins and as a consequence influence their dynamics and biological properties. The biological activities of lipids also extend far beyond membranes into e.g., the immune system such as glycolipids with their specific and complex carbohydrate moieties.

Recently, system-wide lipid analysis has attained more interest due to their importance in medical, biological, biotechnological and industrial applications (5-11). Lipids as a whole have shown a direct implication in an important number of human diseases, including cancer and cardiovascular disease. These biological entities are therefore interesting for biomarker discovery. For example, total lipid profiles are measured when trying to assess the efficacy of a certain cholesterol lowering drug such as the 'statins' (12-14) by measuring; triglycerides, cholesterol and high density lipoprotein (HDL)/ low density lipoprotein (LDL) relationships. Profiling of the individual lipids in a system-wide approach is expected to be even more suited to describe an individual's state with regards to health and disease. It is important to understand the classification of lipids in terms of mass spectrometry (MS) as they will have characteristic properties when analyzed by liquid chromatography LC-MS. Therefore, lipids can be catalogued into eight main distinctive classes. Their diversity is mainly based on their fingerprint chemical structure and mainly by the head group of the lipid class: fatty acids, glycerolipids, glycerophospholipids, sphingolipids, sterol lipids, prenol lipids, saccharolipids,

and polyketides (15). For the analysis of lipids in biological samples, LC-MS has played an important role in the detection and identification of lipids. In particular the advent of electrospray has completely transformed the way in which these compound classes are characterized and quantified with extreme sensitivity in the low femtogram levels. Electrospray is a soft ionization technique and in the vast majority of cases will generate protonated or deprotonated molecules depending on the polarity of the ionization mode utilized. In addition to this, it is not uncommon to generate molecular adducts provided by cations such as Na^+, K^+, or NH_4^+ in positive ion mode. These adducts mainly originate from the specific mobile phase used for the analysis. On the other hand, chromatography has also further evolved with, e.g., developments in the fabrication of small particle sizes such as in the sub 2μm range to obtain chromatographic separations in a much shorter analytical run without the loss of specificity and chromatographic fidelity. This so-called ultra performance LC (UPLC) (16-19) is now widely used and applied to not only lipid analysis but also other areas such as pharmaceutical, metabolomic, proteomic, biopharmaceutical and chemical analyses. There are several strategies which are widely used for the separation of lipids prior to introduction in the mass spectrometer. Normal phase LC-MS separates phospholipids into their respective classes. The separation is important as a means of classification because the separation is attained based on their respective polar head groups with complete disregard of their *sn*-1 and *sn*-2 fatty acid substituents. This is not an uncommon approach to lipid analysis by LC-MS and suitable MS 'friendly' solvents have been used to achieve such separations. In contrast to normal phase separations for lipid analysis reverse phase (RP) separations have the signature characteristic of cataloguing the lipids according to the overall polarity and the fatty acid composition in the *sn*-1, *sn*-2 and *sn*-3 locations. Such a RP separation is more or less orthogonal to normal phase. The ideal situation would be the use of two-dimensional LC in which normal and reversed phases are comprehensively coupled, but such a coupling is not straightforward, and was not the aim of the current project. In terms of mass spectrometric analyzers, lipid analysis has been developed and implemented successfully with tandem quadrupoles and linear ion traps (21-26). In addition there are other mass analyzers, like orbitraps, fourier transform ion cyclotron resonance (FTICR) and hybrid quadrupole orthogonal time-of-flight technology (Q-Tof), which may be utilized for the analysis of phospholipids. It is important for these studies that the mass analyzer of choice can provide exact mass information as this will help to determine the elemental composition of the lipid of interest. The Q-ToF (27) provides such mass measurement and is designed as follows; the first quadrupole focuses all ions (in RF –only mode) or selected ions into the second quadrupole, which acts as a collision cell. Ions entering this collision cell will either be fragmented by collision induced dissociation (CID) or will be transferred without fragmentation into the time of flight region for subsequent detection. Technological advances have made hybrid mass spectrometers such as the Q-ToF superior over more conventional tandem quadrupole or linear ion trap with regards to enhanced mass accuracy and spectral resolution next to sensitivity in full scan mode. A clear example of this is the ability of the Q-ToF to conduct many precursor and neutral loss acquisitions over a single experimental run using an instrument acquisition mode called MS^E (28-30). This overcomes duty cycle issues associated with other scanning instruments with a high number of precursor or neutral loss ions per single injection. Furthermore, during an MS^E acquisition exact mass information is obtained, which is used to remove false positives. In this paper, a rapid and simple

reversed phased UPLC/ TOF MS^E strategy to detect and identify multiple classes of lipids in extracted human plasma will be demonstrated. The methodology is applied to the study of osteoarthritis in humans.

MATERIALS AND METHODS

Chemicals

Mass spectrometry grade isopropanol, acetonitrile and ammonium formate (AmmFm 99.995%) were purchased from Sigma (St. Louis, MO). Water was obtained from a Millipore high purity water dispenser (Billerica, MA). Dichloromethane and methanol were obtained from Thermo Fisher Scientific (New Jersey, NJ) The mobile phase for this study was prepared as follows; solvent A was prepared by adding 400 mL of H_2O to 600mL of acetonitrile followed by the addition of 0.6306 ± 0.1 g of AmmFm to yield a 10mM total concentration of AmmFm. For solvent B, 100 mL of acetonitrile was added to 900 mL of isopropanol followed by the addition of 0.6306 ± 0.01 g of AmmFm to yield a 10 mM total concentration of AmmFm. Prior to use, both solvents A and B were degassed in an ultrasonic bath for 30 minutes. Lipid standards of 1-heptadecanoyl-2-hydroxy-*sn*-glycero-3-phosphocholine LPC (17:0/0:0), 1-nonadecanoyl-2-hydroxy-*sn*-glycero-3-phosphocholine LPC (19:0/0:0), 1,2-dipentadecanoyl-*sn*-glycero-3-phosphoethanolamine PE (15:0/15:0), 1,2-diheptadecanoyl-*sn*-glycero-3-phosphoethanolamine PE (17:0/17:0), 1,2-dimyristoyl- *sn*-glycero-3-[phospho-rac-(1-glycerol)] (sodium salt) PG (14:0/14:0), 1,2-diheptadecanoyl*sn*-glycero-3-[phospho-rac-(1-glycerol)] (sodium salt) PG (17:0/17:0), 1,2-diheptadecanoyl-*sn*-glycero-3-phosphocholine PC (17:0/17:0) and 1,2-dinonadecanoyl-*sn*-glycero-3-phosphocholine PC (19:0/19:0) were purchased from Avanti Polar Lipids (Alabaster, AL, USA). 1,2,3-Tripentadecanoylglycerol TG (15:0/15:0/15:0), 1,2,3-triheptadecanoylglycerol TG (17:0/ 17:0/17:0) were obtained from Sigma (Zwijndrecht, The Netherlands). Leucine enkephalin (Sigma, St. Louis, MO, USA) was used as the lockmass solution at a concentration of 1 ng/µL in a solution of acetonitrile/water +0.1% Formic acid (50/50 v/v).

Lipid nomenclature

Throughout the entire paper and in order to follow a common standard lipid language, the lipid nomenclature described by LIPIMAPS (http://www.lipidmaps.org) was followed.

Lipid preparation and extraction

Lipid extracts from human plasma were prepared according to the protocol described by Hu (35). Human plasma samples were prepared and extracted in a biosafety level 2 (BL2) fume hood. The reproducibility and efficacy of the methodology was tested with a set of human plasma extracts over the total procedure. The validation extracts were prepared by spiking 5 different non-endogenous lipids (LPC 19:0/0:0, PG 14:0/14:0, PE 15:0/15:0, PC 19:0/19:0 and TG 15:0/15:0/15:0) and their corresponding internal standards into pooled healthy human plasma. The concentration ranges for each of the non-endogenous lipids and their internal standards were; LPC 19:0/0:0 0, 1.25, 2.5, 5, 20, 80, 160 µg/mL and the internal

standard LPC 17:0/0:0 were used at a final concentration of 15μg/ml; PG 14:0/14:0 0, 5, 10, 20, 80, 320   g/mL and the internal standard PG 17:0/17:0 were used at a final concentration of 20μg/ml ; PE 15:0/15:0 0, 2.5, 5, 10, 40, 160, 320 μg/mL and the internal standard PE 17:0/17:0 were used at a final concentration of 20 μg/ml; PC 19:0/19:0 0, 3.75, 7.5, 15, 60, 240, 480μg/mL and the internal standard PC 17:0/17:0 were used at a final concentration of 40 μg/ml; TG 15:0/15:0/15:0 0, 1.25, 2.5, 5, 20, 80,160μg/mL and the internal standard TG 17:0/17:0/17:0 were used at a final concentration of 25μg/ml. Each calibration standard was injected in triplicate. The lipid fraction was extracted using a simple liquid-liquid extraction (LLE) methodology in which 30 μL of human plasma was mixed with a dichloromethane (DCM) /methanol mixture (31) (2:1,v/v) in accordance with the method described by Bligh and Dyer (31).

The method was validated by spiking the samples before and after preparation as follows; before the sample preparation; 30 μL of IS and 30 μL of the validation calibration mixture were added to 30μL of human plasma sample followed by the addition of 180 μL of MeOH and 360 μL of DCM. A total of 340 μL of lipid extract from the lower organic phase was collected and then 60 μL of 2:1 DCM/MeOH was added. This mixture was diluted 5 times with injection solvent; 10 μL was injected into the LC-MS system

The procedure for spiking after the sample preparation was the same as that described for spiking before except the order in which the 60 μL of 2:1 DCM/MeOH and 30μL of IS plus 30 μL of validation standard mixture was added. For the blank sample, 30 μL of human plasma was replaced by 30 μL of HPLC-MS grade water and the 60 μL of the two sets of standard mixtures were replaced by 60 μL of 2:1 DCM/ MeOH.

Osteoarthritis sample analysis

Heparinized plasma samples were collected from 59 subjects (all female donors) that were part of the Dutch CHeCK cohort (31). Permission was granted to analyze the samples for the purpose of this particular study. Subjects were classified based on radiologic features of osteoarthritis in knee and hip joints (Kellgren-Lawrence Grading). The KL-grade (0-4) was determined for each joint and a summed osteoarthritis load was calculated for each subject by summing the KL grade of the individual joints, resulting in a theoretical range from 0 (no OA in knees of hips) to 16 (severe OA in all joints). Since the CHeCK cohort comprised subjects with mild OA, the actual range in the current 59 subjects was 0 to 8. The samples were analyzed by LC-MS individually, each sample group contained the following number of subjects ; group 0 (n =26) , group 1 (n = 6), group 2 (n = 8), group 3 (n = 4), group 4 (n = 8) , group 5 (n =1), group 6 (n = 2), group 7 (n = 2), group 8 (n = 2). For the purpose of the statistical analysis the samples were classified under the following groups;   Control subjects with a total OA score of 0 (no OA in knees of hips); Early OA subjects with a total OA score of 1-3 and Moderate OA, subjects with a total OA score of 4-8. All patients had similar body mass index (BMI).

UPLC analysis

An Acquity UPLC (Waters, Milford, MA, USA) was used for the inlet. Human plasma extracts were injected onto a 1.8 μm particle 100 x 2.1 mm id Waters Acquity HSS T3 column (Waters, Milford, MA, USA) which was heated to 55 °C in the column oven. The average column pressure was ca. 10,000 psi. A binary gradient system consisting of acetonitrile and water with 10 mM ammonium formate (60:40, v/v) was used as eluent A. As for eluent B, it consisted of acetonitrile and isopropanol both containing 10mM ammonium formate (10:90, v/v). The sample analysis was performed by using a linear gradient (curve 6) over a 15 minute total run time; during the initial portion of the gradient, it was held at 60% A and 40% B. For the next 10 minutes the gradient was ramped in a linear fashion to 100% B and held at this composition for 2 minutes hereafter the system was switched back to 60% B and 40% A and equilibrated for an additional 3 minutes. The flow rate used for these experiments was 0.4mL/min and the injection volume was 10 μL.

Mass Spectrometry

The inlet (UPLC system) was coupled to a hybrid quadrupole orthogonal time of flight mass spectrometer (SYNAPT HDMS, Waters, MS Technologies, Manchester, and UK). Electrospray positive and negative ionization modes were used. A capillary voltage and cone voltage of ±3 kV and ±35 V respectively were used for both polarities. The desolvation source conditions were as follows; for the desolvation gas 700 L/hr was used and the desolvation temperature was kept at 400°C. Data acquisition took place over the mass range of 50-1200 Da for both MS and MS^E modes. The system was equipped with an integral LockSpray unit with its own reference sprayer that was controlled automatically by the acquisition software to collect a reference scan every 10 seconds lasting 0.3 seconds. The LockSpray internal reference used for these experiments was Leucine enkephalin. The reference internal calibrant was introduced into the lock mass sprayer at a constant flow rate of 50 μL/min using an external pump. A single lock mass calibration at m/z 556.2771 in positive ion mode and m/z 554.2615 in negative ion mode was used for the complete analysis. The mass spectrometer was operated in the MS^E mode of acquisition for both polarities. During this acquisition method, the first quadrupole Q1 is operated in a wide band RF mode only, allowing all ions to enter the T-wave collision cell. Two discrete and independent interleaved acquisitions functions are automatically created. The first function, typically set at 5 eV, collects low energy or unfragmented data while the second function collects high energy or fragmented data typically set by using a collision energy ramp from 20-30 eV. In both instances, Argon gas is used for CID. The advantage of this acquisition mode lies in the fact that it is an unbiased strategy to collect both unfragmented and fragmented ions which consecutively can be used for e.g. quantification and fragment-ion information, without prior knowledge of the sample composition. The latter experiment can be considered to be a product-ion scan, a pre-cursor ion- or neutral-loss "like" scan. This technique was able to produce a more generic, simple, fast and yet elegant profiling approach to complex lipidomic samples. Applying

this technology allowed the specific detection of intact [M+H] $^+$ or [M-H] $^-$ ions, precursor- and neutral loss-like ions in either positive or negative ionization mode upon collision-induced dissociation.

The specificity and reliability of this methodology allowed us to use this technology as a 'shotgun' LC-MS approach to search for fatty acids (FA), cholesteryl esters (ChoE), phospholipids (PL), monoacyglycerides (MG), diacylglycerides (DG) and triacylcerides (TG) in an unbiased and reliable manner. For instance, in positive ion mode PCs and SMs are readily detected as protonated molecules or cations. Upon CID they both generate the m/z 184.0739 fragment-ion corresponding to the polar hear group, $[(CH_3)_3N^+C_2H_4OP\ (OH)_2\ O]$. Ions yielding structural information are of low abundance and typically other solvents/modifiers such as LiOH are added either in the mobile phase or post-column (32) to obtain information on the FA chain length and number of carbon atoms. As a matter of interest, the fragmentation pathway for the generation of this particular fragment-ion (m/z 184.0739) has been extensively studied which indicates direct involvement of a α-hydrogen mainly of the fatty acyl chain at *sn*-2 (33).

Data Processing

 For the determination of the repeatability, linearity and recovery, the ratio of the peak areas of the endogenous lipid and the corresponding internal standard was calculated. The internal standard for the lipids LPC 19:0/0:0, PG 14:0/14:0, PE 15:0/15:0, PC 19:0/19:0 and TG 15:0/15:0/15:0 were LPC 17:0/0:0, PG 17:0/17:0, PE 17:0/17:0, PC 17:0/17:0 and TG 17:0/17:0/17:0, respectively.

A quantitative and qualitative software tool called TargetLynx (Waters MS Technologies, Manchester, UK) was utilized for the determination of the peak areas of calibration analytes and internal standards followed by the generation of calibration lines. In addition to this, the above mentioned software algorithm was also capable of generating a peak list (m/z, retention time, peak area, mass accuracy) containing a pre-defined list of lipids, from which the raw data was mined verifying the presence or absence of these biochemicals. A master list was generated in a .txt format and was used for further evaluation.

For the MS^E data processing, the software tool MetaboLynx XS (Waters MS Technologies) was utilized to align the low energy information with the high energy information. Typically this tool is utilized for processing xenobiotics but it is equally applicable to this concept. This algorithm allowed for the search of common precursor ions, diagnostic precursor ions and neutral losses from the high energy data and by parallel alignment with the low energy data and thus locating the unfragmented molecule.

In the case of the osteoarthritis sample analysis, MarkerLynxXS (Waters MS Technologies) was used as the primary tool for data deconvolution and multivariate statistical analysis. The data set was normalized to the total number of peaks identified as variables (exact mass-retention time pairs (EMRT) and peak intensities) and pareto scaling was utilized for

the multivariate statistical analysis. For the database search, lipidmaps *on-line* searching tools (http://www.lipidmaps.org) was used.

RESULTS AND DISCUSSION

UPLC-TOF MS^E Analysis

In order to understand the lipidome and the biological implications it is important to be able to catalogue and quantify lipids into their respective molecular classes. The use of UPLC enabled a fast sample turn around in a total time of 15 minutes which is suitable for a rapid profiling screening strategy. This is about 3x faster than it would take for a similar HPLC method under the same conditions (34). Figure 1 highlights the retention time windows of the lipid classes in the UPLC/TOF MS chromatogram in positive and negative ion mode. In other words, these are region-specific chromatographic areas where we could focus our attention when searching for certain lipid classes or for specific fraction collection experiments.
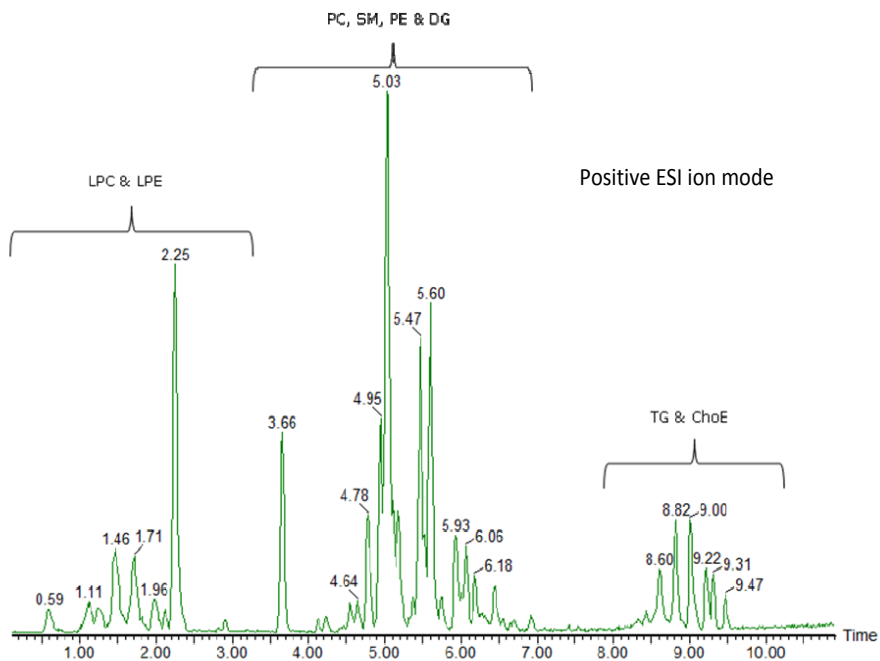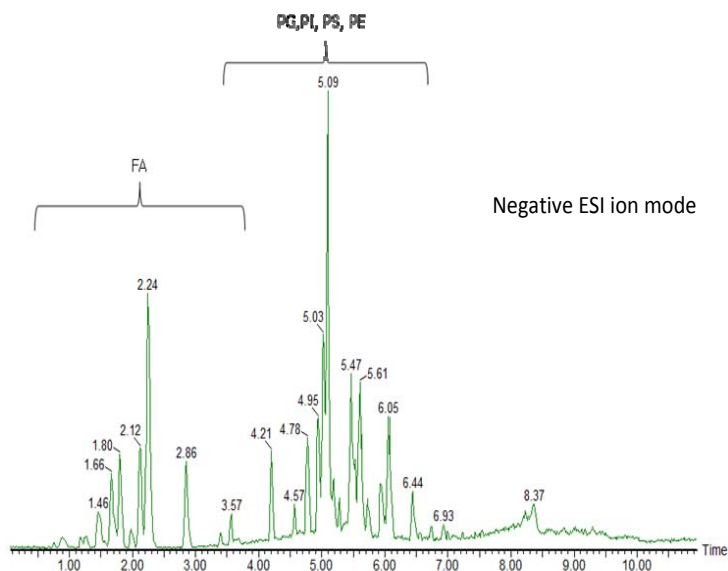
Figure 1. Base peak UPLC/TOFMS chromatogram of a human plasma extract using electrospray ionization in positive and negative mode; different lipid classes elute in different elution time windows. For the experimental details see Materials and Methods.

Abbreviations: ChoE= cholesterol ester; PC = phosphatidylcholine; FA = free fatty acid; TG = triglyceride; DG = diacylglyceride; PS = phosphatidylserine; PI = phosphatidylinositol; PG = phosphatidylglycerol; PE = phosphatidylethanolamine; LPE = Lyso phosphatidylserine; LPC = Lyso phosphatidylcholine; SM= sphingomyelin.

Linearity

For the developed RP-UPLC-TOFMS^E method, five different non-endogenous lipids were spiked to 30 µL of human plasma at six different concentrations (C0-C6), where the calibration ranges were different for the five non-endogenous lipids (Table 1). For each of the five lipids a calibration line was generated using the ratios of the non-endogenous lipid peak areas and their corresponding internal standard (IS). Different polarity ionization modes were used for the different lipids, due to the difference in the preferential ionizations for the different polar head groups. They were divided in the following order for all the validation experiments; positive ion electrospray mode (LPC 19:0/0:0, PC 19:0/19:0 and TG 15:0/15:0/15:0) and negative ion electrospray mode (PG 14:0/14:0 and PE 15:0/15:0). The linear regression r^2 was better than 0.994 for all five non endogenous lipid species (Table 1). These results are comparable to those published by Laaksonen and Hu (35, 36). In order to prove the robustness of the methodology described in this paper, good linearity was also obtained when PC 17:0/17:0 was used as the internal standard for LPC 19:0/0:0 (r^2, 0.995) and for TG 15:0/15:0/15:0 (r^2, 0.996) in electrospray positive ion mode. A good correlation was obtained in electrospray negative ion

mode when PE 15:0/15:0 was used as the internal standard for PG 14:0/14:0 (r2, 0.998). In all these cases also the RSDs were acceptable (data not shown).

Table 1. Validation results of non-endogenous validation standards; response determined as ratio of response of validation standard and corresponding internal standard; 5 non-endogenous lipids and internal standards were spiked to human plasma prior to sample preparation. Each calibration point was injected in triplicate.

	Validation Standards/IS Results									
	LPC (19:0/0:0)/ LPC (17:0/0:0)		PC (19:0/19:0)/ PC (17:0/17:0)		PE (15:0/15:0)/ PE (17:0/17:0)		PG (14:0/14:0)/PG (17:0/17:0)		TG (15:0/15:0/15:0)/TG (17:0/17:0/17:0)	
conc. Level	conc (µg/mL)	Average RSD (%)	conc (µg/mL)	Average RSD (%)	conc (µg/mL)	Average RSD (%)	conc (µg/mL)	Average RSD (%)	conc (µg/mL)	Average RSD (%)
C1	1.25	-4.6	3.75	-7.7	2.5	-9.0	5	-7.2	1.25	1.0
C2	2.5	-6.1	7.5	-0.4	5	-0.1	10	8.3	2.5	-1.2
C3	5	-2.8	15	15.9	10	1.8	20	12.1	5	9.2
C4	20	-6.1	60	1.0	40	5.7	80	7.9	20	-7.1
C5	80	0.4	240	1.8	160	-0.2	320	-4.0	80	4.7
C6	160	0.8	480	-1.3	320	-0.7			160.0	-0.8
slope	0.0477		0.0164		0.0142		0.0067		0.0226	
intercept	-0.0117		0.0128		0.0184		0.0173		0.0064	
R^2	0.9993		0.9993		0.999		0.9943		0.9982	

Reproducibility

The intra-day and inter-day variation was assessed by performing repeated sample preparations and analysis during three consecutive days; this consisted of sample preparation, extraction and analysis in triplicates. One human plasma sample was divided into several aliquots stored at -20°C for each sample preparation step. Quality controls for each of the 5 non-endogenous lipid standards were prepared in plasma at the following concentration levels; LPC 19:0/0:0 (20µg/mL), PG 14:0/14:0 (80µg/mL), PE 15:0/15:0 (40µg/mL), PC 19:0/19:0 (60µg/mL) and TG 15:0/15:0/15:0 (20µg/mL). The intra-day and inter-day variation were calculated as the mean ratios of the peak area of the selected lipid with the corresponding IS spiked to human plasma (Supplemental information Figure S1). The RSD for the intra-day variation for all the 5 non-endogenous lipids ranged from 4.3-6.2%. For the inter-day variation, the RSD for all the non-endogenous lipids ranged from 4.8-8%.

Recovery

In the recovery section of the validation, the same 5 non-endogenous lipids with their respective internal standards already cited in the method were used. These lipids were spiked before and after extraction. Each plasma and pretreated sample was prepared in triplicate in 3 consecutive days, and analyzed in triplicate. The recovery for each non-endogenous lipid in the validation set was calculated as the ratio of the peak area for the particular lipid in the sample prior to extraction and in the samples spiked after extraction. The recoveries were calculated at the following concentration levels for all the lipids in the validation set; LPC 19:0/0:0 (20µg/mL), PG 14:0/14:0 (80µg/mL), PE 15:0/15:0 (40µg/mL), PC 19:0/19:0

(60μg/mL) and TG 15:0/15:0/15:0 (20μg/mL). The average recoveries over the 3 day recovery test (Supplemental information Figure S2) were 74% for the LPC 19:0/0:0, 94% for the PC 19:0/19:0, 81% for the PE 15:0/15:0, 79% for the PG 14:0/14:0 and 82% for the TG 15:0/15:0/15:0. The recoveries were considered to be acceptable for routine lipid profiling experiments.

Lipid Identification and MS[E]

With respect to the lipid identification step, it was possible to identify 275 major fatty acids lipids and TG's (Table S1 in the supplemental information) in these human plasma samples. It is worth pointing out that in total more than 1500 peaks were detected but it was beyond the scope of this paper to identify each one of all entries and we only focused on the most abundant lipid species. This methodology and in particular the use of the highly efficient LC separation allowed for the separation of isomers of several lipids.

These 275 human fatty acids, lipids and TG's are classified according their respective groups, TGs (77), PC (65), SM (43), PS (31), LPC (22), FA (14), PI (7), ChoE (6), PE (4), PG (3), LPE (2) and DG (1). By observing this table closely (Table S1 in the supplemental information section) it is obvious that the top 10 most abundant ions (Table S2 in the supplemental information) belong to the PC, SM and TG lipid class. The most abundant phospholipid was a PC with an absolute peak area of 311 at a retention time of 5.02 minutes. At this particular retention time a protonated molecule $[M+H]^+$ with an m/z of 758.5718 corresponding to the elemental composition $C_{42}H_{80}NO_8P$ (error of +2.4 ppm) was assigned to a PC compound with a 1-acyl 34:2 moiety. The most abundant peak of the second most abundant phospholipid class found in the top 10 entries had a retention time of 4.78 minutes and a peak area of 60. The corresponding spectrum shows a protonated molecule $[M+H]^+$ at m/z 703.5767 and an elemental composition of $C_{39}H_{79}N_2O_6P$ with an error of +1.9 ppm. This phospholipid was assigned as the 2-amido 16:0 of the SM class. The most abundant peak of the third most abundant lipid class (retention time 8.82 minutes and m/z 874.7885 for the $[M+NH_4]^+$ ion) was assigned to the triacylglyceride (TG) 1-acyl 52:3 ($C_{55}H_{103}NO_6$ +2.5 ppm).

One approach which can be used to obtain MS^2 information is to carry out data-dependent experiments (37). During data-dependent experiments it is possible to collect MS and MS^2 data in a serial process, that is when a specific ion of interest is detected in full scan mode and after a specific set of criteria, e.g. peak intensity, retention time, inclusion- and/or exclusion criteria, are met, the mass spectrometer will switch to MS^2 mode and collect fragment-ion data. However, during these experiments for complex samples co-elution of multiple lipids, at low and high level concentrations will occur, and the data-dependent fragmentation experiments may vary from sample to sample. A 'good' data-dependent method relies heavily on the fact that the scientist has previous knowledge of the type of biochemicals which are expected to be detected, the method itself including m/z ranges and ion intensity thresholds which need to be set accordingly in order to prevent inclusion of false positives, therefore adding complexity to the experiment. As a result, for the qualitative

analysis lipids may be missed, and quantitative analysis is not possible with data-dependent MS/MS data. Also, if the MS/MS experiments are too slow, not enough full scan MS experiments are carried out for quantitative analysis. In this context the acquisition rate of the mass spectrometer and the speed of the chromatography are important factors to be considered.

In contrast, during the MS^E approach all ions generated in the ion source enter the collision cell, and alternating a (i) low energy collision experiment is carried out resulting in only very modest or no fragmentation and a (ii) higher energy collision experiment is carried out resulting in fragment ions; in both cases all product ions are acquired in the TOF MS detector. The use of MS^E data results in multiple levels of information which is extremely useful when trying to confirm the identity of a specific compound. For example, one could focus on determining the polar head group or the carbon length of the FA moiety. With this data independent acquisition mode it is possible to perform an *ad-hoc de-novo* profiling type of experiment. These experiments capture a myriad of information which may be used to data mine complex data sets by extracting accurate mass full scan chromatograms or accurate mass high energy chromatograms which may contain key diagnostic fragment-ions. Since we now have both low and high energy information within the same data file, it is possible to obtain accurate mass, fragment-ion, precursor ion and neutral loss 'like' data to search for diagnostic ions or common neutral losses.

Therefore, the specificity arising from the accurate mass precursor 'like' ion scanning allowed for an extended application of this technique not just for a single diagnostic fragment-ion but for a large number of them without the loss in performance as seen when the same experiment is performed with a tandem quadrupole or linear ion trap. In addition to this, a higher level of specificity is obtained because the use of accurate mass and a high level of mass spectral resolution in both the low and the high energy modes. To illustrate this powerful approach, Figure 2 highlights the possibility to extract an accurate mass ion chromatogram with a narrow mass window of 30mDa for the phosphatidylcholine head group. By alignment of the low energy data with the high energy data, which is carried out automatically with the software (MetaboLynx XS), all low energy corresponding entries which have this product ion of interest will be reported. From this figure it is clearly visible that not only the phosphatidylcholine fragment-ion at m/z 184.0731 was very abundant, but also selectively allowed the search for the LPC, PC and SM phospholipid classes. Of course this is notwithstanding the fact that all other important full scan and fragment-ion information belonging to other lipid classes are acquired within the single LC-MS^E analysis and can be data mined at any time. This approach is totally unbiased and as such it is possible to search for other diagnostic fragments as 'all fragment-ions' should be accounted for. This will allow for the identification of high and low abundance species in a relatively simple manner. However, having said this, the data generated here is very complex and even though it is possible to obtain a 'quick look and see' of what is there in a manual fashion. Ultimately, powerful software algorithms in the MS^E software allows for correlation and alignment between low and high energy data
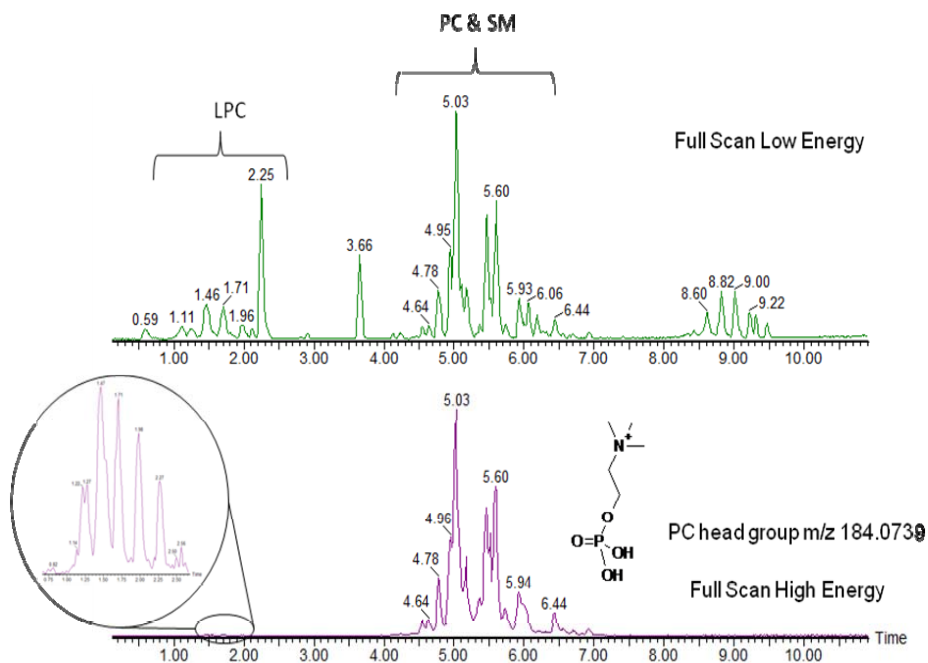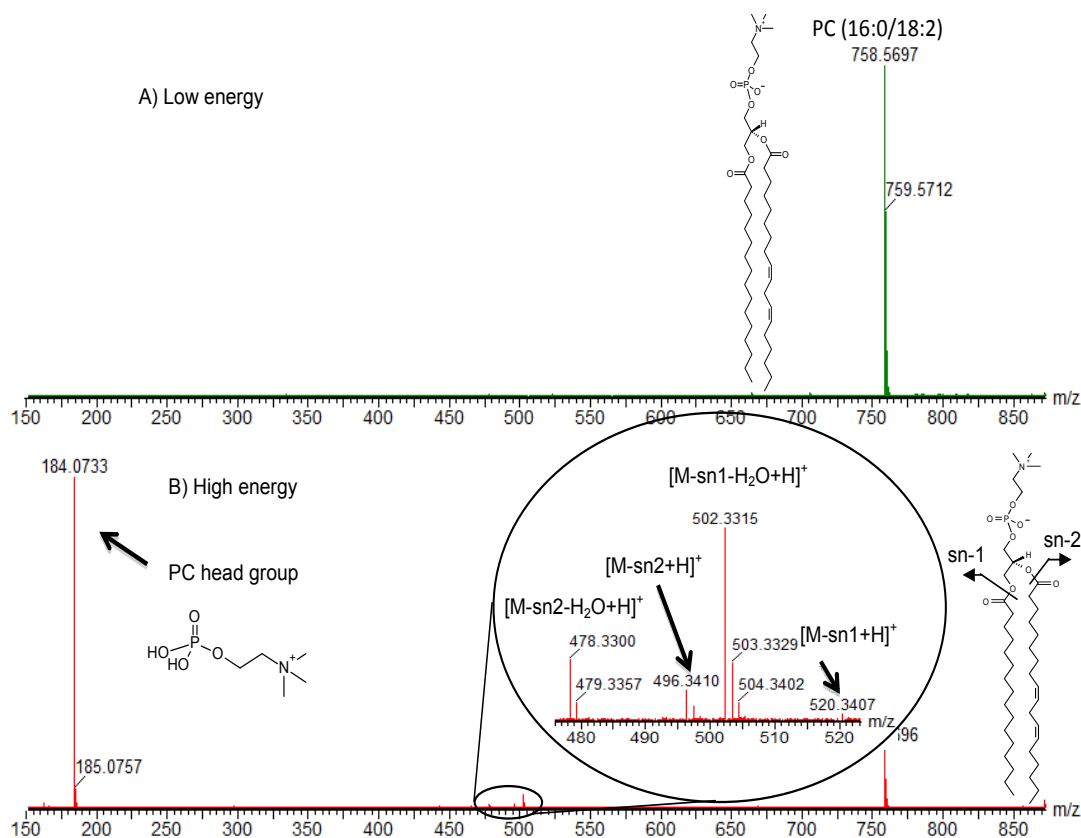
Figure 2. Low-(top) and high-(bottom) collision energy full scan MS chromatogram obtained by MS^E approach using conditions as described in Methods and Materials. It can be clearly seen that the fragment-ion for the phosphocholine head group m/z 184.0739, being characteristic for LPC, PC and SM can clearly be used for identification of individual lipids within one class followed by alignment with the low energy trace.

The high energy data is produced by CID, which in turns gives rise to an extensive number of fragment-ions. If, for instance we take the diagnostic fragment-ion of the phosphatidylcholine species at m/z 184.0733 (error, -3.3 ppm) (Figure 3 section B) it can be observed how the low energy (Figure 3 section A) gives rise to the ion at m/z 758.5697 (-0.5 ppm) [M+H]$^+$ (PC 16:0/18:2). The corresponding fragments of this ion are visible in the high energy spectrum. The ion with the highest abundance is clearly the diagnostic fragment-ion for the PC's of m/z 184.0733 corresponding to the polar head group. However, next to this ion several other fragment-ions are present in the high energy spectrum at a much lower abundance. Further examination of these fragment-ions show that they can be associated with the FA chains of the molecule. Without the use of lithiated adducts, the ion at m/z 184.0733 is the only high abundance ion which dominates the spectrum and hardly any *sn-1* or *sn-2* information as to the assignment for the identities and position of the FA substituent is obtained. Having said that, it is still possible to generate information detailing fatty acid branching information in a chromatographic timeframe. As shown in figure 3 section A of the spectra reveals the low energy information containing the unfragmented PC (16:0/18:2) and section B contains fragment-ion information detailing the

loss of the polar head group at m/z 184.0733 and the cleavages of the *sn-2* m/z 496.3410 and *sn-1* m/z 520.3407, subsequent H$_2$O losses from the sn-2 m/z 478.3300 and sn-1 m/z 502.3315 were also detected. Therefore, helping to decipher the lipid polar head and FA composition.

Figure 3. Low- (top) and high- (bottom) collision energy exact mass spectra of PC (16:0/18:2). The low energy spectrum only contains the precursor ion at m/z 758.5697 whereas in the high energy spectrum various diagnostic fragments appear as the loss of the various FA chains at 496.3410 and 520.3407 and their respective water losses. Next also the major fragment ion at m/z 184.0733 can be seen corresponding to the polar head group.

PC can also be presented as plasmanyl-phosphocholines and plasmenyl-phosphocholines (38). These plasmanyl- and plasmenyl- phosphatidylcholine species mainly yield upon MS/MS the fragment-ion at m/z 184.0739, (being the phosphatidylcholine head group) , such as the diacyl-phosphocholines. Sphingomyelins also share the same phosphocholine diagnostic fragment-ion as with the PC. The only difference from the PC is in the fact that they are linked to the phosphocholine polar head group by an *N-acyl* FA linked to a long-chain hydrocarbon. Another example of the

benefit of applying MS^E acquisition and subsequently obtaining more detailed information on *sn-1* and *sn-2* Acyl FA chain length is shown in Figure 4. Here the low energy ion trace of m/z 782.5694 corresponding to PC 36:4, i.e. representing several possible isomers as well as the high energy traces of m/z 502.3292 and m/z 478.3292 are shown (Figure 4B and 4C, respectively). It is possible to see very good alignment between the peak at 4.65 minutes in the low energy scan and the peak with the same retention time (only difference is the inter-scan delay which is consistent throughout the experiment) in the high energy trace for m/z 502.3292. This product ion can be assigned as [(M-*sn-1*-H$_2$O)+H]$^+$ or [(M-*sn-2*-H$_2$O)+H]$^+$ corresponding to either the *sn-1* or *sn-2* acyl FA loss of PC 18:2/18:2. The two low energy peaks in the m/z 782.5694 trace at retention times 4.95 minutes and 5.45 minutes both have corresponding aligned peaks by retention time belonging m/z 478.3292 which is a descriptive ion for [(M-*sn-1*-H$_2$O)+H]$^+$ or [(M-*sn-2*-H$_2$O)+H]$^+$ to either the *sn-1* or *sn-2* acyl FA for PC 16:0/20:4 or PC 20:4/16:0). The other peaks in figure 4B and C correspond to the remaining acyl FA fragments for other lipids which had in common the masses of m/z 478.3292 and m/z 502.3292. From this data, vital information is acquired which gives insight to the FA composition.
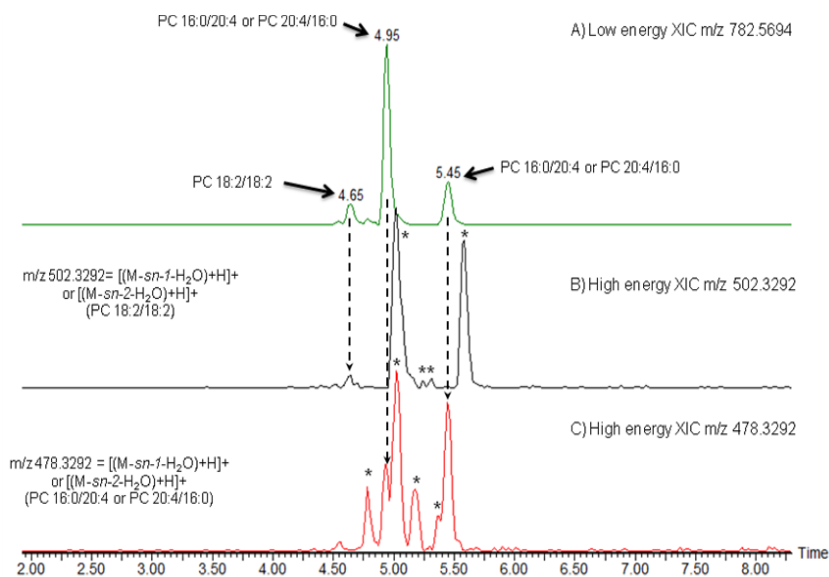

Figure 4. (A) Shows the low energy trace for PC 36:4 (m/z 782.5694) and the high energy traces for (B) m/z 502.3292 and (C) m/z 478.3292 highlighting the corresponding fragment-ions (dashed lines) of the various structures for PC (36:4) providing information on their possible FA composition.

*Acyl FA corresponding to other lipids

Due to its generic nature, this method is not only specific to phospholipids but any other biochemical entity present in the sample, for example TGs and ChoE's detected in electrospray positive ion.

The fragment-ions of TG's (39) have been comprehensively characterized by Murphy *et al* and as in the case of phospholipids it gives rise to diagnostic fragment-ions and neutral losses which may be used to determine the length and composition of the FA chains. It has to be noted that the protonated molecules obtained by the described method are in the form of the ammonium adduct $[M+NH_4]^+$. Under CID reactions in the collision cell, the decomposition of the $[M+NH_4]^+$ ion results in the neutral-loss of i) NH_3 and ii) the acyl-side chains, to generate the diacyl product ion. MS^2 data may be used to determine the acyl group for a given $[M+NH_4]^+$ ion. The exact mass information obtained from the MS^2 spectra can be used in combination with the unfragmented ion to identify possible molecular TG species. Moreover, since in these experiments the two collision cells (Trap T-wave and Transfer T-wave) are used in a parallel fashion to generate the MS^E spectra, it is possible to create a pseudo MS^3 spectrum of all ions. With this in mind, the high energy spectra of the already produced or first generation of product ions (diacyl ions), gave rise to the second generation product ions like the acylium (RCO^+) and the $(RCO+74)^+$ ions. Figure 5A and 5B clearly show the results for the combined spectrum between the low and high energy scans at 8.82 minutes. As it can be observed in the low energy data it is possible to obtain information from precursor ion. The base peak ion is at m/z 874.7885 (+2.4 ppm) which corresponds to TG (52:3). However, at the same retention time there are a number of TG species which co-elute chromatographically. Nevertheless, it is possible to align and recognize the fragment-ions belonging to the unfragmented precursor ion if the co-eluting ions are separated only by a single scan. Having said that, in this particular case we know that we are dealing with TGs due to the elution window in the chromatogram and therefore most of the fragment-ion data will belong to these compounds. It is possible to appreciate that the ions at m/z 601.5197 (loss of 16:0 FA) chain, m/z 577.5194 (loss of 18:2 FA) chain and m/z 575.5036 (loss of the 18:1 FA chain) (Figure 5A) all can be used as diagnostic fragment-ions to identify the presence of the ion at m/z 874.7885 (TG (52:3)). This information is all obtained simultaneously and in the same injection. Figure 5B shows three extracted ion chromatograms at m/z 601.5220, 577.5210 and 575.5040 (window of +/- 30 mDa) a number of chromatographic peaks which are very selective and indicative for these fragment-ions giving indication of the losses of 16:0 FA, 18:2 FA and 18:1 FA chains, respectively. Likewise, the data can be selectively data-mined for specific fragment-ions which correspond to the TG molecular species and confirmed by exact mass in the low energy trace. Exact mass neutral-loss information may also be extracted out of this complex data set for the classification of TGs. There are many different neutral losses which may be used as diagnostic losses for the confirmation of TGs, but in this example we will use one to demonstrate the proof of principle of this powerful analytical strategy. For instance, if the data is interrogated for the loss of the 16:0 FA, corresponding to $[CH_3(CH_2)_{14}CO_2H+NH_3]$ with an exact mass neutral loss of 273.2668, a chromatogram will be obtained showing all precursors displaying this exact mass neutral loss. This is illustrated in more detail in figure 5C, where it is possible to observe how the data can be mined for exact mass neutral losses which correspond to specific FA moieties by comparing the low and high energy acquisitions. The biggest

advantage here is that it is possible to search for an unlimited number of exact mass neutral losses as this methodology is not limited by duty cycle such as in other scanning mass spectrometers.
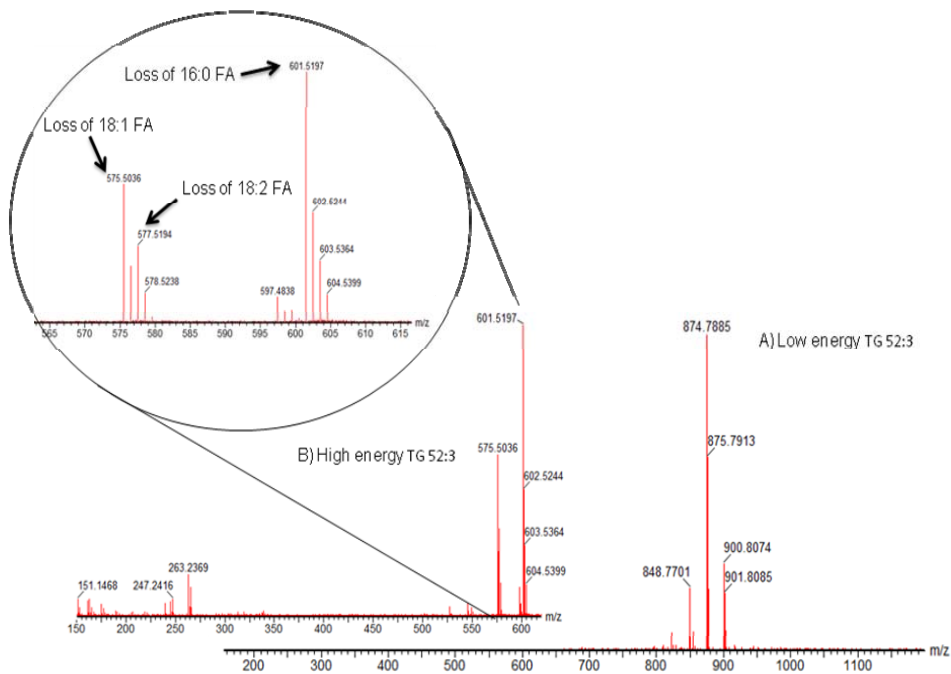
Figure 5A. Shows the low energy (A) for TG (52:3) and the corresponding high energy fragmentation spectra (B) obtained at a retention time of 8.82 min with key diagnostic fragment-ions at m/z 601.5197 (loss of 16:0 FA chain), m/z 577.5194 (loss of 18:2 FA chain) and m/z 575.5036 (loss of the 18:1 FA)
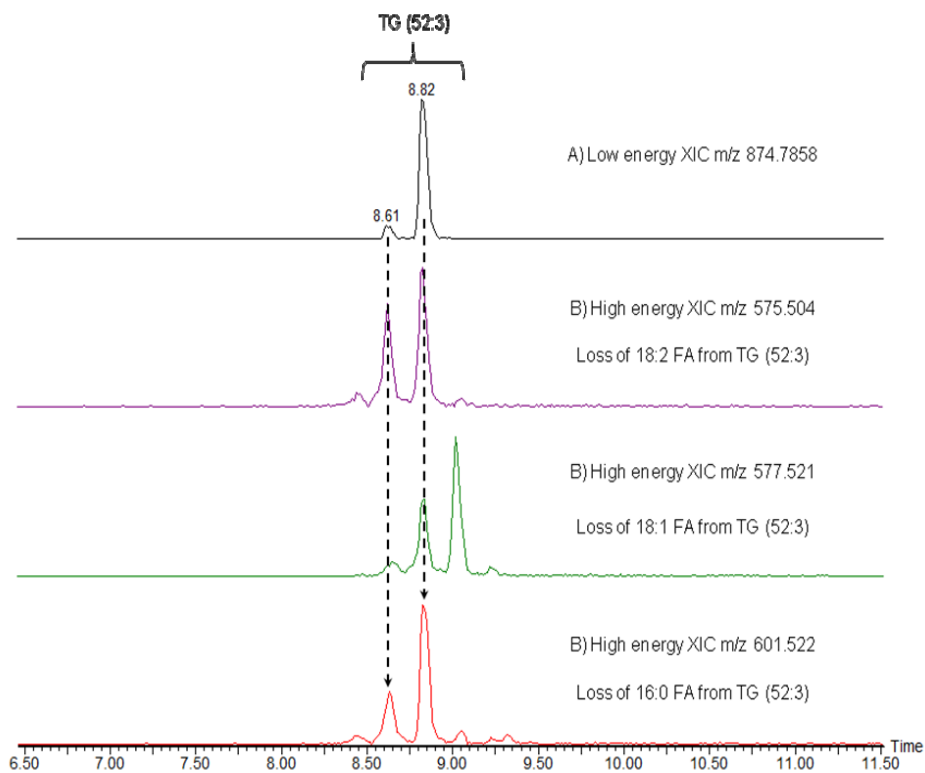
Figure 5B. (A) Low energy extracted ion chromatogram for unfragmented protonated TG (52:3) and (B) high energy extracted ion chromatograms of 'key fragment-ions' which denote losses of acyl FA from the TG (52:3) (m/z 601.5220, loss of 16:0 FA chain; m/z 577.5210, loss of 18:2 FA chain and m/z 575.5040, loss of the 18:1 FA).
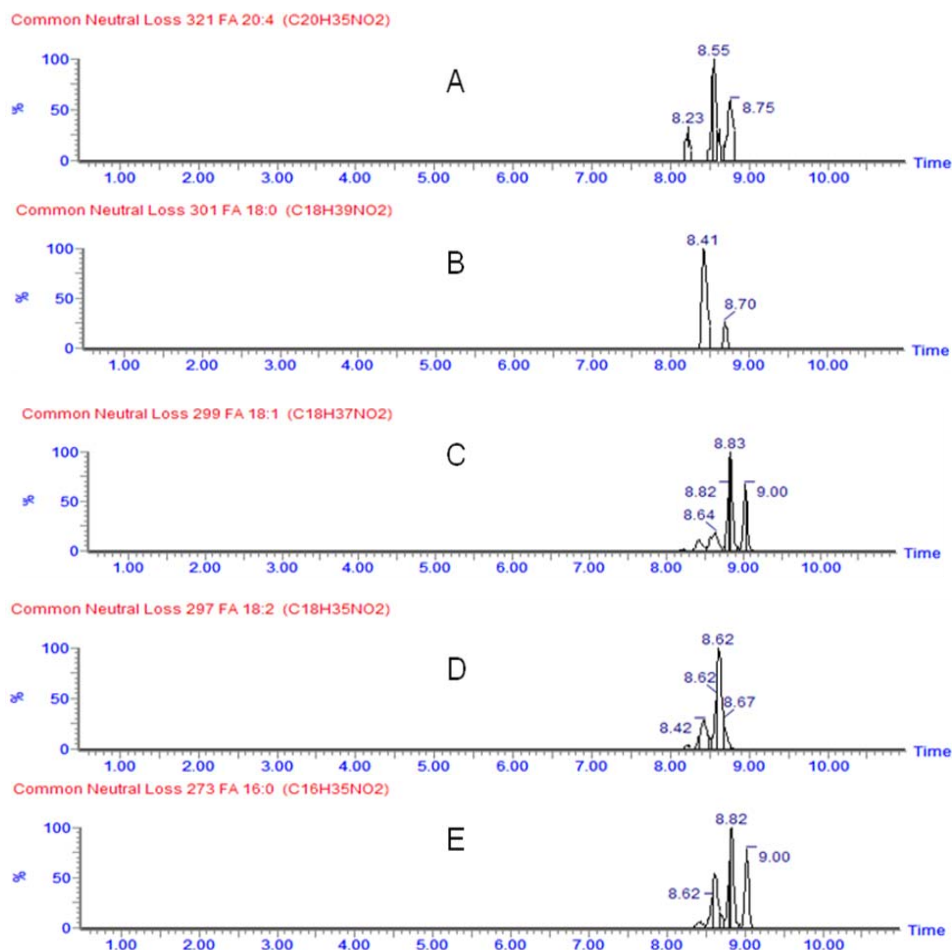
Figure 5C. Use of UPLC-MS^E to search for different FA loses using exact mass neutral loss in extracted human plasma sample. The data was processed using MetaboLynx XS. The losses of different FA moieties corresponded to (A) loss of 20:4 FA, (B) loss of 18:0 FA, (C) loss of 18:1 FA, (D) loss of 18:2 FA, (E) loss of 16:0 FA.

With respect to the cholesterol esters (ChoE), these molecular entities are also well detected by electrospray. For these compounds, the ester bond is formed between the carboxylate group of the fatty acid and the hydroxyl group of the cholesterol. These biochemicals are related to atherosclerosis and inborn errors of lipid metabolism. The main characteristics of the (ChoE) under CID is that they give rise to the cholesteryl motif at m/z 369.3516 (Figure 3S supplemental information) which may be used as the key diagnostic fragment-ion to locate and confirm the presence of the different species of ChoE. If the high energy data is interrogated for the diagnostic fragment-ion at m/z 369.3516, then a number of ChoE entities are identified as observed in Figure 6. Major ChoE at m/z 664.6057 (3.6 ppm) at 9.67 minutes,

m/z 666.6193 (0.6 ppm) at 9.84 minutes, m/z 668.6337 (-1.3 ppm) at 10.14 minutes, m/z 668.6016 (-2.4 ppm) at 9.5 minutes, m/z 690 .6189 (0.1 ppm) at 9.72 minutes and m/z 714.6185 (-0.6 ppm) at 9.61 where all identified using the high energy information together using the correlation with the low energy data.
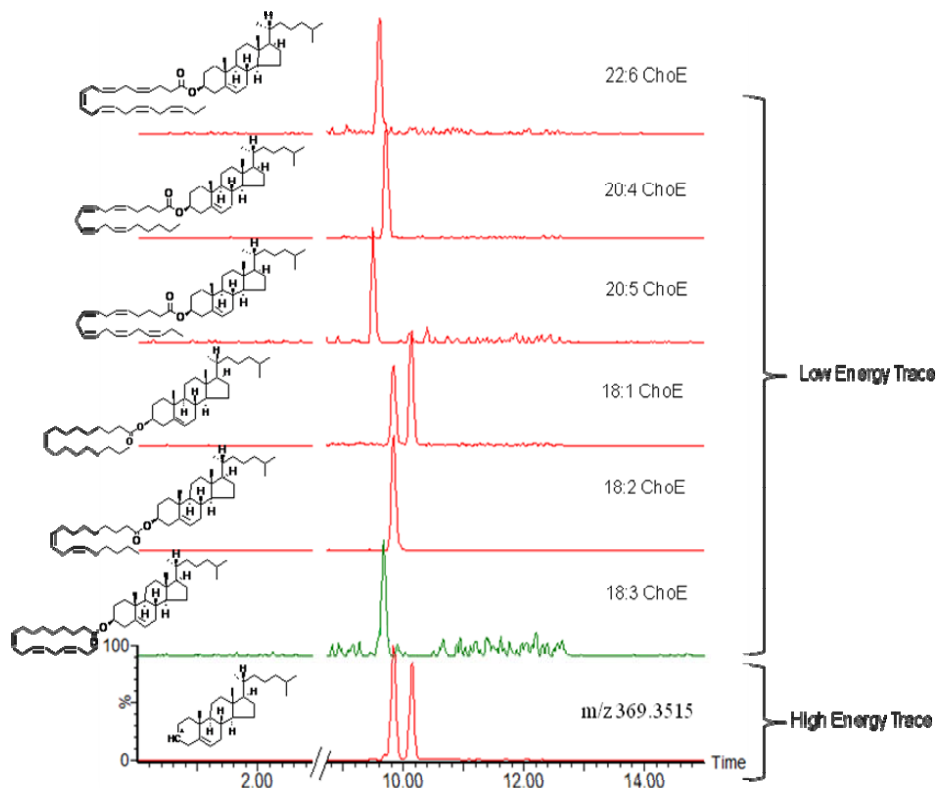

Figure 6. Reconstructed ion chromatograms of UPLC-MS[E] data with low and high energy acquisitions. The high energy reconstructed ion chromatogram of the key fragment-ion from the cholesteryl (m/z 369.3515) is used to identify the possible presence of ChoE's, and subsequently at the indicated low energy UPLC-MS trace as the key fragment-ion from the cholesteryl (m/z 369.3515). Following alignment with the low energy trace it is possible to extract the unfragmented ion information, which corresponds to the ChoE. The structures shown are examples of possible structures.

In electrospray negative ion mode, complementary information is obtained. More specifically, under CID anions or deprotonated molecules of glycerophospholipids produce important and abundant acyl anions of their FA moieties. In this mode of operation and applying MS[E] it is possible to simultaneously profile in a parallel fashion for the FA elemental composition in a large number of molecular species which may be present in any lipid extract. In Figure S4 (supplemental information) this is demonstrated for the extracted high energy precursor ion chromatograms of several fatty acids, i.e. FA 15:0 (precursor ion *m/z* 241.2175), FA 16:0 (precursor ion *m/z* 255.2332,), FA 18:2 (precursor ion *m/z* 279.2332), FA 18:1

(precursor ion *m/z* 281.2489), FA 18:0 (precursor ion *m/z* 283.2646) and FA 20:4 (precursor ion *m/z* 303.2332). For this different FA's the corresponding unfragmented precursor ion could be found in the low-energy trace. An example shown in Figure S5 (supplemental information) where the peak at a retention time of 4.25 minutes for both the low and the high energy corresponded to the calibration standard PG 14:0/14:0. This acidic glycerophospholipid is preferentially ionized in negative electrospray ion mode. In this mode, it yields the [M-H]$^-$ ion as most abundant ion. The fragment-ions obtained by CID yield similar fragments as described for other glycerophospholipid classes such as product ions arising from the following fragmentation mechanisms; a) neutral losses of the free FA ([M-H-R$_n$COOH]$^-$), b) neutral losses of ketenes ([M-H-R'$_n$CH=C=O]$^-$), or from the carboxylate anion fragments (R$_n$COO) $^-$. Additionally, PG fragment-ions also give rise to a specific fragment-ion at m/z 227 which corresponds to the (glycerophosphoglycerol-H-H$_2$O)$^-$. This fragment-ion can be used as a descriptor in electrospray negative ion mode to search for PG's. Figure 7 highlights how this information is obtained in the high energy collision mode where the key fragment-ions at m/z 227.2003 (-3.5 ppm) corresponding to either the [*sn1*-H]$^-$ acid or [*sn2*-H]$^-$ acid, m/z 437.2298 (-1.4 ppm) corresponding to either the [(M-*sn-1*-H$_2$O)-H]$^-$ or [(M-*sn-2*-H$_2$O)-H]$^-$, m/z 455.2420 (2.2 ppm) corresponding to either the [(M-*sn-1*)-H]$^-$ or [(M-*sn-2*)-H]$^-$are generated. The presence of these key diagnostic fragment-ions for the PG together with the exact mass in the low and high energy traces at the same retention time was enough for a positive identification of this type of glycerophospholipid confirming it to the PG 14:0/14:0 at m/z 665.4406 (1.8 ppm).
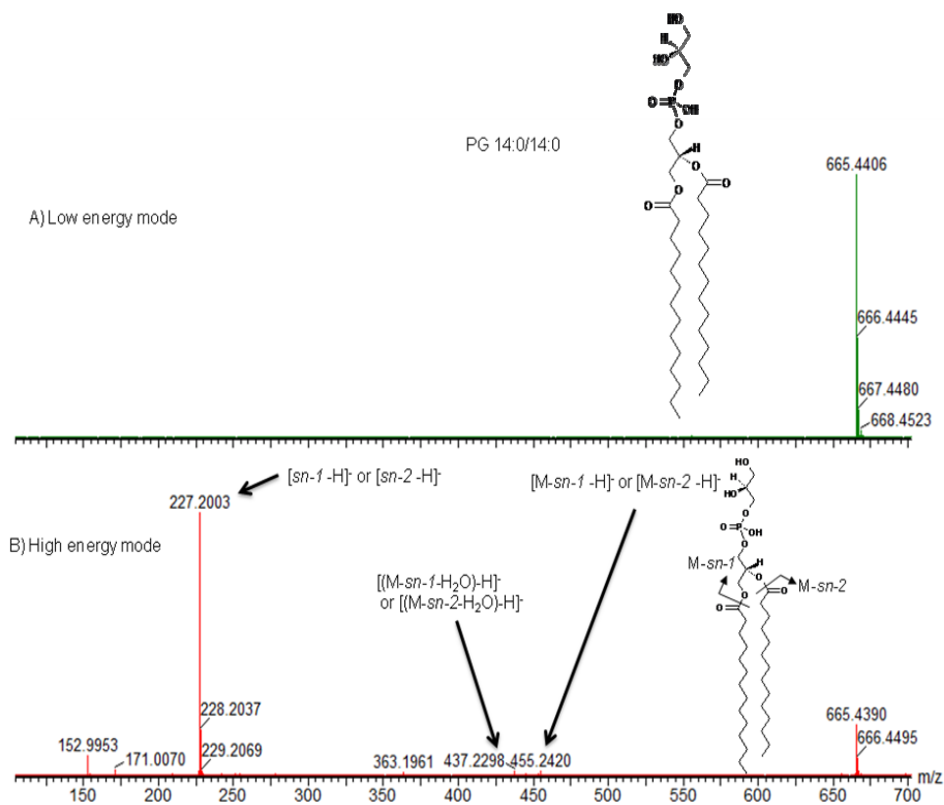
Figure 7. Low energy spectra (A) and the fragment-ions in the high energy mode (B) of PG 14:0/14:0 (negative ionization mode)

"Shotgun Lipidomic" Method Application: Osteoarthritis Samples

The potential of the lipidomic method was explored for the discovery of biomarkers for OA. Plasma samples from patients with various levels of OA were analyzed to detect and identify putative lipids which may be able to differentiate between the different levels of OA. Usually the first chemometrical tool used in the evaluation of a metabolomics study is Principal Component Analysis (PCA) to provide a fast overview of the most important variations and differences between objects. PCA as an unsupervised data analysis (40) technique did not provide an obvious separation between the groups with different stages of OA (data not shown). For the statistical data analysis, the individual data sets for each subject was organized in 3 groups; Control was comprised of group 0, Early OA contained groups 1-2, Moderate OA contained groups 3-8. The created model was evaluated by inspecting the goodness of fit (R^2X) and predictive power (Q^2X) with values of 0.41 and 0.30 respectively. In order to localize subtle differences between the groups, partial least squares-discrimination analysis (PLS-DA) was used for data analysis. After applying this methodology, it was possible to obtain a

significant separation between all the different groups that is; the control sample, the early OA and the moderate OA (Figure 8).
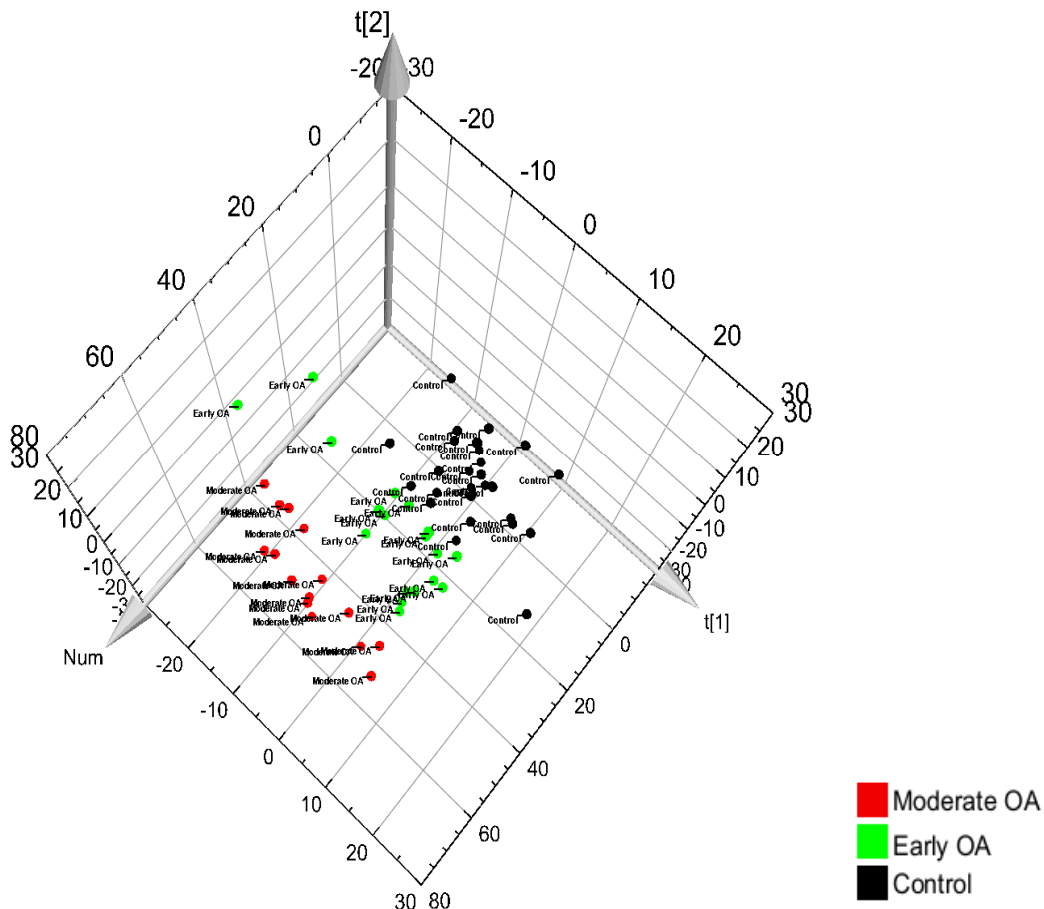
Figure 8. Partial Least Squares- Discrimination Analysis (PLS-DA) score plot of different OA samples of different disease state (Control, Early OA, and Moderate OA).

These results suggest that altered lipid metabolism is involved in OA. In OA, inflammatory pain is a typical occurrence. Phospholipases A_1 and A_2 hydrolyze the *sn-1*(PLA_1) or *sn-2* (PLA_2) acyl bond of phospholipids, for example arachidonic acid (41) (C20:4) is released from a PC that contains a C20:4 acyl FA chain. As a consequence of this reaction, arachidonic acid is formed together with a corresponding lysophospholipid. Arachidonic acid is an inflammatory mediator, and therefore an increased activity of Phospholipase can be expected in the case of inflammation. The activity of the Phospholipase enzyme was gauged by monitoring the ratios between LPC (16:0) /PC (36:4) and LPC (18:0) /PC

(38:4). In the extracted ion chromatograms (low energy trace) of the protonated PC 36:4 and the PC 38:4 a number of isomers showed up as chromatographically separated peaks. In order to include only those PC's which did contain FA 20:4, the high energy data were used to determine those isomers which contained FA 20:4 in either the *sn-1* or *sn-2* position. By monitoring the ratio of the sum of the normalized response of LPC 16:0 and LPC 18:0 and the sum of the response of PC 36:4 and PC 38:4 it can be observed that there was a considerable change of the ratio; this change indicated an changed activity of Phospholipase from control to early OA and moderate OA. This latter showed an increased level in the ratio of LPC/PC as noted with respect to the controls but not as elevated as in early OA (Figure 9).
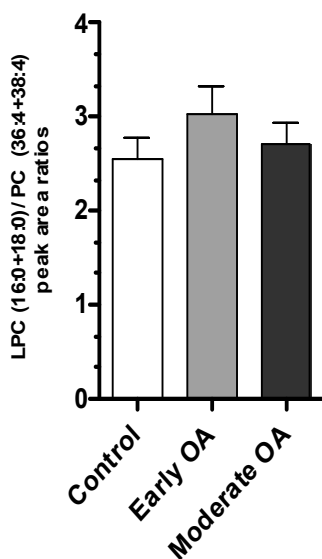
Figure 9. Shows the absolute peak area ratio between LPC (16:0+18:0) / PC (36:4+38:4) for the entire study in all groups (Control, Early OA and Moderate OA). The error bar spread indicates the biological standard deviation of all results for the subjects in each group.

CONCLUSIONS

The usefulness of MS^E as an untargeted methodology for both quantitation and identification in the same analysis has been clearly demonstrated. We applied this approach to lipid profiling but any other biochemicals which may be present in the biological sample could have been monitored in a comparable manner. The qualitative data allowed for the unambiguous identification of FA chain lengths. In principle *all* individual phospholipids and di- and triglycerides, whereas similar LC-MS/MS techniques such as data dependent acquisitions have limitations with respect to coverage for complex samples as the ones studied here. Data dependent analysis would simply miss various lipids due to time constraints and complexity of the samples; different lipids fragment according to different fragmentation mechanisms generating a vast number of different key fragment-ions and specific neutral losses in either positive or negative ion electrospray based techniques. MS^E on the other hand acquires all relevant information in both low energy and high energy acquisitions during the same analysis, and in the subsequent data processing available information on fragmentation pathways, diagnostic precursor and neutral losses allowed us to determine the polar head group and FA composition in a relatively fast and efficient manner.

This analytical strategy has been successfully applied to a study changes in the lipid profile in patients with a different degree of osteoarthritis. In summary, the capabilities of the combination of efficient separation using UPLC combined with detection using a TOF-MS in MS^E mode has been clearly demonstrated for the analysis of a wide range of lipids.

REFERENCES

1. Dowhan, W.; Bogdanov, M. pp. 1-35 (edited by D.E. Vance and J.E. Vance, Elsevier Science) **2002**.

2. Wenk, M. R. *Nat. Rev. Drug Discovery* **2005**, *4*, 594–610.

3. Feng, L.; Prestwich, G.D. (Dekker-CRC, New York, **2005**).

4. Eyster,K.M. *Adv. Physiol. Edu*., **2007,** *31*, 5-16.

5. Jakobsson, A.; Westerberg, R. *Prog. Lipid Res*., **2006**, *45*, 237-249

6. Endo, A. *J. Lipid Res.* **1992**, *33* (11): 1569–82.

7. Fahy, E.; Subramaniam, S.; Brown, H.A.; Glass, C.K.; Merrill, A.H.; Murphy, R.C.; Raetz, C.R.H.; Russell, D.W.; Seyama, Y.; Shaw, W.; Shimizu, T.; Spener F.; Van Meer, G.; Vannieuwenhze, M.S.; White, S.H.; Witztum, J.L.; Dennis, E.A. *Journal of Lipid Research*. **2005**, *46*, 839-861.

8. Goni, F. M.; Alonso, A. (eds Muller, G. & Petry, S.) 79–100 (Wiley-VCH, Weinheim, Germany, **2004**).

9. Athenstaedt, K.; Daum, G. *Eur. J. Biochem.* **1999**, *266*, 1–16

10. Balazy, M. *Prostaglandins Other Lipid Mediat.* **(2004)** , *73*, 173–180

11. Pettus, B. J.; Chalfant, C. E.; Hannun, Y. A. *Curr. Mol. Med.* **2004**, *4*, 405–418.

12. Reynolds, C. P.; Maurer, B. J; Kolesnick, R. N. *Cancer Lett.* **2004**, *206*, 169–180

13. Hla, T. *Semin. Cell Dev. Biol.* **2004**, *15*, 513–520.

14. Muller, G. Lipases and Phospholipases in Drug Development 231–331 (Wiley-VCH, Weinheim, Germany, **2004**).

15. Hollander, P. *Prim. Care* **2003**, *30*, 427–440.

16. Laaksonen, R.; Katajamaa, M.; Paiva, H.; Sysi.Aho, M.; Saarinen, L.; Junni, P.; Lutjohann, D.; Smet, J.; Van Coster, R.; Seppanen-Laakso, T.; Lehtimaki, T.; Soini, J.; Oresic, M. *PLoS One* **2006**, *1* (1), e97.

17. Nagan, N.; R.A. Zoeller. *Progress in Lipid Research*. **2001**, *40*, 199-229.

18. Tiller PR.; Yu S., Castro-Perez J.; Fillgrove KL.; Baillie TA .*Rapid Commun. Mass Spectrom.* **2008**, *22,* 1053-1061.

19. Yu, K.; Di L.; Kern,s E.; Li, S.Q.; Alden, P.; Plumb, S.R.. *Rapid Communications in MassSpectrometry* **2007**, *21*, Issue 6, 893-902.

20. Plumb, R.S.; Johnson, K.A.; Rainville, P.; Shockcor, J.P.; Williams, R.; Granger, J.H.; Wilson, I.D. *Rapid Communications in MassSpectrometry*. **2006** , *20*, Issue 19, 2800-2806.

21. Fenn, J.B.; Mann, M.; Meng, C.K.; Wong, S.F.; Whitehouse, C.M. *Science*, **1989**, *246*:64-71.

22. Watkins, S. M. *Curr. Opin. Drug Discov. Devel.* **2004**, *7*, 112–117.

23. Houjou, T.; Yamatani, K.; Imagawa, M.; Shimizu, T.; Taguchi, R. *Rapid Commun. Mass Spectrom.* **2005**, *19*, 654–666.

24. Hermansson, M.; Uphoff, A.; Kakela, R.; Somerharju, P. *Anal. Chem.* **2005**, *77*, 2166–2175.

25. Han, X.; Gross, R. W. *Anal. Biochem.* **2001**, *295*, 88–100.

26. Sullards, M. C.; Merrill, A. H. Jr. *Sci STKE* PL1 , **2001**.

27. Wenk, M. R.; Lucast, L.; Di Paolo, G.; Romanelli, AJ.; Suchy, SF.; Nussbaum, RL.; Cline, GW.; Shulman, GI.; McMurray, W; De Camilli, P. *Nature Biotechnol.* **2003**, *21*, 813–817.

28. Ekroos, K.; Chernushevich, I. V.; Simons, K.; Shevchenko, A. *Anal. Chem.* **2002**, *74*, 941–949.

29. Wrona, M.; Mauriala, T.; Bateman, K.P.; Mortishire-Smith, R.J.; O'Connor, D. *Rapid Communications in Mass Spectrometry* . **2005**, 19, Issue 18, 2597-2602.

30. Bateman, K.P.; Castro-Perez, J.; Wrona, M.; Shockcor, J.P.; Yu, K.; Oballa R., Nicoll-Griffith, D.A . *Rapid Communications in Mass Spectrometry* **2007**, *21*, Issue 9, 1485-1496.

31. Rainville, P. D.; Stumpf, C. J.; Shockcor, J. P.; Plumb, R. S.; Nicholson, J. K. *J. Proteome Res.* **2007**, *6*, 552–558.

32. Bligh, E.G.;Dyer, W.J. *Can. J. Biochem. Psysiol* **1959**, *37*,911-917

33. Wesseling, J.; Dekker, J.; van den Berg, WB.; Bierma-Zeinstra, SM.; Boers M, Cats HA.; Deckers, P.; Gorter, KJ.; Heuts, PH.; Hilberdink, WK.; Kloppenburg, M.; Nelissen, RG.; Oosterveld, FG.; Oostveen, JC.; Roorda, LD.; Viergever, MA.; Ten Wolde, S.; Lafeber, FP.; Bijlsma, JW. *Ann Rheum Dis*. **2009** , *68* (9), 1413-9

34. Hsu, F.F.; Bohrer, A.; Turk, J. *J. Am. Soc. Mass Spectrom.* **1998** *,9* , 516-526

35. Hsu, F.F.; Turk, J. *J. Am. Soc. Mass Spectrom.* **2003**, *14,* 352-363.

36. Barroso, B.; Bischoff, R. *J. Chromatogr., B* **2005**, *814*, 21–28.

37. Laaksonen, R.; Katajamaa, M.; Paiva, H.; Sysi.Aho, M.; Saarinen, L.; Junni, P.; Lutjohann, D.; Smet, J.; Van Coster, R.; Seppanen-Laakso, T.; Lehtimaki, T.; Soini, J.; Oresic, M. *PLoS One* **2006**, *1* (1), e97.

38. Chunxiu, H,.; van Dommelen, J.; van der Heijden, R.; Spijksma, G.; Reijmers, T. H.; Wang, M.; Slee, E.; Lu, X.; Xu, G.; van der Greef, J.; Hankemeier, T. *Journal of Proteome Research.* **2009**, *7*, 4982–4991.

39. Ding, J.; Sorensen, C.M.; Jaitly, N.; Jiang, H.; Orton, D.J.; Monroe, M.E.; Moore, R.J.; Smith, R.D.; Metz, T.O. *Journal of Chromatography B*, **2008**, *871* ,243-252.

40. Hsu, F.F.; Turk, J.; Thukkanni,A.K.; Messner, M.C.; Wildsmith, K.R.; Ford, D.A. *J. Am. Soc. Mass Spectrom.* **2003**, *38*, 752-763.

41. Murphy, R.C.; Wu, C.C.; MacAnoy, A.M. *J Am Soc Mass Spectrom* **2005**, *16*, 1498-1509

42. Jackson, J. E. *A User's Guide to Principal Components*; Wiley: New York, **1991**.

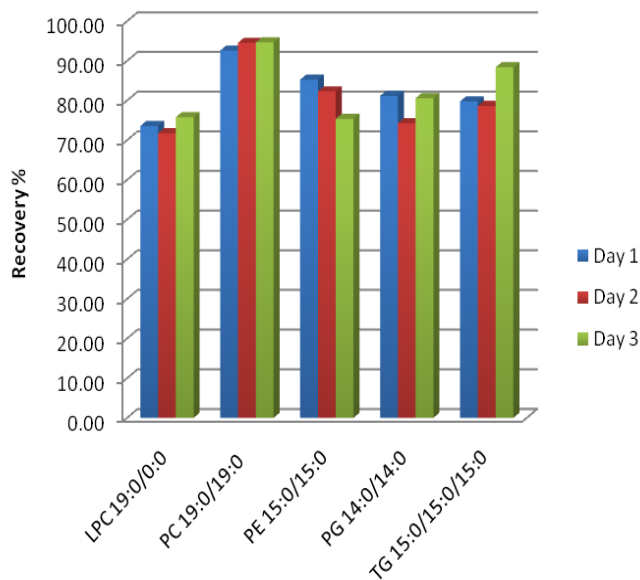43. Macrides, TA; Treschow, AP. Abstract, 88th American Oil Chemists Society.

SUPPLEMENTARY INFORMATION

Supplemental Figure S1. Intraday and interday variation bar chart for all non-endogenous lipids used in the validation set
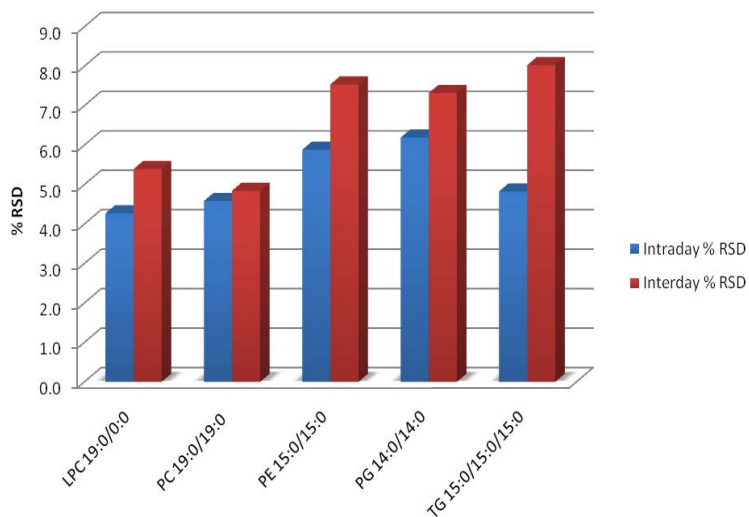
Supplemental Figure S2. Recovery for all non-endogenous lipids used in the validation set during three consecutive days

Table S1. List of all major lipids identified in the human extracted plasma; the m/z of the most abundant ion, the mass error, retention time, provisional lipid assignment and the ionization mode (positive/negative) are given.

Class	Formula	m/z Found	ppm	Time (min)	provisional assignment class		Ionization mode
ChoE	C47H77NO2	688.6016	-2.4	9.5	ChoE	20:5	[M+NH$_4$]$^+$
	C49H79NO2	714.6185	-0.6	9.61	ChoE	22:6	[M+NH$_4$]$^+$
	C45H77NO2	664.6057	3.6	9.67	ChoE	18:3	[M+NH$_4$]$^+$
	C47H79NO2	690.6189	0.1	9.72	ChoE	20:4	[M+NH$_4$]$^+$
	C45H79NO2	666.6193	0.6	9.84	ChoE	18:2	[M+NH$_4$]$^+$
	C45H81NO2	668.6337	-1.3	10.14	ChoE	18:1	[M+NH$_4$]$^+$
DG	C39H71NO5	634.5411	0	6.41	DG	36:4	[M+NH$_4$]$^+$
FA	C18H30O2	277.2150	-6.4	1.46	FA	18:3	[M-H]-
	C22H32O2	327.2301	-7.1	1.52	FA	22:6	[M-H]-
	C14H28O2	227.2023	5.1	1.55	FA	14:0	[M-H]-
	C16H30O2	253.2170	0.9	1.65	FA	16:1	[M-H]-
	C20H32O2	303.2309	-5	1.7	FA	20:4	[M-H]-
	C18H32O2	279.2319	-1.9	1.8	FA	18:2	[M-H]-
	C20H34O2	305.2476	-1.6	1.98	FA	20:3	[M-H]-
	C16H32O2	255.2324	-0.1	2.12	FA	16:0	[M-H]-
	C22H36O2	331.2635	-0.7	2.18	FA	22:4	[M-H]-
	C18H34O2	281.2479	-0.6	2.24	FA	18:1	[M-H]-
	C17H34O2	269.2484	1.2	2.47	FA	17:0	[M-H]-
	C18H36O2	283.2638	0.2	2.86	FA	18:0	[M-H]-
	C20H38O2	309.2786	-2.5	2.95	FA	20:1	[M-H]-
	C20H40O2	311.2971	6.6	3.68	FA	20:0	[M-H]-
PC	C42H76NO8P	754.5411	3.2	4.89	PC	34:4	[M+H]$^+$
	C40H76NO8P	730.5409	3.1	4.4	PC	32:2	[M+H]$^+$
	C44H78NO8P	780.5551	1	4.54	PC	36:5	[M+H]$^+$
	C46H76NO8P	802.5403	2	4.54	PC	38:8	[M+H]$^+$
	C46H80NO8P	806.5709	1.2	4.55	PC	38:6	[M+H]$^+$
	C44H76NO8P	778.5371	-2.1	4.59	PC	36:6	[M+H]$^+$
	C44H80NO8P	782.5715	2	4.62	PC	36:4	[M+H]$^+$
	C42H78NO8P	756.5535	-1.1	4.71	PC	34:3	[M+H]$^+$

C42H82NO7P	744.5935	3.8	4.71	PC-plasm	34:1	[M+H]+
C44H80NO8P	782.5718	2.4	4.78	PC	36:4	[M+H]+
C46H80NO8P	806.5729	3.7	4.78	PC	38:6	[M+H]+
C40H78NO8P	732.5576	4.5	4.89	PC	32:1	[M+H]+
C46H78NO8P	804.5527	-2	4.93	PC	37:0	[M+H]+
C44H80NO8P	782.5728	3.6	4.94	PC	36:4	[M+H]+
C35H70NO8P	664.4935	2.7	4.96	PC	28:7	[M+H]+
C46H82NO8P	808.5896	4.9	4.96	PC	38:5	[M+H]+
C42H80NO8P	758.5718	2.4	5.02	PC	34:2	[M+H]+
C44H78NO8P	780.5545	0.2	5.04	PC	36:5	[M+H]+
C44H82NO8P	784.5876	2.5	5.09	PC	36:3	[M+H]+
C44H80NO7P	766.5762	1.4	5.15	PC-plasm	36:4	[M+H]+
C44H82NO8P	784.5876	2.5	5.15	PC	36:3	[M+H]+
C46H82NO8P	808.5851	-0.6	5.15	PC	38:5	[M+H]+
C46H80NO8P	806.5684	-1.9	5.18	PC	38:6	[M+H]+
C43H82NO8P	772.5861	0.6	5.22	PC	35:2	[M+H]+
C46H82NO7P	792.5931	3	5.23	PC-plasm	38:5	[M+H]+
C45H82NO8P	796.5875	2.4	5.23	PC	37:4	[M+H]+
C46H84NO8P	810.6044	3.9	5.23	PC	38:4	[M+H]+
C48H82NO8P	832.5808	-5.8	5.23	PC	39:0	[M+H]+
C46H80NO7P	790.5731	-2.5	5.3	PC-plasm	38:6	[M+H]+
C43H82NO8P	772.5858	0.2	5.31	PC	35:2	[M+H]+
C44H78NO7P	764.5595	0.1	5.32	PC-plasm	36:5	[M+H]+
C46H84NO8P	810.6016	0.4	5.35	PC	38:4	[M+H]+
C48H84NO8P	834.6031	2.2	5.36	PC	40:6	[M+H]+
C40H80NO8P	734.5718	2.5	5.43	PC	32:0	[M+H]+
C44H84NO7P	770.6059	-0.6	5.43	PC-plasm	36:2	[M+H]+
C46H84NO7P	794.6064	0	5.43	PC-plasm	38:4	[M+H]+
C42H82NO8P	760.5883	3.5	5.44	PC	34:1	[M+H]+
C48H86NO7P	820.6230	1.2	5.44	PC-plasm	40:5	[M+H]+
C44H80NO8P	782.5695	-0.6	5.45	PC	36:4	[M+H]+
C46H84NO8P	810.6037	3	5.51	PC	38:4	[M+H]+
C48H82NO8P	832.5830	-3.1	5.51	PC	40:7	[M+H]+
C48H86NO8P	836.6119	-6	5.51	PC	40:5	[M+H]+

	C46H82NO8P	808.5830	-3.2	5.58	PC	38:5	[M+H]$^+$
	C44H84NO8P	786.6025	1.6	5.59	PC	36:2	[M+H]$^+$
	C43H78NO8P	768.5568	3.2	5.66	PC	35:4	[M+H]$^+$
	C43H84NO8P	774.6008	-0.6	5.71	PC	35:1	[M+H]$^+$
	C42H84NO7P	746.6033	-4.2	5.72	PC-plasm	34:0	[M+H]$^+$
	C46H86NO8P	812.6152	-2.1	5.72	PC	38:3	[M+H]$^+$
	C48H84NO8P	834.5981	-3.8	5.72	PC	40:6	[M+H]$^+$
	C42H84NO8P	762.6032	2.6	5.91	PC	34:0	[M+H]$^+$
	C44H82NO8P	784.5865	1.1	5.91	PC	36:3	[M+H]$^+$
	C44H86NO8P	788.6165	-0.5	5.98	PC	36:1	[M+H]$^+$
	C46H84NO8P	810.5992	-2.5	5.98	PC	38:4	[M+H]$^+$
	C46H88NO8P	814.6338	1.5	6.03	PC	38:2	[M+H]$^+$
	C41H76NO8P	742.5365	-2.9	6.06	PC	33:3	[M+H]$^+$
	C39H78NO8P	720.5533	-1.4	6.06	PC	31:0	[M+H]$^+$
	C46H92NO8P	818.6649	1.3	6.83	PC	38:0	[M+H]$^+$
	C52H96NO8P	894.6934	-2	8.44	PC	44:4	[M+H]$^+$
	C50H96NO8P	870.6982	3.5	8.57	PC	42:2	[M+H]$^+$
	C52H98NO8P	896.7118	1.1	8.6	PC	44:3	[M+H]$^+$
	C52H100NO8P	898.7225	-4.4	8.82	PC	44:2	[M+H]$^+$
	C54H102NO8P	924.7462	4.4	8.83	PC	46:3	[M+H]$^+$
	C48H94NO8P	844.6763	-3.8	8.9	PC	40:2	[M+H]$^+$
	C52H102NO8P	900.7373	-5.3	9.02	PC	44:1	[M+H]$^+$
	C54H106NO8P	928.7690	-4.8	9.21	PC	46:1	[M+H]$^+$
PE	C43H76NO8P	764.5237	0.8	5.16	PE	38:5	[M-H]-
	C39H74NO8P	714.5103	4	5.18	PE	34:2	[M-H]-
	C43H78NO8P	766.5403	2.1	5.65	PE	38:4	[M-H]-
	C41H78NO8P	742.5404	2.3	5.74	PE	36:2	[M-H]-
PG	C32H63O10P	637.4073	-1.2	2.79	PG	26:0	[M-H]-
	C36H71O10P	693.4739	4.6	4	PG	30:0	[M-H]-
	C52H99O10P	913.6851	-5.1	6.26	PG	46:2	[M-H]-
PI	C45H79O13P	857.5202	2.5	3.99	PI	36:4	[M-H]-
	C43H79O13P	833.5187	0.8	4.07	PI	34:2	[M-H]-
	C49H83O13P	909.5511	1.9	4.42	PI	40:6	[M-H]-
	C43H81O13P	835.5377	4.8	4.5	PI	34:1	[M-H]-

	C47H83O13P	885.5524	3.5	4.57	PI	38:4	[M-H]-
	C45H83O13P	861.5481	-1.4	4.64	PI	36:2	[M-H]-
	C47H85O13P	887.5643	-0.8	4.76	PI	38:3	[M-H]-
PS	C37H72NO10P	720.4839	3.2	4.11	PS	31:0	[M-H]-
	C44H80NO10P	812.5402	-4.9	4.32	PS	38:3	[M-H]-
	C42H80NO10P	788.5465	2.9	4.42	PS	36:1	[M-H]-
	C46H82NO10P	838.5621	2.7	4.42	PS	40:4	[M-H]-
	C44H82NO10P	814.5624	3.1	4.53	PS	38:2	[M-H]-
	C46H82NO10P	838.5647	5.8	4.56	PS	40:4	[M-H]-
	C48H84NO10P	864.5773	2.1	4.56	PS	42:5	[M-H]-
	C46H84NO10P	840.5766	1.3	4.66	PS	40:3	[M-H]-
	C43H82NO10P	802.5607	1.1	4.73	PS	37:1	[M-H]-
	C48H84NO10P	864.5776	2.4	4.79	PS	42:5	[M-H]-
	C39H72NO10P	744.4801	-2	4.96	PS	33:2	[M-H]-
	C48H86NO10P	866.5933	2.5	4.98	PS	42:4	[M-H]-
	C44H84NO10P	816.5768	1.6	5.05	PS	38:1	[M-H]-
	C46H86NO10P	842.5944	3.9	5.11	PS	40:2	[M-H]-
	C48H86NO10P	866.5925	1.6	5.16	PS	42:4	[M-H]-
	C46H86NO10P	842.5911	0	5.19	PS	40:2	[M-H]-
	C45H86NO10P	830.5872	-4.7	5.26	PS	39:1	[M-H]-
	C45H86NO10P	830.5933	2.6	5.31	PS	39:1	[M-H]-
	C46H86NO10P	842.5946	4.1	5.37	PS	40:2	[M-H]-
	C50H88NO10P	892.6071	0.4	5.37	PS	44:5	[M-H]-
	C44H86NO10P	818.5949	4.6	5.46	PS	38:0	[M-H]-
	C48H88NO10P	868.6103	4	5.53	PS	42:3	[M-H]-
	C50H90NO10P	894.6236	1.3	5.54	PS	44:4	[M-H]-
	C45H86NO10P	830.5903	-1	5.61	PS	39:1	[M-H]-
	C46H88NO10P	844.6032	-4.2	5.61	PS	40:1	[M-H]-
	C50H90NO10P	894.6234	1.1	5.72	PS	44:4	[M-H]-
	C48H90NO10P	870.6227	0.3	5.74	PS	42:2	[M-H]-
	C45H88NO10P	832.6057	-1.3	5.77	PS	39:0	[M-H]-
	C50H92NO10P	896.6399	2	5.91	PS	44:3	[M-H]-
	C46H90NO10P	846.6190	-4.1	6.01	PS	40:0	[M-H]-
	C43H80NO10P	800.5396	-5.7	6.08	PS	37:2	[M-H]-

LPC	C24H48NO7P	494.3251	0.8	1.15	LPC	16:1	[M+H]+
	C28H48NO7P	542.3225	-4.1	1.21	LPC	20:5	[M+H]+
	C22H47NO7P	468.3079	-2.3	1.21	LPC	14:0	[M+H]+
	C26H50NO7P	520.3397	-1.1	1.21	LPC	18:2	[M+H]+
	C30H50NO7P	568.3428	4.4	1.22	LPC	22:6	[M+H]+
	C28H50NO7P	544.3421	3.3	1.23	LPC	20:4	[M+H]+
	C26H50NO7P	520.3394	-1.7	1.26	LPC	18:2	[M+H]+
	C23H48NO7P	482.3244	-0.6	1.42	LPC	15:0	[M+H]+
	C26H48NO7P	518.3246	-0.1	1.43	LPC	18:3	[M+H]+
	C24H50NO7P	496.3399	-0.8	1.45	LPC	16:0	[M+H]+
	C26H52NO7P	522.3538	-4.1	1.57	LPC	18:1	[M+H]+
	C25H52NO7P	510.3568	1.7	1.69	LPC	17:0	[M+H]+
	C27H50NO7P	532.3395	-1.5	1.69	LPC	19:3	[M+H]+
	C26H54NO7P	524.3726	1.9	1.84	LPC	18:0	[M+H]+
	C24H50NO6P	480.3436	-3.7	1.88	LPC	15:1	[M+H]+
	C24H52NO6P	482.3603	-1.7	1.93	LPC	15:0	[M+H]+
	C26H54NO7P	524.3726	1.9	1.97	LPC	18:0	[M+H]+
	C28H52NO7P	546.3549	-1.9	1.99	LPC	20:3	[M+H]+
	C28H52NO7P	546.3559	-0.1	2.02	LPC	20:3	[M+H]+
	C26H54NO6P	508.3758	-1.8	2.06	LPC	17:1	[M+H]+
	C27H56NO7P	538.3885	2.3	2.14	LPC	19:0	[M+H]+
	C27H56NO7P	538.3873	0.1	2.27	LPC	19:0	[M+H]+
LPE	C27H44NO7P	524.2787	1.9	1.21	LPE	22:6	[M-H]-
	C25H44NO7P	500.2798	4.2	1.25	LPE	20:4	[M-H]-
SM	C37H75N2O6P	675.5440	-0.1	4.7	SM	14:0	[M+H]+
	C39H77N2O6P	701.5564	-4.7	4.23	SM	16:1	[M+H]+
	C41H75N2O6P	723.5447	0.9	4.23	SM	18:4	[M+H]+
	C38H77N2O6P	689.5617	2.9	4.45	SM	15:0	[M+H]+
	C39H79N2O6P	703.5767	1.9	4.78	SM	16:0	[M+H]+
	C41H77N2O6P	725.5600	0.4	4.78	SM	18:3	[M+H]+
	C41H81N2O6P	729.5917	0.9	4.89	SM	18:1	[M+H]+
	C43H79N2O6P	751.5771	2.3	4.89	SM	20:4	[M+H]+
	C43H81N2O6P	753.5944	4.5	5.39	SM	20:3	[M+H]+
	C40H81N2O6P	717.5898	-1.8	5.71	SM	17:0	[M+H]+

	C47H87N2O6P	807.6346	-4.2	5.96	SM	24:4	[M+H]$^+$
	C43H87N2O6P	759.6407	3.6	5.98	SM	20:0	[M+H]$^+$
	C41H83N2O6P	731.6089	3	6	SM	18:0	[M+H]$^+$
	C47H91N2O6P	811.6653	-4.9	6.02	SM	24:2	[M+H]$^+$
	C49H89N2O6P	833.6518	-2.2	6.02	SM	26:5	[M+H]$^+$
	C47H87N2O6P	807.6377	-0.3	6.03	SM	24:4	[M+H]$^+$
	C45H89N2O6P	785.6536	0	6.06	SM	22:1	[M+H]$^+$
	C43H85N2O6P	757.6225	0.1	6.12	SM	20:1	[M+H]$^+$
	C37H63N2O6P	663.4521	2.9	6.18	SM	14:6	[M+H]$^+$
	C46H91N2O6P	799.6657	-4.5	6.2	SM	23:1	[M+H]$^+$
	C44H89N2O6P	773.6563	3.5	6.24	SM	21:0	[M+H]$^+$
	C46H91N2O6P	799.6701	1	6.3	SM	23:1	[M+H]$^+$
	C47H93N2O6P	813.6838	-1.4	6.43	SM	24:1	[M+H]$^+$
	C49H91N2O6P	835.6685	-0.9	6.43	SM	26:4	[M+H]$^+$
	C45H91N2O6P	787.6719	3.3	6.44	SM	22:0	[M+H]$^+$
	C47H89N2O6P	809.6506	-3.7	6.44	SM	24:3	[M+H]$^+$
	C47H93N2O6P	813.6871	2.7	6.54	SM	24:1	[M+H]$^+$
	C49H91N2O6P	835.6672	-2.5	6.54	SM	26:4	[M+H]$^+$
	C48H95N2O6P	827.7049	5.2	6.57	SM	25:1	[M+H]$^+$
	C46H93N2O6P	801.6882	4.1	6.68	SM	23:0	[M+H]$^+$
	C48H91N2O6P	823.6712	2.3	6.7	SM	25:3	[M+H]$^+$
	C47H95N2O6P	815.7028	2.7	6.91	SM	24:0	[M+H]$^+$
	C49H93N2O6P	837.6869	2.4	6.92	SM	26:3	[M+H]$^+$
	C45H89N2O6P	785.6570	4.3	8.38	SM	22:1	[M+H]$^+$
	C49H95N2O6P	839.7038	3.8	8.72	SM	26:2	[M+H]$^+$
	C46H93N2O6P	801.6851	0.2	8.78	SM	23:0	[M+H]$^+$
	C49H97N2O6P	841.7189	3.2	8.9	SM	26:1	[M+H]$^+$
	C53H101N2O6P	893.7510	3.9	8.92	SM	30:3	[M+H]$^+$
	C48H97N2O6P	829.7124	-4.6	8.97	SM	25:0	[M+H]$^+$
	C40H75N2O6P	711.5465	3.4	9.11	SM	17:3	[M+H]$^+$
	C50H99N2O6P	855.7324	0.6	9.21	SM	27:1	[M+H]$^+$
	C52H105N2O6P	885.7817	3.2	9.44	SM	29:0	[M+H]$^+$
	C55H109N2O6P	925.8089	-1.3	9.48	SM	32:1	[M+H]$^+$
TG	C47H89NO6	764.6807	5.1	8.03	TG	44:2	[M+NH$_4$]$^+$

C49H91NO6	790.6967	5.3	8.11	TG	46:3	[M+NH4]+
C53H95NO6	842.7266	3.3	8.23	TG	50:5	[M+NH4]+
C57H99NO6	894.7515	-4	8.23	TG	54:7	[M+NH4]+
C45H89NO6	740.6752	-2.1	8.24	TG	42:0	[M+NH4]+
C57H99NO6	894.7515	-4	8.25	TG	54:7	[M+NH4]+
C50H93NO6	804.7063	-2.2	8.25	TG	47:3	[M+NH4]+
C55H97NO6	868.7400	0.7	8.3	TG	52:6	[M+NH4]+
C47H91NO6	766.6937	1.6	8.3	TG	44:1	[M+NH4]+
C49H93NO6	792.7114	4.2	8.3	TG	46:2	[M+NH4]+
C61H101NO6	944.7735	3	8.31	TG	58:10	[M+NH4]+
C51H95NO6	818.7251	1.7	8.33	TG	48:3	[M+NH4]+
C51H95NO6	818.7239	0.1	8.34	TG	48:3	[M+NH4]+
C59H101NO6	920.7708	0.1	8.34	TG	56:8	[M+NH4]+
C46H91NO6	754.6968	5.8	8.36	TG	43:0	[M+NH4]+
C53H97NO6	844.7397	0.4	8.36	TG	50:4	[M+NH4]+
C53H97NO6	844.7397	0.4	8.39	TG	50:4	[M+NH4]+
C57H101NO6	896.7740	3.7	8.41	TG	54:6	[M+NH4]+
C55H99NO6	870.7558	0.8	8.42	TG	52:5	[M+NH4]+
C61H103NO6	946.7879	1.6	8.43	TG	58:9	[M+NH4]+
C50H95NO6	806.7217	-2.5	8.47	TG	47:2	[M+NH4]+
C52H97NO6	832.7440	5.5	8.49	TG	49:3	[M+NH4]+
C59H103NO6	922.7908	4.8	8.54	TG	56:7	[M+NH4]+
C57H101NO6	896.7720	1.5	8.55	TG	54:6	[M+NH4]+
C49H95NO6	794.7220	-2.2	8.57	TG	46:1	[M+NH4]+
C53H99NO6	846.7567	2	8.58	TG	50:3	[M+NH4]+
C51H97NO6	820.7375	-2.3	8.58	TG	48:2	[M+NH4]+
C55H101NO6	872.7720	1.5	8.62	TG	52:4	[M+NH4]+
C53H99NO6	846.7554	0.4	8.63	TG	50:3	[M+NH4]+
C57H103NO6	898.7861	-0.3	8.64	TG	54:5	[M+NH4]+
C48H95NO6	782.7242	0.6	8.65	TG	45:0	[M+NH4]+
C52H99NO6	834.7592	5	8.67	TG	49:2	[M+NH4]+
C54H101NO6	860.7722	1.8	8.7	TG	51:3	[M+NH4]+
C50H97NO6	808.7390	-0.5	8.7	TG	47:1	[M+NH4]+
C59H105NO6	924.8026	0.7	8.75	TG	56:6	[M+NH4]+

C49H97NO6	796.7368	-3.3	8.78	TG	46:0	$[M+NH_4]^+$
C51H99NO6	822.7565	1.8	8.79	TG	48:1	$[M+NH_4]^+$
C53H101NO6	848.7715	1	8.8	TG	50:2	$[M+NH_4]^+$
C55H103NO6	874.7885	2.5	8.82	TG	52:3	$[M+NH_4]^+$
C58H108NO6	916.8366	3.6	8.82	TG	55:3	$[M+NH_4]^+$
C61H115NO6	958.8865	6.5	8.82	TG	58:3	$[M+NH_4]^+$
C57H105NO6	900.8053	3.7	8.83	TG	54:4	$[M+NH_4]^+$
C54H103NO6	862.7913	5.8	8.92	TG	51:2	$[M+NH_4]^+$
C61H109NO6	952.8344	1.2	8.99	TG	58:6	$[M+NH_4]^+$
C51H101NO6	824.7726	2.3	8.99	TG	48:0	$[M+NH_4]^+$
C59H107NO6	926.8182	0.5	9	TG	56:5	$[M+NH_4]^+$
C53H103NO6	850.7871	0.9	9	TG	50:1	$[M+NH_4]^+$
C55H105NO6	876.8063	4.9	9	TG	52:2	$[M+NH_4]^+$
C60H115NO6	946.8836	3.6	9	TG	57:2	$[M+NH_4]^+$
C58H11NO6	918.8494	0.4	9.01	TG	55:2	$[M+NH_4]^+$
C61H117NO6	960.8916	-4.5	9.01	TG	58:2	$[M+NH_4]^+$
C59H109NO6	928.8317	-1.7	9.02	TG	56:4	$[M+NH_4]^+$
C57H107NO6	902.8207	3.4	9.04	TG	54:3	$[M+NH_4]^+$
C51H101NO6	824.7700	-0.8	9.06	TG	48:0	$[M+NH_4]^+$
C54H105NO6	864.8056	4.2	9.07	TG	51:1	$[M+NH_4]^+$
C56H107NO6	890.8201	2.7	9.08	TG	53:2	$[M+NH_4]^+$
C54H105NO6	864.8061	4.8	9.12	TG	51:1	$[M+NH_4]^+$
C59H111NO6	930.8494	0.4	9.21	TG	56:3	$[M+NH_4]^+$
C55H109NO6	880.8375	4.8	9.21	TG	52:0	$[M+NH_4]^+$
C55H107NO6	878.8224	5.4	9.21	TG	52:1	$[M+NH_4]^+$
C54H99NO6	858.7546	-0.6	9.22	TG	51:4	$[M+NH_4]^+$
C57H109NO6	904.8358	2.8	9.22	TG	54:2	$[M+NH_4]^+$
C54H107NO6	866.8201	2.8	9.31	TG	51:0	$[M+NH_4]^+$
C59H113NO6	932.8600	1.4	9.45	TG	56:2	$[M+NH_4]^+$
C57H111NO6	906.8511	2.4	9.46	TG	54:1	$[M+NH_4]^+$
C58H113NO6	920.8690	4.8	9.52	TG	55:1	$[M+NH_4]^+$
C59H115NO6	934.8801	-0.2	9.59	TG	56:1	$[M+NH_4]^+$
C57H113NO6	908.8682	4	9.59	TG	54:0	$[M+NH_4]^+$
C60H117NO6	948.9012	5.6	9.7	TG	57:1	$[M+NH_4]^+$

C61H113NO6	956.8646	2.2	9.8	TG	58:4	[M+NH$_4$]$^+$
C56H109NO6	892.8337	0.4	9.9	TG	53:1	[M+NH$_4$]$^+$
C63H121NO6	988.9258	-1.4	9.93	TG	60:2	[M+NH$_4$]$^+$
C65H123NO6	1014.9415	-1.4	9.93	TG	62:3	[M+NH$_4$]$^+$
C62H121NO6	976.9298	2.7	9.95	TG	59:1	[M+NH$_4$]$^+$
C62H123NO6	978.9465	3.7	10.09	TG	59:0	[M+NH$_4$]$^+$
C65H125NO6	1016.9623	3.7	10.12	TG	62:2	[M+NH$_4$]$^+$
C63H123NO6	990.9436	0.7	10.12	TG	60:1	[M+NH$_4$]$^+$

Table S2 in the supplemental information. 10 most abundant* lipid species found in extracted human plasma

Class	Formula	m/z Found	Ppm	Time (min)	Area Abs	provisional assignment
PC	C42H80NO8P	758.5718	2.4	5.02	311	1-acyl 34:2
PC	C44H84NO8P	786.6025	1.6	5.59	210	1-acyl 36:2
PC	C42H82NO8P	760.5883	3.5	5.44	189	1-acyl 34:1
PC	C44H80NO8P	782.5728	3.6	4.94	154	1-acyl 36:4
PC	C44H82NO8P	784.5876	2.5	5.15	134	1-acyl 36:3
TG	C55H103NO6	874.7885	2.5	8.82	109	1-acyl 52:3
TG	C55H105NO6	876.8063	4.9	9	84	1-acyl 52:2
SM	C39H79N2O6P	703.5767	1.9	4.78	60	2-amido 16:0
PC	C46H80NO8P	806.5729	3.7	4.78	58	1-acyl 38:6
TG	C51H99NO6	822.7565	1.8	8.79	15	1-acyl 48:1

* Most abundant as determined by the peak area of the most abundant m/z of each lipid.

Supplemental information Figure S3. High energy fragmentation for the ChoE 18:1 giving rise to the diagnostic fragment-ion at m/z 369.3504 corresponding to the cholesteryl motif which in turn can be used as a precursor ion to 'hunt' in the data set for ChoE lipids in the low energy trace.
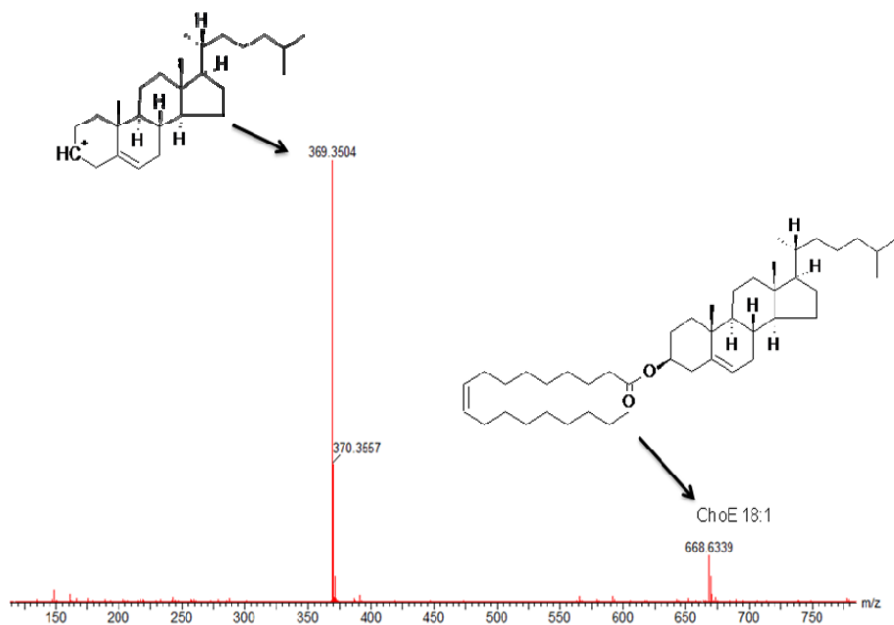
Supplemental information Figure S4. High energy extracted ion precursor ion chromatograms in negative ion mode. In this figure it can be observed (from top to bottom; m/z 303.2332 FA (20:4), m/z 283.2646 FA (18:0), m/z 281.2489 FA (18:1), m/z 279.2332 FA (18:2), m/z 255.2332 FA (16:0), m/z 241.2175 FA (15:0)) the fact that fragment-ion information determining the length of the FA can be search against the low energy mode with exact mass to determine the elemental composition of the lipid and to even quantify the levels present (the low energy data is not shown in this example)

Supplemental information Figure S5. Low energy extracted ion chromatogram of PG 14:0/14:0 with m/z 665.4406 and the corresponding high energy extracted ion chromatogram of m/z 227.2003.

Chapter 3

Ion mobility mass spectrometry with dual stage CID fragmentation enables localization of fatty acyl and double bond positions in phosphatidylcholines

Ion mobility mass spectrometry with dual stage CID fragmentation enables localization of fatty acyl and double bond positions in phosphatidylcholines

SUMMARY

A high content molecular fragmentation for the analysis of phosphatidylcholines (PC) was achieved utilizing a two-stage (trap (1st generation fragmentation) and transfer (2nd generation fragmentation)) collision-induced dissociation (CID) in combination with travelling-wave ion mobility spectrometry (TWIMS). The novel aspects of this work reside in the fact that a TWIMS arrangement was used to obtain a high level of structural information including location of fatty acyl substituents and double bonds for PCs in plasma in the absence of alkali metal adduct ions such as $[M+Li]^+$. Elemental compositions for fragment ions were confirmed by accurate mass measurements. A very specific 1st generation fragment ion m/z 577 (M – Phosphoryl choline) from the PC (16:0/18:1 (9Z)) was produced which by further CID generated acylium ions containing either the fatty acyl 16:0 ($C_{15}H_{31}CO^+$, m/z 239) or 18:1 (9Z) ($C_{17}H_{33}CO^+$, m/z 265) substituent. Subsequent water loss from these acylium ions was key in producing hydrocarbon fragment ions mainly from the α-proximal position of the carbonyl group such as the hydrocarbon ion m/z 67 ($+H_2C$-HC=CH-CH=CH$_2$). Formation of these ions was of important significance for determining double bonds in the fatty acid chains. In addition to this, and with the aid of ^{13}C labeled lyso-phosphatidylcholine (LPC) 18:1 (9Z) in the ω-position (methyl). TAP fragmentation produced the ion at m/z 57, and was proven to be derived from either (i) the α-proximal (carboxylate) or (ii) the distant ω-position (methyl) in the LPC.

INTRODUCTION

Lipids play a very important role in human physiology and nutrition (1-5). In this research, we will focus on the structural analysis of phosphatidylcholines (PC). This specific phospholipid subclass contains a polar head group and a glycerol backbone which can be esterified by one (Lyso Phospholipids) or two (PC) different fatty acids occupying *sn-1* or *sn-2* positions (6, 7). PCs represent the most abundant class of phospholipids in plasma, and play a pivotal role directly or indirectly in several major enzymatic reactions occurring in circulation and in tissues. For example, PCs can be hydrolyzed by endothelial lipase (EL) (8) to generate Lyso PCs which can turn on signaling pathways in many tissues upon absorption. Since the position of double bonds bears an impact on the Lyso PCs signaling properties, it is of high interest to locate the position of the double bond in the fatty acyl chains of PCs. In addition, certain enzymes have a prevalence to select different fatty acyl compositions in the PC. For example, Lecithin: cholesterol acyltransferase (LCAT) in circulation favors fatty acyl 18:1 and 18:2 over 20:4 and 22:6 at the *sn-2* position of PC in human beings (9).

Positional determination of fatty acyl groups in PCs and subsequent location of the double bond is a laborious and complex process. In the past, location of the fatty acyl group in PCs has been achieved either by enzymatic means in combination with mass spectrometry, or solely relying on mass spectrometry. Enzymatic assays involved digestions of PCs using Phospholipase A1 or A2. As a result specific cleavage by hydrolysis takes place for either the *sn-1* or *sn-2* position.

Over the years, there has been a variety of different mass analyzers (10) which have been applied to lipid analysis ranging from sector instruments, tandem quadrupoles, time-of-flight mass spectrometers, Orbitrap, Fourier Transform-Ion Cyclotron Resonance (FT-ICR), and linear ion traps all using a variety of different ionization techniques including electron impact (EI), fast atom bombardment (FAB), matrix-assisted laser desorption ionization (MALDI) (11) and electrospray (ESI) ionization. The early pioneering work of Gross and co-workers paved the path in the research of lipid fragmentation mechanisms and double bond localization by the use of high-energy collision-induced dissociation of the carboxylate anions of free fatty acids, generated by FAB and without a derivatization step (12-14). Their research showed that by high-energy collision-induced charge-remote fragmentation the position of the double bond in a mono-unsaturated fatty acid could be determined. This method worked also for poly-unsaturated fatty acids, but the localization of double bonds increased in complexity.

As electrospray became more widely adopted, Murphy *et al*. (15) and Kerwin *et al.* (16) implemented this ionization technique for the analysis of PCs using either positive or negative ion electrospray. In positive ion electrospray mode and in the absence of alkali metal adduct ions such as lithium (which is introduced post-column) PCs are primarily ionized as $[M+H]^+$ ions. Under these conditions, low-energy collisional induced dissociation (CID) mainly yields the favorable loss of the phosphocholine head group, with little or no information about the fatty acyl groups or double bond position (17,18). In negative ion mode PCs are detected in an ammonium acetate buffered methanol solution as $[M+CH_3COO]^-$ or

[M-CH$_3$]$^-$, the latter being due to loss of methyl acetate formed via abstraction of a methyl cation from the quaternary ammonium group by the acetate anion. The [M-CH$_3$]$^-$ ions do generate upon low-energy CID relatively low abundant R$_1$COO$^-$ and R$_2$COO$^-$ ions from which therefore it could be difficult to generate by charge-remote fragmentation sufficiently abundant fragment ions to locate their double bond position.

The use of alkali metal adducts and more specifically lithium adducts to generate fragmentation of fatty acyl chains for localization of double bonds has been extensively utilized in the electrospray ionization mode. For instance, Hsu *et al.* (19,20) has comprehensively studied the fragmentation mechanism of PCs showing that it is possible to obtain fatty acyl information by low-energy CID using a tandem quadrupole. With respect to the utilization of a multi-stage CID approach for the localization of double bonds in the fatty acyl chains, Bryant *et al.* (21) demonstrated that it was possible to obtain FAB-MS[3] fragmentation with a four sector MS instrument for the analysis of phosphatidylcholines present in a human immunodeficiency virus. In spite of the fact that at the time this was an innovative approach, the sensitivity obtained from this instrument arrangement is relatively low when compared to other mass spectrometers currently available such as tandem quadrupoles or time-of-flight mass spectrometers. MS^n experiments involving the use of lithiated adducts have also been studied using linear ion trap mass spectrometers as described by Hsu *et al* (22). Different phospholipid classes were analyzed using the lithiated approach yielding detection as [M+ Li]$^+$, [M−H+ 2Li]$^+$ and [M−2H+ 3Li]$^+$ ions. Hydrocarbon fragment ions from this approach are generated from the fatty acyl chains, forming allylic and vinylic fragment ions. In some cases (phosphatidic acid (PA), phosphatidylserine (PS) and lyso phospholipids) further multi-stage fragmentation up to MS^5 is required to obtain double bond information. Consequently, fragment ions belonging to the fatty acyl moiety result in yielding very low ion abundances, thus making interpretation challenging.

An alternative technique involving the use of ozone gas to oxidize the carbon-carbon double bond/s in fatty acids and provide real-time double bond analysis in the MS has been previously investigated by Thomas *et al.* (23,24). There are different ways to introduce this reactive gas into the mass spectrometer. It can be introduced directly in the electrospray ionization source which entails the use of oxygen as the nebulization gas and using a high voltage on the capillary producing a corona discharge to generate ozone gas. An alternative method, involves the direct supply of ozone to the ion source. This latter approach permits for a superior management of ozone gas introduced in the ionization chamber. Fragmentation information in this fashion arising from 'ozonolysis' is very complicated and especially in complex lipid mixtures containing isobaric lipids which may contain similar fragment ions. As of recently, introduction of ozone post-ionization has been thoroughly documented using an ion trap mass analyzer (25). The most immediate advantage here is the fact that complex mixtures can be handled in a much better fashion by mass selection of specific lipids and subsequent MS^n experiments. Although this technique so-called 'ozonolysis' is extremely useful, there are health hazards involved in the use of ozone gas in the laboratory thereby requiring constant monitoring of its level.

As technology evolved in mass spectrometry, ion mobility mass spectrometry (IMS) has become a key component in proteomic and lipidomic analysis (26-34). IMS has the capability of separating ions based on the size, collisional cross

sections, and charge state. Monitoring these ions under the influence of a gas, typically nitrogen, in the presence of an electric field produces different mobility times in the drift tube. Hence, this offers an additional level of selectivity on top of m/z, retention times and peak intensity values. Ion mobility has been used as a tool to achieve a better understanding of the stochiometry of large molecular weight proteins in the gas phase (35-37). Yet, this type of configuration can be employed as well in studying small molecules as demonstrated by the IMS separation of regional isomers (38,39).

In this report we describe the use of a travelling-wave ion mobility spectrometry procedure (TWIMS) which enables the identification of the fatty acid substituents at *sn-1* or *sn-2* positions of the PC as well as the location of double bonds in the fatty acid chains. This TWIMS device (40) consists of an ion mobility drift tube positioned between a quadrupole mass analyzer and an orthogonal time-of-flight mass spectrometer. Another important aspect of this study is that up to now there has been no report using LC/MS in electrospray positive ion mode without any derivatization agent or adducts that has been able to localize double bonds in the fatty acyl substituents of PCs.

MATERIAL AND METHODS

Chemicals and reagents

Lipid standards were obtained from Avanti Polar lipids (Alabama, USA). PC (16:0/14:0); PC(16:0/18:0); PC(16:0/18:1(9Z)); PC(16:0/18:2(9Z,12Z)); PC (16:0/20:4(5Z,8Z,11Z,14Z)); PC(16:0/22:6(4Z,7Z,10Z,13Z,16Z,19Z)); LPC (18:0); LPC (18:1) were prepared as stock solutions in dichloromethane (1mg/mL) and stored at -20°C until further analysis. Labeled lipid standards, PC (16:0/^{13}C labeled at ω carbon 18:1(9Z)); LPC (^{13}C labeled at ω carbon 18:1(9Z)) were purchased from Cambridge Isotec (MA, USA). These standards were also prepared as stock solutions in dichloromethane (1mg/mL) and stored at -20°C. A solution of leucine enkephalin (Sigma Aldrich, LO, USA) at a concentration of 2 ng/μL in 50/50 v/v acetonitrile/ water (0.1% formic acid) was used for lock mass correction.

Biological sample preparation

All animal protocols were reviewed and approved by the Merck Research Laboratories Institutional Animal Care and Use Committee (Rahway, NJ). Male C57Bl/6 mice (Taconic Farms, Inc., Germantown, NY) were maintained on a regular chow diet. Mice were tail bled and the plasma was collected in EDTA tubes with lipase inhibitors added. In addition to this, human and rhesus macaque plasma samples (Bioreclammation, SC) were also used. An aliquot of plasma (20 μL) was extracted by the Bligh and Dyer method (41).

Liquid interface and Ion mobility TOF mass spectrometric conditions

Two types of liquid introduction systems were utilized for mass spectrometric experiments on a SYNAPT G2 HDMS (Waters, MS Technologies, Manchester, UK). Synthetic lipid samples were examined by flow injection analysis (FIA), using a robotic chip-based nano-electrospray delivery device (Advion Nanomate, NY, USA). Samples were introduced to the mass spectrometer by infusing through a 5-μm nozzle. A voltage of +1.5 kV was applied to the conductive disposable sample pick-up tip. For standard lipid samples (concentration 100 ng/μL), 5-μL aliquots were injected using a new tip for each delivery, to minimize the risk of sample contamination. Data was collected for 10 min per sample. For the analysis of plasma samples, an Acquity UPLC (Waters, MA, USA), a high-pressure solvent delivery system was coupled to the mass spectrometer; same chromatographic conditions were used as described in previous work (42). Electrospray (ESI) ionization mass spectra were recorded under positive ion generating conditions while maintaining the capillary, extraction cone and cone voltages at +2 kV, +4 V and +30 V respectively for LC related experiments. The desolvation nitrogen gas was used at a flow rate of 700 L/hr, the source and desolvation temperatures were set at 120, and 450 °C respectively. Mass spectra (*m/z* 50-1200) were acquired at a resolving power of 25,000 [full width half height mass resolution

(FWHM)]. Leucine enkephalin was used as the lockmass for all the experiments described herein. The lockmass was introduced automatically with a built-in solvent delivery system at a flow rate of 10 µL/min, and acquired for 0.3 seconds; this event was repeated every 10 seconds in a separate acquisition channel. Lockmass corrections were applied in a post-processing manner.

Ion mobility Time-Aligned Parallel (TAP) fragmentation experimental conditions

For fragmentation experiments the instrument was set up in a mode called time-aligned parallel fragmentation (TAP), in which both collision cells (trap and transfer) were maintained at a collision energy setting of 35 eV. The collision gas utilized was argon at a pressure of $9.11e^{-3}$ mbar. Under this mode of operation, ions of interest were selected in the quadrupole region Q1 at a resolution of 1 Dalton to allow only ions of one m/z ratio to pass through. Ions isolated in this way, were subjected to subsequent fragmentation in the "trap" region of the IMS device. These first generation fragment ions entered the helium cell region that was operated at 150 mL/min, the main function of the helium cell was to reduce the internal energy of ions and minimize further fragmentation. First generation daughter ions then entered the IMS cell, held under 80 mL/min flow of nitrogen, to be separated according to their charge, *m/z* and collisional cross section areas. As the separated ions exited the IMS cell they were subjected to a second fragmentation event where each ion produced a series of second generation grand- daughter ions. Each spectrum produced in this way corresponds to a specific drift time that can be aligned with a first generation daughter ion or mixture of ions. The trap T-wave, IMS T-wave and the transfer T-wave all carried different wave velocities; these were 314 m/sec, 652 m/sec and 190 m/sec respectively. The total cycle span for a TAP fragmentation experiment was 10.75 msec. Each total fragmentation including IMS separation adds up to 200 IMS scans or bins, thus each scan accounting for 53.75 µsecs, so that over the course of an LC run or FIA a large number of ion mobility scans can be attained.

TWIMS calibration procedure

The movement of ions through the T-wave mobility device is somewhat different from that in more conventional drift tubes that use a constant electric field. Thus, it is necessary to calibrate the TWIMS device with a calibration mixture of known collision cross sectional (CCS) areas as reference markers. For the calibration of the TWIMS device, a mixture of poly-DL-alanine (Sigma-Aldrich, LO, USA) (1mg/mL) in 50/50 v/v methanol/water was infused for a total of 5 minutes to collect sufficient data points for the calibration. Only singly charged species of the calibrant ions were processed for the calibration curve. The drift time (t_c) was plotted against normalized cross section and a linear trend line ($y = ax + b$) was constructed. The linear calibration curve ($r^2 = 0.9908$; Figure S-1) obtained in this way was then used to calculate

collision cross section areas (Å^2) of other ions subjected to mobility in the T-Wave cell. The same calibration line was applied to all measurements by maintaining all IMS parameters constant throughout the experiments.

All the data generated in these experiments was processed by a special software algorithm designed by the manufacturer (DriftScope 2.1) as part of the MassLynx 4.1 software package. The main function of DriftScope was to deconvolute IMS data from a multidimensional format (retention time, *m/z*, peak intensity, and drift time) to a two-dimensional display (drift time and *m/z*). In other words, the data was first deconvoluted in the DriftScope and then exported to MassLynx for further data processing.

Lipid nomenclature

Throughout this study the lipid nomenclature utilized was the same as cited by LIPIDMAPS (http://www.lipidmaps.org) following the article by Fahy *et al.*(6)

RESULTS AND DISCUSSION

LC-IMS/TOF-MS plasma lipid analysis

Data obtained from an LC-IMS/TOF-MS analysis of mouse plasma are illustrated in Figure 1A. Although the presence of a large number of components in the plasma mixture is evident from the reverse-phase LC-MS profile obtained (Figure 1A, top), the occurrence of three major different drift-time regions (Figure 1A, bottom, bright yellow patches) indicate the existence of three different cluster of lipids classes in the lipid plasma extract. Even though, recording of TOF spectra in conjunction with IMS has some merit, enhanced structural information can be generated if the two collision cells are operated in tandem with the IMS device. This procedure named TAP protocol is the main focus of the research reported here. For example, the ion m/z 760.6 from one of the major lipids of interest PC (16:0/18:1 (9Z)) in plasma that eluted at retention time 6.0 min, was selected with the quadrupole mass filter (1-Da wide isolation window) and subjected to fragmentation in the first collision cell (Figure 1B), A packet of daughter ions produced in the trap region were subjected to ion mobility separation followed by secondary fragmentation in the transfer region, resulting in a driftogram containing the different drift regions for each of the 1st generation and 2nd generation fragment ions generated in this arrangement (Figure 1B). Figure 1C shows in detail the spectra contained in each of the drift time regions generated by TAP fragmentation from mouse plasma; the peak centered at 1.46 ms represents the m/z 184 ion derived from the phosphocholine head group. The drift region centered around 4.37 ms represents a composite of several ions that originated from the loss of the acyl chains (M – *sn-1* and M – *sn-2*). The drift time region at 5.67 ms corresponds to the M-Phosphoryl choline fragment ion. Finally the drift time region centered at 6.91 ms represents the 1st generation fragment ions of precursor (PC (16:0/18:1 (9Z)). The sensitivity obtained from this LC on-line IMS-TOF experiment was adequate. Even though the hydrocarbon fragment ions generated in drift time region 4 were of low abundance, it was possible to detect them without the need of fraction collection of the peak followed by infusion analysis. To determine whether low PCs levels may affect our ability to obtain a good degree of fragmentation information for region 4 in the driftogram, a 1μL injection of the extracted plasma sample was carried out. The data shown in figure S-2 clearly depicted the fact that we were able to detect with a good ion count the lower injection volume for the same drift time region 4.

In order to confirm the fragmentation content of the ions present in the trap region in detail, a sample of synthetic (PC (16:0/18:1 (9Z)) was infused by flow injection and product-ion spectra corresponding to each region were obtained. Typically CID spectra of PCs show only a very intense peak at m/z 184, which corresponds to the phosphocholine head group, and provide little information on the fatty acyl chains at the *sn-1* or *sn-2* positions. With the use of TAP fragmentation in combination with ion mobility, more structural information on these ions can be obtained. All fragmentation reported herein was a direct result of charged-induced fragmentation (CIF). Stable isotope ^{13}C labeling of the terminal carbon at position 18 of the *sn-2* fatty acyl chain has been used for the PC and LPC, not only to guide us in the data interpretation, but also to find out whether fragmentation originated in the distant or proximal carbon position from the carbonyl group. This will be discussed later in more detail.
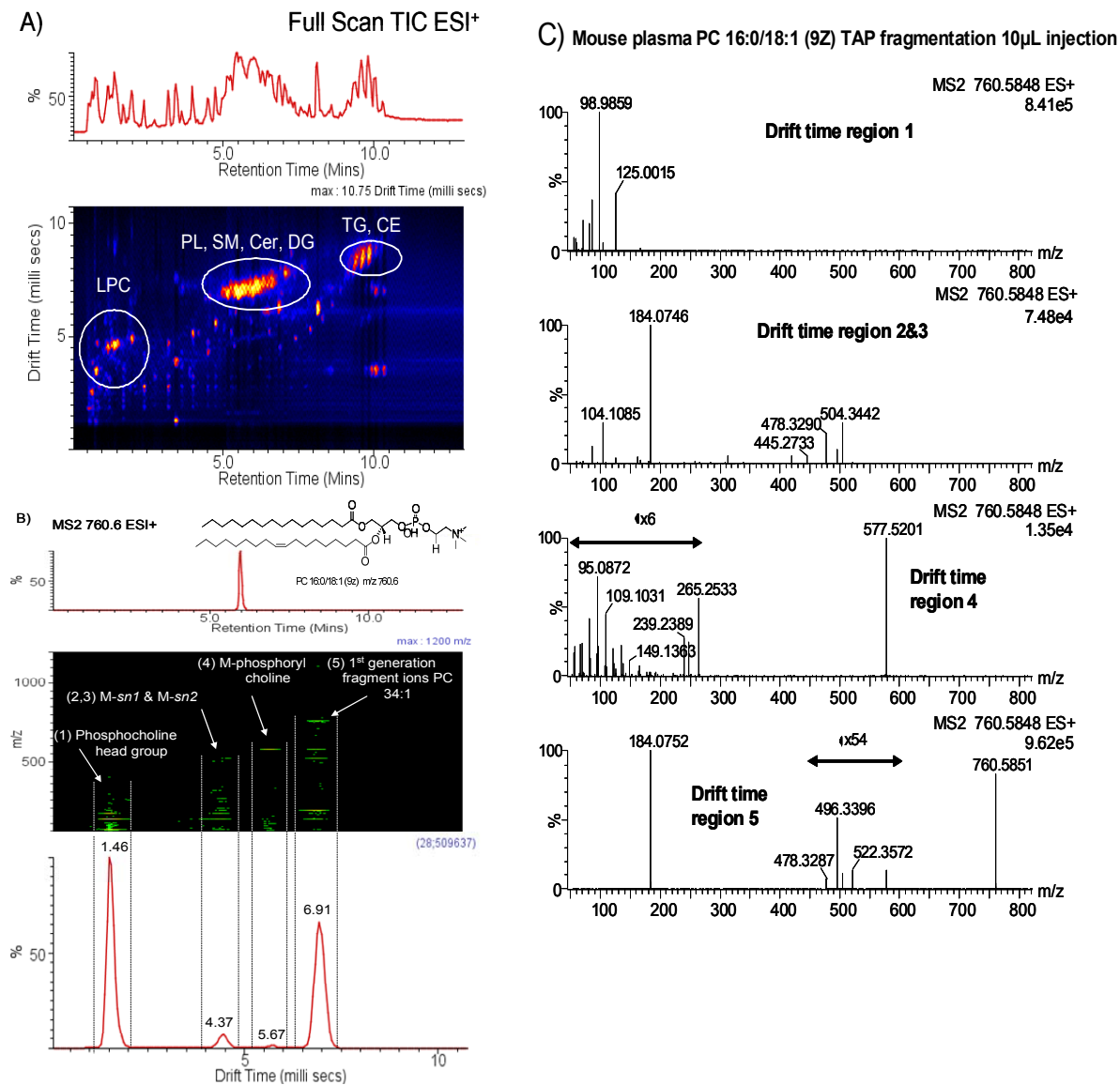
Figure 1. LC/IMS-TOF full scan MS and TAP analysis in mouse plasma. (A) A chromatogram recorded by acquiring *m/z* 50-1200 mass range (top) and ion mobility data (bottom) for 13.0 min on an LC/IMS-TOF instrument from an extracted mouse plasma sample (LPC = Lyso phosphatidylcholine; PL = Phospholipid, SM = Sphingomyelins; Cer = Ceramides; DG = Diacylglycerides; TG = Triacylglycerides, CE = Cholesterol ester) (B) TAP data from the m/z 760.6 ion, for PC 16:0/18:1 (9Z) from an extracted mouse plasma sample, isolated in Q1 and then subjected to fragmentation. (C) TAP fragmentation spectra corresponding to each of the drift time regions in the driftogram shown in panel B.

Loss of the phosphoryl choline head group

Use of a synthetic standard to confirm the TAP fragmentation results in Figure 1C was important in this study. Figures 2A-D give the corresponding spectra for all the driftogram regions shown in Figure 1C using the synthetic standard. The *m/z* 577.5201 (+0.9 ppm from that calculated for $C_{37}H_{69}O_4$) ion represented by the peak at 5.67 ms in Figure 1C, produced the product ion spectrum observed in Figure 2C. The *m/z* 577.5 ion in fact corresponds to the loss of the phosphoryl choline head group from the precursor ion m/z 760.5; this particular fragmentation step is not energetically favorable. This is supported by the observation that the relative peak intensity of the m/z 577 ion driftogram is significantly smaller than those of the other peaks in the driftogram (Figure 1B). The subsequent fragments from this ion resulted from a secondary fragmentation process in the transfer region being derived from the parent ion. The generation of the *m/z* 577 ion is postulated in Scheme 1, sequence **a → b**. Presumably, this fragmentation step arises from CIF in which heterolytic cleavage of the C-N bond in ion **a** is successively accompanied by a concomitant 1,2-hydride shift and loss of CH_3CO, followed by loss of HPO_3 and again a concomitant 1,2-hydride shift to give ion **b** with m/z 577. The two 1,2-hydride shifts during this fragmentation avoid the formation of primary carbenium ion centers, which theoretically are known not to correspond to energy minima. Without the use of lithiated PC adducts, there is little evidence in the literature for this particular fragmentation process; Trimpin *et al.* (43) have indicated the occurrence of this fragment ion without support from accurate mass measurements. Furthermore, the IMS configuration used in that work was different from the one applied in the present research. Table S-1 shows all the different fragment ions generated in each of the drift time regions together with their accurate mass. All first and second generation fragment ion accurate mass measurements gave a total RMS error of 1.56 ppm, which is very acceptable in view of the fact that such measurements by use of IMS TOF have not been reported earlier. From Table S-1, it can be noted that drift fragmentation region 4 contains fragment ions which for the major part may contain 0, 1, 2 or 3 double bonds. These ions are generated from CIF events which will be discussed below.
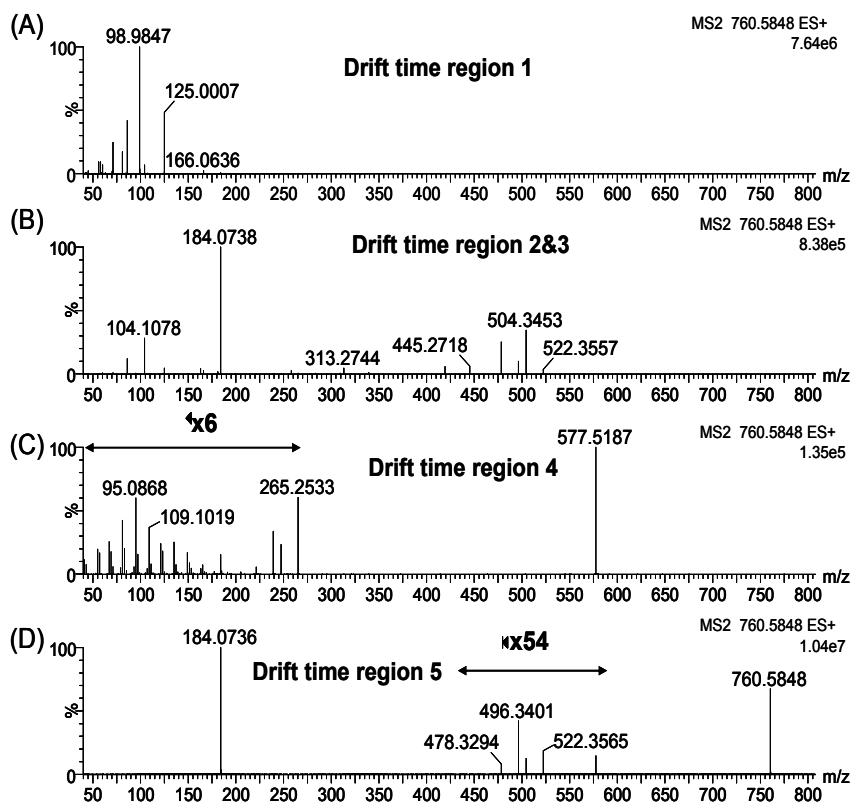
Figure 2. Synthetic standard of m/z 760.5848 (PC 16:0/18:1 (9Z)) showing collision induced dissociation mass spectra of ions arising from the TAP experiment with drift times corresponding to 1.45 (A), 4.37 (B), 5.67 (C) and 6.91 (D) ms. (A) Drift time region 1; Phosphocholine head group (transfer fragments). (B) Drift time region 2 & 3; M-*sn1* & M-*sn2* (transfer fragments). (C) Drift time region 4; M-Phosphoryl choline (transfer fragments).(D) Drift time region 5; First generation fragment ions from PC 16:0/18:1 (9Z) (trap fragments)

Location of the fatty acyl substituent positions

For the determination of the position of the fatty acyl chain in the *sn-1* or *sn-2* positions, m/z 760.5 corresponding to PC 16:0/18:1 (9Z) was selected in the quadrupole region (Q1). This was followed by CID fragmentation in the trap region and drift times belonging to region 2 and 3 were used (see Figure 3). Figure 3A shows in detail the results from three different biological matrices (rhesus, mouse and human plasma) injected on the LC column and detected by the IMS-CID-TOF. In all cases, the data show that *sn-2* is preferentially fragmented over *sn-1*. This was confirmed by the use of synthetic standards where the FA 16:0 constituent was either in the *sn-1* or *sn-2* positions (PC 16:0/ 18:1 (9Z) or PC 18:1 (9Z) / 16:0). In Figure 3B can be observed that if the same synthetic standard (PC 16:0/18:1 (9Z)) is used as in the plasma samples the same fragmentation pattern is detected. In contrast to this, if the FA 16:0 substituent is now in the *sn-2*

position (PC 18:1/ 16:0 (9Z)) the opposite is observed. This finding leads to the postulation that it is possible to predict the location of the fatty acyl groups on the basis of the intensity ratios between the different losses of the fatty acyl moieties. The observation that the [M-*sn2*+H]$^+$ ions are most abundant may well be due to the tertiary α-hydrogen atom which can form a hydrogen bond with the carbonyl oxygen of the *sn-1* group and thus may hinder the formation of the [M-*sn1*+H]$^+$ ions.
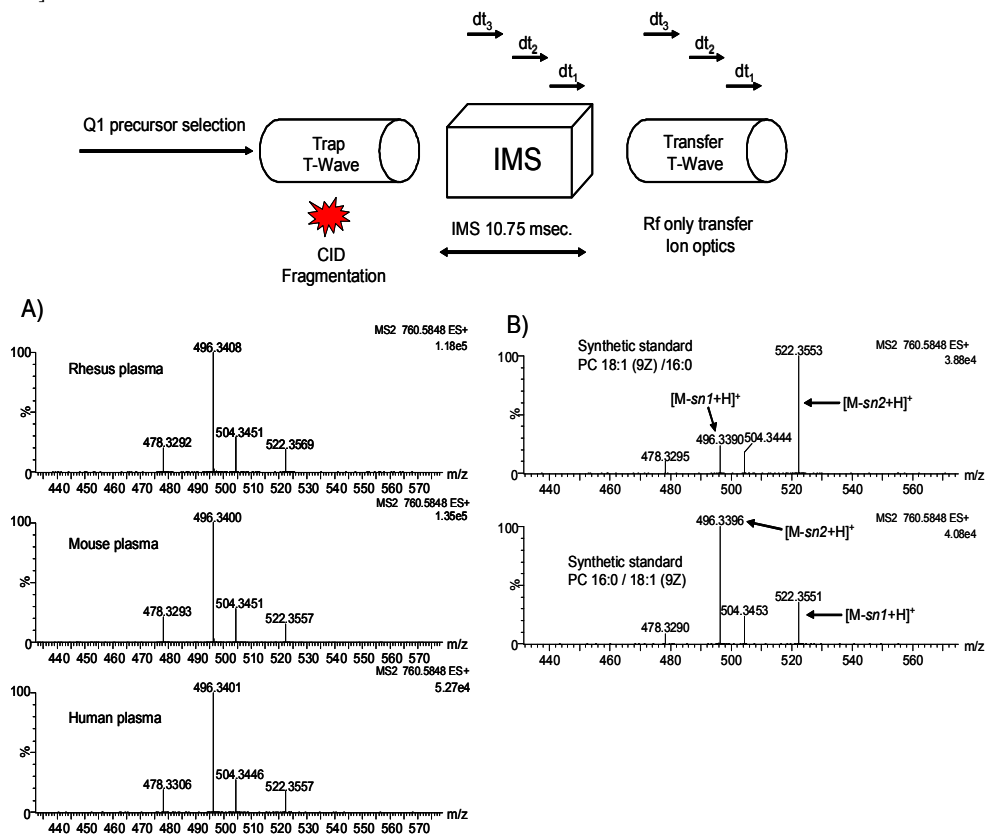
Figure 3. Localization of fatty acyl substitutent in phosphatidylcholines ; PC 16:0/18:1 (9Z) fragmentation was conducted by selecting the ion at m/z 760.5 in the quadrupole region Q1 followed by collision-induced fragmentation in the trap (A) Shows the m/z 430-580 region of collision –induced dissociation mass spectra for drift time region 2 &3 for rhesus *(upper panel)* , mouse *(mid panel)* and human *(lower panel)* plasma samples. (B) Depicts the fragmentation pattern for synthetic standards PC 18:1 (9Z) /16:0 and PC 16:0/ 18:1 (9Z) in drift time regions 2&3.

Abbreviations: dt (drift time for fragment ions generated in the trap region)

a, m/z 760

	N(CH$_3$)$_3$
	CH$_3$CHO
	HPO$_3$
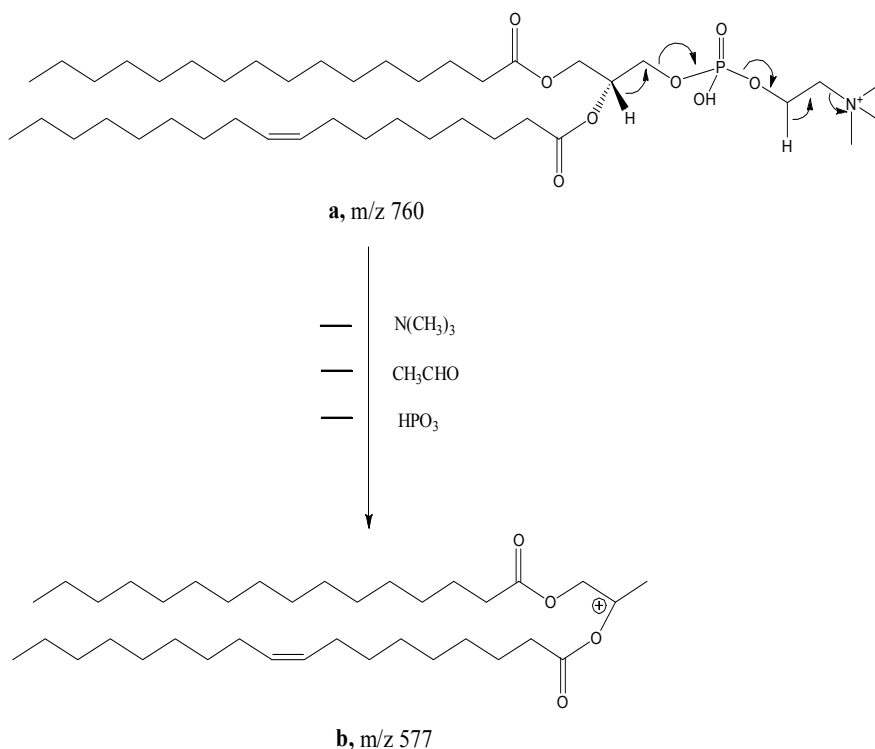
b, m/z 577

Scheme 1. Proposed mechanism for the formation of M-Phosphoryl choline ion *m/z* 577 arising from TAP charge-induced fragmentation of PC 16:0/18:1 (9Z).

Location of the double bond position in the fatty acyl substituent

The data generated from the drift time region 4 shows clear isolation in the drift tube of the ion that contains the M-Phosphoryl choline *m/z* 577 (Figure 1C and 2C). This fragment ion gives rise to the formation of the acylium ions (Figure 5A) corresponding to FA 18:1 (9Z) (*sn*-2-CO$^+$) with *m/z* 265.2533 (+0.8 ppm) and FA 16:0 (*sn*1-CO$^+$) with *m/z* 239.2380 (+2.1 ppm) as visualized in Scheme 2 by sequences **b → c** and **b → d → e.** These acylium ions eliminate a molecule of water to give the ions *m/z* 247 and *m/z* 221, respectively. In Scheme 3, a mechanism is proposed for the loss of water from ion **c** with *m/z* 265. It involves a successive 1,5-hydride shift from the C5 methylene group to the carbonyl carbon atom, a proton abstraction by the carbonyl oxygen from the C4 methylene group, a 1,3-hydride shift from the C3 methylene group to the carbonyl carbon atom and a proton abstraction from the C2 methylene group by the generated hydroxyl group, as visualized by the sequence **c → f → g → h → i**. Ion **i** can then eliminate by heterolytic cleavage a water molecule to give

ion **j** with *m/z* 247. The latter ion thus contains at its original carbonyl end a delocalized pentadienyl cation moiety being consistent with the presence of a relatively abundant ion at *m/z* 67 having the elemental composition of C_5H_7 (see Table S-1, section 4) that can be formed by a 1,2-elimination reaction from ion **j** to give ion **k** (see Scheme 3). In a similar way a molecule of water can be eliminated from ion **e** with *m/z* 239 (see Scheme 2) to give the ion with *m/z* 221 that can generate by a 1,2-elimination reaction the $C_5H_7^+$ ion **k** with *m/z* 67 as well.

At this point, it should be noted that the most abundant hydrocarbon fragment ions as observed in Figure 4A also have 2 double bonds, indicating that the dehydrated acylium ions $C_{16}H_{29}^+$ and $C_{18}H_{33}^+$ are the key precursor ions for their formation (note that Figure 4A refers to PC 16:0/18:0 having two saturated fatty acid groups). A very interesting and important observation is made when comparing the $C_5H_7^+$ ion to its higher homologues. It can be seen that from C_9 containing ions onwards the hydrocarbon fragments not only possess 2 double bonds, but also 3 double bonds. The latter must originate from the FA 18:1(9Z) chain and the fact that $C_9H_{13}^+$ is the first ion having 3 double bonds is in perfect agreement with the double bond at position 9 of the fatty acid chain *sn-2* (Figure 4B), irrespective of the pathway of its formation. Such location of the double bond is also possible with an increased level of unsaturation as in the case of PC 16:0/18:2 (9Z, 12Z). This is shown by the spectrum in Figure 4C, where the C_5 to C_8 containing ions have 2 double bonds, the C_9 to C_{11} containing ions have 3 double bonds and the C_{12} and higher homologue ions have 4 double bonds. This is again in perfect agreement with the double bonds at positions 9 and 12 of the fatty acid chain *sn-2*.

Research has been recently undertaken (22) to locate the double bond in long chain unsaturated fatty acids by the use of lithium adduct and a linear ion trap mass spectrometer. The majority of the fragment ions generated in that work arises from β-cleavage with a γ–H shift via a McLafferty-type of rearrangement (44). Although that research yielded an important set of information, this was conducted using a simpler and less complex system by flow injection analysis infusion and free fatty acids standards. In contrast, in the present study it has been demonstrated that hydrocarbon ions from the fatty acyl chains using the ion mobility set-up can be relatively easily generated and that they were of general high abundance for performing accurate mass measurements, which in itself was key to postulate the fragmentation mechanism described here.

It is well known that unsaturated hydrocarbon ions may suffer from hydrogen and skeletal rearrangements. It is therefore surprising that in the present research double bond location in the fatty acid chain, discussed above, can be relatively easily derived from the spectra. A reason may be that the proposed dehydrated acylium ions do have a highly resonance-stabilized pentadienyl cation moiety that on energetic grounds prevents hydrogen and skeletal rearrangements to occur. Yet, in Table S-1 and Figure 4 the saturated $C_4H_9^+$ ion with a notable abundance is present. This prompted us to study PC (16:0/18:1 (9Z)) specifically labeled with ^{13}C at the terminal methyl group of the *sn-2* fatty acid chain in order to find out which hydrocarbon ion fragments do contain ^{13}C and thus whether also fragmentation from the ω end might take place. The spectra of the unlabeled and ^{13}C-labeled compound are given in Figures 5A and 5B, respectively. Apart from the peaks at *m/z* 266.2554 (-4.1 ppm, $^{13}C_1{}^{12}C_{18}H_{33}O$) and *m/z* 248.2455 (+1.6 ppm, $^{13}C_1{}^{12}C_{18}H_{31}$) in Figure 5B which are due
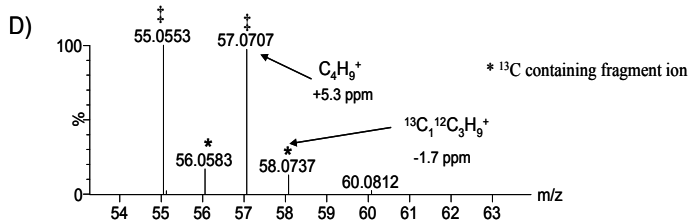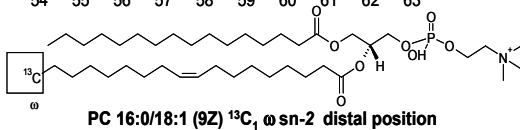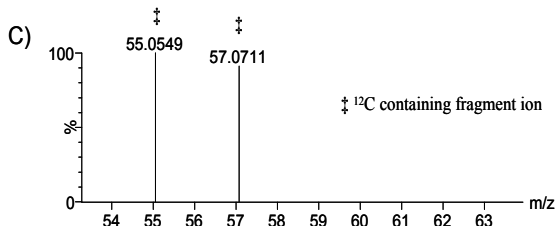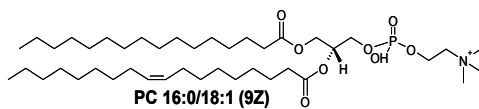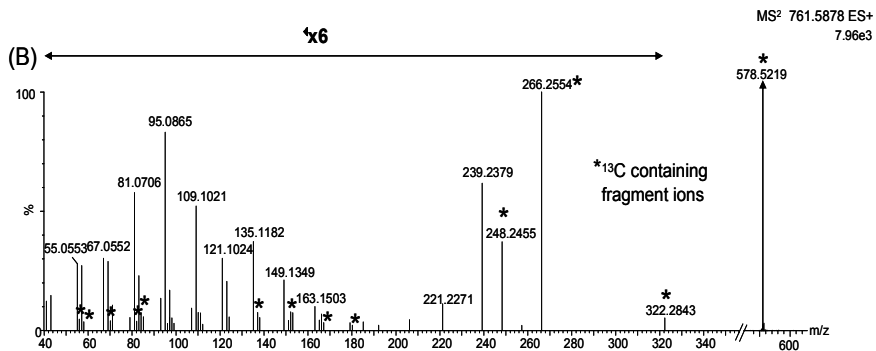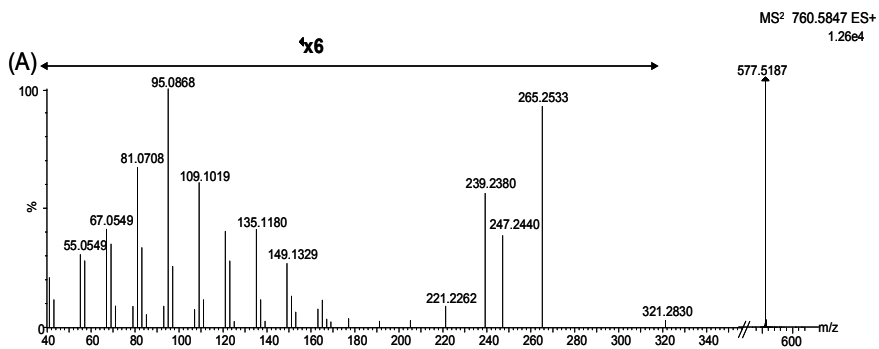
to the ^{13}C-labeled acylium ion and its dehydrated fragment ion from the *sn-2* fatty acid chain, the peaks denoted with an asterisk in the lower mass region correspond to hydrocarbon ions containing the ^{13}C-label. These peaks have a low intensity and from comparison of Figure 5B with Figure 5A it may be concluded that the majority of the hydrocarbon ions are generated from the dehydrated acylium ions by elimination of neutrals containing the ^{13}C-label. It is not clear how the low abundant ^{13}C containing hydrocarbon ions are formed, but if a small fraction of the dehydrated acylium ions would eliminate the pentadienyl moiety as a neutral, for example as 1,3,5-hexatriene, then the resulting hydrocarbon fragment ion may undergo skeletal rearrangements prior to fragmentation. This would lead to scrambling of the carbon atoms and indeed Figure 5B shows that the peaks at *m/z* 55 ($C_4H_7^+$) and *m/z* 57 ($C_4H_9^+$) of spectrum Figure 5A have only shifted to a minor extent to *m/z* 56 ($^{13}C_1C_3H_7^+$) and *m/z* 58 ($^{13}C_1C_3H_9^+$); see also the corresponding zoomed regions in the spectra Figure 5C and Figure 5D.

A further study was performed by using LPC 18:1 (9Z), labeled with ^{13}C in the terminal ω-methyl group and having only one fatty acid chain. Figure 6A depicts the fragmentation of LPC 18:1 (9Z) under TAP conditions. The ^{13}C label was retained in the hydrocarbon fragment ions until the 'C8 position (Table S-2) and then it was only present in the dehydrated acylium ion *m/z* 248.2568 ($^{12}C_{17}\,^{13}C_1\,H_{31}$, 10.1 ppm), the acylium ion *m/z* 266.2568 ($^{12}C_{17}{}^{13}C_1H_{33}O$, +1.1 ppm) and the ions with *m/z* 310.2929 ($^{12}C_{19}{}^{13}C_1H_{37}O_2$, -1.6 ppm) and *m/z* 340.2929 ($^{12}C_{20}{}^{13}C_1H_{39}O_3$, -1.2 ppm) (Figure 6B). Interestingly, further inspection of the lower mass range revealed the presence of two fragment ions; *m/z* 57.0341 (+1.8 ppm, C_3H_5O) and *m/z* 57.0705 (+1.8 ppm C_4H_9) (Figures 6C and 6D). The mass spectral resolution was sufficient to mass resolve these two fragment ions which were 36.4 mDa apart. These two ions were only observed for the LPC and a more detailed mechanistic scheme for the formation of the ion with *m/z* 57.0341 is proposed in Scheme 4 as sequence **l → m → n → o**, where the first step is similar to sequence **a → b** in Scheme 1 and where ion **o** is a resonance stabilized 2-hydroxy-allyl cation. Like in the case of PC (16:0/18:1 (9Z)), the ion at *m/z* 57.0705 shifts only partly to *m/z* 58.0740 ($^{13}C_1{}^{12}C_3H_9$, +3.4 ppm) upon ^{13}C-labeling indicating the occurrence of carbon skeletal rearrangements as noted before. Nevertheless, the majority of the hydrocarbon fragment ions originate from the dehydrated acylium ions by elimination of neutrals containing the ^{13}C-label and again it is equally well possible to locate the double bond position in the LPC lipid classes as shown above for the PC lipid classes.
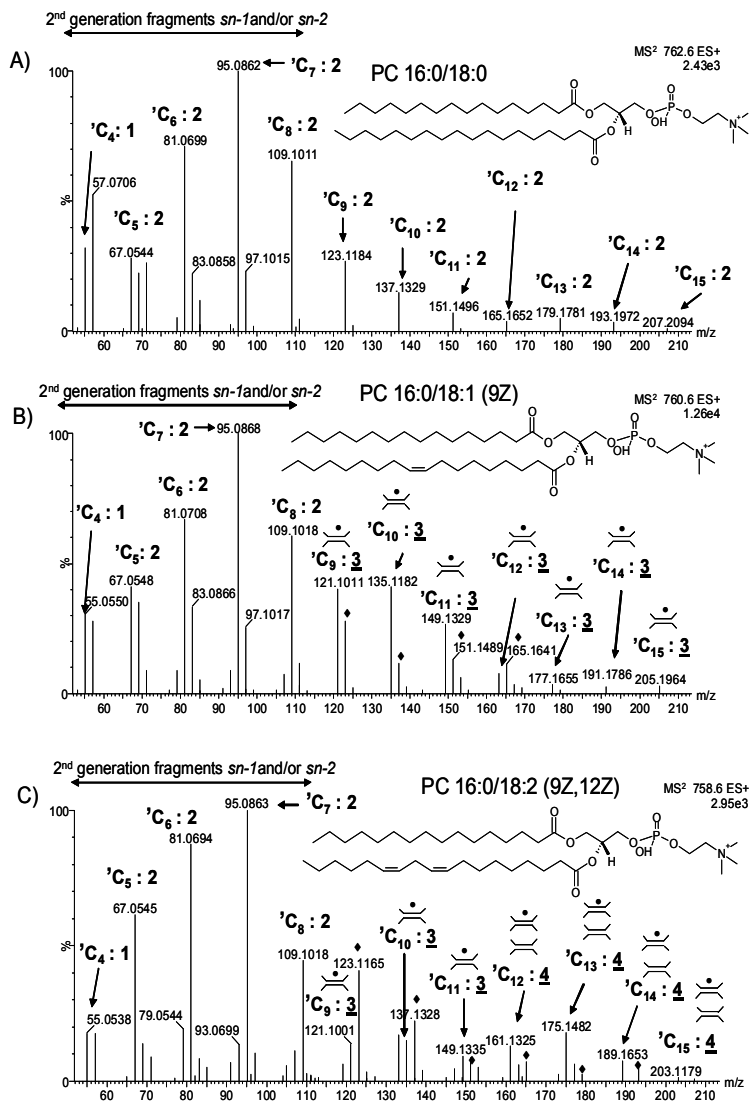
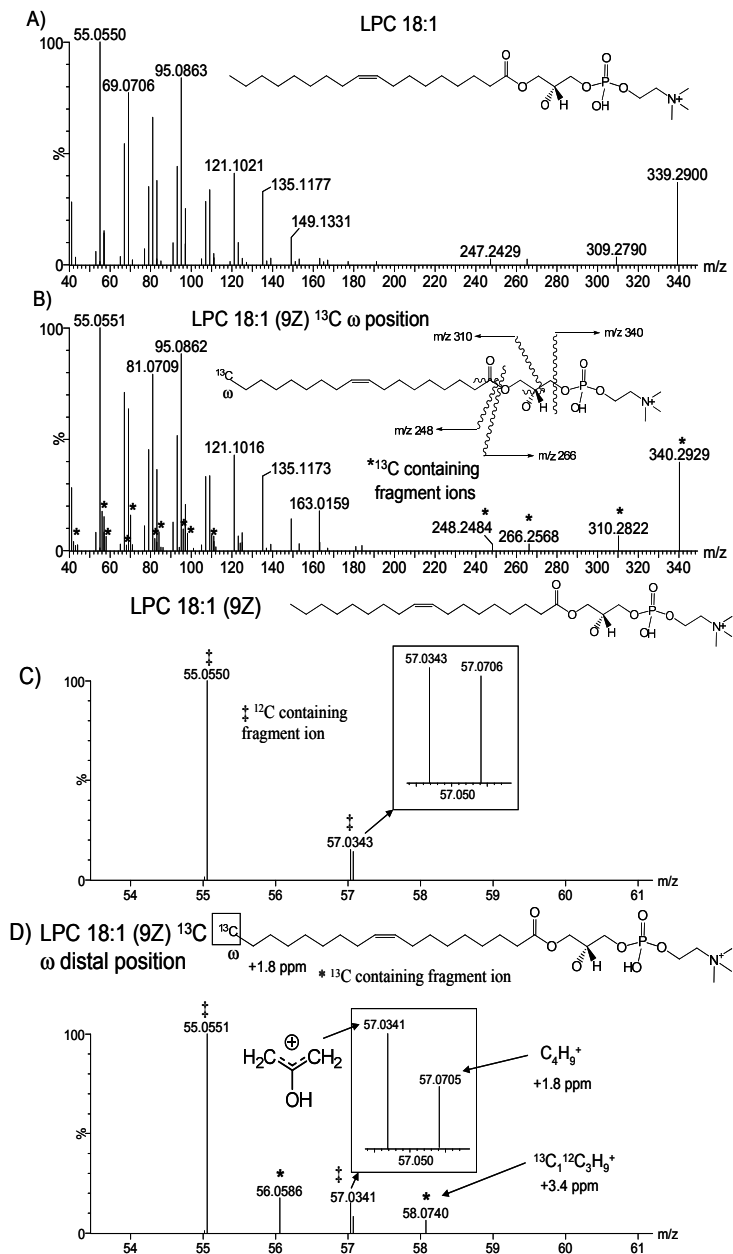**Figure 4.** (A) 2nd generation of fragment ions region 4 for PC (16:0/18:0). (B) 2nd generation of fragment ions region 4 for PC (16:0/18:1(9Z)). (C) 2nd generation of fragment ions region 4 for PC (16:0/18:2(9Z, 12Z)).

Nomenclature: Fragment ions which belongs to either *sn-1* or *sn-2* fatty acyl chain are denoted by "•" for FA 18:1 (9Z) or FA 18:1 (9Z, 12Z) containing and "♦" for FA 16:0 containing

(A)

MS² 760.5847 ES+
1.26e4

x6

577.5187

95.0868
265.2533
81.0708
109.1019
239.2380
67.0549
135.1180
247.2440
55.0549
149.1329
221.2262
321.2830

(B)

MS² 761.5878 ES+
7.96e3

x6

578.5219 *

266.2554 *

95.0865

81.0706
109.1021
239.2379
*13C containing
fragment ions

67.0552
135.1182
248.2455 *
55.0553
121.1024
149.1349
322.2843 *
163.1503
221.2271

PC 16:0/18:1 (9Z)

C)

55.0549 ‡
57.0711 ‡

‡ 12C containing fragment ion

PC 16:0/18:1 (9Z) 13C₁ ω sn-2 distal position

D)

55.0553 ‡
57.0707 ‡

C₄H₉⁺
+5.3 ppm

* 13C containing fragment ion

56.0583 *
58.0737 *
13C₁12C₃H₉⁺
-1.7 ppm
60.0812

Figure 5. Fragment ion spectra from region 4 using the unlabeled synthetic version of PC (16:0/18:1(9Z)) and the synthetic stable isotopic labeled ^{13}C in the ω terminal position. (A) Unlabeled 2nd generation of fragment ions region 4 for PC (16:0/18:1(9Z)). (B) Stable isotope ^{13}C labeled 2nd generation of fragment ions region 4 for PC (16:0/18:1(9Z)). (C) Unlabeled 2nd generation of fragment ions region 4 for PC (16:0/18:1(9Z)) showing zoomed region for lower mass range. (D) Stable isotope ^{13}C labeled 2nd generation of fragment ions region 4 for PC (16:0/18:1(9Z)) showing zoomed region for lower mass range.
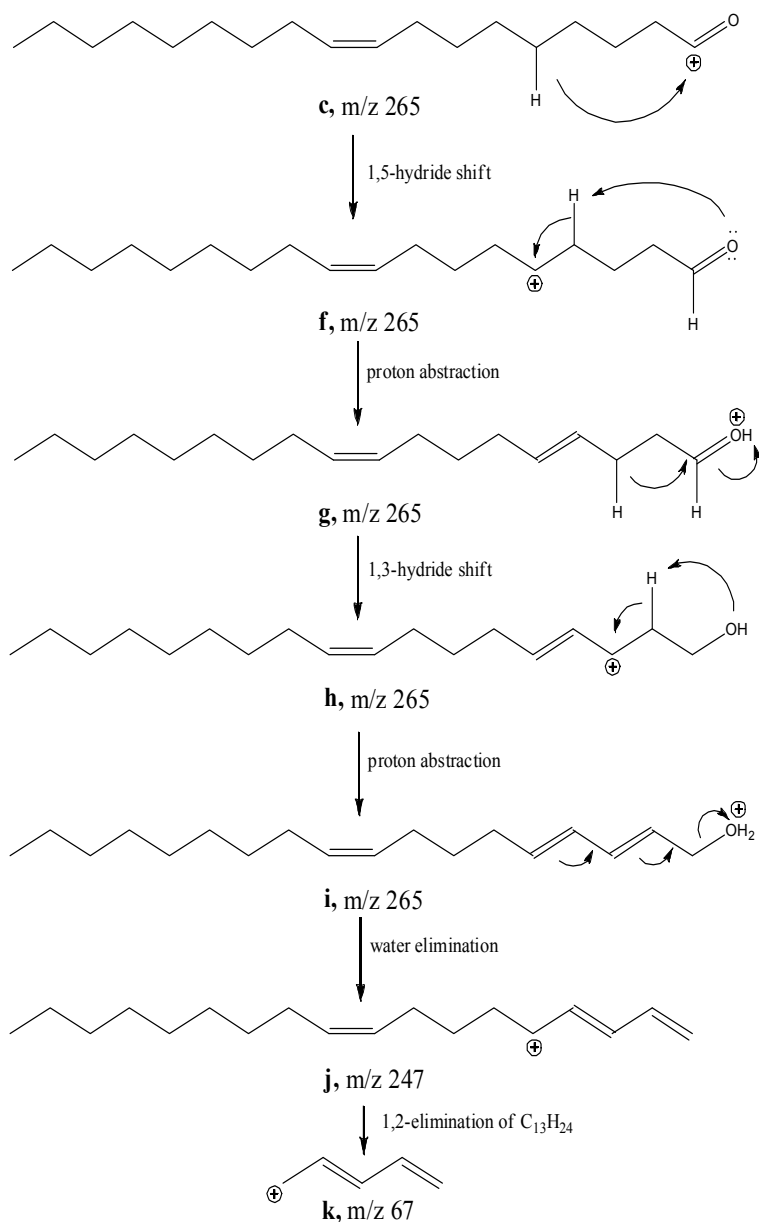
Figure 6. Fragment ion spectra from region 2 using the unlabeled version of LPC 18:1(9Z) and the stable isotopic labeled ^{13}C in the ω terminal position. (A) Unlabeled 2nd generation of fragment ions region 2 for LPC 18:1(9Z). (B) Stable isotope ^{13}C labeled 2nd generation of fragment ions region 2 for LPC 18:1(9Z). (C) Unlabeled 2nd generation of fragment ions region 2 for LPC 18:1(9Z) showing zoomed region for lower mass range. (D) Stable isotope ^{13}C labeled 2nd generation of fragment ions region 2 for LPC 18:1(9Z) showing zoomed region for lower mass range.
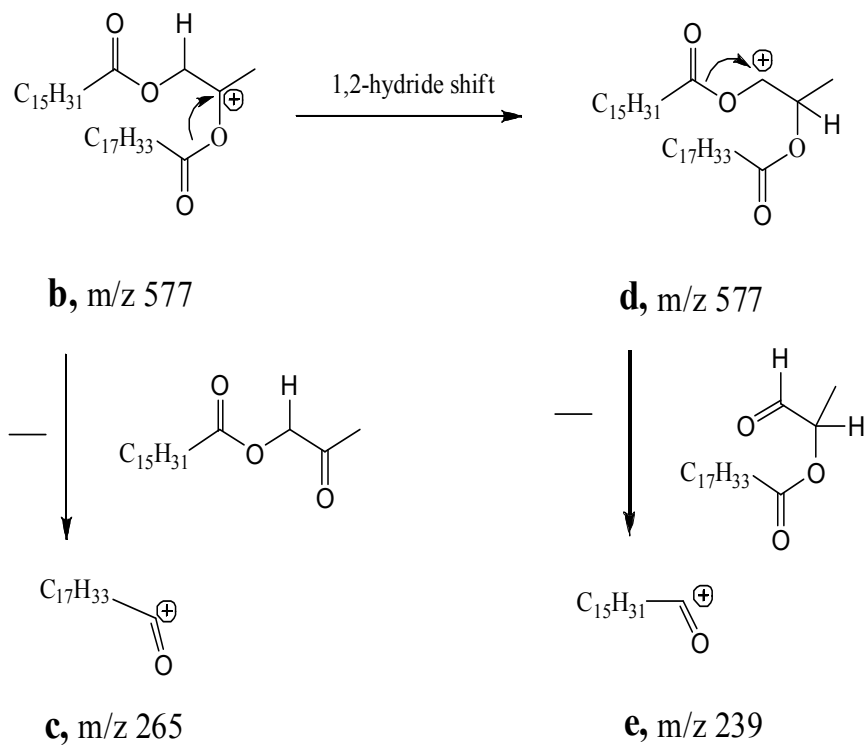

Scheme 2. Formation of the acylium ions $C_{17}H_{33}CO^+$ with *m/z* 265 and $C_{15}H_{31}CO^+$ with *m/z* 239 from the M-Phosphoryl choline ion *m/z* 577.

c, m/z 265

1,5-hydride shift

f, m/z 265

proton abstraction

g, m/z 265

1,3-hydride shift

h, m/z 265

proton abstraction

i, m/z 265

water elimination

j, m/z 247

1,2-elimination of $C_{13}H_{24}$

k, m/z 67

Scheme 3. Proposed mechanism for the loss of water from the acylium ion with *m/z* 265 and one of its further fragmentations to give the hydrocarbon ion $C_5H_7^+$ with *m/z* 67.

l, m/z 522

m, m/z 339

Proton abstraction

n, m/z 339

Loss of C$_{17}$H$_{33}$COOH

o, m/z 57
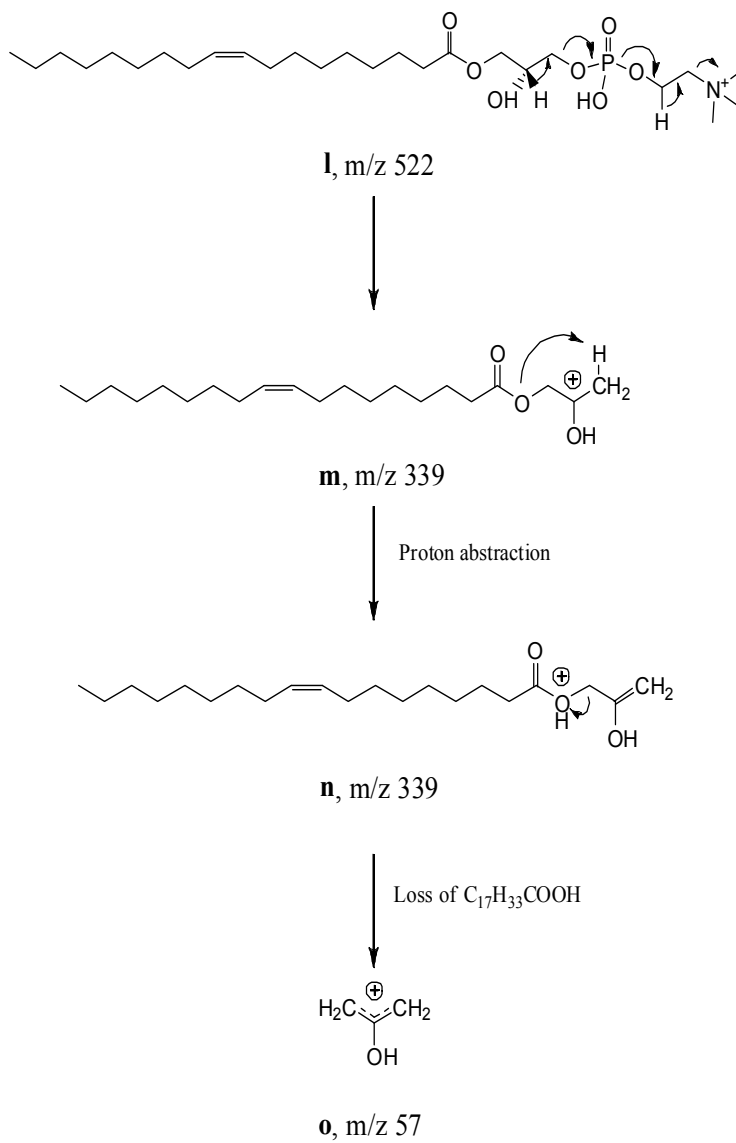
Scheme 4. Proposed mechanism for the formation of the fragment ion C$_3$H$_5$O$^+$ ion with *m/z* 57.0341 arising from the TAP fragmentation of LPC 18:1(9Z)

CONCLUSION

A faster, selective and a more simplistic approach was employed in this study for the comprehensive fragmentation of PCs either by FIA/MS using synthetic standards or by LC/MS using plasma from different species (human, rhesus and mouse). The use of TAP fragmentation together with ion mobility separation of fragment ions enabled the localization of the fatty acyl positions and double bonds in PCs and LPCs. The capability to generate fragment ion information concerning the *sn-1* and *sn-2* positions of the fatty acyl substituents has streamlined our identification process and minimized the need for time-consuming enzymatic assays to determine *sn-1* and *sn-2* fatty acyl substituent positions. The method described in this study has the advantage to speed up the analysis and simplify the identification process via enhanced fragmentation in combination with accurate mass.

This study is an extension of the investigations initiated by other researchers (12-14,17,18,20,22,45,46). The observations in this current study recapitulate and further validate previous findings obtained either by the use of alkali metal adducts (lithium or sodium) in positive ion, or by the use of negative ion FAB. Nonetheless, the main difference is the use of a different mass analyzer which allowed for accurate mass confirmation of the fragment ions and provided an extra level of selectivity by the application of high-resolution accurate mass ion mobility time-of-flight mass spectrometry. Additionally, hydrocarbon fragmentation data was generated by protonated PCs and LPCs which aided in the subsequent localization of double bonds.

In our particular context, a more simplistic approach was utilized in which not only qualitative information was obtained but also applicable to quantitative information. Analysis of plasma samples for lipid analysis is already a complicated affair due to the myriad number of lipids present in the sample. Adding another variable to the analysis such as introduction post-column of an alkali metal to generate ions, such as Li+ adduct ions will further complicate the detection and identification process of an already challenging analysis. Even though volatile lithium salts can be utilized to obtain fatty acyl and double bond position, there is always a risk of unwanted ion source block contamination occurring from prolonged usage. This can pose difficulties in the routine operation of a laboratory such as ours in which a large number of metabolite profiling samples (>1000 per week) measuring different analytes (lipids, bile acids, amino acids, sugars, polar metabolites, etc) are analyzed. Furthermore, in the strategy described in this study, lower molecular weight species were observed in Figure 6 (m/z 57 scheme 4) generated by TAP fragmentation from the LPC 18:1 (9Z) showing that there are two fragment ions with different elemental compositions which have not been described before. Accurate mass measurement and high-resolution ion mobility permitted this observation.

Extension of this methodology may be applied to other phospholipid classes and this will be the subject of future research. Besides this, ion mobility added an extra level of selectivity, not only in the MS^2 mode, but also in full scan MS because it has provided additional descriptors, such as drift time information besides *m/z*, chromatographic retention time, peak intensity, and peak area.

In summary, it has been possible to analyze biological samples, such as plasma for lipid analysis and to obtain structural information in this way. Our methodology and results thus pave the way for precise characterization of lipid profiles in our future studies of various disease models and potential therapies for dyslipidemia and atherosclerosis.

REFERENCES

1.   Brown, H. A. *Methods Enzymol* **433**, XV-XVI (2007).

2.   Astarita, G., Ahmed, F. & Piomelli, D. *Methods Mol Biol* **579**, 201-19 (2009).

3.   Gross, R. W., Jenkins, C. M., Yang, J., Mancuso, D. J. & Han, X. *Prostaglandins Other Lipid Mediat* **77**, 52-64 (2005).

4.   Gross, R. W. & Han, X. *Methods Enzymol* **433**, 73-90 (2007).

5.   German, J. B., Gillies, L. A., Smilowitz, J. T., Zivkovic, A. M. & Watkins, S. M. *Curr Opin Lipidol* **18**, 66-71 (2007).

6.   Fahy, E. et al.. *J Lipid Res* **50 Suppl**, S9-14 (2009).

7.   Fahy, E. et al.. *J Lipid Res* **46**, 839-61 (2005).

8.   Yasuda, T., Ishida, T. & Rader, D. J. *Circ J* **74**, 2263-70.

9.   Angell, R., Mitsuhashi, Y., Bigley, K. & Bauer, J. E. *Lipids* **44**, 415-24 (2009).

10.   Griffiths, W. J.. *Mass Spectrom Rev* **22**, 81-152 (2003).

11.   Pittenauer, E. & Allmaier, G. *J Am Soc Mass Spectrom* **20**, 1037-47 (2009).

12.   Tomer, K. B., Crow, F. W. & Gross, M. L. *Journal of the American Chemical Society* **105**, 5487-5488 (1983).

13.   Jensen, N. J., Tomer, K. B. & Gross, M. L. *Lipids* **21**, 580-8 (1986).

14.   Jensen, N. J., Tomer, K. B. & Gross, M. L. *Lipids* **22**, 480-9 (1987).

15.   Murphy, R. C., Fiedler, J. & Hevko, J. *Chem Rev* **101**, 479-526 (2001).

16.   Kerwin, J. L., Tuininga, A. R. & Ericsson, L. H.. *J Lipid Res* **35**, 1102-14 (1994).

17.   Murphy, R. C. & Harrison, K. A. *Mass Spectrometry Reviews* **13**, 57-75 (1994).

18.   Pulfer, M. & Murphy, R. C.. *Mass Spectrom Rev* **22**, 332-64 (2003).

19.   Hsu, F. F. & Turk, J. *J Am Soc Mass Spectrom* **19**, 1681-91 (2008).

20.   Hsu, F. F. & Turk, J. *J Am Soc Mass Spectrom* **14**, 352-63 (2003).

21.   Bryant, D. K., Orlando, R. C., Fenselau, C., Sowder, R. C. & Henderson, L. E. *Anal Chem* **63**, 1110-4 (1991).

22.   Hsu, F. F. & Turk, J. *J Am Soc Mass Spectrom* **19**, 1673-80 (2008).

23.   Thomas, M. C., Mitchell, T. W. & Blanksby, S. J. *J Am Chem Soc* **128**, 58-9 (2006).

24.   Thomas, M. C. et al. *Anal Chem* **79**, 5013-22 (2007).

25.   Thomas, M. C. et al. *Anal Chem* **80**, 303-11 (2008).

26.   Becker, C. et al. *J Am Soc Mass Spectrom* **20**, 907-14 (2009).

27.   Belov, M. E., Buschbach, M. A., Prior, D. C., Tang, K. & Smith, R. D. *Anal Chem* **79**, 2451-62 (2007).

28.   Fenn, L. S., Kliman, M., Mahsut, A., Zhao, S. R. & McLean, J. A. *Anal Bioanal Chem* **394**, 235-44 (2009).

29.   Fenn, L. S. & McLean, J. A. *Anal Bioanal Chem* **391**, 905-9 (2008).

30.   Hill, H. H., Siems, W. F., Stlouis, R. H. & Mcminn, D. G. *Analytical Chemistry* **62**, A1201-A1209 (1990).

31.   Guo, Y., Ling, Y., Thomson, B. A. & Siu, K. W. *J Am Soc Mass Spectrom* **16**, 1787-94 (2005).

32.   Ruotolo, B. T., Gillig, K. J., Stone, E. G. & Russell, D. H. *J Chromatogr B Analyt Technol Biomed Life Sci* **782**, 385-92 (2002).

33.   Trimpin, S., Clemmer, D. E. & McEwen, C. N. *J Am Soc Mass Spectrom* **18**, 1967-72 (2007).

34.   Zhu, M., Bendiak, B., Clowers, B. & Hill, H. H., Jr. *Anal Bioanal Chem* **394**, 1853-67 (2009).

35.   Ruotolo, B. T. et al. *Science* **310**, 1658-1661 (2005).

36.   Ruotolo, B. T. et al. *Angew Chem Int Ed Engl* **46**, 8001-4 (2007).

37.   Smith, D. P. et al. *Eur J Mass Spectrom (Chichester, Eng)* **15**, 113-30 (2009).

38.   Williams, J. P., Lough, J. A., Campuzano, I., Richardson, K. & Sadler, P. J. *Rapid Commun Mass Spectrom* **23**, 3563-9 (2009).

39.   Williams, J. P. et al. *Journal of the American Society for Mass Spectrometry* **20**, 1119-1122 (2009).

40.   Wildgoose, J. et al. *Molecular & Cellular Proteomics* **5**, S14-S14 (2006).

41.   Bligh, E. G. & Dyer, W. J. *Can J Biochem Physiol* **37**, 911-7 (1959).

42.   Castro-Perez, J. M. et al. *J Proteome Res* **9**, 2377-89.

43.   Trimpin, S. et al. *International Journal of Mass Spectrometry* **287**, 58-69 (2009).

44.   McLafferty, F. *Anal Chem* **31**, 82-7.

45.   Hsu, F. F., Bohrer, A. & Turk, J. *J Am Soc Mass Spectrom* **9**, 516-26 (1998).

46.   Hsu, F. F. & Turk, J. *J Am Soc Mass Spectrom* **10**, 600-12 (1999).

SUPPLEMENTARY INFORMATION

Figure S-1. TWIMS mobility calibration using singly charged ions for poly-DL-alanine
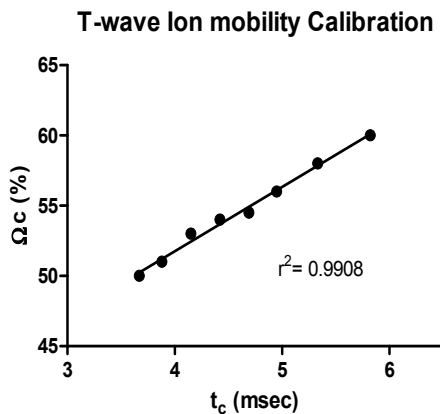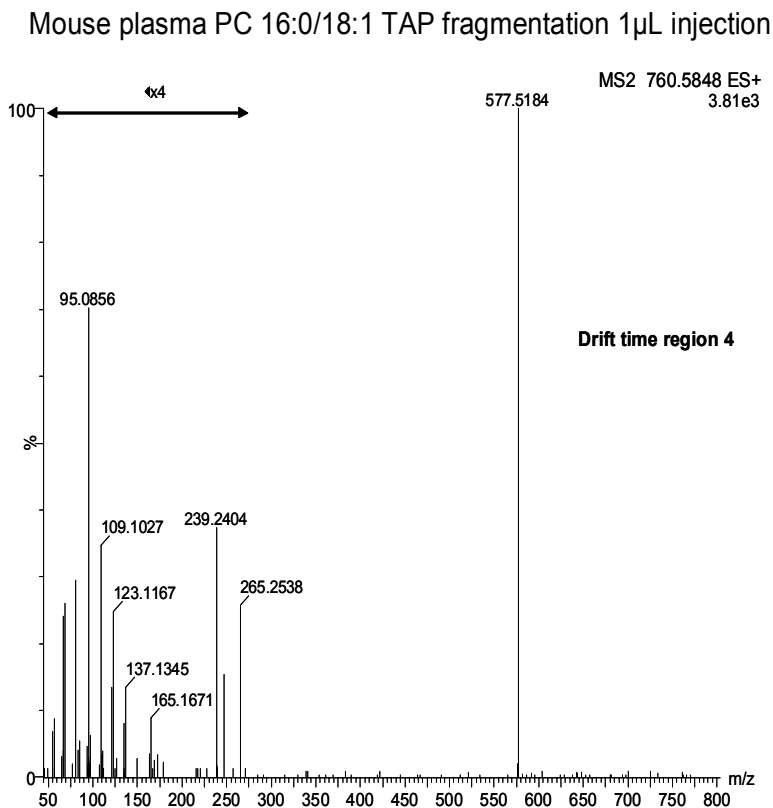

T-wave Ion mobility Calibration

r^2= 0.9908

Figure S-2. Shows a 1µL injection of mouse plasma at selecting m/z 760.5 in the first quadrupole region and further subjected to collision-induced dissociation by TAP fragmentation. The figure depicts drift time region 4 which contain fragment ions belonging to the M-Phosphoryl choline head group

Mouse plasma PC 16:0/18:1 TAP fragmentation 1µL injection

MS2 760.5848 ES+
3.81e3

577.5184

Drift time region 4

95.0856
109.1027   239.2404
123.1167   265.2538
137.1345
165.1671

Table S-1. Collision-induced dissociation spectra of 1st and 2nd generation fragment ions that correspond to different drift times of a TAP experiment conducted on the precursor m/z 760.5 ion from PC (16:0/18:1 (9Z) (synthetic standard).

	m/z (observed)	Relative Intensity (%)	Calc. Mass	mDa	ppm	DBE	Formula
	184.0736	100	184.0739	-0.3	-1.6	-0.5	C5 H15 N O4 P
	478.3295	0.15	478.3298	-0.3	-0.6	1.5	C24 H49 N O6 P
Drift Time (6.91 ms) Section 5	496.3401	0.78	496.3403	-0.2	-0.4	0.5	C24 H51 N O7 P
	504.3452	0.23	504.3454	-0.2	-0.4	2.5	C26 H51 N O6 P
	522.3564	0.34	522.356	0.4	0.8	1.5	C26 H53 N O7 P
	577.5193	0.27	577.5196	-0.3	-0.5	3.5	C37 H69 O4
	760.5848	66.9	760.5856	-0.8	-1.1	2.5	C42 H83 N O8 P
Drift time (5.67 ms) Section 4	41.0397	2.21	41.0391	0.6	14.6	1.5	C3 H5
	43.0552	1.19	43.0548	0.4	9.3	0.5	C3 H7
	55.0549	3.16	55.0548	0.1	1.8	1.5	C4 H7
	57.0711	2.89	57.0704	0.7	12.3	0.5	C4 H9
	67.0549	4.28	67.0548	0.1	1.5	2.5	C5 H7
	69.0709	3.64	69.0704	0.5	7.2	1.5	C5 H9
	81.0708	6.8	81.0704	0.4	4.9	2.5	C6 H9
	83.0865	3.38	83.0861	0.4	4.8	1.5	C6 H11
	95.0868	10.5	95.0861	0.7	7.4	2.5	C7 H11
	97.1019	2.84	97.1017	0.2	2.1	1.5	C7 H13
	109.1019	6.47	109.1017	0.2	1.8	2.5	C8 H13
	111.118	1.2	111.1174	0.6	5.4	1.5	C8 H15
	121.1011	3.91	121.1017	-0.6	-5	3.5	C9 H13
	123.1169	2.78	123.1174	-0.5	-4.1	2.5	C9 H15
	135.118	4.2	135.1174	0.6	4.4	3.5	C10 H15
	137.1338	1.12	137.133	0.8	5.8	2.5	C10 H17
	149.1329	2.74	149.133	-0.1	-0.7	3.5	C11 H17
	151.1494	1.35	151.1487	0.7	4.6	2.5	C11 H19

163.1501	0.76	163.1487	1.4	8.6	3.5	C12 H19
165.1641	1.09	165.1643	-0.2	-1.2	2.5	C12 H21
221.2262	0.97	221.2269	-0.7	-3.2	2.5	C16 H29
239.238	5.87	239.2375	0.5	2.1	1.5	C16 H31 O
247.244	3.82	247.2426	1.4	5.7	3.5	C18 H31
265.2533	9.57	265.2531	0.2	0.8	2.5	C18 H33 O
577.5187	100	577.5196	-0.9	-1.6	3.5	C37 H69 O4
86.0973	11.67	86.097	0.3	3.5	0.5	C5 H12 N
104.1078	28.62	104.1075	0.3	2.9	-0.5	C5 H14 N O
125.0006	4.26	125.0004	0.2	1.6	0.5	C2 H6 O4 P
163.0165	3.88	163.016	0.5	3.1	2.5	C5 H8 O4 P
166.0635	2.32	166.0633	0.2	1.2	0.5	C5 H13 N O3 P
184.0738	100	184.0739	-0.1	-0.5	-0.5	C5 H15 N O4 P
258.1111	2.58	258.1107	0.4	1.5	-0.5	C8 H21 N O6 P
313.2744	4.24	313.2743	0.1	0.3	1.5	C19 H37 O3
419.2569	5.35	419.2563	0.6	1.4	2.5	C21 H40 O6 P
445.2718	5.66	445.2719	-0.1	-0.2	3.5	C23 H42 O6 P
478.3296	23.48	478.3298	-0.2	-0.4	1.5	C24 H49 N O6 P
496.3402	9.5	496.3403	-0.1	-0.2	0.5	C24 H51 N O7 P
504.3453	32.83	504.3454	-0.1	-0.2	2.5	C26 H51 N O6 P
522.3557	3.54	522.356	-0.3	-0.6	1.5	C26 H53 N O7 P
45.0345	2.09	45.034	0.5	11.1	0.5	C2 H5 O
56.0503	8.45	56.05	0.3	5.4	1.5	C3 H6 N
58.0661	8.53	58.0657	0.4	6.9	0.5	C3 H8 N
60.0816	6.39	60.0813	0.3	5	-0.5	C3 H10 N
71.0736	22.86	71.0735	0.1	1.4	1	C4 H9 N
80.9743	17.2	80.9742	0.1	1.2	0.5	H2 O3 P
86.0973	39.25	86.097	0.3	3.5	0.5	C5 H12 N
98.9847	100	98.9847	0	0	-0.5	H4 O4 P
104.1077	6.33	104.1075	0.2	1.9	-0.5	C5 H14 N O

The "Drift time (4.37 ms) Section 2 &3" label spans the second group of rows (86.0973 through 522.3557). The "Drift time (1.46 ms) Section 1" label spans the third group of rows (45.0345 through 104.1077).

125.0007	44.39	125.0004	0.3	2.4	0.5	C2 H6 O4 P
166.0636	2.09	166.0633	0.3	1.8	0.5	C5 H13 N O3 P

Table S-2. Results showing the drift time region 2 (M-Phosphocholine head group) of LPC 18:1 (9Z), labeled with ^{13}C in the terminal methyl group (synthetic standard).

Mass	Relative Abundance (%)	Calc. Mass	mDa	PPM	DBE	Formula
41.0397	28.21	41.0391	0.6	14.6	1.5	C3 H5
42.0428	**4**	**42.0425**	**0.3**	**7.1**	**1.5**	**H5 12C2 13C ***
43.0557	2.27	43.0548	0.9	20.9	0.5	C3 H7
44.059	**2.52**	**44.0581**	**0.9**	**20.4**	**0.5**	**H7 12C2 13C ***
53.0399	8.17	53.0391	0.8	15.1	2.5	C4 H5
55.0193	1.16	55.0184	0.9	16.4	2.5	C3 H3 O
55.0551	100	55.0548	0.3	5.4	1.5	C4 H7
56.0586	**17.62**	**56.0581**	**0.5**	**8.9**	**1.5**	**H7 12C3 13C ***
57.0341	15.17	57.034	0.1	1.8	1.5	C3 H5 O
57.0705	8.26	57.0704	0.1	1.8	0.5	C4 H9
58.074	**6.31**	**58.0738**	**0.2**	**3.4**	**0.5**	**H9 12C3 13C ***
65.0384	2.84	65.0391	-0.7	-10.8	3.5	C5 H5
67.0552	70.97	67.0548	0.4	6	2.5	C5 H7
68.0588	**2.34**	**68.0581**	**0.7**	**10.3**	**2.5**	**H7 12C4 13C ***
69.0709	63.56	69.0704	0.5	7.2	1.5	C5 H9
70.0739	**15.88**	**70.0738**	**0.1**	**1.4**	**1.5**	**H9 12C4 13C ***
77.039	11.05	77.0391	-0.1	-1.3	4.5	C6 H5
79.0549	45.26	79.0548	0.1	1.3	3.5	C6 H7
81.0709	79.2	81.0704	0.5	6.2	2.5	C6 H9
83.0865	36.37	83.0861	0.4	4.8	1.5	C6 H11
84.0887	**8.27**	**84.0894**	**-0.7**	**-8.3**	**1.5**	**H11 12C5 13C***
91.0546	12.74	91.0548	-0.2	-2.2	4.5	C7 H7
93.0708	51.62	93.0704	0.4	4.3	3.5	C7 H9

94.0741	**1.41**	**94.0738**	**0.3**	**3.2**	**3.5**	**H9 12C6 13C ***
95.0862	88.37	95.0861	0.1	1.1	2.5	C7 H11
96.0894	**9.61**	**96.0894**	**0**	**0**	**2.5**	**H11 12C6 13C ***
97.0654	11.84	97.0653	0.1	1	2.5	C6 H9 O
97.1012	20.66	97.1017	-0.5	-5.1	1.5	C7 H13
98.1053	**7.64**	**98.1051**	**0.2**	**2**	**1.5**	**H13 12C6 13C ***
107.0857	33.23	107.0861	-0.4	-3.7	3.5	C8 H11
109.1022	33.53	109.1017	0.5	4.6	2.5	C8 H13
110.1059	**7.02**	**110.1051**	**0.8**	**7.3**	**2.5**	**H13 12C7 13C ***
111.0818	6.43	111.081	0.8	7.2	2.5	C7 H11 O
111.1182	4.1	111.1174	0.8	7.2	1.5	C8 H15
121.1016	42.88	121.1017	-0.1	-0.8	3.5	C9 H13
122.1059	**0.81**	**122.1051**	**0.8**	**6.6**	**3.5**	**12C8 13C H13 ***
123.1176	6.49	123.1174	0.2	1.6	2.5	C9 H15
125.0958	3.59	125.0966	-0.8	-6.4	2.5	C8 H13 O
135.1173	33.37	135.1174	-0.1	-0.7	3.5	C10 H15
149.1332	14.17	149.133	0.2	1.3	3.5	C11 H17
153.1279	3.06	153.1279	0	0	2.5	C10 H17 O
163.1481	3.66	163.1487	-0.6	-3.7	3.5	C12 H19
167.1436	1.08	167.1436	0	0	2.5	C11 H19 O
248.2484	**2.7**	**248.2459**	**2.5**	**10.1**	**3.5**	**12C17 13C H31 ***
266.2568	**2.86**	**266.2565**	**0.3**	**1.1**	**2.5**	**H33 O 12C17 13C ***
310.2822	**6.55**	**310.2827**	**-0.5**	**-1.6**	**2.5**	**H37 O2 12C19 13C ***
340.2929	**39.68**	**340.2933**	**-0.4**	**-1.2**	**2.5**	**H39 O3 12C20 13C***

*[13]C containing fragment ion

Part II

Lipid modulating therapies; evaluation of animal models and siRNA mediated KD

Chapter 4

Anacetrapib a novel cholesteryl ester transfer protein inhibitor and its evaluation on the dyslipidemic Syrian golden hamster animal model

Anacetrapib a novel cholesteryl ester transfer protein inhibitor and its evaluation on the dyslipidemic Syrian golden hamster animal model

SUMMARY

Anacetrapib (ANA), a reversible inhibitor of cholesteryl ester transfer protein (CETP) raises HDL cholesterol and lowers LDL cholesterol in dyslipidemic patients. The purpose of this study was to determine the utility of a dyslipidemic hamster model to characterize compositional changes in plasma lipoproteins and fecal sterols in response to CETP inhibition, using an analytical LC/MS platform in combination with gel electrophoresis and fast protein liquid chromatograpy. Treatment of hamsters with ANA (60mg/kg/d, 2 weeks) inhibited CETP activity and increased total and HDL-cholesterol. In HDL, free cholesterol and cholesteryl esters were increased with ANA treatment, with the largest increase in cholesterol observed in large HDL compared to intermediate HDL. Major triglycerides (10 species of TG) were reduced in HDL and reciprocally increased in LDL with ANA-treatment. Fecal bulk cholesterol and cholic acid were increased with ANA treatment compared to vehicle, this finding was further substantiated by a macrophage-to-feces excretion experiment using ^{3}H-cholesterol where an increment of the levels of radioactivty were recorded for animals treated with ANA. In vitro, serum from ANA-treated hamsters also displayed greater cholesterol efflux capacity. These data indicate that ANA stimulates cholesterol efflux and cholesterol accumulation in HDL, which is associated with increased fecal cholesterol excretion. This study demonstrates the utility of the dyslipidemic Syrian golden hamster model to study regulation of lipoprotein composition by CETP and to evaluate the potential benefit of CETP inhibition on lipoprotein and cholesterol metabolism.

INTRODUCTION

Cardiovascular disease (CVD) is one of the major underlying causes for mortality in the USA and Europe (1-3) and increasingly in other geographies (4). Despite the significant number of therapies which specifically target the modulation of LDL cholesterol, cardiovascular events still remain high. Statins are the most widely prescribed drugs to treat dyslipidemia; however a large unmet medical need in the management of atherosclerosis still exists. Epidemiological studies have suggested that the presence of higher levels of HDL is associated with reduced cardiovascular risk (5-9). Therefore, alternative therapies that increase HDL cholesterol are being explored to take advantage of the inverse relationship between HDL and risk.

Cholesteryl ester transfer protein (CETP) has re-gained momentum as a possible target for treating cardiovascular disease. This is largely due to the recent discharging of the increased mortality observed with torcetrapib treatment in the ILLUMINATE study (10) as being attributed to off-target effects (11-14), and a lack of such effects with other CETP inhibitors including anacetrapib and dalcetrapib. Anacetrapib is a potent CETP inhibitor that has been shown to increase HDL cholesterol and reduce LDL cholesterol in humans in addition to statin therapy (15), and a recent phase III safety study (DEFINE) further supports the safety and tolerability of anacetrapib (16).

Preclinical animal models commonly utilized for studying CETP include rabbits and hamsters which naturally express CETP, in contrast to mice and rats which do not express CETP. The hamster model has been widely used for studying specific lipid therapies including ezetimibe and other lipid regulatory pathways (17-20). Although recent studies have reported the effects of CETP inhibition on cholesterol metabolism in normolipidemic hamsters (21), there are no reports of the effects of anacetrapib in dyslipidemic hamsters, which may better reflect human dyslipidemia.

The purpose of this study was to test the hypothesis that CETP inhibition with anacetrapib will raise HDL and lower LDL in a similar manner to what is observed in humans, and to test the effect of anacetrapib on plasma and fecal cholesterol parameters in Syrian golden hamsters fed a high fat diet.

MATERIALS AND METHODS

Animals

All animal work was performed in accordance with the Merck Research Laboratories Institutional Animal Care and Use Committee (Rahway, NJ). Male Syrian golden hamsters (weight at start of studies between100-120g) were placed on a dyslipidemic diet (Research Diets D08092301, 45% kcal from fat/lard, 0.12% cholesterol), provided *ad libitum* for 3 weeks prior to initiation of treatment. Anacetrapib was administered in the high fat diet to deliver a 60 mg/kg dosage. This dose was selected based on a pilot dose ranging study in which 60mg/kg produced maximum efficacy (effects on lipoproteins and CETP activity). Animals (n=8) were treated with Anacetrapib for 2 weeks. Control group consisted of animals (n=8) on a high fat diet with no drug treatment. A single time point terminal bleed was collected at the end of the study and serum samples were stored at -80°C until analyzed. Fecal samples were collected for 24 hrs prior to and after treatment with control and anacetrapib-containing diets. All individual fecal samples were weighed and recorded accordingly.

In a separate set of studies, the effects of anacetrapib on cholesterol absorption were examined. This was performed in two separate cohorts of dyslipidemic Syrian golden hamsters. In one group, animals were made dyslipidemic and treated with anacetrapib-containing diet or control diet as described above. In another cohort, dyslipidemic hamsters were treated with ezetimibe-containing diet (1.5mg/kg/day) or control diet for 2 weeks. For both studies, following treatment hamsters were treated with D_6-cholesterol (Sigma, St Louis, USA) at an oral dose of 12 mg/kg; feces were collected post tracer treatment for 24 hr, 48 hr, 72 hr and 96 hr. The fecal samples were frozen at -20°C until analyzed by LC/MS.

In vivo macrophage-to-feces reverse cholesterol transport

For this study, separate cohorts of animals (n= 12 vehicle and n=12 Anacetrapib 60mg/kg) were utilized and maintained at the same conditions as already mentioned. Preparation of J774 cells were performed as previously described (22). J774 cells obtained from the American Type Culture Collection (ATCC; Manassas, VA), were grown in suspension in RPMI/HEPES supplemented with 10% FBS and 0.5% gentamicin in suspension in Nalgene Teflon flasks. Cells were radiolabeled with 5 µCi/mL ^{3}H-cholesterol and cholesterol loaded with 50µg/mL oxidized LDL over 48 hours. Radiolabeled cells were then washed with RPMI/HEPES and equilibrated for 4 hr in fresh RPMI/HEPES supplemented with 0.2% BSA and gentamicin. Cells were pelletted by low speed centrifugation and resuspended in MEM/HEPES prior to injection into hamsters.

^{3}H-cholesterol–labeled and oxidized LDL-loaded J774 cells (2.5×10^6 cells containing 10×10^6 dpm in 0.5 mL minimum essential medium) were injected intraperitoneally into individually caged hamsters. Animals had free access to food and water, and were maintained on diet and treatment during the 72 hr experiment. Blood was collected by from the jugular vein under isoflurane anesthesia at 24, 48 and 72 hr to measure radioactivity released into the plasma and HDL after

phosphotungstate/MgCl$_2$ precipitation (50μL of plasma or HDL counted). Hamsters were then sacrificed by cervical dislocation, exsanguinated and liver was harvested from each animal. A ≈ 50mg-piece of liver was homogenized using an ultrasound probe in 500 μL water then 100 μL were counted in a liquid scintillation counter. Feces were collected over 72 hr and were stored at 4°C before extraction of cholesterol and bile acids.

Fecal cholesterol and bile acid extraction was performed as previously described (22). The total feces collected from 0 to 72 hr were weighed and soaked in Millipore water (1 mL water per 100 mg feces) overnight at 4°C. The following day, an equal volume of absolute ethanol was added, and the mixtures were homogenized. To extract the ^{3}H-cholesterol and ^{3}H-bile acid fractions, 1 mL of the homogenized samples was combined with 1 mL ethanol and 200 μL NaOH. The samples were saponified at 95°C for 1 hr and cooled to room temperature, and then ^{3}H-cholesterol was extracted 2 times with 3 mL hexane. The extracts were pooled, evaporated, resuspended in toluene, and then counted in a liquid scintillation counter. To extract ^{3}H-bile acids, the remaining aqueous portion of the feces was acidified with concentrated HCl and then extracted 2 times with 3 mL ethyl acetate. The extracts were pooled together, evaporated, resuspended in ethyl acetate, and counted in a liquid scintillation counter.

Results were expressed as % of the radioactivity injected recovered in plasma, HDL and liver and feces. The plasma volume was estimated as 3.5% of the body weight.

Serum CETP activity

CETP activity was determined by measuring the transfer of ^{3}H- cholesteryl oleate and ^{3}H- triolein from pre-labeled exogenous LDL to HDL by CETP in serum as previously described (23). Briefly, the assay was performed by incubating the serum with ^{3}H- labeled exogenous LDL for 90 min at 37°C. The transfer reaction was terminated by precipitation of LDL with 20% w/v PEG 8000 (1:1 vol.). The samples were centrifuged and an aliquot of the HDL-containing supernatant was counted for radioactivity measurement by liquid scintillation.

Ex-vivo cholesterol efflux assay

 Ex-vivo cholesterol efflux capacity of hamster serum was measured as described by Fournier *et al* (24) and Mweva *et al* (25) (VascularStrategies LLC, Wynnewood PA). ABCA1-mediated cholesterol efflux was determined in J774 mouse macrophages and SR-BI-mediated cholesterol efflux was assessed in Fu5AH rat hepatoma cells.

ApoB measurement by LC/MS

Serum samples (2μL) were diluted with 50 mM ammonium bicarbonate pH 8.0 followed by addition of GFEPT-[^{2}H$_{10}$]L-EALFGK (Bachem, Torrance, CA). The following peptide sequence was measured GFEPTLEALFGK for quantitation

purposes. 10 µL of a 10% sodium de-oxycholate solution was added to delipidate the lipoproteins, followed by reduction with dithiothreitol for 30 min at 60 °C, alkylation with iodoacetamide for 60 min at 25 °C in the dark, and protein digestion with trypsin overnight. A final volume of 200 µL 20% formic acid was added to stop digestion and precipitate sodium de-oxycholate. This was immediately followed by centrifugation at 15,800 rpm for 15 min. The supernatant was removed for LC/MS analysis using a Waters Acquity UPLC and Xevo triple quadrupole mass spectrometer (Xevo TQ, Waters, Manchester, UK). The gradient employed was 95% A (0.1% formic acid in water)/5% B (0.1% formic acid in acetonitrile) ramped to 80% A at 1 minute, 65% A at 4 min, 5% A at 5 min. The chromatographic separation was achieved by the use of a reverse phase column (Phenomenex Kinetex C18 50 x 2.1mm 1.7µm) operated at 50 °C with a column flow rate of 0.7 mL/min. The mass spectrometer was operated in electrospray positive ion mode.

Serum lipoprotein analysis by Fast Protein Liquid Chromatography and Gel Electrophoresis

Both fast protein liquid chromatography (FPLC) and gel electrophoresis were employed in this study to quantitate the cholesterol component in VLDL, LDL and HDL fractions.

For the FPLC method, EDTA serum was filtered and treated with lipase inhibitor (Paraoxan, Sigma, St Louis, USA) prior to analysis. The method comprised of a system equipped with fast performance liquid chromatography (FPLC) gel filtration using a Superose-6 size exclusion column (~24 ml, GE LifeSciences, Inc.) attached to a Dionex HPLC system. 25µl of serum was injected onto the column and eluted with PBS -/-buffer containing 1mM EDTA at a flow rate of 0.4 ml/min. The column effluent was mixed with a commercially available enzymatic colorimetric cholesterol detection reagent (total cholesterol E, Wako USA) that was delivered at a rate of 0.2 ml/min. After passing through a 1,500ul knitted reaction coil (~15 min) that was maintained in a 37°C heated chamber, the reaction mixture was read at 600nm absorbance using a photodiode array (PDA) detector. The first peak of cholesterol eluted from the column was attributed to VLDL, the second peak to IDL/LDL and the third to HDL. The area under each peak was calculated using Chromeleon software™ provided with the HPLC (Dionex, Inc). To calculate the cholesterol concentration for each lipoprotein fraction, the ratio of the corresponding peak area to total peak area was multiplied by the total cholesterol concentration measured in the sample as determined using the Total Cholesterol E Kit by Wako (Richmond, VA).

Gel electrophoresis was carried out using a commercially available kit according to the manufacturer's instructions (Lipoprint®, Quantimetrix, Redondo Beach, CA). Briefly, 25 µL of serum was loaded in the gel followed by staining with Sudan black B for cholesterol and cholesterol esters quantitation in the lipoprotein bands. The gels were scanned and cholesterol measurements were conducted by entering the total cholesterol levels previously measured by the Wako E cholesterol kit (Richmond, VA).

To assess lipid composition in lipoprotein particles, VLDL, LDL and HDL lipoprotein bands were cut from Lipoprint gels. The gel fragments were placed in homogenization tubes, 400 µL phosphate buffered saline (PBS) was added to the

VLDL and HDL bands and 1000 µL of PBS was used for the IDL and LDL bands. The gel fragments were homogenized at 5,000 rpm for 15 secs at room temperature. Homogenates were centrifuged at a speed of 20,000 rpm 10°C, for 10 min. And the resulting supernatant was extracted for lipids using the Bligh and Dyer method (26).

Lipid analysis by LC/MS was conducted using non endogenous internal standards [(1,2-diheptadecanoyl-sn-glycero-3-phosphocholine (PC 17:0/17:0), 1-heptadecanoyl-2-hydroxy-sn-glycero-3-phosphocholine (LysoPC 17:0), triheptadecanoin (TG 17:0/17:0/17:0) , cholesteryl ester (CE 17:0) (Avanti Lipids, Alabaster, AL) and D_6-cholesterol (Sigma, St Louis, MO)] standards were added to samples at a final concentration of 1 µg/mL. In addition to this, external lipid calibrants (cholest-5-en-3β-yl hexadecanoate (CE 16:0), cholest-5-en-3β-yl octadecanoate (CE 18:0), cholest-5-en-3b-yl (9Z-octadecenoate) (CE 18:1), cholest-5-en-3β-yl (9Z,12Z-octadecadienoate) (CE 18:2), cholest-5-en-3β-yl (9Z,12Z,15Z-octadecatrienoate) (CE 18:3), cholest-5-en-3β-yl (5Z,8Z,11Z,14Z-eicosatetraenoate) (CE 20:4), and cholest-5-en-3β-yl (4Z,7Z,10Z,13Z,16Z,19Z-docosahexaenoate) (CE 22:6) and free cholesterol (Avanti Lipids, Alabaster, AL)) in buffer ranging from 0.01 - 2 µg/mL were used for free cholesterol and cholesteryl ester lipid quantitation.

The subsequent lipid extracts were analyzed on a hybrid orthogonal quadrupole time of flight mass spectrometer (Synapt G2 HDMS, Waters, Manchester, UK). Positive electrospray ionization (ESI) mode was utilized for the CE and TG analysis and atmospheric pressure photoionization (APPI) mode was utilized for the measurement of free cholesterol in the lipoprotein fractions as described by Castro-Perez *et al* (27). The mass spectrometer was coupled to an inlet system comprised of an Acquity UPLC (Waters, Milford, MA, USA). The lipid extracts were injected (10µL) onto a 1.8 µm particle 100 x 2.1 mm id Waters Acquity HSS T3 column (Waters, Milford, MA, USA); the column was maintained at 55 °C. The flow rate used for these experiments was 0.4 mL/min. A binary gradient system consisting of acetonitrile (Burdick & Jackson, USA) and water with 10 mM ammonium formate (Sigma-Aldrich, St Louis, MO) (40:60, v/v) was used as eluent A. Eluent B, consisted of acetonitrile and isopropanol (Burdick & Jackson, USA) both containing 10 mM ammonium formate (10:90, v/v). The sample analysis was performed by using a linear gradient (curve 6) over a 15 min total run time; during the initial portion of the gradient, it was held at 60% A and 40% B. For the next 10 min the gradient was ramped in a linear fashion to 100% B and held at this composition for 2 min hereafter the system was switched back to 60% B and 40% A and equilibrated for an additional 3 min.

Fecal cholesterol and bile acid composition analysis by LC/MS

Fecal samples from each time point were weighed and homogenized as follows; 10 mL of 80% methanol 20% water was added to the fecal samples in 50mL Falcon tubes. The volume was increased to 20 mL if the weight of feces per animal exceeded 2g. The samples were then allowed to stand at room temperature for approximately 30 min. After this process was completed, the fecal matter was homogenized at a speed of 30,000 rpm for 3 min. For neutral lipid extraction 200µL of the homogenate was transferred to a 1.5 mL eppendorff tube, and 320 µL of dichloromethane containing 10ug/mL D_6-cholesterol (ISTD) and 5 µg/mL D_6-cholesterol ester 18:2 internal standard was added to all the samples. For cholesterol

absorption, instead $^{13}C_{18}$ CE 18:1 was used as the internal standard. Samples were vortexed for 60 secs and 80µL of H_2O was added to each sample followed by another vortex cycle of 60 secs. In order to create a two-phase liquid layer, the samples were centrifuged at 20,000 rpm, 10ºC for 10 min. 75µL of the lower organic layer was transferred to a deep 96-deep well plate and diluted with 300 µL of injection solvent (65% Acetonitrile: 30% Isopropanol: 5 % water). The plate was then centrifuged at 4,000 rpm for 10 minutes to pellet any residual solids. 100µL of the supernatant was transferred to a new 96-well plate which was then sealed before analysis by LC/MS. An external cholesterol calibration curve (0.01-20 µg/mL) in buffer was used to quantify D_6-cholesterol.

For bile acid extraction from the fecal samples, 10µL of the fecal homogenate was transferred to a 1.5mL eppendorff tube and diluted with 490µL of 80% methanol containing 500nM D_4-cholic acid, D_4-glycocholic acid, D_4-chenodeoxycholic acid & D_5-lithocholic acid as the internal standards. The resulting mixture was then vortexed for 60 seconds. This was followed by centrifugation at 10,000 RPM for 10 minutes at 10ºC. Finally, the samples were transferred (100µL) of the supernatant to a 96 well plate and centrifuged again for 10 minutes to pellet any residual solids. The supernatant was transferred to a new 96-well plate and care was taken to avoid disturbance of any pellet for analysis. For quantitation of bile acids present in the feces, external calibrants in buffer were utilized in the range of 0.02µM -4µM for Lithocholic acid (LCA) , Glycholic acid (GCA) , Taurocholic acid (TCA), Deoxycholic acid (DCA), Cholic acid (CA), Chenodeoxycholic acid (CDCA), Glycochenodeoxycholic acid (GCDCA) and Taurochenodeoxycholic acid (TCDCA) (Sigma, St Louis, MO). Resulting analyte concentrations for the samples were computed against each calibration line for the corresponding bile acid.

Data processing and statistical analysis

Data processing was conducted using the instrument manufacturer software for the lipoprotein analysis using FPLC and GGE. Lipid composition and quantitation analysis work by LC/MS was carried out using MassLynx (Waters, Milford, USA). For statistical analysis; all the figures are presented as ± standard error mean (SEM). Differences between groups were computed by unpaired Student's *t-test* with two-tailed p-values statistical analysis (GraphPad Prism, La Jolla, CA). A p-value of <0.05 was considered as being statistically significant.

Lipid nomenclature

The lipid nomenclature utilized throughout the manuscript is the same as described by Fahy *et al.* (28). For instance, CE 18:1 denotes cholesteryl ester containing 18 hydrocarbons and 1 double bond as the fatty acyl substituent. Equally the same applies to triglycerides cited in the manuscript. For example TG 54:3, translates to a triglyceride containing 54 hydrocarbons attached to the glycerol back-bone and a total of 3 double bonds, which forms part of the 3 fatty acyl substituents.
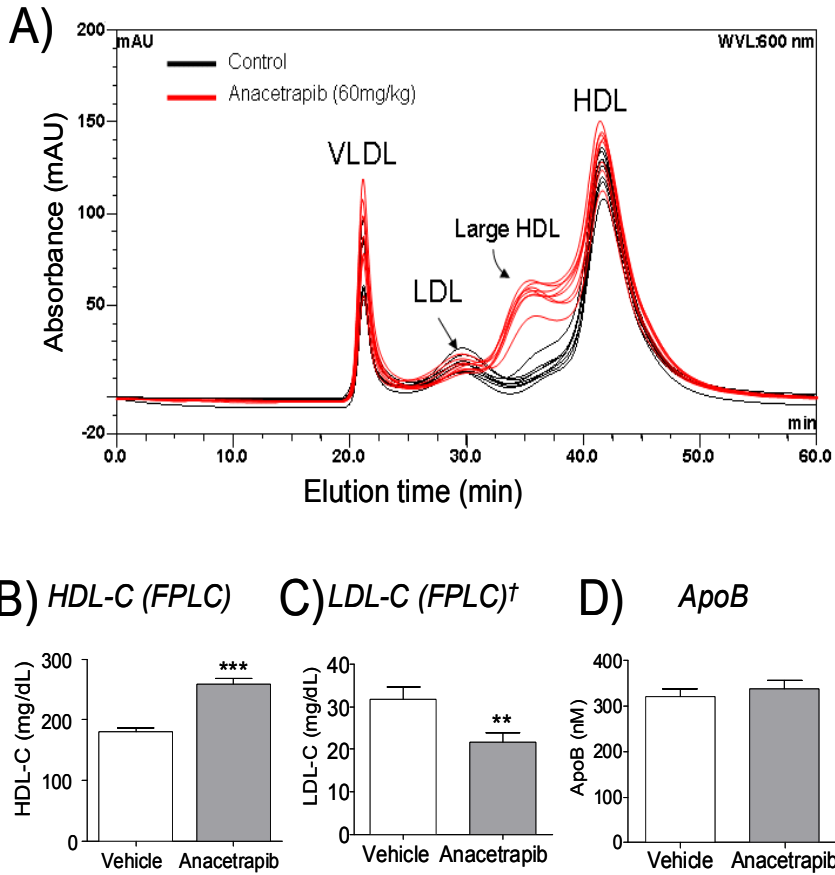
RESULTS

Anacetrapib treatment of dyslipidemic Syrian golden hamsters results in reduced CETP activity

Anacetrapib-treated hamsters showed a reduction in serum CETP activity, manifest as a reduction in both cholesteryl ester and triglyceride transfer (46% and 47% reduction respectively) compared to the vehicle treated animals (Figure 1A, B).
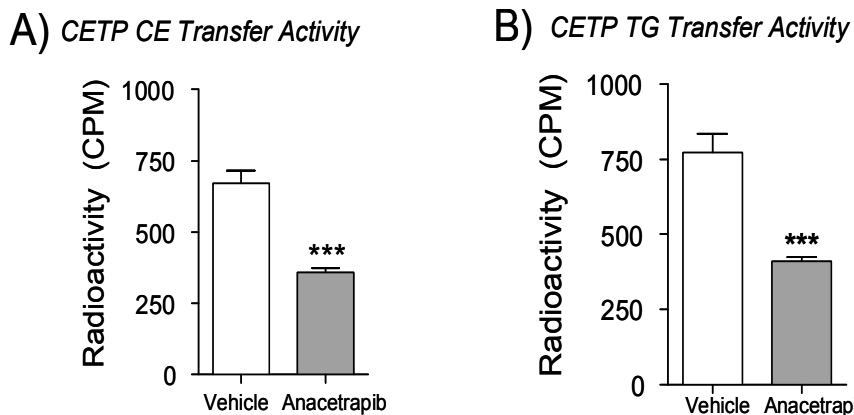
Figure 1. Anacetrapib treatment (60mg/kg, 2 weeks) inhibits serum CETP transfer activity for (A) cholesterol esters (B) and triglyceride ***P<0.001 vs. vehicle.

FPLC analysis of hamster serum (Figure 2A) showed a 43% increase in HDL-cholesterol (Figure 2B) and 32% reduction in LDL-cholesterol (Figure 2C) compared to vehicle-treated controls. Figure 3A depicts the analysis of the same samples by GGE showing a very comparable increase in the level of HDL-cholesterol (53% increase compared to vehicle), but no change in LDL-cholesterol (Figure 3B and C respectively).
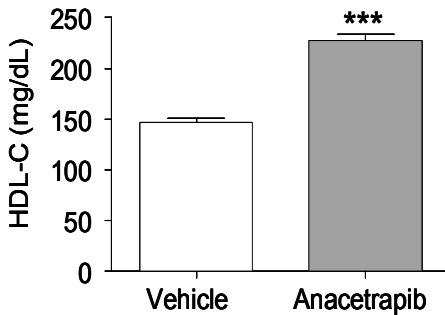
Figure 2. Anacetrapib treatment (60mg/kg, 2 weeks) results in (A) formation of large HDL particles, (B) increased HDL-cholesterol, (C) apparent reduction in LDL from FPLC analysis and (D) no change in plasma apoB **$P<0.01$, ***$P<0.001$ vs. vehicle. †*presence of large HDL confounds resolution of LDL peak*
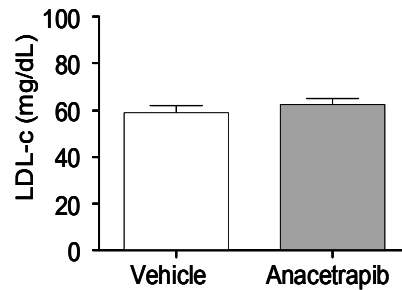
A) *Lipoprint analysis of lipoprotein associated cholesterol*
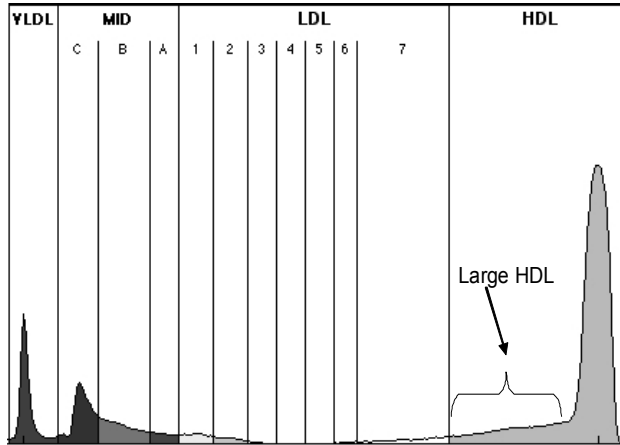

## B) *Total HDL-c (Lipoprint)*   C) *Total LDL-c (Lipoprint)*

Figure 3. Gradient gel electrophoresis separation of lipoproteins (A) Trace from Lipoprint® scan following gradient gel electrophoresis of Ana-treated hamster serum (60mg/kg, 2 weeks) (B) Anacetrapib treatment increases total HDL-cholesterol with (C) no effect on total LDL-cholesterol ***$P<0.001$ vs. vehicle

For analysis of lipid composition in the VLDL and LDL fraction (IDL and LDL bands from gradient gel electrophoresis subfractions were combined as one fraction) CE and FC were measured by LC/MS. These measurements did not reveal any significant changes between the ANA and control groups (Figure 4A, B and C). HDL subfractions were also measured using an HDL specific lipoprotein electrophoresis kit. In this case, the large HDL from anacetrapib-treated hamsters contained 89% more cholesterol than in the vehicle group (p<0.0001) and the intermediate HDL subfraction 29% more cholesterol than in the vehicle group (p<0.01) (Figure 5A)
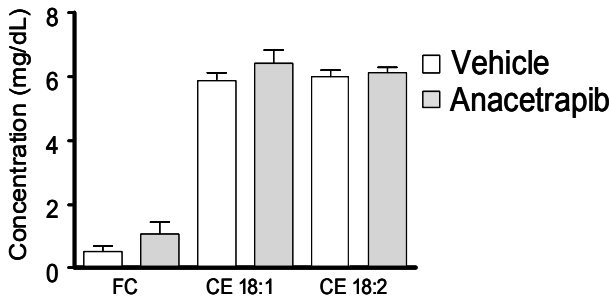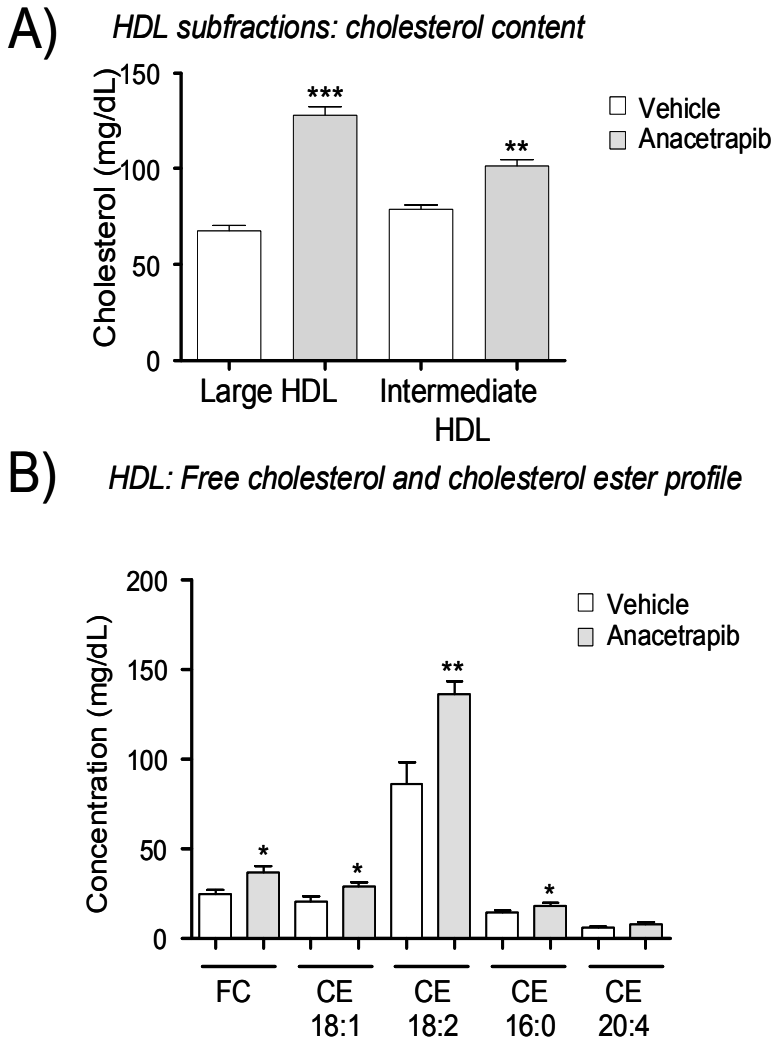
A) LDL subfractions: cholesterol content
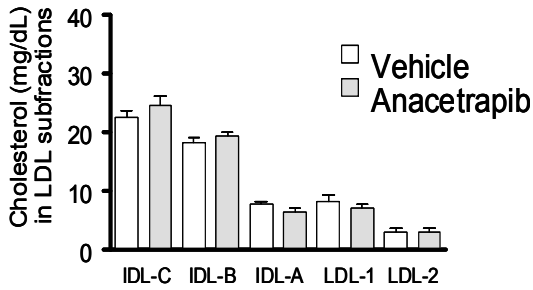
B) LDL: Free cholesterol and cholesterol ester profile
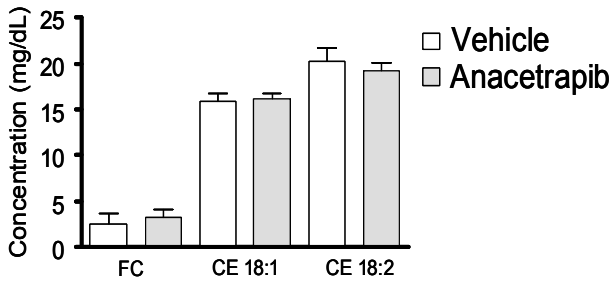
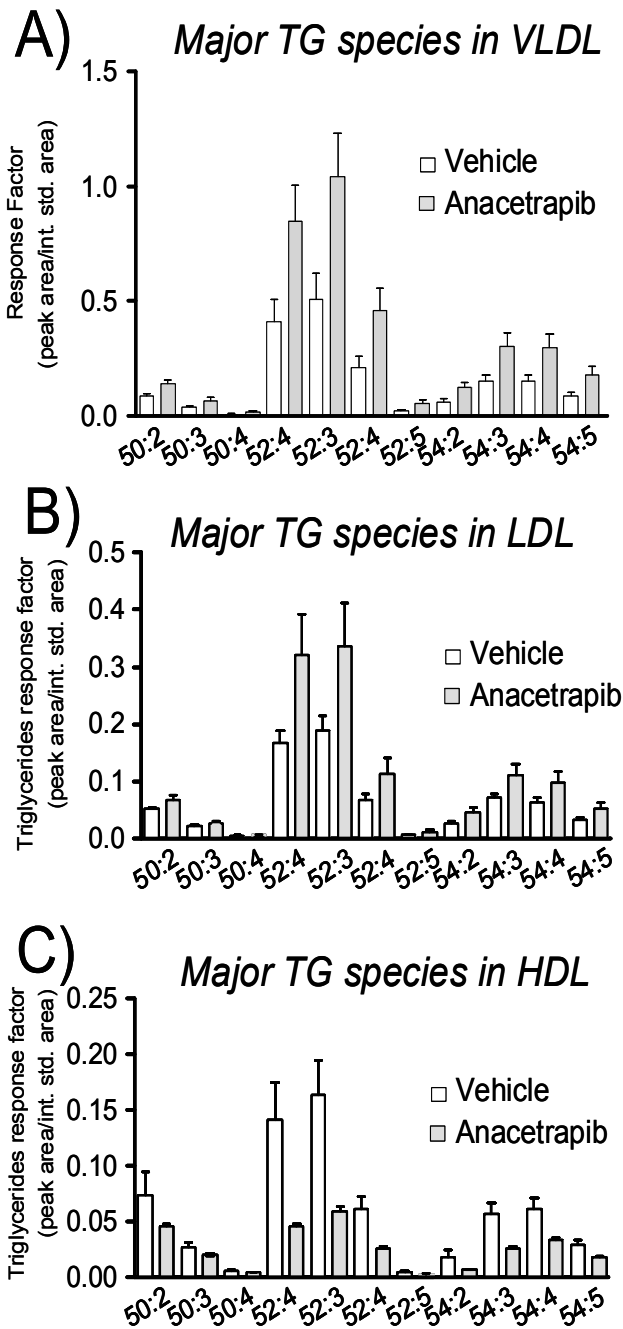## C) VLDL: Free cholesterol and cholesterol ester profile

Figure 4. Gradient gel electrophoresis LDL subfraction analysis. (A) Distribution of cholesterol in subfractions of LDL. VLDL and LDL cholesterol composition analyzed by LC/MS. (B) Free cholesterol and major cholesteryl ester species present in total LDL and (C) Free cholesterol and major cholesteryl ester species present in total VLDL

Figure 5. HDL cholesterol composition analyzed by LC/MA (A) Distribution of cholesterol in subfractions of HDL, (B) Free cholesterol and major cholesteryl ester species present in total HDL.*P<0.05, **P<0.01, ***P<0.001 vs. vehicle

The added specificity of LC/MS permitted investigation of the lipid composition for different CE's and FC in the VLDL, LDL and HDL particles. The HDL fraction measurement by LC/MS (Figure 5B) showed statistically significant increases of FC (33% anacetrapib vs. vehicle (p<0.05), CE 18:1 (41% anacetrapib vs. vehicle (p<0.05), CE 18:2 (57% anacetrapib vs. vehicle (p<0.01), CE 16:0 (26% anacetrapib vs. vehicle (p<0.05) and CE 20:4 (35% anacetrapib vs. vehicle (p=0.0523) in the anacetrapib treated animals vs. the vehicle group. When triglyceride levels in the VLDL, LDL and HDL lipoprotein fractions were measured by LC/MS, it was observed that for the HDL fraction the level of the TG was significantly reduced ~180% (Figure 6C) in the anacetrapib treated group vs. the control group. For the VLDL and LDL

fraction TG levels were ~ 80-100% higher (Figure 6A and B respectively) than in the vehicle group, supporting the notion that CETP mediated TG transfer was inhibited by anacetrapib.

Figure 6. Triglyceride composition of (A) VLDL, (B) LDL and (C)) HDL, isolated by gradient gel electrophoresis and analyzed by LC/MS.

Fecal bulk cholesterol excretion and promotion of reverse cholesterol transport following CETP inhibition

Treatment with anacetrapib resulted in an increased concentration of cholesterol in the feces by 29.6% $p<0.05$ (Figure 7A) with respect to the vehicle groups after the initial 2 week period in which the animals were equilibrated with the HF diet. Cholic acid excretion (Figure 7B) showed a very similar pattern as the cholesterol excretion, reaching steady excretion state at 2 weeks following the HFD and with anacetrapib treatment a net increase on the excretion of CA of 28.5% $p<0.05$.
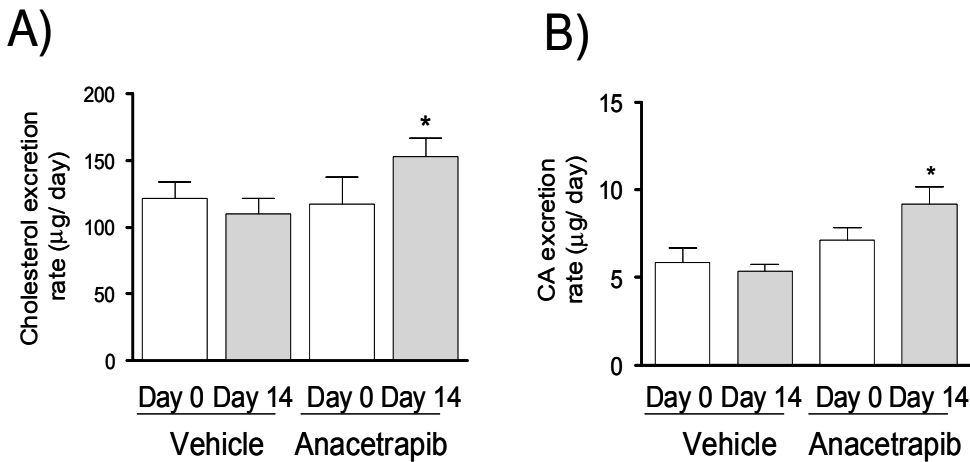
Figure 7. Anacetrapib treatment increases concentration of (A) fecal cholesterol, and (B) fecal cholic acid after 14 days of treatment (24hr collection of feces post-treatment). * *P*<0.05 vs. day 0

In order to evaluate whether anacetrapib treatment influenced RCT, radiolabeled cholesterol-loaded macrophages were injected in hamsters following treatment with either control or anacetrapib-containing diets as described in the materials and methods section. Figure 8A shows the appearance of radio-tracer in plasma was 20% higher in animals treated with anacetrapib compared to controls at 72h. HDL plasma (figure 8B) resulted in an increment of 69% of radio- tracer for anacetrapib-treated animals than that of control animals at 72h. Liver radioactivity data (figure 8C) resulted in a reduction of 29% for animals treated with anacetrapib in comparison to the control group. Fecal excretion of ^{3}H-cholesterol and radiolabeled bile acids for the anacetrapib treatment showed a higher degree of injected radioactivity than in the control group (figure 8D).
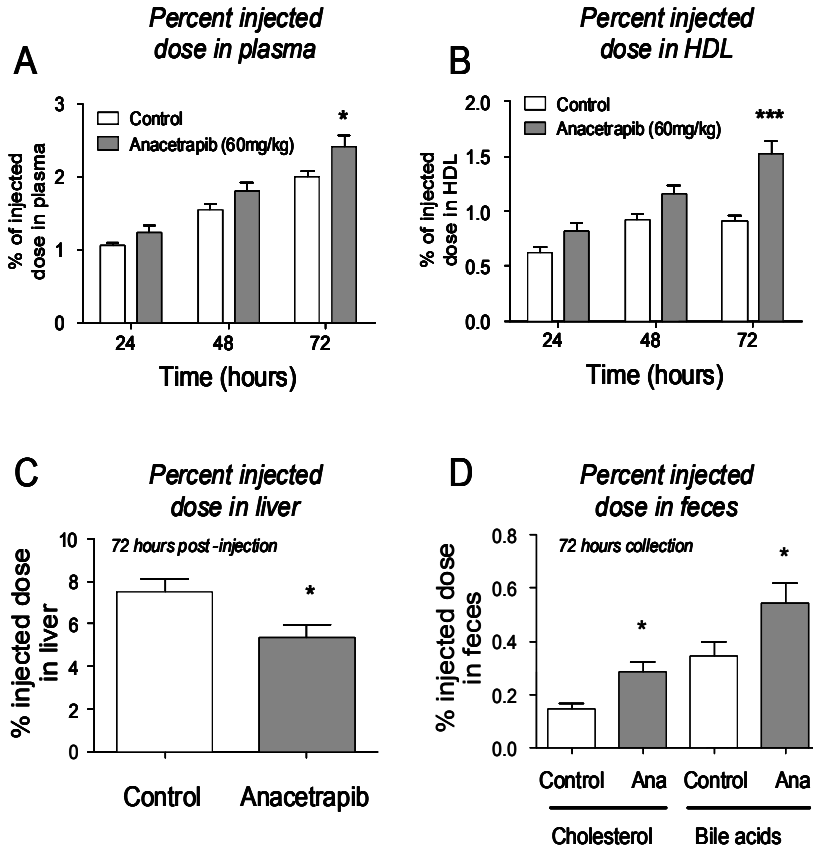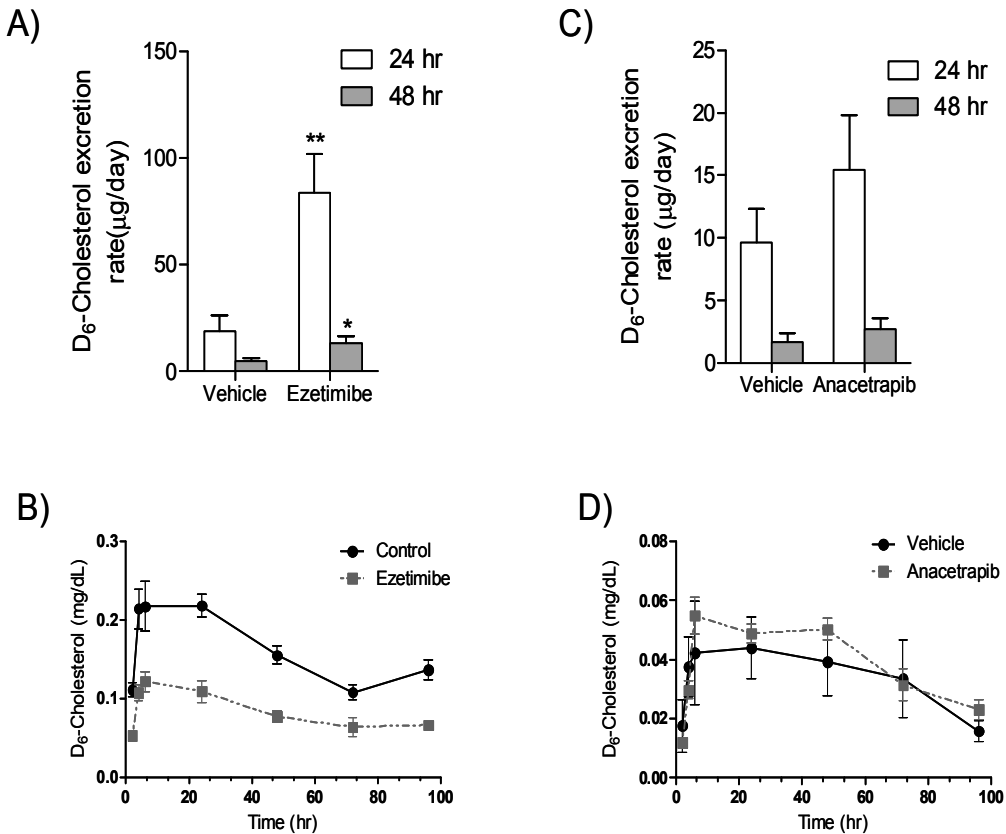
Figure 8.Anacetrapib treatment (60mg/kg, 2 weeks) of dyslipidemic hamsters and effects on macrophage-to-feces RCT. A) ^{3}H-tracer recovery in plasma, B) ^{3}H-tracer recovery in HDL fraction of plasma, C) ^{3}H-tracer recovery in liver tissue, D) ^{3}H-tracer recovery in fecal cholesterol and bile acid fraction. ***$P<0.001$, *$P<0.05$ vs. control. Open bars = control, solid bars = anacetrapib treated

To determine whether the increase in fecal cholesterol content was possibly due to effects on absorption, D_6-labeled cholesterol was used in two experiments to track removal of cholesterol from the gastrointestinal tract, by measurement of changes in D_6-labeled cholesterol in the feces after oral dosing. In both experiments, D_6-cholesterol appeared in the feces over the course of 48hr for control and treated groups (Figure 8A and C), and were undetectable beyond 48hr (data not shown). It should be noted that the ezetimibe and anacetrapib experiments were performed in separate cohorts of animals, which may explain the differences in the absolute values for fecal and plasma D_6-cholesterol between vehicle groups from both experiments.

In the experiment using ezetimibe, treated animals, showed significantly higher levels of D_6 cholesterol in the feces at both 24 and 48 hr compared to control (Figure 9A). In the anacetrapib experiment, animals treated with anacetrapib showed no significant differences in the level of D_6-cholesterol in the feces compared to control at 24 and 48hr (Figure

9C). Plasma circulating levels of D_6-cholesterol were determined by LC/MS measurements. For animals treated with anacetrapib (Figure 9D) there was a slight increase (15%) in plasma D_6-cholesterol compared to vehicle (AUC for all time points) while for ezetimibe-treated animals (Figure 9B) there was a significant drop (99.6% reduction in AUC) in plasma D_6-cholesterol compared to vehicle.

Figure 9. Anacetrapib does not affect cholesterol absorption (2 weeks treatment at 60mg/kg in-feed). (A) Fecal D6-cholesterol excretion over 48hr for vehicle and ezetimibe treated hamsters. (B) Plasma levels of D6-cholesterol in plasma for vehicle and ezetimibe treated hamsters. (C) Fecal D6-cholesterol excretion over 48hr for vehicle and anacetrapib treated hamsters. (D) Plasma levels of D6-cholesterol in plasma for vehicle and anacetrapib treated hamsters **$P<0.01$ ezetimibe 24 hr vs. vehicle 24 hr * $P<0.05$ ezetimibe 48 hr vs. vehicle 48 hr

HDL from dyslipidemic hamsters treated with anacetrapib exhibited increased cholesterol efflux capacity

A statistically significant increase in SR-BI mediated efflux was observed in HDL from anacetrapib treated animals group compared to the vehicle-treated animals (Figure 10A). In the J774 efflux assay, ABCA1-mediated efflux was increased in HDL from anacetrapib-treated hamsters compared to vehicle. In the absence of cAMP (which stimulates ABCA1 expression in these cells), there was no difference in efflux values, indicating the specificity for ABCA1-mediated efflux (Figure 10B).
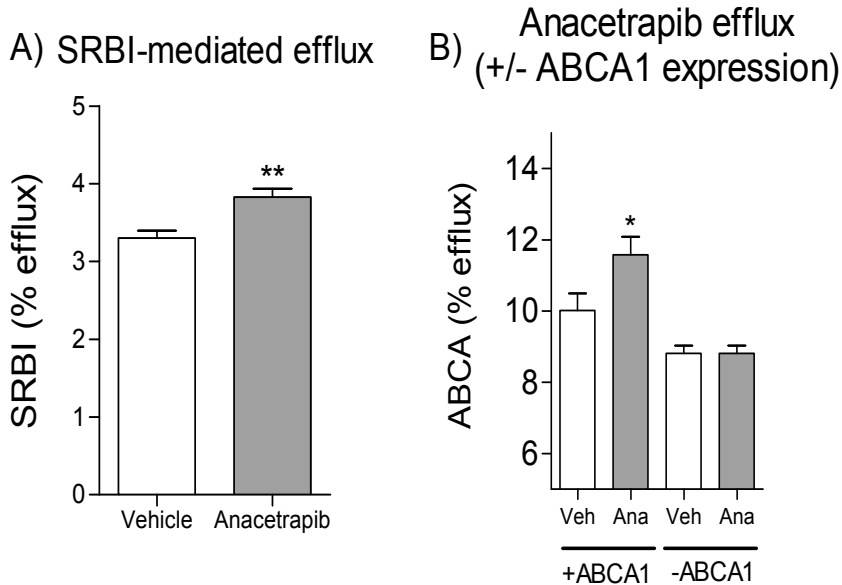
Figure 10. *In vitro* cholesterol efflux was increased by hamsters treated with anacetrapib in comparison with the control. (A) SR-BI mediated cholesterol efflux. (B) Cholesterol efflux +/- ABCA1 expression.

*$P<0.05$, **$P<0.01$ vs. vehicle

DISCUSSION

In order to fully understand the mechanism of action of CETP inhibitors such as anacetrapib, a multi-faceted approach in an appropriate animal model should be used. The purpose of this study was to evaluate the dyslipidemic Syrian golden hamster treated with anacetrapib as a model to study CETP biology. By comprehensively analyzing plasma lipoprotein-associated cholesterol, detailed lipoprotein composition, and parameters related to fecal cholesterol excretion, this study uncovered clear utility in the use of dyslipidemic hamsters for studying HDL cholesterol handling, but also raised some discrepancies which may affect its use in studying integrated lipoprotein metabolism.

One aim of this study was to characterize the cholesterol and triglyceride composition of lipoproteins in response to CETP inhibition. In the case of HDL, LC/MS analysis of the HDL band excised from gradient gels showed that all sterols (free cholesterol and cholesteryl esters) were up-regulated in the HDL fraction, with CE 18:2 (cholesteryl linoleate) being the most abundant cholesteryl ester in HDL. This observation is consistent with studies in rodents that lecithin/cholesteryl acyl transferase (LCAT) preferentially hydrolyses phosphatidylcholines containing linoleate as the fatty acyl motif in the *sn-2* position for esterification of cholesterol on HDL (29, 30). Whether this substrate preference of LCAT for linoleate-containing phosphatidylcholines contributes to the predominance of cholesteryl linoleate in CETP-inhibited hamster HDL requires further study**.**

The increase in HDL free cholesterol is supportive of the notion that cholesterol efflux to HDL is improved with CETP inhibition. Indeed, it was observed *in vitro* that HDL efflux from cultured macrophages was increased in HDL from anacetrapib-treated animals. This observation is in line with studies where HDL from humans treated with anacetrapib (31) or CETP-deficient humans (32) display greater efflux capacity from cultured macrophages, and supports the use of this model to study cholesterol flux regulated by CETP, and to test the effects of CETP inhibition and movement of cholesterol into the feces for excretion.

It was observed that the fecal concentration of cholesterol and cholic acid (in a 24hr collection following 2 weeks of treatment) was increased in hamsters treated with anacetrapib, an effect that could not be attributed to alterations in cholesterol absorption from the intestine. An increase in both fecal neutral sterols and bile acids with CETP inhibition, taken together with the observation of increased free cholesterol and cholesterol ester in HDL and improved HDL efflux capacity, indicates that anacetrapib may be promoting reverse cholesterol transport, shifting cholesterol through the HDL pool and into the feces through biliary excretion. The current study utilized dyslipidemic hamsters, where it is possible that more cholesterol is being exchanged by CETP and could better reflect the human dyslipidemic state. While the combination of changes in lipoprotein composition, fecal cholesterol/bile acid, and HDL efflux capacity all point towards improvement of a net increase in cholesterol excretion, examination of true "macrophage-to-feces reverse cholesterol transport" provides more direct evidence. In this research, it was observed a marked increased of radio-tracer for both 'hot' cholesterol and bile acids in the anacetrapib treatment group, suggesting promotion of macrophage-to-feces reverse

cholesterol transport using standard methods as described by Rader and Rothblat (33-36). In combination, these studies support the hypothesis that anacetrapib promotes reverse cholesterol transport in a hamster model of dyslipidemia. Taken together with the *in vitro* cholesterol efflux data from the current study, which recapitulated observations from anacetrapib-treated and CETP-deficient humans, the dyslipidemic hamster appears to have significant utility in studying HDL-dependent cholesterol excretion.

In the case of LDL-cholesterol, due to the presence of enlarged HDL particles, the apparent reduction of LDL cholesterol observed with FPLC analysis was concluded to be artifactual, by (i) a lack of effect of treatment on serum apoB levels (Figure 2D), and (ii) a lack of effect of treatment on LDL-cholesterol analyzed by gradient gel electrophoresis and LC/MS analysis. From this analysis, gradient-gel electrophoresis with post-hoc LC/MS analysis of cholesterol species was used for more detailed characterization of lipoprotein composition as it appeared to achieve better resolution between LDL and HDL peaks with CETP inhibition. This analysis further supported of a lack of an LDL cholesterol-lowering effect by anacetrapib in this model, with the observation of no change in cholesterol species (free cholesterol, cholesteryl ester) in any of the LDL subfractions or VLDL isolated from gradient gels. Regardless, the reduction of major triglyceride species in HDL and reciprocal increase of triglycerides in LDL and in VLDL showed that inhibition of transfer activity of CETP in the hamster does affect the lipid composition. It is possible that CETP in hamsters plays a greater role in triglyceride transfer out of LDL into HDL rather than movement of cholesterol into LDL, but this requires a more in-depth investigation. Although hamsters express CETP endogenously, they do still carry the majority of their cholesterol on HDL. Placement of hamsters on a high-fat supplemented with cholesterol, as in the current study, has been shown to increase LDL cholesterol (37), but this still did not unmask an effect of CETP inhibition on LDL. Other CETP-containing species, such as nonhuman primates, in which the distribution of cholesterol across lipoproteins is more similar to humans, may be of significant utility in recapitulating the LDL reduction observed in human subject with anacetrapib.

In summary, this study reported changes in lipoprotein composition with CETP inhibition by anacetrapib in the dyslipidemic hamster. The lack of an LDL-lowering effect by anacetrapib in this model, which is not a high-LDL-cholesterol model, limits its utility. However, the changes in HDL lipid composition, coupled with increased fecal sterol excretion and increased HDL cholesterol efflux capacity, indicate that anacetrapib is promoting cholesterol excretion in this model, possibly via reverse cholesterol transport.

REFERENCES

1. Rayner, M., Allender, S., and Scarborough, P. (2009) *Eur J Cardiovasc Prev Rehabil* **16 Suppl 2,** S43-7.

2. Menotti, A., Lanti, M., Puddu, P. E., and Kromhout, D. (2000) *Heart* **84,** 238-44.

3. Rosamond, W., Flegal, K., Furie, K., Go, A., Greenlund, K., Haase, N., Hailpern, S. M., Ho, M., Howard, V., Kissela, B., Kittner, S., Lloyd-Jones, D., McDermott, M., Meigs, J., Moy, C., Nichol, G., O'Donnell, C., Roger, V., Sorlie, P., Steinberger, J., Thom, T., Wilson, M., and Hong, Y. (2008) *Circulation* **117,** e25-146.

4. Zhang, X. H., Lu, Z. L., and Liu, L. (2008) *Heart* **94,** 1126-31.

5. Gordon, T., Castelli, W. P., Hjortland, M. C., Kannel, W. B., and Dawber, T. R. (1977) *Am J Med* **62,** 707-14.

6. Miller, N. E., Thelle, D. S., Forde, O. H., and Mjos, O. D. (1977) *Lancet* **1,** 965-8.

7. Keys, A. (1980) *Lancet* **2,** 603-6.

8. Jacobs, D. R., Jr., Mebane, I. L., Bangdiwala, S. I., Criqui, M. H., and Tyroler, H. A. (1990) *Am J Epidemiol* **131,** 32-47.

9. Kitamura, A., Iso, H., Naito, Y., Iida, M., Konishi, M., Folsom, A. R., Sato, S., Kiyama, M., Nakamura, M., Sankai, T., and et al. (1994) *Circulation* **89,** 2533-9.

10. Barter, P. J., Caulfield, M., Eriksson, M., Grundy, S. M., Kastelein, J. J., Komajda, M., Lopez-Sendon, J., Mosca, L., Tardif, J. C., Waters, D. D., Shear, C. L., Revkin, J. H., Buhr, K. A., Fisher, M. R., Tall, A. R., and Brewer, B. (2007) *N Engl J Med* **357,** 2109-22.

11. Forrest, M. J., Bloomfield, D., Briscoe, R. J., Brown, P. N., Cumiskey, A. M., Ehrhart, J., Hershey, J. C., Keller, W. J., Ma, X., McPherson, H. E., Messina, E., Peterson, L. B., Sharif-Rodriguez, W., Siegl, P. K., Sinclair, P. J., Sparrow, C. P., Stevenson, A. S., Sun, S. Y., Tsai, C., Vargas, H., Walker, M., 3rd, West, S. H., White, V., and Woltmann, R. F. (2008) *Br J Pharmacol* **154,** 1465-73.

12. Stroes, E. S., Kastelein, J. J., Benardeau, A., Kuhlmann, O., Blum, D., Campos, L. A., Clerc, R. G., and Niesor, E. J. (2009) *Br J Pharmacol* **158,** 1763-70.

13. Polakowski, J. S., King, A. J., Campbell, T. J., Nelson, R. A., Preusser, L. C., Kempf-Grote, A. J., Marsh, K. C., Gintant, G. A., Cox, B. F., and Mittelstadt, S. W. (2009) *J Cardiovasc Pharmacol* **54,** 543-51.

14. DePasquale, M., Cadelina, G., Knight, D., Loging, W., Winter, S., Blasi, E., Perry, D., and Keiser, J. (2009) *Drug Development Research* **70,** 35-48.

15.　　Bloomfield, D., Carlson, G. L., Sapre, A., Tribble, D., McKenney, J. M., Littlejohn, T. W., 3rd, Sisk, C. M., Mitchel, Y., and Pasternak, R. C. (2009) *Am Heart J* **157,** 352-360 e2.

16.　　Cannon, C. P., Shah, S., Dansky, H. M., Davidson, M., Brinton, E. A., Gotto, A. M., Stepanavage, M., Liu, S. X., Gibbons, P., Ashraf, T. B., Zafarino, J., Mitchel, Y., and Barter, P. *N Engl J Med* **363,** 2406-15.

17.　　Bilz, S., Samuel, V., Morino, K., Savage, D., Choi, C. S., and Shulman, G. I. (2006) *Am J Physiol Endocrinol Metab* **290,** E716-22.

18.　　Woollett, L. A., and Spady, D. K. (1997) *J Clin Invest* **99,** 1704-13.

19.　　Woollett, L. A., Spady, D. K., and Dietschy, J. M. (1992) *J Clin Invest* **89,** 1133-41.

20.　　Liu, G. L., Fan, L. M., and Redinger, R. N. (1991) *Comp Biochem Physiol A Comp Physiol* **99,** 223-8.

21.　　Niesor, E. J., Magg, C., Ogawa, N., Okamoto, H., von der Mark, E., Matile, H., Schmid, G., Clerc, R. G., Chaput, E., Blum-Kaelin, D., Huber, W., Thoma, R., Pflieger, P., Kakutani, M., Takahashi, D., Dernick, G., and Maugeais, C. *J Lipid Res* **51,** 3443-54.

22.　　Briand F, Treguier M, Andre A, Grillot D, Issandou M, Ouguerram K, Suplice T. *J Lipid Res* **51**:732-770, 2010.

23.　　Ranalletta, M., Bierilo, K. K., Chen, Y., Milot, D., Chen, Q., Tung, E., Houde, C., Elowe, N. H., Garcia-Calvo, M., Porter, G., Eveland, S., Frantz-Wattley, B., Kavana, M., Addona, G., Sinclair, P., Sparrow, C., O'Neill, E. A., Koblan, K. S., Sitlani, A., Hubbard, B., and Fisher, T. S. *J Lipid Res* **51,** 2739-52.

24.　　Fournier, N., Francone, O., Rothblat, G., Goudouneche, D., Cambillau, M., Kellner-Weibel, G., Robinet, P., Royer, L., Moatti, N., Simon, A., and Paul, J. L. (2003) *Atherosclerosis* **171,** 287-93.

25.　　Mweva, S., Paul, J. L., Cambillau, M., Goudouneche, D., Beaune, P., Simon, A., and Fournier, N. (2006) *Eur J Clin Invest* **36,** 552-9.

26.　　Bligh, E. G., and Dyer, W. J. (1959) *Can J Biochem Physiol* **37,** 911-7.

27.　　Castro-Perez, J., Previs, S. F., McLaren, D. G., Shah, V., Herath, K., Bhat, G., Johns, D. G., Wang, S. P., Mitnaul, L., Jensen, K., Vreeken, R., Hankemeier, T., Roddy, T. P., and Hubbard, B. K. *J Lipid Res* **52,** 159-69.

28.　　Fahy, E., Subramaniam, S., Murphy, R. C., Nishijima, M., Raetz, C. R., Shimizu, T., Spener, F., van Meer, G., Wakelam, M. J., and Dennis, E. A. (2009) *J Lipid Res* **50 Suppl,** S9-14.

29.　　Grove, D., and Pownall, H. J. (1991) *Lipids* **26,** 416-20.

30.   Liu, M., Bagdade, J. D., and Subbaiah, P. V. (1995) *J Lipid Res* **36,** 1813-24.

31.   Yvan-Charvet, L., Kling, J., Pagler, T., Li, H., Hubbard, B., Fisher, T., Sparrow, C. P., Taggart, A. K., and Tall, A. R. *Arterioscler Thromb Vasc Biol* **30,** 1430-8.

32.   Matsuura, F., Wang, N., Chen, W., Jiang, X. C., and Tall, A. R. (2006) *J Clin Invest* **116,** 1435-42.

33.   Zhang, Y., Zanotti, I., Reilly, M. P., Glick, J. M., Rothblat, G. H., and Rader, D. J. (2003) *Circulation* **108,** 661-3.

34.   Naik, S. U., Wang, X., Da Silva, J. S., Jaye, M., Macphee, C. H., Reilly, M. P., Billheimer, J. T., Rothblat, G. H., and Rader, D. J. (2006) *Circulation* **113,** 90-7.

35.   Zhang, Y., Da Silva, J. R., Reilly, M., Billheimer, J. T., Rothblat, G. H., and Rader, D. J. (2005) *J Clin Invest* **115,** 2870-4.

36.   Moore, R. E., Navab, M., Millar, J. S., Zimetti, F., Hama, S., Rothblat, G. H., and Rader, D. J. (2005) *Circ Res* **97,** 763-71.

37.   Briand, F. *Curr Opin Investig Drugs* **11,** 289-97.

Chapter 5

Liver steatosis induced by siRNA ApoB KD followed by combination siRNA therapy with loss of function for fatty acid transport protein 5 (Fatp5) KD

Liver steatosis induced by siRNA ApoB KD followed by combination siRNA therapy with loss of function for fatty acid transport protein 5 (*Fatp5*) KD

SUMMARY

The association between hypercholesterolemia and elevated serum apolipoprotein B (APOB) has generated interest in APOB as a therapeutic target for patients at risk of developing cardiovascular disease. In the clinic, mipomersen, an antisense oligonucleotide (ASO) APOB inhibitor, was associated with a trend toward increased hepatic triglycerides and liver steatosis remains a concern. Liver specific siRNA mediated knockdown of *ApoB* led to elevated hepatic triglycerides and liver steatosis in mice exhibiting a human-like lipid profile. This was associated with the reduced expression of many genes required for *de novo* hepatic fatty acid synthesis. As a proof-of-concept for combination dosing using the siRNA-LNP platform, siRNA-mediated knockdown of murine fatty acid transport protein 5 (*Fatp5*/*Slc27a5*) was evaluated to investigate whether this approach was able to alleviate *ApoB* knockdown induced steatosis, since *Fatp5* mediates long chain fatty acid uptake (LCFA) to the liver. Fatty acids are required for triglyceride synthesis, and shRNA mediated *Fatp5* knockdown protects against high fat diet-induced steatosis. *Fatp5* siRNA treatment failed to influence the degree, zonal distribution, or composition of the hepatic triglyceride population that accumulated following *ApoB* siRNA treatment. These findings suggest that loss of FATP5 activity is not sufficient to prevent the accumulation of triglycerides caused by *ApoB* knockdown and also provides a proof-of-concept for combination dosing *in vivo* utilizing our siRNA-LNP technology.

INTRODUCTION

Elevated LDL cholesterol (LDL-c) promotes atherosclerosis, and it is well established that reducing LDL-c helps mitigate the risk of developing cardiovascular disease in patients with hypercholesterolemia (1-7). LDL-c consists of a single apolipoprotein B-100 (APOB-100) molecule, cholesterol, cholesterol-esters and triacylglycerols that are comprised of various dietary and *de novo* synthesized fatty acids (8). In the liver, APOB is required for very low density lipoprotein (VLDL) formation and serves as the scaffold that solubilizes cholesterol and fatty acids (in the form of triglycerides) for secretion into the blood for circulation (8). An association between hypercholesterolemia and increased APOB protein levels, together with the observation that reductions in *ApoB* synthesis reduce LDL-c and the incidence of atherosclerosis has generated interest in APOB as a therapeutic target (9-13). Both antisense oligonucleotides (ASOs) and small interfering RNAs (siRNAs) targeting *ApoB* reduce LDL-c in mice and in non-human primates (14-18). In mice, *ApoB* ASOs reduced LDL-c without inducing hepatic steatosis, a liability of microsomal transfer protein (MTP) inhibitors that block triglyceride-rich lipoprotein assembly and secretion (19). In patients, mipomersen, an *ApoB* targeting ASO, reduces both LDL-c and APOB demonstrating the potential for an *ApoB* targeted therapeutic (20-24). Liver steatosis induced by inhibiting *ApoB*, however, remains an important concern. Recently, mipomersen administration at a sub-maximum efficacious dose was shown to be associated with a trend toward increased intra-hepatic triglyceride (IHTG) content for mipomersen treated patients with one of the ten patients developing mild steatosis (20). In addition, mice harboring a base-pair deletion in the coding region of *ApoB* (*ApoB-38.9*) exhibited hepatic triglyceride accumulation (25). In order to attenuate the risk of liver steatosis associated with an *ApoB* targeted therapeutic, one approach would be to combine an *ApoB* ASO or siRNA with another therapeutic that increases the clearance of hepatic triglycerides.

Fatty acid transport protein 5 (*Fatp5*/*Slc27a5*) mediates the uptake of long-chain fatty acids (LCFAs) to the liver and is involved in bile acid reconjugation during enterohepatic recirculation (26, 27). *Fatp5* knockout mice exhibit lower levels of hepatic triglycerides and free fatty acids due to decreased liver fatty acid uptake (27). Furthermore, Doege *et al.* recently showed that adenovirus-shRNA mediated silencing of *Fatp5* mRNA not only protected mice from high fat diet-induced liver steatosis but also reversed steatosis once it was established (25). This suggested that a FATP5 inhibitor may be an attractive combination therapy with an APOB targeted therapeutic.

Besides its role in free fatty acid uptake, FATP5 also plays a critical role in reconjugation of bile acids during enterohepatic recirculation to the liver, and complete deletion of *Fatp5* resulted in a significant increase in unconjugated bile acids in both bile and serum (26). Activation of FXR, a bile acid nuclear receptor, with bile acids or synthetic activators has been shown to reduce the secretion of triglyceride-rich VLDL from the liver in mice, which was associated with a decrease in *Srebp1* and 2 pathway genes (28). The involvement of FATP5 in bile acid metabolism suggests that it too may play a role in hepatic triglyceride metabolism via FXR. However, the contributions of the bile acid reconjugation activity of FATP5 on hepatic steatosis or the contribution of FATP5 on APOB-induced steatosis are currently unknown.

By utilizing two siRNAs specifically targeting *Fatp5* and *ApoB* it was possible to provide a proof-of-concept for combination dosing *in vivo* and evaluate the ability of *Fatp5* siRNA treatment to alleviate *ApoB* siRNA-induced liver steatosis. Significant increases in IHTG content were found following liver specific siRNA-mediated knockdown of *ApoB* mRNA and serum protein in a mouse model that has a human-like lipid profile. Following *ApoB* siRNA administration, mice exhibited an increase in the total triglyceride pool found within the liver, which consisted largely of non-essential fatty acids. Lipid accumulation, which exhibited a periportal to midzonal distribution in many of the control and *Fatp5* siRNA treated groups spread across all zones following *ApoB* siRNA treatment. Dual treatment with *ApoB* and *Fatp5* siRNAs resulted in similar levels of knockdown for either a 1.5 mg/kg dose of each (a 3mg/kg total siRNA dose) or a 3 mg/kg dose of a single siRNA. The simultaneous knockdown of both *ApoB* and *Fatp5* led to an increase in the proportion of unconjugated bile acids, consistent with FATP5's role in bile acid reconjugation, yet it failed to influence the size, distribution, or composition of the triglyceride population induced by the knockdown of *ApoB*.

MATERIALS AND METHODS

siRNA design

 siRNAs were designed to the mRNA transcripts using a previously published design algorithm (29). siRNA sequences contained the following chemical modifications added to the 2' position of the ribose sugar when indicated: deoxy (d), 2' fluoro (f), or 2' O-methyl (o) (30). Modification abbreviations are given immediately preceding the base to which they were applied. Passenger strands were capped with an inverted abasic nucleotide on the 5' and 3' ends. The control siRNA sequence (Cntrl siRNA) consists of:

 iB;fluU;fluC;fluU;fluU;fluU;fluU;dA;dA;fluC;fluU;fluC;fluU;fluC;fluU;fluU;fluC;dA;dG;dG;dT;dT;iB

passenger strand and

fluC;fluC;fluU;omeG;omeA;omeA;omeA;omeG;omeA;omeG;omeA;omeG;fluU;fluU;omeA;omeA;omeA;rA;rG;rA;omeU;ome U guide strand sequences.

The *Fatp5* (951) siRNA sequence consists of:

iB;fluC;fluU;dG;fluC;fluC;dA;fluU;dA;fluU;fluU;fluC;dA;fluU;fluC;fluU;fluU;fluU;dA;fluC;dT;dT;iB

passenger strand and

rG;rU;rA;omeA;omeA;omeG;omeA;fluU;omeG;omeA;omeA;fluU;omeA;fluU;omeG;omeG;fluC;omeA;omeG;omeU;om eU guide strand sequences.

The *ApoB* (10168) siRNA sequence consists of:

iB;fluU;fluC;dA;fluU;fluC;dA;fluC;dA;fluC;fluU;dG;dA;dA;fluU;dA;fluC;fluC;dA;dA;dT;dT;iB

passenger strand and

rU;rU;rG;omeG;fluU;omeA;fluU;fluU;fluC;omeA;omeG;fluU;omeG;fluU;omeG;omeA;fluU;omeG;omeA;omeU;omeU guide strand sequences.

siRNA synthesis

siRNAs were synthesized by methods previously described (31). For each siRNA, the two individual strands were synthesized separately using solid phase synthesis, and purified by ion-exchange chromatography. The complementary

strands were annealed to form the duplex siRNA. The duplex was then ultra filtered and lyophilized to form the dry siRNA. Duplex purity was monitored by LC/MS and tested for the presence of endotoxin by standard methods.

Preparation of siRNA-Lipid Nanoparticle (LNP) complex

LNPs were made using the cationic lipid CLinDMA (2-{4-[(3b)-cholest-5-en-3-yloxy]-butoxy}-N,N-dimethyl-3-[(9Z,12Z)-octadeca-9,12-dien-1-yloxy]propan-1-amine), cholesterol, and PEG-DM (monomethoxy(polyethyleneglycol)-1,2-dimyristoylglycerol) in 60:38:2 molar ratio, respectively. siRNAs were incorporated in the LNPs with high encapsulation efficiency by mixing siRNA in citrate buffer with an ethanolic solution of the lipid mixture, followed by a stepwise diafiltration process. Cholesterol was purchased from Northern Lipids, PEG-DMG was purchased from NOF Corporation (Japan) and CLinDMA was synthesized by Merck and Co. The encapsulation efficiency of the particles was determined using a SYBR Gold fluorescence assay in the absence and presence of triton, and the particle size measurements were performed using a Wyatt DynaPro plate reader. The siRNA and lipid concentrations in the LNP were quantified by a HPLC method, developed in house, using a PDA detector.

In vivo siRNAs treatments

All *in vivo* work was performed according to an approved animal protocol as set by the Institutional American Association for the Accrediation of Laboratory Animal Care. C57Bl/6 mice engineered to be hemizygous for a knockout of the LDL receptor and hemizygous for the overexpression of the human cholesterol ester transfer protein (CETP) driven by the endogenous apoA1 promoter within a C57Bl/6 background (B6-Ldlr<tm1>Tg(apoA1-CETP, Taconic) were used for these studies. Mice ~16-20 weeks of age were fed Lab Diets (5020 9F) starting two weeks prior to the start of the study. siRNAs were administered by intravenous (i.v.) injection. Animals were dosed on day 0 and day 14 with either 3 mg/kg of a single LNP formulated siRNA or 1.5 mg/kg of two LNP formulated siRNAs for a 3 mg/kg total siRNA combination dose. For siRNA combinations, siRNA were formulated individually and hand-mixed immediately prior to injections. Animals were euthanized by CO_2 inhalation. Immediately after euthanasia, serum was collected using serum separator tubes and allowed to clot at room temperature for 30 minutes. Liver sections were excised, placed in either RNA Later (Qiagen) (right medial lobe), 10% buffered formalin (10% NBF, left medial lobe), or flash frozen (the remainder) and stored until further use.

RNA isolation and qRT-PCR

RNA was isolated using an RNeasy96 Universal Tissue Kit (Qiagen) according to the supplied product protocol. An on-column DNase I treatment was performed and samples were washed three times prior to elution in 100 uL of RNase-free water. Reverse transcription was performed using the Cells to Ct kit (Ambion) in a 20 uL volume with 350 ng of RNA in 1X reverse transcriptase and buffer incubated at 37 °C for 1 hr. TaqMan Gene Expression Assays (Applied Biosystems) were performed as described within the product protocol using the following primer probes, Mm00447768_m1 for *Fatp5*, Mm01545154_g1 for *ApoB*, and Cat# 4352339E for the reference, *Gapdh*. All reactions were performed in duplicate, and

data were analyzed using the ddCt method with *Gapdh* serving as the reference (32). Data represented as both the log2 fold change (ddCt) and % expression ($100*2^{ddCt}$) relative to the control siRNA. For analysis of the selected *Srebp1c* and *Srebp2* pathway genes and *Scd1*, expression was normalized to an average of that of mouse *β-actin* (*Actb*), Glyceraldehyde 3-phosphate dehydrogenase (*Gapdh*), Beta-glucuronidase (*Gusb*), Hypoxanthine-guanine phosphoribosyltransferase (*Hprt1*), Peptidylprolyl isomerase A (*Cyclophilin A/ Ppia*) and ribosomal protein 113a (*Rp113a*) in each sample. Expression levels of all genes analyzed were normalized to an average of the housekeeping genes (listed above) to obtain dCt. Fold regulation is calculated as: ddCt of gene in treatment group/dCt of gene in control group. Significance (p value) was calculated from a two-tailed *t*-test between control and treatment group. Accession numbers for the primer/probes used are listed in Supplemental Table 1.

Cholesterol and triglyceride analysis

For serum cholesterol analysis, serum clot tubes were centrifuged for 10 minutes at 10,000 rpm. Lipase inhibitor (Sigma-Aldrich) was added at a 1:100 (v:v) ratio of inhibitor to serum followed by iterative rounds of mixing (600 rpm at 4 °C for 1.5 minutes, Eppendorf ThermoMixer R) and centrifugation (2,000 rpm at 4 °C for 2 minutes) until sufficient RBCs coated the bottom of the wells. Serum was replated into a new deep well plate so RBCs were not resuspended in serum. Serum total and HDL cholesterol levels were measured using Wako's total and HDL cholesterol kits according to the supplied product protocol. Non-HDL, which serves as an approximation for LDL, was calculated by subtracting HDL from total cholesterol measurements. The percent difference relative to the control siRNA was calculated using the following equation (100*(1-(experimental/control))).

Histology and hematology

Mouse livers were fixed with 10% neutral buffered formalin. One hepatic lobe was treated with osmium tetroxide solution, to visualize lipids, overnight at room temperature prior to paraffin embedding and processing. The other hepatic lobe was embedded and processed in paraffin and H&E stained. Samples were sectioned at a thickness of 5 micron. The osmium stained samples were digitalized using an Aperio ScanScope XT. Percent area (positive pixel count) was calculated using the positive pixel count algorithm (MAN-0024) supplied with the imaging software (Aperio). Samples were also reviewed by a board certified veterinary pathologist and scored for inflammation and lipidosis using a semi-quantitative score (0 = normal, 1 = minimal, 2 = mild, 3 = moderate, 4 = marked and 5 = severe).

Measurement of serum APOB

The APOB levels in serum were measured by LC/MS. Briefly, 4 uL of serum was diluted with 138 uL of 50 mM ammonium bicarbonate (pH 8.0), 50 uL of 80 nM internal standard APOB peptides and 10 uL of 10% sodium deoxycholate. Samples were reduced with dithiothreitol for 30 min at 60ºC, alkylated with iodoacetamide for 60 min at 25 ºC in the dark and digested overnight with 3 ug trypsin (1:50 serum proteins). To stop digestion, 10 uL of 20% formic

acid was added to precipitate the sodium deoxycholate. Samples were then centrifuged for 15 minutes at 15800 rcf and 120 uL of the supernatant was removed for LC/MS analysis. Serum APOB levels in the samples were then analyzed on a Waters Acquity UPLC and Xevo triple quadrupole mass spectrometer. The gradient was 95%A (0.1% formic acid in water)/5%B (0.1% formic acid in acetonitrile) ramped to 80%A at 1 minute, 65%A at 4 minutes, 5%A at 5 minutes. A Phenomenex Kinetex C18 50x2.1mm 1.7μm column maintained at 50ºC was used at a flow rate of 0.7mL/min. The concentration of APOB peptide was calculated by dividing the area under the curve for the analyte by the area of its internal standard and multiplying by the internal standard concentration. The concentration of APOB was then converted to and reported as mg/dL.

LC/MS sample preparation and analysis for bile acid conjugation and hepatic triglycerides

Terminal bile samples from each group were collected using the stick and pull method. Samples were diluted 1:1000 v/v in 50% acetonitrile + 0.1% formic acid / 50% water + 0.1 % formic acid, followed by the addition of 1μM total internal standard solution (D$_4$-TCA, D$_4$-CA, D$_4$-GCA) (Sigma-Isotec St. Louis, MO). The mixture was vortexed for 10 seconds, centrifuged for 10 minutes at 15,000 g, then stored at -20 °C until LC/MS analysis. Supernatant was injected (10 μL) directly onto the LC/MS system.

A 50 mg slice of frozen liver from each animal was homogenized in 2 mL polypropylene tubes containing a 14 mm ceramic bead using a Precellys 24 homogenizer (Bertin Technologies, Montigny-le-Bretonneux, France). A non-naturally occurring internal standard solution (20μL) containing 1,2,3-triheptadecanoyl-glycerol (TG 51:0) (Sigma Aldrich, St Louis, MO) 0.8 mg/mL along with dichloromethane/methanol (2:1 v/v) was added to each sample prior to homogenization (126). Samples were homogenized at 5,500 RPM, 2 x 30 seconds, with a 15 second pause between cycles. In order to generate a two layer liquid separation, 200 μL of distilled water was added, vortexed for 30 seconds, followed by centrifugation at 20,000 rpm at 5 °C for 10 minutes. 10 μL of the lower layer, containing the lipids, was removed without disrupting the liver tissue homogenate disk. This was followed by dilution of the extracted lipid sample 1/50 in a solvent mixture (65% ACN, 30% IPA, 5% H$_2$O). External endogenous calibration standards (cholic acid, deoxycholic acid, chenodeoxycholic acid, lithocholic acid, taurocholic acid, glycolic acid, taurochenodeoxycholic acid, 1,2-dihexadecanoyl-3-(9Z,12Z-octadecadienoyl)-sn-glycerol (TG 50:3), 1-hexadecanoyl-2-octadecanoyl-3-(9Z-octadecenoyl)-sn-glycerol (TG 52:1), 1-hexadecanoyl-2,3-di-(9Z-octadecenoyl)-sn-glycerol (TG 52:2), 1-hexadecanoyl-2-(9Z-octadecenoyl)-3-(9Z,12Z-octadecadienoyl)-sn-glycerol (TG 52:3), 1-hexadecanoyl-2,3-di-(9Z,12Z-octadecadienoyl)-sn-glycerol (TG 52:4), 1,2,3-tri-(9Z-octadecenoyl)-glycerol (TG 54:3), 1,3-di-(9Z-octadecenoyl)-2-(9Z,12Z-octadecadienoyl)-sn-glycerol (TG 54:4) in buffer solution were used to cover the endogenous bile acids and triglycerides concentrations present in the bile and liver tissues. The inlet system was comprised of an Acquity UPLC (Waters, Milford, MA, USA). Bile and lipid extracts were injected (2 μL) onto a 1.8 μm particle 100 x 2.1 mm id Waters Acquity HSS T3 column (Waters, Milford, MA, USA). The column was maintained at 55 °C with a 0.4 mL/min flow rate for the

lipid analysis and 65 °C with a 0.7 mL/min flow rate for the bile analysis. A binary gradient system was utilized for the analysis of both sample sets. Two different gradient conditions were used. For the lipid analysis, acetonitrile (Burdick & Jackson, USA) and water with 10 mM ammonium acetate (Sigma-Aldrich, St Louis, MO) (40:60, v/v) was used as eluent A. Eluent B, consisted of acetonitrile and isopropanol (Burdick & Jackson, USA) both containing 10 mM ammonium acetate (10:90, v/v). A linear gradient (curve 6) was performed over a 15 min total run time. The initial portion of the gradient was held at 60% A and 40% B. For the next 10 min the gradient was ramped in a linear fashion to 100% B and held at this composition for 2 min.   Hereafter the system was switched back to 60% B and 40% A and equilibrated for an additional 3 minutes. For the bile acid analysis, water + 0.1% formic acid was used as eluent A. Eluent B consisted of acetonitrile + 0.1% formic acid (Burdick & Jackson, USA). A linear gradient (curve 6) was performed over a 13 min total run time. During the initial portion of the gradient, it was held at 80% A and 20% B. For the next 10 minutes the gradient was ramped in a stepped linear fashion to 35% B (curve 5) in 4 minutes, 45% B in 7.5 minutes and 99% B in 9.5 minutes and held at this composition for 1.6 minutes. Hereafter the system was switched back to 80% B and 20% A and equilibrated for an additional 2.9 minutes.

The inlet system described was directly coupled to a hybrid quadrupole orthogonal time of flight mass spectrometer (SYNAPT G2 HDMS, Waters, MS Technologies, Manchester, UK). Electrospray (ESI) positive and negative ion ionization modes were used. In both ESI modes a capillary voltage and cone voltage of ±2 kV and ±30 V respectively were used. The desolvation source conditions were as follows; for the desolvation gas 700 L/hr was used and the desolvation temperature was kept at 450°C. Data were acquired over the mass range of 50-1200 Da.

The LC/MS data acquired was processed by the use of a quantitative data deconvolution package (Positive software by MassLynx, Waters, MA, USA). Data are presented as ± standard error of the mean (S.E.M.). Differences between groups were computed by either student's *t-test* or by 2-way ANOVA (GraphPad Prism, La Jolla, CA). Post-test analysis for quantifiable variables was conducted using either Bonferroni or Mann-Whitney *U* non-parametric test with two-tailed *p*-values. Values of *p* <0.05 was considered statistically significant.

RESULTS

Sustained knockdown of both ApoB and Fatp5 mRNA transcripts were achieved with siRNAs administered either alone or in combination

To investigate if we can simultaneously silence both *ApoB* and *Fatp5*, we administered siRNAs specifically targeting both *ApoB* and *Fatp5* alone and in combination to CETP/LDLR hemizygous female mice (mice exhibiting a human-like lipid profile) fed a low-fat western diet. Changes to the lipid profile were obtained through a hemizygous mutation of the LDL receptor (+/- LDLR) and the hemizygous overexpression of a mouse apoA1 promoter driven human CETP transgene (+/- apoA1-hCETP). This lead to an elevation in LDL and a cholesterol profile that more closely resembled the HDL to LDL ratio observed in humans (29). Female mice were fed a low-fat western diet and treated with siRNAs formulated in a lipid nanoparticle (LNP) to achieve delivery to the liver. Animals were dosed on day 0 and day 14 with either 3 mg/kg of a single siRNA or 1.5 mg/kg of two siRNAs for a 3 mg/kg total siRNA combination dose. Efficacy was analyzed using qRT-PCR on liver samples collected on day 21 and day 28 following the initial dose. Analysis of mRNA expression levels revealed no appreciable differences in knockdown between *ApoB* siRNA treatments administered either alone or in combination with the *Fatp5* siRNA (Figure 1 A-B). On day 21, we observed robust knockdown of the *ApoB* mRNA transcript (≥ 90%) across all groups that became slightly attenuated (≥ 86%) on day 28. Similar results were observed for the *Fatp5* siRNA, where ≥ 89% knockdown of *Fatp5* was observed across all groups on day 21 and ≥ 70% reduction was observed across groups on day 28 (Figure 1 C-D). Together, these data revealed robust knockdown of both *ApoB* and *Fatp5* mRNA transcripts demonstrating the utility of using siRNAs to specifically silence more than one gene, and thus more than one biological pathway, with a single siRNA combination dose.
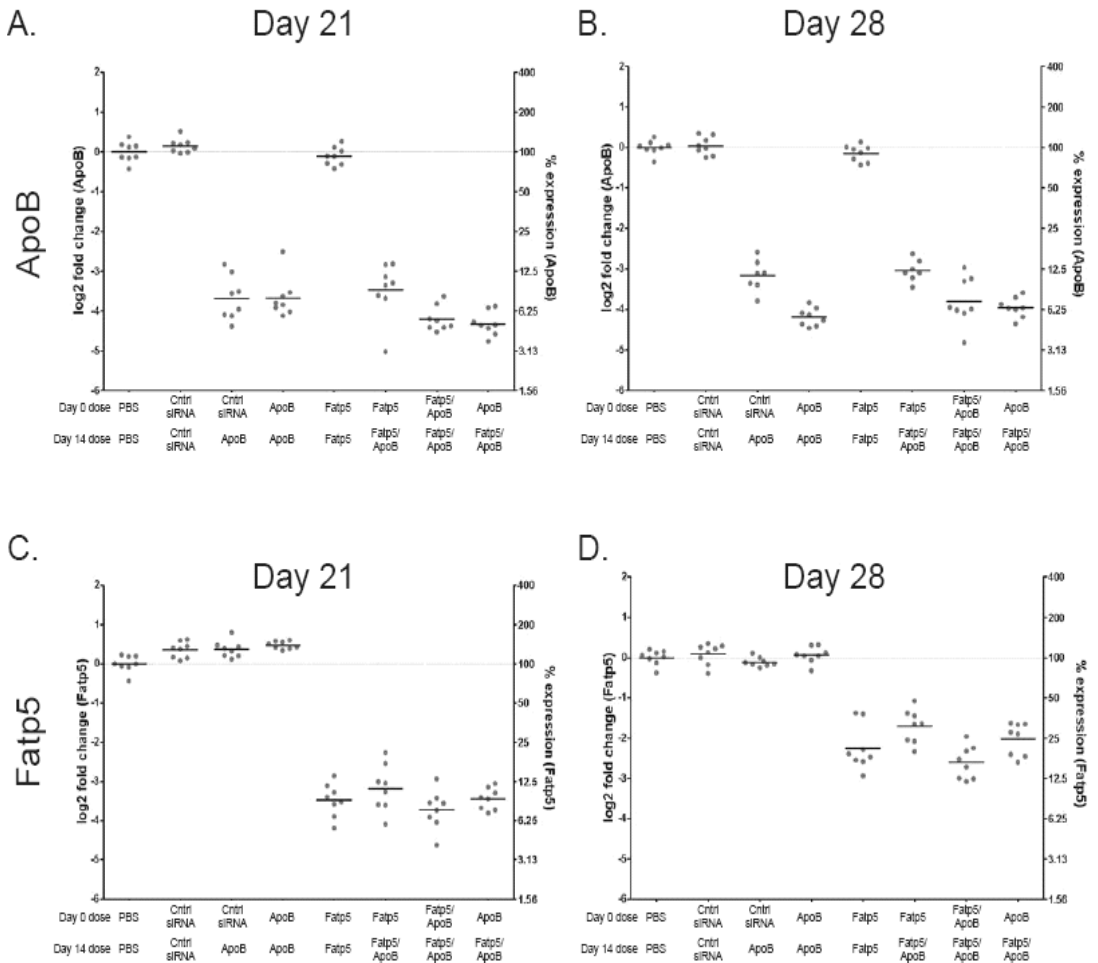
Figure 1. Similar levels of *ApoB* and *Fatp5* mRNAs were observed for all groups containing siRNAs targeting these genes, either alone or in combination. Mice were treated with siRNAs targeting *ApoB* and *Fatp5* alone or in combination (*ApoB*, *Fatp5*, *Fatp5/ApoB*) at day 0 and day 14. Gene expression was analyzed using qRT-PCR (TaqMan) on day 21 (**A**, **C**) and day 28 (**B**, **D**) post the initial dose. PBS and a control siRNA (cntrl siRNA) served as negative controls. Data represented as the log2 fold change (ddCt), left axes, and % expression, right axes, relative to the cntrl siRNA treatment of individual animals (circles) and the group means (bars).

Fatp5 knockdown impairs bile acid reconjugation

The ratio of unconjugated/conjugated bile acid in the bile was used as a biological indicator for the loss of FATP5 activity following siRNA treatment to female mice fed a low-fat western diet (26). Figure 2A shows a significant increase in the proportion of unconjugated bile acids for all *Fatp5* siRNA treatment groups, indicative of the loss of FATP5 activity ($p = 0.0003$ t-test, Mann Whitney post-test, cntrl siRNA groups vs. *Fatp5* siRNA groups). The unconjugated/conjugated ratio

for the cntrl/cntrl siRNA group and the *Fatp5*/*Fatp5* siRNA group was 0.004 and 2.2 respectively. The ratio was lower for some of the *Fatp5* siRNA treatment groups when combined with the *ApoB* siRNA, but nevertheless exhibited a significant level of target engagement when compared with the control siRNA. Cholic acid in the *Fatp5* groups was the most predominant unconjugated bile acid found in bile (Figure 2B), which showed a dramatic increase in concentration (0.77 mM in control siRNA vs. 77.95 mM in *Fatp5*) after knockdown of *Fatp5* ($p = 0.0003$ *t*-test, Mann Whitney post-test). Conjugated bile acids, specifically taurocholic acid (TCA), showed the reverse effect with *Fatp5* knockdown ($p = 0.1304$ *t*-test, Mann Whitney post-test). The levels of TCA decreased to 43.2 mM in comparison with the cntrl siRNA group 69.7 mM (data not shown). The ratio of unconjugated/conjugated bile acids in the serum reflected that of the bile, with a significant increase in the unconjugated levels (data not shown).
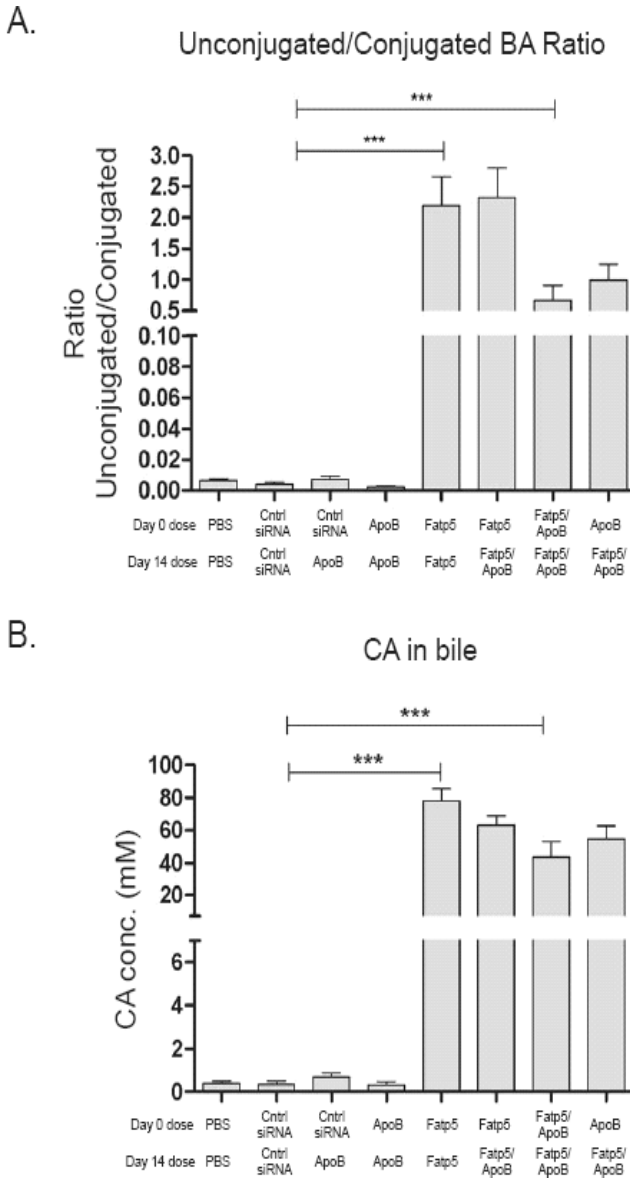
Figure 2. *Fatp5* knockdown reduces bile acid (BA) reconjugation. (A) An increase in the level of unconjugated/conjugated bile acid ratio (***, $p \leq$ *0.001* t-test, Mann Whitney post-test) was observed following *Fatp5* knockdown. (B) Cholic acid (CA) concentrations exhibited an increase in the concentration measured (***, $p \leq 0.001$ t-test, Mann Whitney post-test) by LC/MS after treatment with the *Fatp5* siRNA.

ApoB siRNA treatment led to significant reductions in serum APOB protein, cholesterol and triglyceride levels alone and in combination with a Fatp5 targeting siRNA ApoB siRNA treatment, either alone or in combination with a siRNA

targeting Fatp5, caused a significant reduction ($p \leq 0.001$) in serum APOB levels in female mice fed a low-fat western diet (Figure 3). APOB protein reductions were consistent with the reductions in hepatic *ApoB* mRNA levels (Figure 1). This led to reductions in circulating cholesterol and triglyceride levels. On day 21, similar reductions in total (76% to 84%), HDL (67% to 78%), and non-HDL (79% to 90%) cholesterol were observed across all *ApoB* siRNA treatment groups (Figure 4 A-C). No significant decrease in cholesterol levels were observed for the *ApoB+Fatp5* siRNA combination group relative to the *ApoB* siRNA individual treatment group.
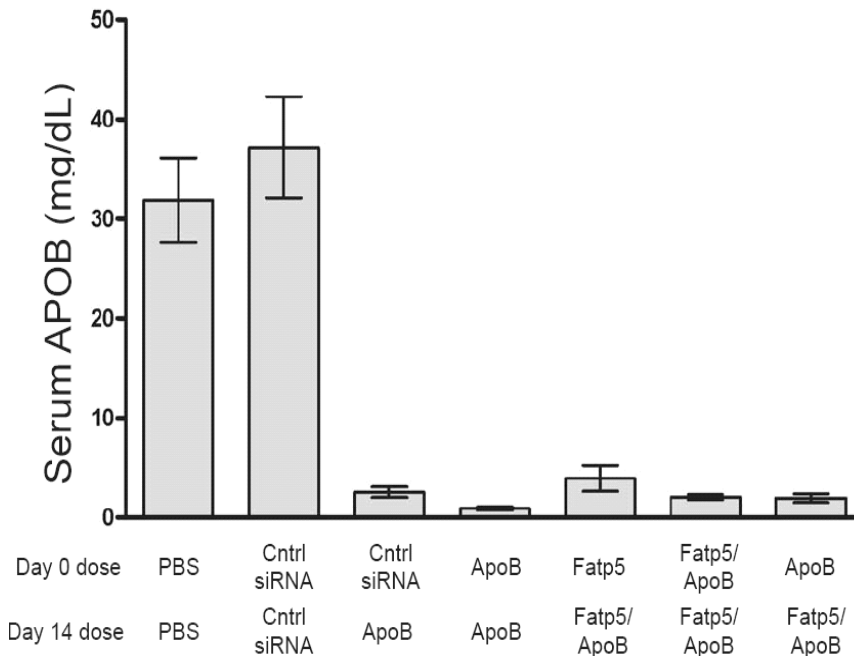
Figure 3. Serum APOB protein levels were reduced following *ApoB* siRNA treatment. APOB levels in serum were measured by LC/MS. Data represented as the group means (bars) +/- S.D.

Serum triglycerides were also significantly reduced for both *ApoB* and *Fatp5* siRNA treatments either alone or in combination on day 21, with a more modest effect observed on day 28 (Supplementary Figure 1 A-B). As with serum non-HDL, serum triglycerides were also significantly reduced (17%, $p \leq 0.05$, student t-test, 2-tailed) for the *Fatp5* (day 0 and day 14 dose) group (Supplementary Figure 1 A). On day 28, significant reductions in total (67% to 81%), HDL (41-73%), and non-HDL (82-93%) were also observed for the *ApoB* siRNA treatment groups (Figure 4 D-F). Taken together,

these data point to similar and significant changes in serum cholesterol across *ApoB* siRNA treatment groups that correlate with observed reductions in *ApoB* mRNA and serum protein levels.
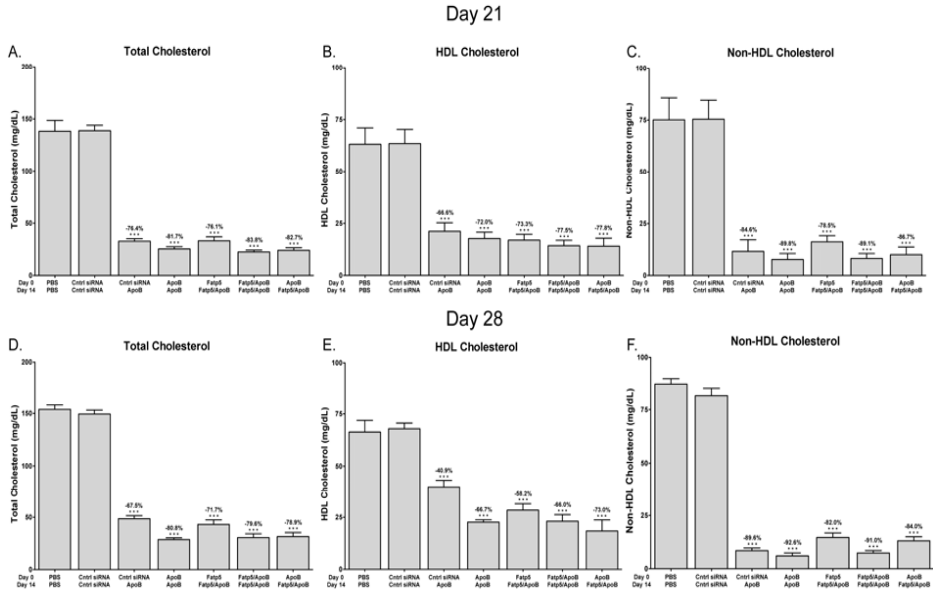

Figure 4. Comparable levels of serum cholesterol were observed for *ApoB* siRNA treatments either alone or in combination with a siRNA targeting *Fatp5*. Total (A, D) and HDL (B, E) cholesterol were measured on day 21 and on day 28 following a day 0 and day 14 dose as indicated on the x-axis. Non-HDL cholesterol (C, F) was calculated by subtracting the HDL cholesterol value from the total cholesterol value. Data represented as group means (bars) +/- S.D. The percent difference relative to the control siRNA is shown. Significance (***, $p \leq 0.0001$, **, $p \leq 0.001$) was calculated using a two-tailed t-test between siRNA control (cntrl siRNA) and treatment groups.

Fatp5 siRNA treatment failed to alleviate ApoB siRNA induced liver steatosis

To determine if *Fatp5* siRNA treatment was sufficient to alleviate *ApoB* siRNA induced liver steatosis, liver sections were processed, sectioned, and stained with either osmium or hematoxylin and eosin (H&E). Image analysis of the osmium stained slides revealed similar levels of significant lipid accumulation across all *ApoB* siRNA treatment groups relative to the PBS, *Fatp5*, or control siRNA groups (Figure 5 A-B). These data indicate that *Fatp5* siRNA treatment failed to alleviate *ApoB* siRNA induced liver steatosis in female mice fed a low-fat western diet. For the PBS, *Fatp5*, and control siRNA groups, there was some evidence of a periportal to midzonal (zones 1 and 2) distribution of lipid droplets within hepatocytes (Figure 5 C, PBS/PBS, Control siRNA/Control siRNA, and *Fatp5*/*Fatp5*). This contrasts the lipid distribution following *ApoB* siRNA treatment, where diffuse infiltration (all zones) was observed (Figure 5 C, *ApoB*/*ApoB*, *ApoB+Fatp5*/*ApoB+Fatp5*, *Fatp5*/*ApoB+Fatp5* groups). The *ApoB* treated groups (control siRNA/*ApoB* and

ApoB/ApoB) displayed lipid droplets that were smaller and more evenly distributed, while fewer but larger lipid droplets were observed for the remaining groups in many instances and as shown in figure 5C. By H&E staining, hepatocytes in the *ApoB* siRNA treatment groups appeared diffusely swollen, with granular to vacuolated cytoplasmic spaces (data not shown).
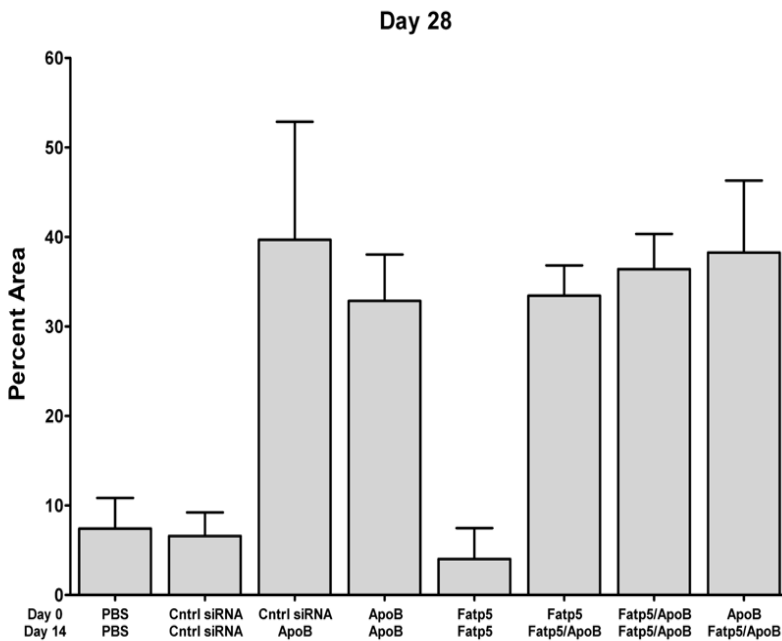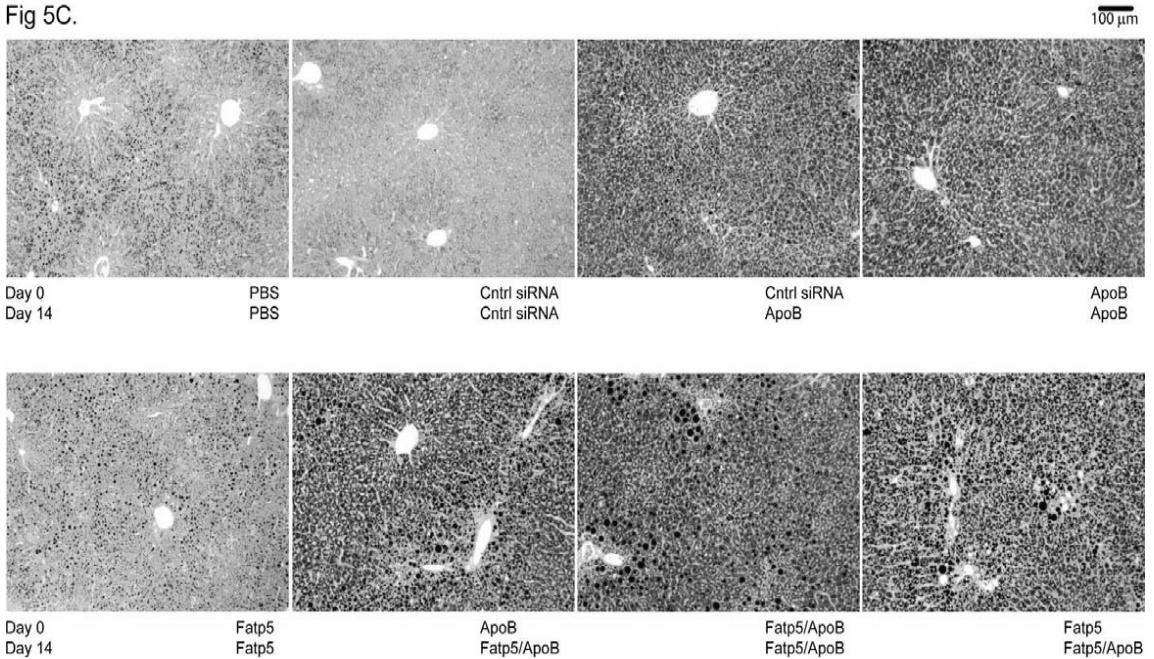
A.
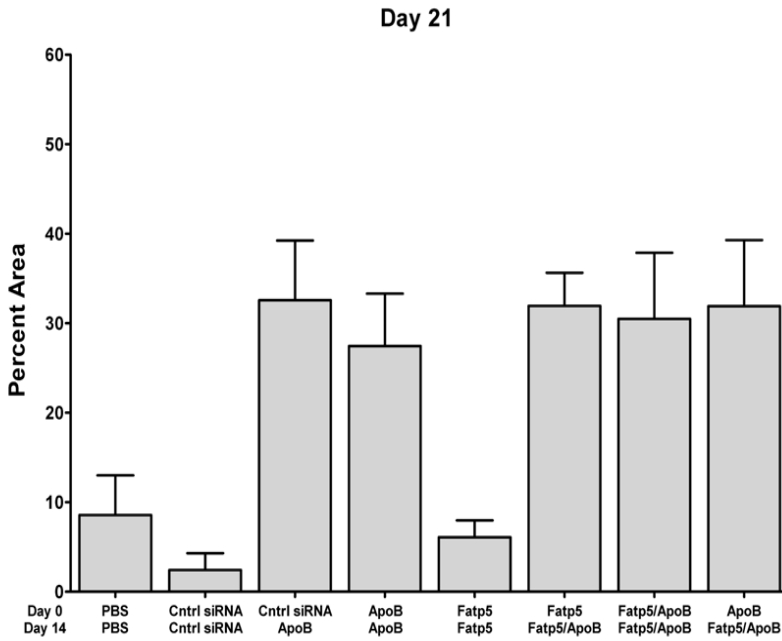
B.

Fig 5C.

Figure 5. Similar levels of liver steatosis were observed across all *ApoB* siRNA treatment groups. A-B. Osmium stained images were scanned and pixel intensities were quantitated for day 21 (A) and day 28 (B). Data represented as the group mean +/- S.D. (C) Images representative of each of the treatment groups are shown.

Fatp5 knockdown failed to alter ApoB siRNA induced liver triglyceride levels or composition

 Total triglyceride composition analysis by LC/MS revealed a significant increase in the level of triglycerides found in the liver following treatment with *ApoB* siRNA when compared with siRNA control (Figure 6 A, Control siRNA 7.5 μg/mg of tissue vs. *ApoB* siRNA 35.5 μg/mg of tissue*, p = 0.0002, t-test* with Mann-Whitney post-test).   Comparative measurements between the *ApoB*/*ApoB* and the *Fatp5*/*Fatp5+ApoB* group did not show protection from triglyceride accumulation in female mice fed a low-fat western diet. LC/MS indicated that 1-hexadecanoyl-2,3-di-(9Z-octadecenoyl)-sn-glycerol (TG 52:2) and 1-hexadecanoyl-2-(9Z-octadecenoyl)-3-(9Z,12Z-octadecadienoyl)-sn-glycerol (TG 52:3)were significantly higher (*p ≤ 0.0001,* 2-way ANOVA with Bonferroni post-test) following *Fatp5*/*Fatp5+ApoB* treatment relative to *ApoB*/*ApoB* treatment (Figure 6 B). 1-Hexadecanoyl-2,3-di-(9Z,12Z-octadecadienoyl)-sn-glycerol (TG 52:4) and 1,2,3-tri-(9Z-octadecenoyl)-glycerol (TG 54:3) although not statistically significant also showed an increased in the *Fatp5*/*Fatp5+ApoB* cohort in comparison with the *ApoB*/*ApoB* cohort.   Structure elucidation by collision induced dissociation MS/MS provided information about the possible fatty acid composition for each triglyceride;   1-hexadecanoyl-2,3-di-(9Z-octadecenoyl)-sn-glycerol   (TG   52:2),   1-hexadecanoyl-2-(9Z-octadecenoyl)-3-(9Z,12Z-octadecadienoyl)-sn-glycerol (TG 52:3), 1,2,3-tri-(9Z-octadecenoyl)-glycerol (TG 54:3) and 1,3-di-(9Z-octadecenoyl)-2-(9Z,12Z-octadecadienoyl)-sn-glycerol (TG 54:4).   .   These triglycerides were confirmed by exact mass and the use of

external standards (Supplementary Figure 2). All of these significantly relevant triglycerides have constituent fatty acids which are non-essential suggesting that these triglycerides may be derived from *de novo* synthesis.
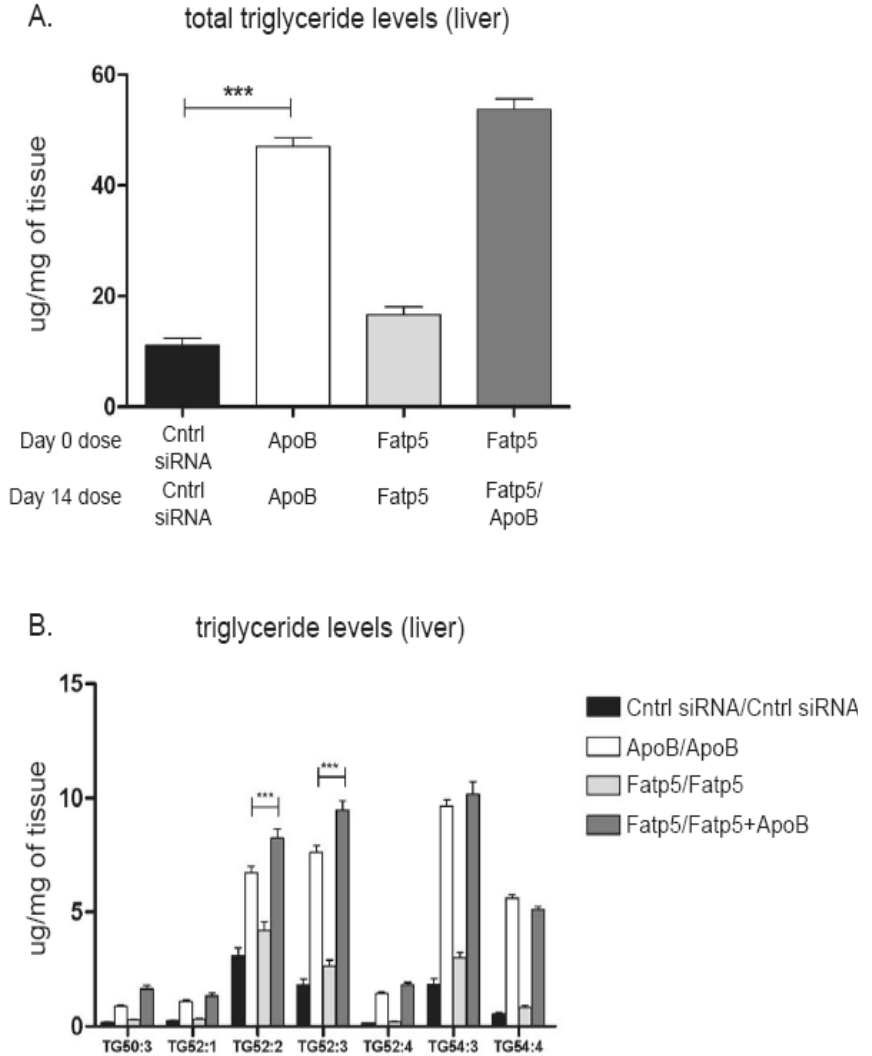
Figure 6. *Fatp5* siRNA treatment fails to alter *ApoB* siRNA induced liver triglyceride levels or composition. The total triglyceride pool size and composition was measured for different siRNA administrations (Control siRNA/Control siRNA, *ApoB/ApoB*, *Fatp5/Fatp5* and *Fatp5/Fatp5+ApoB*). (A) A large increase in liver triglycerides was observed for the *ApoB/ApoB* group relative to the control siRNA (***, $p = 0.0002$, *t-test* with Mann-Whitney post-test). *Fatp5* siRNA treatment (*Fatp5/Fatp5+ApoB*) did not show protection from *ApoB* siRNA induced liver steatosis. (B) Specific triglycerides 1-hexadecanoyl-2,3-di-(9Z-octadecenoyl)-sn-glycerol (TG 52:2) and 1-hexadecanoyl-2-(9Z-octadecenoyl)-3-(9Z,12Z-octadecadienoyl)-sn-glycerol (TG 52:3) showed an increase in their concentrations in both the *ApoB/ApoB* and *Fatp5/Fatp5+ApoB* groups suggesting that *Fatp5* KD fails to alter the triglyceride composition induced by *ApoB* knockdown (***, $p \leq 0.0001$, 2-way ANOVA with Bonferroni post-test).

The hepatic sterol response differed after ApoB and Fatp5 siRNA treatments

To investigate the hepatic gene response to *ApoB*, *Fatp5* or combination treatments, we performed qRT-PCR analysis on genes involved in the sterol response element binding protein 1 and 2 pathways (*Srebp1* and *Srebp2*). Interestingly, although *ApoB* knockdown induced steatosis, it resulted in a significant decrease in many genes in involved both pathways (Table 1), including genes that are key regulators of fatty acid and triglyceride synthesis (*Fasn*, *Scd*, *Fads1/2*, *Acsl3/5*). As previously described, deletion (31) or silencing (25) of *Fatp5* caused a reduced uptake of hepatic free fatty acids from serum, which caused a subsequent increase in genes involved in fatty acid synthesis. In contrast to *ApoB* siRNA treatment, Table 1 shows that *Fatp5* siRNA treatment resulted in a significant increase in both *Srebp1* and *Srebp2* pathways. Although bile acid conjugation levels changed and there was a significant increase in cholic acid in bile (Figure 3B), transcription of FXR or key regulators of FXR did not change (data not shown). *ApoB* siRNA treatment appeared to have a stronger effect on the *Srebp1/2* pathways than *Fatp5* siRNA since the simultaneous reductions of both resulted in a hepatic gene signature more similar to that of *ApoB* siRNA treatment alone.

Table 1.

	Gene	ApoB		Fatp5		Fatp5/Fatp5+ApoB	
		Fold regulation	p value	Fold regulation	p value	Fold regulation	p value
Srebp1c pathway	Acaca	-1.46	0.0705	1.78	0.0156	-1.86	0.0266
	Acacb	-1.69	0.0084	1.61	0.0070	-5.40	0.0098
	Fasn	-2.99	0.0026	2.05	0.0203	-2.03	0.0830
	Scd	-3.62	0.0009	1.95	0.0007	-2.91	0.0104
	Fads1	-2.18	0.0000	1.13	0.0514	-2.18	0.0000
	Fads2	-2.39	0.0000	1.24	0.0705	-2.36	0.0001
	Acsf2	1.36	0.0075	1.12	0.0792	1.28	0.0074
	Acsl1	1.19	0.1635	-1.18	0.3571	1.06	0.6852
	Acsl3	-2.16	0.0002	1.05	0.8005	-1.76	0.0202
	Acsl4	-1.24	0.1148	-1.10	0.3702	-1.25	0.0948
	Acsl5	-1.28	0.0405	1.40	0.0020	-1.40	0.0475
Srebp2 pathway	Hmgcs1	-1.60	0.0238	1.93	0.0020	-1.24	0.3368
	Hmgcr	-2.23	0.0034	1.72	0.0740	-1.30	0.5900
	Mvk	-1.11	0.3513	1.51	0.0086	-1.02	0.8580
	Pmvk	-2.30	0.0004	1.52	0.0068	-2.33	0.0033
	Mvd	-3.26	0.0033	1.94	0.0072	-1.98	0.0528
	Idi1	-1.63	0.0212	1.99	0.0017	-1.24	0.3330
	Fdps	-2.60	0.0022	1.88	0.0039	-2.20	0.0237
	Fdft1	-1.43	0.0095	1.72	0.0011	-1.10	0.6770
	Cyp51a1	-1.75	0.0058	1.81	0.0010	-1.40	0.1238
	Dhcr7	-1.65	0.0065	1.65	0.0007	-1.54	0.1193

Table 1. *Srebp1c* and *Srebp2* gene expression changes observed following *ApoB*, *Fatp5,* and combination siRNA treatments. Selected *Srebp1* and *Srebp2* pathway genes were analyzed after siRNA treatments. Mice were treated with siRNAs targeting *ApoB* and *Fatp5* alone or in combination (*ApoB*, *Fatp5*, *Fatp5*/*ApoB*) at day 0 and day 14. Gene expression was analyzed using qRT-PCR (TaqMan) on day 21. Fold regulation was calculated for the treatment group relative to the control siRNA group. Red indicates a significant induction (p ≤ *0.05*) and green indicates a significant reduction (p ≤ *0.05*) in expression relative to the control siRNA group. Significance (p value) was calculated using a two-tailed t-test between control and treatment groups.

DISCUSSION

By utilizing two siRNAs specifically targeting *Fatp5* and *ApoB* we were able to provide a proof-of-concept for the combination of two siRNAs *in vivo* using our siRNA-LNP platform. It is worth noting that the *ApoB* / *Fatp5* siRNA combination resulted in similar levels of knockdown relative to each single 3 mg/kg siRNA dose, even though the dose for each siRNA was reduced by half for the combination (1.5/1.5 mg/kg vs. 3 mg/kg). Similar levels of knockdown for a 1.5 /1.5 mg/kg combination dose relative to a 3 mg/kg single dose has been observed for other siRNA combinations (data not shown). Knockdown is maintained even though half the siRNA dose is used, in part, by the additional LNP included through the addition of a second siRNA. Thus, by balancing the total amount of LNP within the treatment, we are able to lower the dose of a single siRNA by half and still maintain similar levels of knockdown.

Simultaneously targeting of *ApoB* and *Fatp5* as a proof-of-concept and found that siRNA mediated knockdown of *ApoB* (mRNA and protein) for 4 weeks led to a significant reduction in serum cholesterol, including HDL, and a concomitant elevation in hepatic triglycerides leading to liver steatosis in CETP/LDLR hemizygous mice (a mouse model having a human-like lipid profile). Osmium stained liver sections revealed that *ApoB* siRNA treatment led to the accumulation of numerous small lipid droplets that were diffusely infiltrated across all hepatic zones. This contrasts the lipid staining for the remaining treatments, where lipid droplets appeared larger in many instances and exhibited evidence of a periportal to midzonal distribution (zones 1 and 2).

FATP5 is a transporter of long chain fatty acids (LCFAs) into hepatocytes. We rationalized that reducing LCFA uptake would reduce hepatic triglyceride levels following *ApoB* knockdown, since fatty acids are required for triglyceride synthesis and *ApoB* knockdown leads to the reduced expression of many of the genes involved in *de novo* hepatic fatty acid synthesis (29). We found that *Fatp5* knockdown does not influence the size, composition, or zonal distribution of the hepatic triglyceride pool generated by *ApoB* siRNA treatment suggesting that fatty acids are not transported to the liver from dietary uptake or from a store such as adipocytes.

Lipid levels for the *Fatp5* siRNA treatment alone were too low to reliably assess differences in the hepatic triglyceride population relative to the control siRNA group, although results reported by Doege *et al*. would suggest that reductions in FATP5 would disproportionately decrease the saturated and polyunsaturated fatty acid containing triglycerides relative to monounsaturated fatty acid containing triglycerides (27). The fact that the loss of FATP5 did not influence the size or composition of the triglyceride population generated by the loss of *ApoB* suggests that the means by which triglycerides accumulate within the liver influences the impact of FATP5 activity on the composition of the overall triglyceride population. In light of these data, together with the observation that the majority of accumulated triglycerides consist of non-essential fatty acids suggests that *ApoB* siRNA induced steatosis in this model is the product of the build up of triglycerides generated by *de novo* synthesis.

ApoB siRNA mediated steatosis contrasts results reported for ASO mediated *ApoB* knockdown where only modest but not significant increases in hepatic triglycerides were observed following 6 weeks of biweekly (25mg/kg) treatment that resolved by week 20 (14). Crooke *et al.* reasoned that a compensatory mechanism, which included the activation of AMPK leading to increased fatty acid oxidation and the down regulation of genes involved in fatty acid synthesis and transport led to the resolution of hepatic triglyceride accumulation (14). However, we also observed decreased gene expression within these pathways following the knockdown of *ApoB*. In addition, we observed increased serum ketone levels following *ApoB* siRNA treatment, which is indicative of increased fatty acid oxidation (data not shown). Furthermore, mice harboring a base-pair deletion in the coding region of *ApoB* (*ApoB-38.9*) also exhibited hepatic triglyceride accumulation and decreased expression of genes involved in fatty acid synthesis (25). Taken together, these data suggest that an alternative mechanism may explain the lack of ASO mediated steatosis and the discrepancy between *ApoB* siRNA and ASO treatments. It should be noted that we are observing slightly greater *ApoB* knockdown (~90% vs. ~75%) and cholesterol lowering (~80% (non-HDL) vs. 66% (LDL)) relative to the treatment concentration used for evaluating ASO mediated changes in hepatic triglyceride content in mice (25 mg/kg), which may help explain why we observe significant elevations in hepatic triglycerides compared to ASO treatment.

Finally, it was demonstrated that loss of FATP5 activity resulted in a significant increase in genes involved in hepatic cholesterol biosynthesis (*Srebp2* pathway) and fatty acid synthesis (*Srebp1* pathway). One could, therefore, speculate that changes in bile acid conjugation levels would result in an increase in *de novo* cholesterol synthesis, requiring more acetyl-CoA, which may promote fatty acid synthesis and is consistent with the failure of *Fatp5* knockdown to reverse *ApoB* siRNA induced liver steatosis and the observed small but significant increase in hepatic triglyceride content for the *Fatp5*/*ApoB* siRNA combination over *ApoB* siRNA treatment alone. These data are consistent with the increase in fatty acid synthase expression and defects in bile acid reconjugation reported for the loss of FATP5 activity, suggesting that *Fatp5* siRNA treatment was sufficient to influence FATP5 activity (26, 27).

REFERENCES

1.   Steinberg, D. 2004. *J. Lipid Res.* **45**:1583-1593.

2.   Steinberg, D. 2005. *J. Lipid Res.* **46**:179-190.

3.   Steinberg, D. 2005. *J Lipid Res* **46**:2037-2051.

4.   Steinberg, D. 2006 *J. Lipid Res.* **47**:1339-1351.

5.   Davis, R.A., and Hui, T.Y. 2001. *Arterioscler Thromb Vasc Biol* **21**:887-898.

6.   Skalen, K., Gustafsson, M., Rydberg, E.K., Hulten, L.M., Wiklund, O., Innerarity, T.L., and Boren, J. 2002.. *Nature* **417**:750-754.

7.   Hulthe, J., and Fagerberg, B. 2002. *Arterioscler Thromb Vasc Biol* **22**:1162-1167.

8.   Davidson, N.O., and Shelness, G.S. 2000. *Annu Rev Nutr* **20**:169-193.

9.   Gaffney, D., Forster, L., Caslake, M.J., Bedford, D., Stewart, J.P., Stewart, G., Wieringa, G., Dominiczak, M., Miller, J.P., and Packard, C.J. 2002. *Atherosclerosis* **162**:33-43.

10.   Veerkamp, M.J., de Graaf, J., Bredie, S.J., Hendriks, J.C., Demacker, P.N., and Stalenhoef, A.F. 2002. *Arterioscler Thromb Vasc Biol* **22**:274-282.

11.   Tybjaerg-Hansen, A., Steffensen, R., Meinertz, H., Schnohr, P., and Nordestgaard, B.G. 1998. *N Engl J Med* **338**:1577-1584.

12.   Boren, J., Lee, I., Zhu, W., Arnold, K., Taylor, S., and Innerarity, T.L. 1998. *J Clin Invest* **101**:1084-1093.

13.   Innerarity, T., Mahley, R., Weisgraber, K., Bersot, T., Krauss, R., Vega, G., Grundy, S., Friedl, W., Davignon, J., and McCarthy, B. 1990. *J. Lipid Res.* **31**:1337-1349.

14.   Crooke, R.M., Graham, M.J., Lemonidis, K.M., Whipple, C.P., Koo, S., and Perera, R.J. 2005. *J Lipid Res* **46**:872-884.

15.   Rozema, D.B., Lewis, D.L., Wakefield, D.H., Wong, S.C., Klein, J.J., Roesch, P.L., Bertin, S.L., Reppen, T.W., Chu, Q., Blokhin, A.V., et al. 2007 *Proceedings of the National Academy of Sciences* **104** 12982-12987

16.   Zimmermann, T.S., Lee, A.C., Akinc, A., Bramlage, B., Bumcrot, D., Fedoruk, M.N., Harborth, J., Heyes, J.A., Jeffs, L.B., John, M., et al. 2006. *Nature* **441**:111-114.

17. Soutschek, J., Akinc, A., Bramlage, B., Charisse, K., Constien, R., Donoghue, M., Elbashir, S., Geick, A., Hadwiger, P., Harborth, J., et al. 2004. *Nature* **432**:173-178.

18. Merki, E., Graham, M.J., Mullick, A.E., Miller, E.R., Crooke, R.M., Pitas, R.E., Witztum, J.L., and Tsimikas, S. 2008. *Circulation* **118**:743-753.

19. Chandler, C.E., Wilder, D.E., Pettini, J.L., Savoy, Y.E., Petras, S.F., Chang, G., Vincent, J., and Harwood, H.J., Jr. 2003. *J Lipid Res* **44**:1887-1901.

20. Visser, M.E., Akdim, F., Tribble, D.L., Nederveen, A.J., Kwoh, T.J., Kastelein, J.J., Trip, M.D., and Stroes, E.S. *J Lipid Res* **51**:1057-1062.

21. Akdim, F., Visser, M.E., Tribble, D.L., Baker, B.F., Stroes, E.S., Yu, R., Flaim, J.D., Su, J., Stein, E.A., and Kastelein, J.J. *Am J Cardiol* **105**:1413-1419.

22. Akdim, F., Stroes, E.S., Sijbrands, E.J., Tribble, D.L., Trip, M.D., Jukema, J.W., Flaim, J.D., Su, J., Yu, R., Baker, B.F., et al. *J Am Coll Cardiol* **55**:1611-1618.

23. Raal, F.J., Santos, R.D., Blom, D.J., Marais, A.D., Charng, M.J., Cromwell, W.C., Lachmann, R.H., Gaudet, D., Tan, J.L., Chasan-Taber, S., et al. *Lancet* **375**:998-1006.

24. Kastelein, J.J., Wedel, M.K., Baker, B.F., Su, J., Bradley, J.D., Yu, R.Z., Chuang, E., Graham, M.J., and Crooke, R.M. 2006. *Circulation* **114**:1729-1735.

25. Lin, X., Schonfeld, G., Yue, P., and Chen, Z. 2002. *Arterioscler Thromb Vasc Biol* **22**:476-482.

26. Hubbard, B., Doege, H., Punreddy, S., Wu, H., Huang, X., Kaushik, V.K., Mozell, R.L., Byrnes, J.J., Stricker-Krongrad, A., Chou, C.J., et al. 2006.. *Gastroenterology* **130**:1259-1269.

27. Doege, H., Grimm, D., Falcon, A., Tsang, B., Storm, T.A., Xu, H., Ortegon, A.M., Kazantzis, M., Kay, M.A., and Stahl, A. 2008. *J Biol Chem* **283**:22186-22192.

28. Mencarelli, A., Renga, B., Distrutti, E., and Fiorucci, S. 2009. *Am J Physiol Heart Circ Physiol* **296**:H272-281.

29. Tadin-Strapps, M., Peterson, L.B., Cumiskey, A.M., Rosa, R.L., Mendoza, V.H., Castro-Perez, J., Puig, O., Zhang, L., Strapps, W.R., Yendluri, S., et al. *J Lipid Res*.

30. Majercak, J., Ray, W.J., Espeseth, A., Simon, A., Shi, X.P., Wolffe, C., Getty, K., Marine, S., Stec, E., Ferrer, M., et al. 2006. *Proc Natl Acad Sci U S A* **103**:17967-17972.

31.   Wincott, F., DiRenzo, A., Shaffer, C., Grimm, S., Tracz, D., Workman, C., Sweedler, D., Gonzalez, C., Scaringe, S., and Usman, N. 1995. *Nucleic Acids Res* **23**:2677-2684.

32.   Livak, K.J., and Schmittgen, T.D. 2001. *Methods* **25**:402-408.

33.   Bligh, E.G., and Dyer, W.J. 1959. *Can J Biochem Physiol* **37**:911-917.

SUPPLEMENTARY INFORMATION

Supplementary Figure 1. Comparable levels of triglycerides were observed for *ApoB* siRNA treatments either alone or in combination with a siRNA targeting *Fatp5*. Triglycerides were measured on day 21 (A) and on day 28 (B) following a day 0 and day 14 dose as indicated on the x-axis. Data represented as group means (bars) +/- S.D. The percent difference relative to the control siRNA is shown. Significance (***, p $\leq$ *0.0001*, **, p $\leq$ *0.001*, *, p $\leq$ *0.01*) was calculated using a two-tailed t-test between siRNA control (control siRNA) and treatment groups.
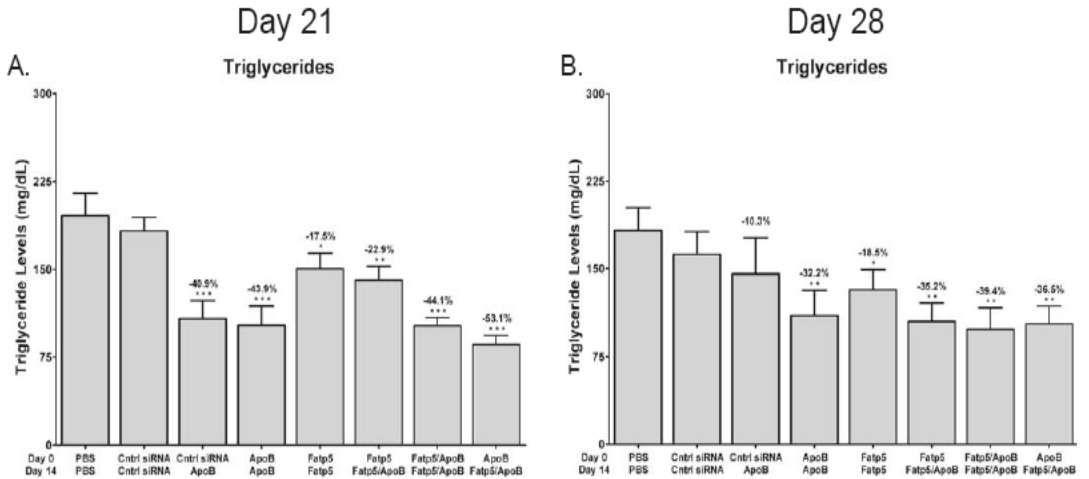
Supplementary Figure 2. Structure elucidation of hepatic triglycerides by collisional induced dissociation (MS/MS). 4These triglycerides were confirmed by exact mass and the use of external standards.
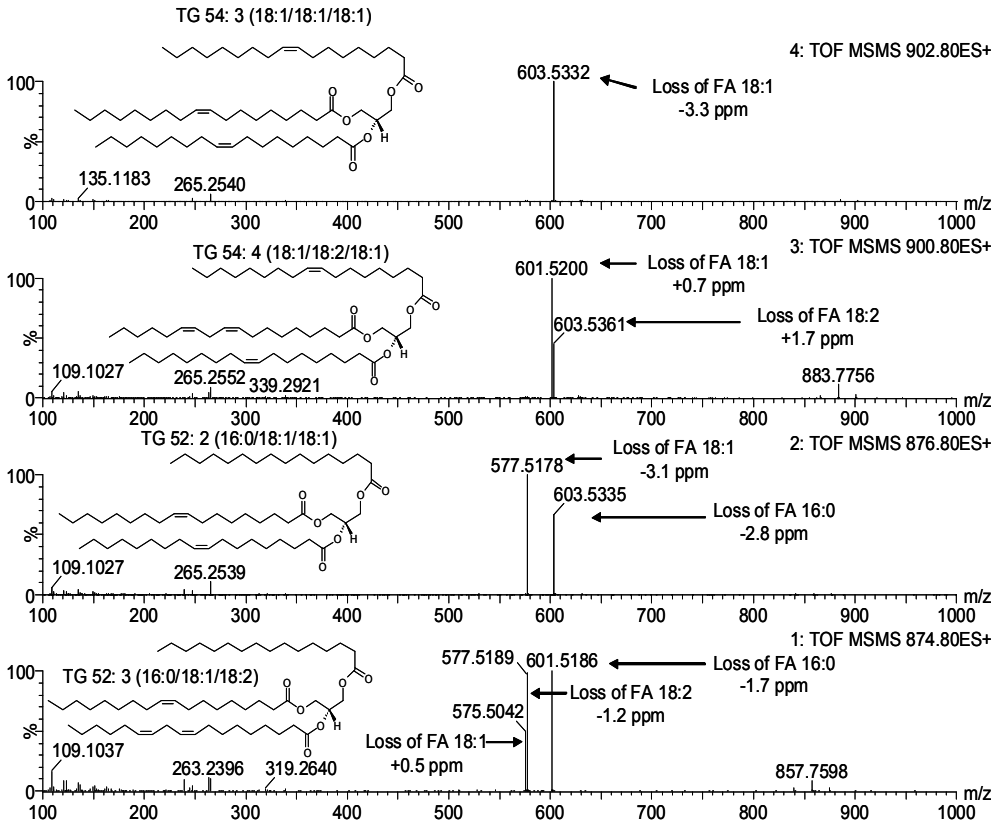
Abbreviations;

TG 52:2 ; 1-hexadecanoyl-2,3-di-(9Z-octadecenoyl)-sn-glycerol

TG 52:3 ; 1-hexadecanoyl-2-(9Z-octadecenoyl)-3-(9Z,12Z-octadecadienoyl)-sn-glycerol

TG 54:3 ; 1,2,3-tri-(9Z-octadecenoyl)-glycerol

TG 54:4 ; 1,3-di-(9Z-octadecenoyl)-2-(9Z,12Z-octadecadienoyl)-sn-glycerol

Supplementary Table 1. The gene expression assays used for *Srepb1c* and *Srebp2* pathway analysis are listed along with the gene symbol, official gene name and probe number.

	Gene	Accession #	Official Full Name	Probe #
Genes involved in Srebp1c pathway	Acaca	NM_133360	Acetyl-Coenzyme A carboxylase alpha	PPM05109
	Acacb	NM_133904	Acetyl-Coenzyme A carboxylase beta	PPM05086
	Fasn	NM_007988	Fatty acid synthase	PPM03816
	Scd	NM_009127	Stearoyl-Coenzyme A desaturase 1	PPM05664
	Fads1	NM_146094	Fatty acid desaturase 1	PPM27749
	Fads2	NM_019699	Fatty acid desaturase 2	PPM28583
	Acsf2	NM_153807	Acyl-CoA synthetase family member 2	PPM32224
	Acsl1	NM_007981	Acyl-CoA synthetase long-chain family member 1	PPM33300
	Acsl3	NM_001033606	Acyl-CoA synthetase long-chain family member 3	PPM63570
	Acsl4	NM_019477	Acyl-CoA synthetase long-chain family member 4	PPM31539
	Acsl5	NM_027976	Acyl-CoA synthetase long-chain family member 5	PPM58825
Genes involved in Srebp2 pathway	Hmgcs1	NM_145942	3-hydroxy-3-methylglutaryl-Coenzyme A synthase 1	PPM05651
	Hmgcr	NM_008255	3-hydroxy-3-methylglutaryl-Coenzyme A reductase	PPM40190
	Mvk	NM_023556	Mevalonate kinase	PPM27182
	Pmvk	NM_026784	Phosphomevalonate kinase	PPM28175
	Mvd	NM_138656	Mevalonate (diphospho) decarboxylase	PPM27199
	Idi1	NM_145360	Isopentenyl-diphosphate delta isomerase	PPM27659
	Fdps	NM_134469	Farnesyl diphosphate synthetase	PPM04626
	Fdft1	NM_010191	Farnesyl diphosphate farnesyl transferase 1	PPM05519
	Cyp51a1	NM_020010	Cytochrome P450, family 51	PPM03876
	Dhcr7	NM_007856	7-dehydrocholesterol reductase	PPM34999

Chapter 6

Non-HDL cholesterol and ApoB was lowered following in-vivo silencing of Slc27a5 gene expression in C57Bl/6 mice

Non-HDL cholesterol and ApoB was lowered following *in-vivo* silencing of Slc27a5 gene expression in C57Bl/6 mice

SUMMARY

Slc27a5, also known as fatty acid transporter 5 (FATP5), is a critical enzyme involved in the reconjugation of bile acids during enterohepatic bile acid recycling. Reported deletion and adenovirus-mediated small hairpin RNA (shRNA) silencing in mice resulted in favorable metabolic phenotypes that included a lack of diet-induced obesity (DIO) and liver steatosis, and an increase in insulin sensitivity. To further understand the role of Slc27a5 in vivo, we generated and characterized a novel C57Bl/6 mouse that constitutively express shRNA sequences which stably silence gene and hepatic protein expression (Slc27a5-cKD mice). On the high fat diet, Slc27a5-cKD male mice were resistant to DIO and had a significant decrease in plasma non-HDL cholesterol, total cholesterol and apolipoprotein-B (apoB). Female Slc27a5-cKD mice were resistant to DIO on the low-fat diet and had a significant decrease in non-HDL cholesterol on the high-fat diet. Acute silencing of Slc27a5 by short-interfering RNA (siRNA) in CETP+/-/LDLr+/- hemizygous mice resulted in lowering of non-HDL cholesterol and apoB. In both models, there were significant elevations of plasma total and unconjugated bile acids. Together, these data extend the role of Slc27a5 in vivo and demonstrate that loss of hepatic gene function results in a significant decrease in proatherogenic lipoprotein particles.

INTRODUCTION

Coronary artery disease (CAD) is the leading cause of death in the Western world, generally caused by atherosclerosis which can produce myocardial infarction, stroke, and peripheral artery disease. Attributes of CAD are caused by many factors, such as genetics, diet and life style (1-4). Atherosclerosis is a chronic inflammatory disease that is accelerated by high levels of plasma apoB-containing lipoproteins (non-HDL cholesterol). Therapies, such as statins, that significantly lower plasma LDL/non-HDL cholesterol have been shown to be effective in treating atherosclerosis and in preventing associated complications. However, some patients cannot tolerate statins, or do not reach their non-HDL cholesterol goal while on a statin (5), therefore additional therapies that reduce proatherogenic apoB-containing lipoproteins are needed. Bile acids (BAs) have a well-known function as detergents in the gastrointestinal tract to help adsorb fat-soluble vitamins and lipids.

In addition, BAs play an important role in cholesterol excretion. Increased interests have focused on the effects of BAs on lipoprotein metabolism, and recent studies have shown that BAs can act as signaling molecules affecting both glucose and lipid metabolism (6-9). BAs may exert biological effects on lipid metabolism by several mechanisms, including activating specific nuclear receptors (farnesoid X receptor (FXR), pregnane X receptor (PXR), and vitamin D receptor (VDR)), by binding to the G protein coupled receptor TGR5 (also known as M-BAR or BG37 or GPBAR1 or GPR131), and by activating specific cell signaling pathways (c-jun N-terminal kinase 1/2, AKT, and ERK 1/2) in the liver and gastrointestinal tract.

BAs can also regulate the expression of proprotein convertase subtilisin/kexin type 9 (PCSK9) and LDL receptor levels in cultured human hepatocytes and in intestinal epithelial cells (10, 11). Interestingly, the conjugation state of BAs (unconjugated and conjugated) exhibited different effects on PCSK9 and LDL receptor levels in intestinal epithelial cells, demonstrating that the BA conjugation state could have differential biological effects. These studies suggest that transcriptional repression of PCSK9 by BAs may have beneficial effects on atherogenic lipids and may potentiate the effects of statins.

The link between BAs and LDL and apoB was demonstrated several years ago with the use of the BA sequestrant cholestyramine, where treatment reduced LDL and apoB levels in humans and in animal models (12-14). Colesevelam hydrochloride treatment of patients with type 2 diabetes and hypercholesterolemia resulted in a significant reduction in LDL and apoB, in addition to significant reductions in glucose/HbA1c (15-20). The exact mechanism of how BA sequestrants reduce LDL and apoB levels is still unknown, yet one possible explanation is that BA sequestrants change the total concentration and synthesis of BAs and possibly affect the activity of FXR or TGR5. Recently, BA activation of FXR has been shown to suppress the expression of the microsomal triglyceride transfer protein (MTP), the transcription factor sterol regulatory element binding protein (SREBP)-1c, other lipogenic genes involved in apoB-lipoprotein metabolism, and reduce atherosclerosis in various animal models (21-23). Moreover, patients who underwent gastric

bypass surgery have reduced apoB-containing lipoproteins and an increase in total circulating BAs, with a trending increase in unconjugated BAs (24). From these data, one could speculate that plasma BA levels and the BA conjugation state may be linked to apoB lipoprotein metabolism. Slc27a5 is an enzyme expressed predominantly in liver that is involved in the reconjugation of BAs to glycine or taurine (conjugated BAs) during the enterohepatic recycling process (Figure 1); conjugation here refers to the N-acyl amidation of BAs with glycine or taurine. Conjugation aids in the solubility and hydrophilicity of BAs, as well as renders conjugated BAs fully ionized at physiological pH (8). Mice genetically deficient in Slc27a5 have a significant increased in unconjugated BAs in the plasma and bile, and result in a lack of diet induced obesity (25, 26). Although silencing gene expression using adenovirus-shRNA virus reduced diet induced liver steatosis (27), transient siRNA-LNP silencing did not protect from apoB-induced liver steatosis (see Chapter 4). These findings highlight an additional function of Slc27a5, as a free fatty acid transporter in liver, and show that loss of its function can inhibit dietary fatty acids from contributing to hepatic steatosis. Accordingly, BAs have been shown to have physiologic effects on glucose, lipid, and liver metabolism, yet the role Slc27a5 may have on cholesterol metabolism is undefined.

Here, a novel role of Slc27a5 in non-HDL cholesterol and apoB metabolism was demonstrated. Reduced expression of Slc27a5 in C57Bl/6 mice constitutively expressing Slc27a5 shRNA transgene or in CETP+/-/LDLr+/- hemizygous mice treated with Slc27a5 siRNA-LNP resulted in a significant increase in plasma total and unconjugated BAs and a significant decrease in plasma non-HDL cholesterol and apoB. As with genetic deficiency, chronic reduction by shRNA resulted in a lack of diet-induced obesity in male mice on both low-fat and high-fat diets, and in female mice on low-fat diet. Acute reduction of Slc27a5 expression resulted in a significant increase in plasma unconjugated BAs and a significant decrease in plasma non-HDL cholesterol and apoB, without any effects on body weight, suggesting that the lipid effects are independent of the effects on body weight. Thus, chronic or acute reduction of Slc27a5 gene expression and function in vivo results in lowering of circulating proatherogenic lipoprotein particles containing apoB.
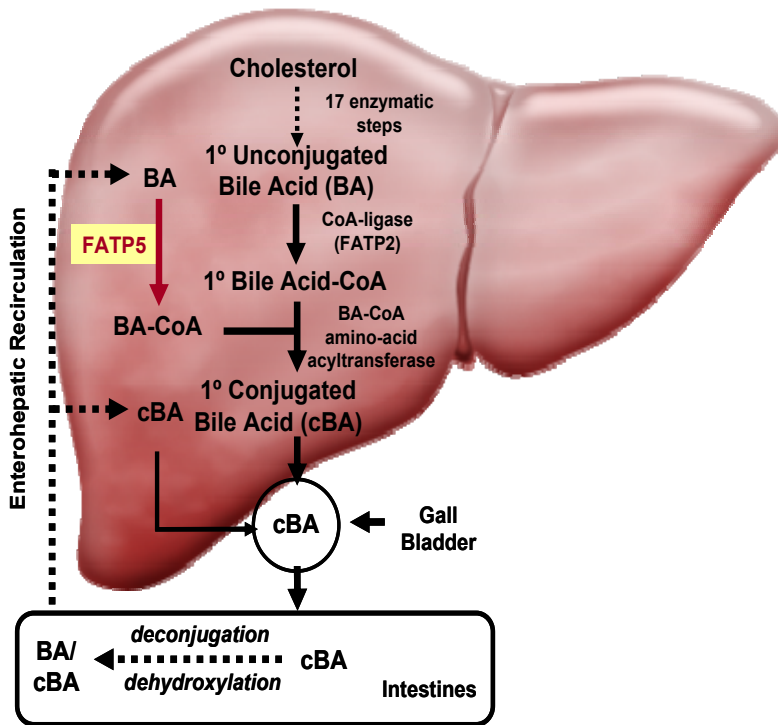
Figure 1. Schematic of bile acid metabolism and enterohepatic recycling. BAs are synthesized in the liver from cholesterol by multiple enzymatic steps that include the rate-limiting step catalyzed by Cyp7a1. Amino acid conjugation of primary bile acids by the bile acid coenzyme A:amino acid N-acyltransferase (BAAT) is first activated by a hepatic coenzyme-A ligase (CoA-ligase); Slc27a2 (FATP2) may act in this capacity. Primary conjugated BAs are then transported to the gall bladder and stored for use. After a meal, "BA flux" is activated when the gall bladder is stimulated by gastric incretins to promote BAs transport to the intestines where they solubilize dietary lipids and vitamins. BAs are then excreted into feces or reabsorbed by intestinal transporters into the portal system and plasma, and are returned to the liver. Microbial enzymes dehydroxylate and deconjugate BAs in the intestines. Secondary unconjugated BAs are reconjugated in the liver by BAAT after CoA-ligase activation by Slc27a5 (FATP5).

MATERIAL AND METHODS

Generation of Slc27a5 shRNA constitutive knockdown C57Bl/6 mice.

19- mer Slc27a5 shRNA (GAGTCCAATCGGAAACTTG [sense] ttcaagaga [loop] CAAGTTTCCGATTGGACTC [antisense]) was cloned into a recombinase- mediated cassette exchange (RMCE) vector downstream of H1 promoter and transfected to the RMCE-ready C57Bl/6 mouse embryonic stem (ES) cells as described (28, 29). ES clones that had undergone successful RMCE with Slc27a5 shRNA expression cassette integrated into rosa26 locus (Figure 2A) were identified by PCR genotyping. The shRNA transgenic ES cells with >70% reduction of Slc27a5 mRNA, determined by TaqMan gene expression analysis (Applied Biosystems, Inc.), were injected into tetraploid blastocysts to generate chimeric founder mice. Male chimeras were mated with C57BL/6 females and resulted in germline transmitted offspring (Slc27a5-cKD mice). mRNA and protein levels of Slc27a5 were determined using 10-12-week-old Slc27a5-cKD mice and the wild-type littermates (bred at Taconic Farms, Inc., Germantown, NY). For all subsequent experiments, heterozygous Slc27a5-cKD mice were used since mRNA and protein levels in mice containing one copy of the shRNA were reduced > 90% of wild type levels.

Measure of hepatic Slc27a5 mRNA and protein expression.

Blood and liver samples were collected from mice immediately following euthanasia. Total RNA was isolated using the RNeasy 96 Tissue Kit (Qiagen) according to the manufacturer's instructions. All RNA samples were treated with DNase I (Qiagen) on a column for 15 minutes at room temperature. First strand cDNA was generated from 1.0µg of total RNA using the MultiScribe™ Reverse Transcriptase and Random Primers contained in a High-Capacity cDNA Reverse Transcription Kit (Applied Biosystems). TaqMan qPCR analysis was done on an ABI 7900 Real-Time PCR System. cDNA derived from 20ng total RNA was used as template for each reaction. Reactions were set up in Triplicate, singleplex with a final volume of 10µl using TaqMan Gene Expression Master Mix (Applied Biosystems). Slc27a5 mRNA was quantified using primer/probe set Mm00447768_m1 purchased from Applied Biosystems, which spans the exon 6 and 7 junction of Slc27a5, detecting only the cDNA, not genomic DNA. Relative quantitation of Slc27a5 expression was determined by standard .Ct-methods, using GAPDH as the endogenous control (Applied Biosystems). The mRNA knockdown (KD) was calculated relative to either WT mice or to a non-targeting control siRNA (nt control) in each experiment. Slc27a5 protein levels were determined by western blot analysis of liver extracts. WT and Slc27a5-cKD livers were snap-frozen on liquid nitrogen and protein extracts were made by sonication in RIPA buffer, with freshly added protease inhibitor (Roche). 20µg of protein extracts was separated by 4-12% Bis-Tris gel (Invitrogen), transferred to PVDF membranes by electro-blotting, and then blotted with a 1:500 dilution of antibodies against Slc27a5 (Sigma). ß-Actin was blotted as a control for protein loading (Cell Signaling).

Analysis of Slc27a5-cKD and WT littermate mice on low-fat and high-fat diets. 8 week old male and female wild type (WT) and Slc27a5-cKD mice (bred at Taconic Farms, Inc., Germantown, NY) were randomized into two groups. Group 1

contained 9 male and 8 female Slc27a5-cKD, and 8 male and 7 female WT mice on a low-fat diet (LFD; 5021, 9% fat, Research Diets, NJ). Group 2 contained 10 male and 9 female Slc27a5-cKD, and 10 male and 9 female WT mice on high-fat diet (HFD; D12492, 60% fat from lard, Research Diets, NJ). The diet intervention proceeded for 13 weeks with weekly body weight and food-intake measurements and then the studies were terminated by euthanasia after a 4 hour fast. Significance of body weight and caloric intake changes were determined after one-way ANOVA analysis. Blood was collected by cardiac bleed to generate plasma or serum, gall bladder content removed and measured by syringe, and tissues (liver, gall bladder) excised and snap-frozen in liquid nitrogen. Samples were stored at -80°C until analyzed. All animal protocols were reviewed and approved by the Merck Research Laboratories Institutional Animal Care and Use Committee (Rahway, NJ).

Plasma lipid measurements.

HDL cholesterol, non-HDL cholesterol, and total cholesterol (TC) serum levels were determined using standard biochemical methods. HDL cholesterol levels were determined using the HDL cholesterol E kit by WAKO Diagnostics. 20μl of precipitating reagent was combined with 20μl of serum in a Costar 3894 V-bottom non-pyrogenic polystyrene sterile plate, mixed, and incubated at room temperature for 5 minutes. Plate was subsequently spun at 4680 rpm for 30 minutes. 5μl of supernatant was aliquoted onto a flat bottom 96-well plate. A standard curve was generated in duplicate by diluting Cholesterol-E standard solution (WAKO Diagnostics) from 0-20μg in water. 200μl of WAKO color reagent solution was added to each well, and incubated at 37°C for 15 minutes or room temperature for 30 minutes. The odometer readings were determined at 600nm using Spectramax plate reader, and the 700nm background reading was subtracted. TC levels were determined using the Total Cholesterol E Kit by WAKO Diagnostics. 5μl of serum was added to a flat bottom 96-well plate, and the standard curve and assay were generated as outlined in the HDL assay. The non-HDL cholesterol levels were calculated indirectly by subtracting HDL cholesterol from TC (non-HDL includes LDL, VLDL and chylomicron fractions). All assays were performed according to the manufacturer's instructions.

Quantitation of plasma apoAI and apoB.

Serum apoA1 levels were measured using a specific murine apoA1 ELISA. Black plates (Thermo Labsystems) were coated with 50μl per well of goat polyclonal anti-mouse apoA1 (Rockland 600-101-196) diluted to 1μg/ml in PBS containing 0.6mM EDTA overnight at 4°C with shaking. Plates were then blocked with 200μl per well of Blocking buffer (1XTBST with 1% BSA) at room temperature for 1 hour, washed with wash buffer (1XTBST supplemented with 0.05% Tween20). Test serum samples were then added to the plates at 1:2000 dilution in Assay buffer (PBS with 1% BSA and 0.1% Tween20), incubated at room temperature for 2 hours with shaking.

Purified mouse HDL was used as the standard and processed in the same way. The plates were washed again, and then incubated with 1μg/ml biotinylated 2° antibody (Rockland 600-101-196) at room temperature with shaking for 1 hour.

Plates were further processed with the Streptavidin/Europium solution and the DELFIA Enhance solution for detection on a Perkin Elmer EnVision 2103 Multi-label reader following the guidelines for DELFIA detection platform.

ApoB was measured by two methods: by semi-quantitative SDS-PAGE- western blot analysis and by LC/MS. For SDS-PAGE-western blot analysis, mouse serum was diluted 200-fold in PBS, and then resolved by SDS-PAGE using the 3-8% NuPAGE Tris-Acetate gradient gel (Invitrogen). A calibrator sample at 1:50 and 1:800 dilutions and the HiMark Pre-Stained HMW protein standard were included on every gel. Gels were run for 90 minutes (125V), transferred onto nitrocellulose membrane, and then subjected to anti-apoB Western blotting in standard procedures. Rabbit anti-mouse apoB (Abcam) and anti-rabbit IgG HRP (GE Healthcare) were used as primary and secondary antibodies, respectively. ECL Plus (GE Healthcare) was used for detection. Densitometric image was obtained by scanning the membranes on a Typhoon Scanner (fluorescence, Blue1 457Laser, 520BP40Cy2; BlueFAM). The absolute intensity of apoB100 and apoB 48 bands was quantified using the ImageQuant Software. Relative quantitation of total apoB (apoB100 + apoB48) in each sample was then achieved by extrapolating from the calibrator curves and reported as arbitrary units.

For LC/MS quantitation, serum apoB protein levels were measured by measuring the GFEPTLEALFGK peptide of apoB using UPLC-MS/MS. Briefly, 4μL of serum was diluted with 138μL of 50 mM ammonium bicarbonate (pH 8.0), 50μL of 80nM internal standard apoB peptides and 10μL of 10% sodium deoxycholate. Samples were reduced with dithiothreitol for 30 min at 60°C, alkylated with iodoacetamide for 60 min at 25°C in the dark and digested overnight with 3μg trypsin (1:50 serum proteins). To stop digestion, 10μL of 20% formic acid was added to precipitate the sodium deoxycholate. Samples were then centrifuged for 15 minutes at 15800 rcf and 120μL of the supernatant was removed for LC/MS analysis. Serum apoB levels in the samples were then analyzed on a Waters Acquity UPLC and Xevo triple quadrupole mass spectrometer. The gradient was 95%A (0.1% formic acid in water)/5%B (0.1% formic acid in acetonitrile) ramped to 80%A at 1 minute, 65%A at 4 minutes, 5%A at 5 minutes. A Phenomenex Kinetex C18 50x2.1mm 1.7μm column maintained at 50°C was used at a flow rate of 0.7mL/min. ApoB peptide concentration was calculated by dividing the area under the curve for the analyte by the area of its internal standard and multiplying by the internal standard concentration. The concentration of apoB was then converted and reported as mg/dL.

High resolution LC/MS measurements of BAs.

Plasma and bile was analyzed for BA concentration and conjugation states. For plasma extraction, 10μl of 1μM internal standard solution (D$_4$-TCA, D$_4$-CA, D$_4$-GCA; Sigma-Isotec St. Louis, MO) was added to 50μL of plasma, and then 450μL of ice-cold ACN solution was added and then mixed. The extracts were centrifuged for 10 minutes at 15,000 g, and the supernatant aspirated and evaporated under vacuum at 10°C. Samples were then reconstituted with 100μL 50% ACN + 0.1% formic acid/50% water + 0.1 % formic acid. The final mixture was placed into a 96 well plate, and stored at -20°C until ready for LC/MS analysis. Bile extraction started with a 1:1000 dilution of bile fluid with 50% ACN + 0.1% formic acid/50% water + 0.1 % formic acid and the addition of 1μM total internal standard above. This mixture was mixed for 10

seconds and centrifuged for 10 minutes at 15,000 g. Then, it was placed on a 96-well and stored at -20°C until ready for LC/MS analysis. The configuration of the LC/MS system was comprised of an Acquity UPLC (Waters, Milford, MA, USA) coupled with a hybrid quadrupole orthogonal time of flight mass spectrometer (SYNAPT G2 HDMS, Waters, MS Technologies, Manchester, UK). Electrospray (ESI) negative ion ionization mode, capillary voltage and cone voltage of -2 kV and -30 V respectively was used. Extracts were injected (10μL) onto a 1.8μm particle 100 x 2.1mm id Waters Acquity HSS T3 column (Waters, Milford, MA, USA) maintained at 65°C, with a flow rate of 0.7 mL/min. A binary gradient system consisting of water + 0.1% formic acid was Eluent A, and Eluent B consisted of acetonitrile + 0.1% formic acid (Burdick & Jackson, USA). A linear gradient was performed over a 13 min total run from 20%B to 99%B. LC/MS data was processed by the manufacturer software (MassLynx) and quantitation determined by TargetLynx. For statistical analysis, all data are presented as ± standard error means (SEM). Differences between groups were computed by student's t-test and 1-way ANOVA (Analysis of Variance) statistical analysis (GraphPad Prism, La Jolla, CA). Post test analysis for quantifiable variables was conducted using Mann-Whitney U non-parametric test with two-tailed p-values and Tukey's post-test. Values of $p < 0.05$ were considered as being statistically significant.

siRNA design.

siRNAs were designed as described previously (30). siRNA sequences contained the following chemical modifications added to the 2' position of the ribose sugar when indicated: deoxy (d), 2' fluoro (flu), or 2' O-methyl (ome). Modification abbreviations are given immediately preceding the base to which they were applied. Passenger strands are blocked with an inverted abasic nucleotide on the 5' and 3' ends. The three siRNA sequences used for the in vivo studies have the following sequences (all in the 5'-3' direction):

non-targeting (nt) control Passenger Strand:

iB;fluU;fluC;fluU;fluU;fluU;fluU;dA;dA;fluC;fluU;fluC;fluU;fluC;fluU;fluU;fluC;dA;dG;dG;dT;dT;iB.

non-targeting (nt) control Guide Strand:

fluC;fluC;fluU;omeG;omeA;omeA;omeG;omeA;omeG;omeA;omeG;fluU;fluU;omeA;omeA;omeA;rA;rG;rA;omeU;omeU.

Slc27a5 Passenger Strand:

iB;fluC;fluU;dG;fluC;fluC;dA;fluU;dA;fluU;fluU;fluC;dA;fluU;fluC;fluU;fluU;fluU;dA;fluC;dT;dT;iB.

Slc27a5 Guide Strand:

rG;rU;rA;omeA;omeA;omeG;omeA;fluU;omeG;omeA;omeA;fluU;omeA;fluU;omeG;omeG;fluC;omeA;omeG;omeU;omeU.

ApoB Passenger Strand:

iB;fluU;fluC;dA;fluU;fluC;dA;fluC;dA;fluC;fluU;dG;dA;dA;fluU;dA;fluC;fluC;dA;dA;dT;dT;iB.

ApoB Guide Strand:

rU;rU;rG;omeG;fluU;omeA;fluU;fluU;fluC;omeA;omeG;fluU;omeG;fluU;omeG;omeA;fluU;omeG;omeA;omeU;omeU.

Synthesis and encapsulation of siRNA.

siRNAs were synthesized by methods previously described (31). In brief, two separate complementary strands were synthesized by solid phase synthesis for each siRNA. The two strands were then purified and annealed to form the double strand siRNA duplex. The duplex was ultra-filtered and lyophilized to form the dry siRNA. Duplex purity was tested with LCMS. Duplex material was tested for the presence of endotoxin by standard methods. Encapsulation of siRNAs was done as described by Tadin-Strapps et al. (manuscript in press JLR 2011). In brief, liposome OCD was made using the cationic lipid CLinDMA (2-{4-[(3b)-cholest-5-en-3-yloxy]-octyl}-N,N-dimethyl-3-[(9Z,12Z)- octadeca-9,12-dien-1-yloxy]propan-1-amine), cholesterol, and PEG-DMG (monomethoxy(polyethyleneglycol)-1,2-dimyristoylglycerol) in 60:38:2 molar ratio respectively. siRNAs were incorporated into the LNPs with high encapsulation efficiency by mixing siRNA in citrate buffer with an ethanolic solution of the lipid mixture, followed by a stepwise diafiltration process. Cholesterol was purchased from Northern Lipids, PEG-DMG was purchased from NOF Corporation and CLinDMA was synthesized by Merck and Co. The encapsulation efficiency of the particles was determined using a SYBR Gold fluorescence assay in the absence and presence of triton, and the particle size measurements were performed using a Wyatt DynaPro plate reader. The siRNA and lipid concentrations in the LNP were quantified by a HPLC method, developed in house, using a PDA and ELSD detector respectively.

*Analysis of CETP+/-/LDLr+/- hemizygous mice treated with siRNA-LNP.*

In vivo efficacy studies were conducted in CETP-tg/Ldlr KO F1 (+/-) (CETP/LDLr hemizygous) mice obtained from Taconic Laboratories. Animals weighed approximately 20-25 g at the time of the study. In an initial study, mice were dosed i.v. via tail vein injections with 3.0, 1.0, 0.3 or 0.1 mg/kg of LNP- encapsulated siRNAs. The Slc27a5 LNPs were diluted in the non-targeting control LNP to ensure that each dose contained comparable lipid content. Animals were sacrificed at days 1, 3, or 7 days following dosing. In a second study, mice were dosed i.v. via tail vein injections with a single 3 mg/kg dose of LNP-encapsulated siRNAs at day 0 and then with another 3 mg/kg re-dose at day 14 for all of the day 21 and day 28 groups. Animals were sacrificed at days 7, 14, 21 or 28 following dosing. In both studies, cohorts for controls and each siRNA tested consisted of eight animals. Blood and liver samples were collected immediately following

euthanasia. In addition, BAs via the gall bladder were also collected. Target gene knockdown in the liver was assessed by TaqMan analysis of total RNA as described above.

RESULTS

### *Slc27a5-cKD mice have significantly reduced hepatic Slc27a5 mRNA and protein expression*.

Slc27a5-cKD mice were generated as described in the Materials and Methods. Germline transmitted Slc27a5 cKD mice were bred with WT C57Bl/6 mice to create and maintain a heterozygous colony (mice containing one copy of Slc27a5 shRNA expression cassette docked at rosa26 locus, Figure 2A). Since Slc27a5 is predominantly expressed in the liver (25, 26), we examined liver mRNA and protein expression to determine efficacy of shRNA silencing. Figure 2B and 2C showed the level of Slc27a5 mRNA (qRT-PCR) and protein (western blot) in Slc27a5 cKD mice respectively. Approximately 90% of the Slc27a5 mRNA was reduced in the liver (Figure 2B) as compared to WT littermate controls. The low level of mRNA remaining did not yield any detectable Slc27a5 protein by western blot analysis of liver extracts (Figure 2C). Gene expression of other Slc27 protein family members found in the liver, Slc27a2 (FATP2) and Slc27a4 (FATP4), were not changed in the Slc27a5-cKD mice (data not shown).

A.

B.

C.
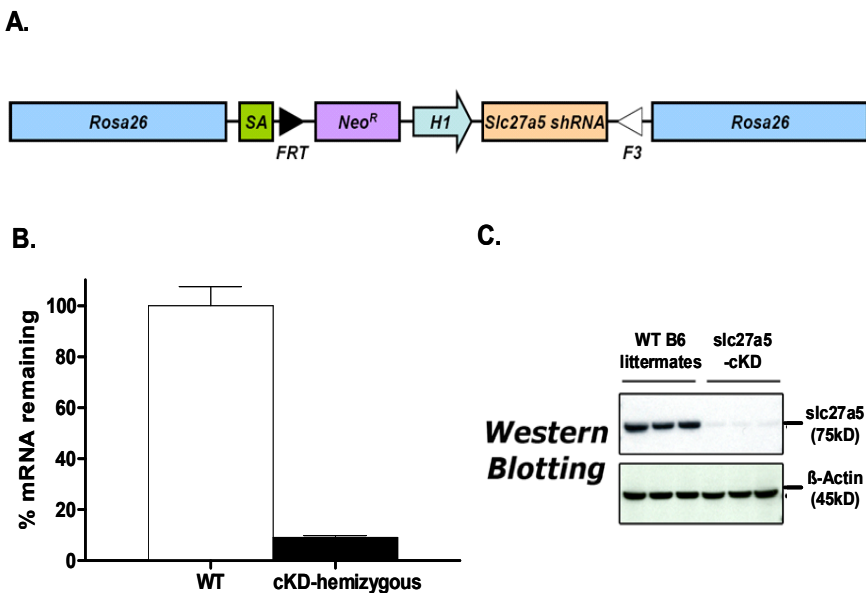
Figure 2. Slc27a5-cKD mice have reduced hepatic mRNA and protein expression. (A) Configuration of RMCE exchanged Rosa26 allele with Slc27a5 shRNA expression cassette under the control of the H1 promoter. NeoR is used for positive selection. (B) Liver total RNA was extracted from C57Bl/6 (WT) littermates (n=7) and Slc27a5-cKD mice (n=9) TaqMan analysis was performed to evaluate Slc27a5 mRNA levels in cKD mice relative to WT mice as described in Materials and Methods. (C) Western blot analyses using 20μg of RIPA protein extracts of liver from cKD mice (n=3) or wild-type mice (n=3). Beta-actin (ß- actin) was blotted as protein loading control.

Slc27a5-cKD mice are resistant to diet-induced obesity

It has been previously reported that Slc27a5 genetic deficiency protected male mice from diet-induced obesity (25). To determine if Slc27a5-cKD mice confer this phenotype, male and female WT and Slc27a5-cKD mice were placed on a low- fat (9% fat) or high-fat (60% fat) diet for 13 weeks. As with the genetically deficient male mice, Slc27a5-cKD male mice were resistant to both low-fat (Figure 3A) and high-fat (Figure 3B) diet-induced obesity; differences became significant ($p<0.01$) after only 1 week on either diet. On the high-fat diet, lack of significant body weight gain occurred while male cKD mice consumed the same amount of calories as the WT mice (1251 ± 157 vs. 1144 ± 79 kcal/13 weeks for WT and Slc27a5-cKD mice respectively, $p<0.26$). Female Slc27a5-cKD mice also had similar caloric intake as WT mice (1357 ± 127 vs. 1404 ± 166 kcal/13 weeks for WT and Slc27a5-cKD mice, respectively, $p<0.69$), but did not show a significant difference in body weight after 13 weeks on the high-fat diet. On the low-fat diet, caloric intake for female Slc27a5-cKD mice were trending towards an increase compared to WT female mice (1468 ± 173 vs. 1797 ± 175 for WT and Slc27a5 mice, respectively, $p<0.08$), yet female Slc27a5-cKD mice gained significantly less weight than WT littermates after 5 to 13 weeks on the diet. Male mice had similar caloric intake (1395 ± 183 vs. 1459 ± 221 for WT and Slc27a5-cKD mice, respectively, $p<0.70$) but still resulted with significantly less body weight gain. Though not examined here, Slc27a5-cKD mice probably failed to gain weight because of an increase in energy expenditure as described for the genetically deficient animals (25). While both male and female cKD mice had less body weight gain on the low-fat diet, the gender disparity observed on the high-fat diet may suggest a differential role of Slc27a5 in male and female mice under different types of caloric intake conditions.
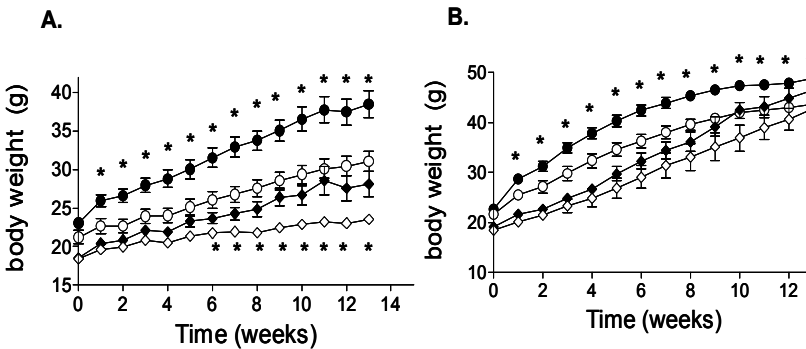
Figure 3. Slc27a5-cKD mice are protected from diet-induced obesity on low-fat and high-fat diets. (A) Body weights were measured weekly for Slc27a5-cKD male (n=9) and female (n=8) and WT littermate control male (n=8) and female (n=7) mice on a low-fat diet (9% fat). Differences in body weights were significant in males starting at week 1 (one-way ANOVA $p<0.01$) and in females at week 6 (one-way ANOVA $p<0.04$). (B) Body weights were measured weekly for Slc27a5-cKD male (n=10) and female (n=9) and WT littermate control male (n=10) and female (n=9) mice on a high-fat diet (60% fat). Differences in body weights were significantly lower in Slc27a5-cKD males starting at week 1 (one-way ANOVA $p<0.02$) compared to WT mice, and no difference was observed in Slc27a5-cKD female mice. WT male, •; WT female, .; Slc27a5-cKD male, .; Slc27a5-cKD female, .. Each data point represents the mean of the group ± standard deviations.

BA conjugation states and concentration in plasma and bile are significantly changed in Slc27a5-cKD mice.

Slc27a5 function is critical for the reconjugation of BAs upon return to the liver during enterohepatic recirculation (Figure 1), therefore we quantified the conjugation levels of all BAs in the plasma and gall bladder after 13 weeks on the low-fat or high-fat diets using high- resolution LC/MS. Table 1 summarizes the BAs found in plasma and bile. Slc27a5-cKD mice had a significant decrease in conjugated BAs and a significant increase in unconjugated BAs in the plasma and bile compared to WT mice. The diet significantly changed the conjugation state of BAs detected in the plasma but not in the bile. Greater than 90% of the BAs in the bile were found conjugated for all groups under all conditions, even in the Slc27a5-cKD mice.

On the low-fat diet, WT mice had ~50% unconjugated BAs in the plasma while cKD mice had >80%. In general, female mice had higher concentrations of BAs in plasma as compared to their male counterparts, particularly the Slc27a5-cKD females which had 16 times more BAs in the plasma as compared to Slc27a5-cKD males on the low-fat diet. Interestingly, male Slc27a5-cKD mice had 2 times more, and female Slc27a5-cKD mice had 20 times more, unconjugated BAs in the plasma than WT mice. Even though there was a significant decrease in conjugated BAs in the plasma, total BA concentration in the plasma increased with Slc27a5 silencing. In the bile, male and female cKD mice had 19 to 31 times more unconjugated BAs than WT mice, respectively. The increase in unconjugated BAs correlated with a significant decrease in conjugated BAs (3 - 5 times less than WT mice), resulting with the total BA concentration in the bile decreasing significantly after Slc27a5 silencing. The high-fat diet caused a change in the composition of BAs detected in the plasma (compared to the low-fat diet), and resulted in ~20% of the BAs in plasma being unconjugated for all groups, except for female Slc27a5-cKD mice which had greater than 60%. On this diet, cKD mice had significantly higher amounts of both unconjugated and conjugated BAs in the plasma, with Slc27a5-cKD male and female mice having 1.5 to 15 times more unconjugated BAs than WT littermates, respectively. Contrary to cKD mice on the low-fat diet, both genders had a significant increase in conjugated BAs in plasma on the high-fat diet (1.4 to 2 times more than WT mice), consistent with an increased BA flux from the gall bladder. The bile contained a significant increase in unconjugated BAs (32 to 100 times more than WT) and a significant decrease in conjugated BAs (1.2 to 1.4 times than WT). While the majority of the BAs were conjugated in the bile (>90%), Slc27a5-cKD mice still had a significant increase in the amount of unconjugated BAs as compared to WT mice. Interestingly, the total BA concentration (plasma + bile) was significantly lower in all cKD mice as compared to WT littermates, except in male cKD mice on the high-fat diet. The samples also contained primary and secondary BAs in both plasma and bile, with a significant increase in tetra-hydroxylated unconjugated BAs in the Slc27a5-cKD mice (see supplemental Figure 1). All together, these data show that Slc27a5 silencing increased the amount of unconjugated BAs in plasma and bile under both diets, further supporting that Slc27a5 plays a critical role in BA reconjugation. In addition, since Slc27a5-cKD mice have an increase in BA concentration in the plasma and a decrease in BA concentration in the bile, loss of Slc27a5 function alters the distribution of BAs resulting

with more BAs in the plasma. Although the Slc27a5-cKD mice had 2-3 fold higher gall bladder volumes than WT mice on the low-fat diet (Table 1), feeding the high-fat diet caused a major reduction. This data suggest that these BAs may still act as substrates for transporters involved in moving BAs into and out of tissues.

TABLE 1. Bile acid concentration and gall bladder volumes

	Low-Fat Diet				High-Fat Diet			
Plasma	**M-WT**	**M-cKD**	**F-WT**	**F-cKD**	**M-WT**	**M-cKD**	**F-WT**	**F-cKD**
Unconjugated	56	80	40	97	18	19	23	67
Conjugated	44	20	60	3	82	81	77	33
	[nM]				[nM]			
Total unconjugated	14 ± 1	30 ± 1^	30 ± 4	594 ± 26^^	13 ± 1	19 ± 1**	11 ± 1	147 ± 4^^^
Total conjugated	11 ± 0.02	8 ± 0.3^	45 ± 1	17 ± 3***	56 ± 5	81 ± 1**	36 ± 1	72 ± 1^^^
Bile	M-WT	M-cKD	F-WT	F-cKD	M-WT	M-cKD	F-WT	F-cKD
	%				%			
Unconjugated	0.2	10	0.2	29	0.03	1	0.01	6
Conjugated	99.8	90	99.8	71	99.97	99	99.99	94
	[µM]				[µM]			
Total unconjugated	0.31 ± 0.01	5.9 ± 0.2^^^	0.41 ± 0.02	15.6 ± 0.6^^	0.03 ± 0.01	1.1 ± 0.03^^^	0.01 ± 0.01	1.3 ± 0.04^^^
Total conjugated	185 ± 8	55 ± 10***	180 ± 11	38 ± 0.6***	110 ± 11	95 ± 3*	100 ± 7	34 ± 33**
Total (plasma + bile)	186 ± 8	61 ± 10**	181 ± 11	54 ± 12^	110 ± 11	96 ± 3	100 ± 7	35 ± 33#
Bile volume (µL)	14.3 ± 4	35.3 ± 13**	16.6 ± 4	59.9 ± 26***	6.5 ± 4	20.6 ± 8**	10.2 ± 3	23.2 ± 11**

Analysis based on student's t-test and 1-way ANOVA. *$p < 8E-02$; **$p < 0.003$; ***$p < 1E-04$; ^$p < 3E-05$; ^^$p < 3E-06$; ^^^$p < 5E-07$; #$p < 0.03$

Loss of Slc27a5 function significantly reduced plasma non-HDL cholesterol land apoB.

Plasma total cholesterol (TC), HDL cholesterol (HDL) and non-HDL cholesterol (chylomicrons, VLDL, LDL) were measured to determine if loss of Slc27a5 function altered lipid levels. Also, apolipoprotein-AI (apoAI), the major apolipoprotein in anti-atherogenic lipoprotein particles (HDL), and apolipoprotein- B (apoB), the major apolipoprotein in pro-atherogenic lipoprotein particles were measured. Figure 4A shows no changes in TC on the low-fat diet, however Slc27a5 silencing significantly reduced TC in males on the high-fat diet (Figure 4B). Both female groups had significantly less TC than males, and loss of Slc27a5 resulted in no change in TC on either diet. HDL cholesterol was reduced in Slc27a5-cKD male mice on the high-fat diet (Figure 4D), but this change did not correlate with a significant change in plasma apoAI levels (Figure 5B). Female Slc27a5-cKD mice had no change in HDL cholesterol (Figure 4), but had less apoAI levels on both diets (Figure 5A, B). Surprisingly, on the high- fat diet, all Slc27a5-cKD mice had a significant decrease in non-HDL cholesterol (Figure 4F), and male mice also had a significant decrease in apoB (Figure 5D). These are the first data to demonstrate that loss of Slc27a5 function alters non- HDL cholesterol and apoB levels. This lipid effect was independent of the effect on diet-induced obesity since the lipid changes did not always correlate with the observed lack of significant body weight gain.
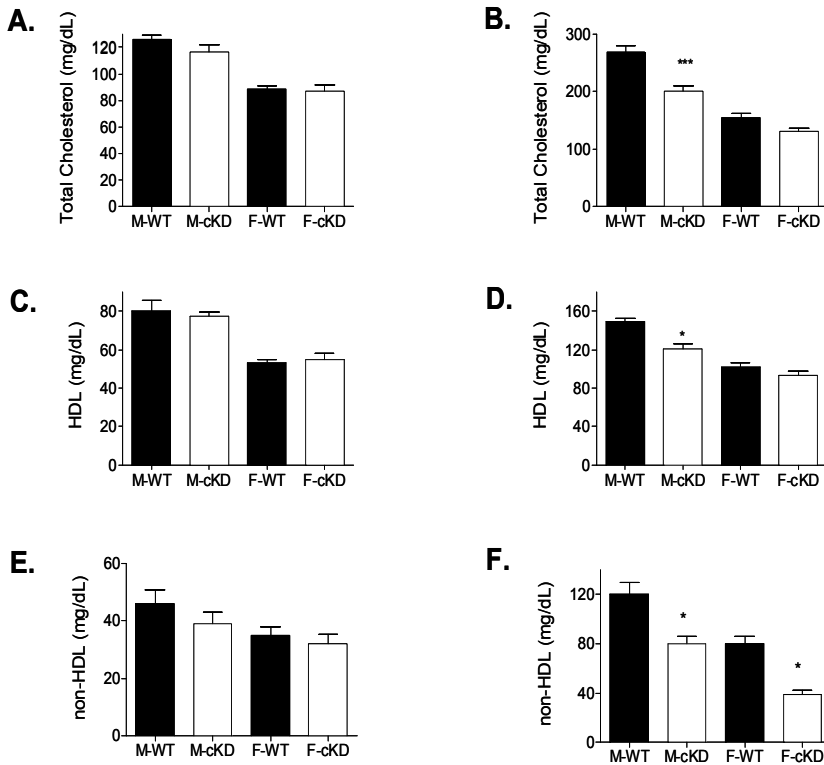
Figure 4. Plasma cholesterol levels in Slc27a5-cKD and WT mice. Plasma TC (A and B), HDL cholesterol (C and D) and non-HDL cholesterol (E and F) levels were measured in male and female Slc27a5-cKD and WT littermates after 13 weeks on low-fat (A, C and E) and high-fat (B, D and F) diets. A significant reduction in TC (one-way ANOVA p<0.001), HDL cholesterol (one-way ANOVA p<0.001) and non-HDL cholesterol (one-way ANOVA p<0.001) levels were observed in Slc27a5-cKD male mice. Female Slc27a5-cKD mice had a significant reduction in non-HDL cholesterol (one-way ANOVA p<0.001) levels on a high-fat diet. Black filled bars represent wild-type mice, and open filled bars represent Slc27a5-cKD mice. M-WT, male WT; F-WT, female WT; M-cKD, male Slc27a5-cKD; F-cKD, female Slc27a5-cKD. All graphs represent the mean of the group ± standard deviations.
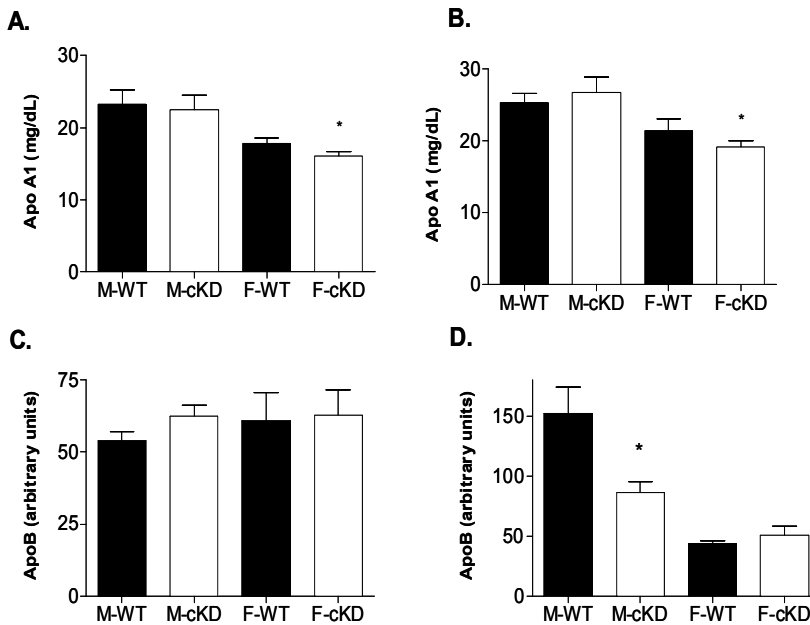
Figure 5. Plasma apoAI and apoB levels in Slc27a5-cKD and WT mice.

Plasma apoAI levels were measured in male and female Slc27a5-cKD and WT littermates after 13 weeks on low-fat (A and C) and a high-fat (B and D) diets. A significant reduction in apoAI was observed in Slc27a5-cKD female mice on both diets (one-way ANOVA $p<0.05$). A significant reduction in apoB was observed in Slc27a5-cKD male mice on the high-fat diet. Black filled bars represent wild-type mice, and open filled bars represent Slc27a5-cKD mice. M-WT, male WT; F-WT, female WT; M-cKD, male Slc27a5-cKD; F-cKD, female Slc27a5-cKD. All graphs represent the mean of the group ± standard deviations.

Systemic administration of LNP-formulated Slc27a5 siRNA altered hepatic Slc27a5 mRNA expression, BA conjugation levels and plasma BA concentration in CETP+/-/LDLr+/- hemizygous mice.

We next evaluated Slc27a5 function in CETP/LDLr hemizygous mice, which have increased non- HDL cholesterol on normal chow, using siRNAs encapsulated in lipid nanoparticles (LNPs). A single intravenous infusion of different doses of Slc27a5 siRNA-LNP resulted in significant, time- and dose-dependent reduction in Slc27a5 mRNA (Figure 6A). The effect was specific, rapid and potent, and resulted in silencing >90% of the mRNA 1 day after infusion of 3 mpk siRNA-LNP, which was sustained for 7 days. Silencing of mRNA was specific for Slc27a5 siRNA-LNP since the non-targeting control siRNA-LNP (nt-control) had no significant change in Slc27a5 gene expression over 7 days. Loss of Slc27a5 function was assessed by quantifying the BA conjugation levels in the plasma and bile. Figure 6B shows a time- and dose-dependent increase in unconjugated BAs with Slc27a5 siRNA-LNP treatment, resulting in a ~40 fold increase in

unconjugated BAs in the bile at day 7 compared to nt-control. As was shown with the cKD mice, Slc27a5 siRNA-LNP treatment also resulted in a significant increase in plasma unconjugated BAs (Figure 6C), which yielded a 3.5 fold increase compared to nt-control. In contrast to the cKD mice, acute siRNA-LNP silencing did not result in an increase in bile volume (data not shown).
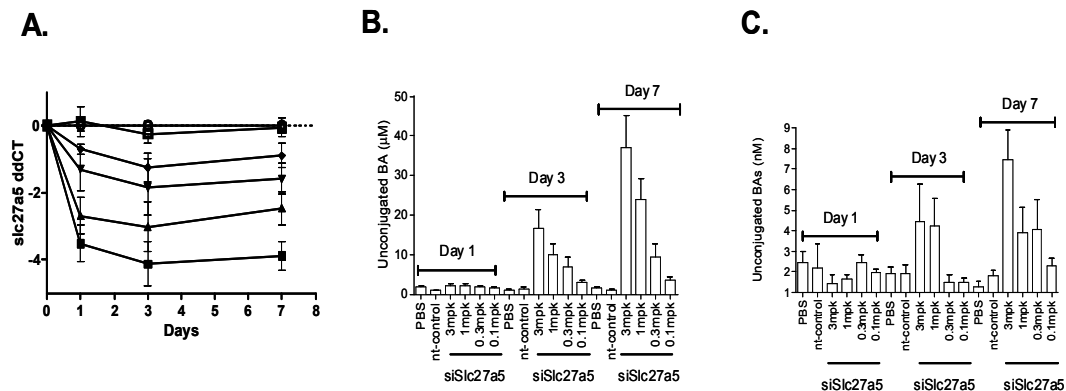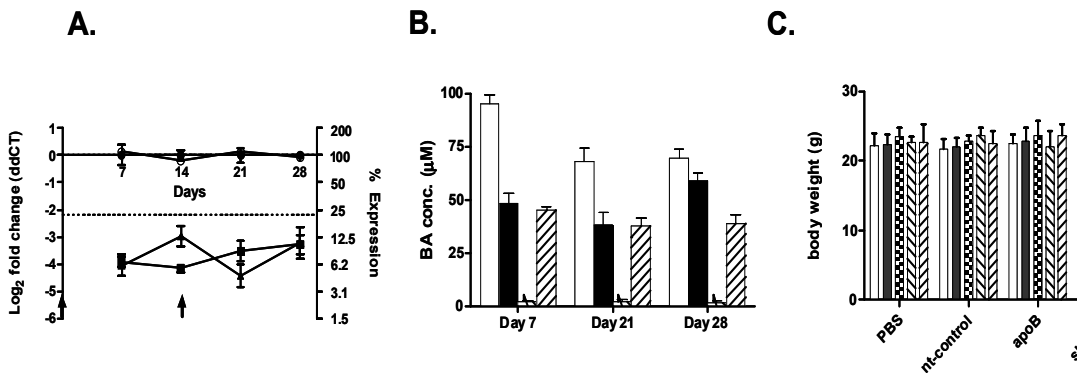

Figure 6. Hepatic Slc27a5 mRNA and BA levels in siRNA-LNP treated CETP+/-/LDLr+/- hemizygous mice. CETP+/-/LDLr+/- hemizygous mice (n=8 per group) were infused with PBS or specific siRNA-LNPs (Slc27a5 or nt-control) on day 0, and then analysis of liver gene expression, unconjugated BAs in bile, and unconjugated BAs in plasma was performed on days 1, 3 and 7. (A) Mice were dosed with PBS or a titrating amounts of Slc27a5 siRNA-LNP (0.1, 0.3, 1.0 and 3.0 mpk). Livers were quickly harvested and qRT-PCR was performed to quantify Slc27a5 mRNA levels. Gene expression levels were directly dependent on the concentration of siRNA-LNP dosed, with >90% of Slc27a5 mRNA reduced with the 3 mpk dose. (B) Unconjugated BAs in the bile were quantified by high- resolution LC/MS at the indicated days after siRNA dosing. The amount of unconjugated BAs depended on the concentration dose of siRNA-LNP and with time after dosing. A specific and significant increase in unconjugated BAs was observed at days 3 and 7. (C) Unconjugated BAs in plasma was quantified by high-resolution LC/MS at the indicated days after PBS or siRNA dosing. A specific and significant increase in unconjugated BAs was observed at days 3 and 7. All graphs represent the mean of the group ± standard deviations.

Repeat dosing of Slc27a5 siRNA-LNP significantly increased unconjugated BA in bile, and did not affect body weight.

We next characterized the BA conjugation levels in CETP+/-/LDLr+/- hemizygous mice after a longer duration of siRNA silencing. To extend the duration of hepatic Slc27a5 silencing, we dosed 3 mpk of siRNA-LNPs on day 0 and then gave a second dose at day 14. Animals were sacrificed on days 7, 14, 21 and 28; therefore animals sacrificed at days 21 and 28 received 2 doses of the same siRNA-LNP. As a positive control for lipid changes, a potent apoB siRNA-LNP, known to reduce plasma non-HDL cholesterol and apoB levels was also used. The effect of siRNA-LNP treatment was specific, rapid and potent and day 7 after treatment resulted in ~95% decrease in Slc27a5 mRNA (Figure 7A). Silencing of mRNA

was specific for Slc27a5 siRNA-LNP since the nt-control and apoB siRNA-LNPs had no significant effects on Slc27a5 gene expression. As expected however, apoB siRNA-LNP specifically and significantly reduced apoB mRNA (~95%). By day 14, the potency of the Slc27a5 siRNA-LNP was slightly reduced, resulting in ~87% of the Slc27a5 mRNA being reduced. The day 14 apoB siRNA-LNP treated animals had sustained reduction of apoB mRNA, demonstrating that duration of mRNA silencing is target-specific. After re-dosing animals at day 14, Slc27a5 mRNA levels were again reduced ~95% at day 21, but the max knockdown slightly reduced again to yield ~90% reduction at day 28.

This is a similar level of mRNA expression seen in the cKD mice (Figure 2A). Also, siRNA-LNP treatment did not induce a significant increase in liver enzymes (AST/ALT) levels as compared to PBS treated animals (data not shown). Figure 7B shows that the function of Slc27a5 correlated with the loss of mRNA since there was a significant increase in unconjugated BAs and a significant decrease in conjugated BAs in bile. The increase in unconjugated BAs was specific since nt-control siRNA-LNP had no effect on BA conjugation levels. In contrast to the cKD mice, acute siRNA-LNP treatment of CETP+/- /LDLr+/- hemizygous mice resulted in >90% unconjugated BAs in bile. This level of unconjugated BAs remained after redosing and throughout the study. These data demonstrate that administration of Slc27a5 siRNA-LNPs significantly reduces mRNA and protein functions in vivo and that a double dose can sustain protein dysfunction out to 28 days. Moreover, Figure 7C shows that during the 28 days of this study, there was no significant difference in body weights of animals treated with nt-control, apoB or Slc27a5 siRNA-LNPs. These data indicate that the effect of Slc27a5 on body weight is decoupled from its effect on BA reconjugation.

Figure 7. Hepatic Slc27a5 mRNA, BA conjugation levels, and body weight measurements in siRNA-LNP treated CETP+/-/LDLr+/- hemizygous mice. CETP+/-/LDLr+/- hemizygous mice (n=8 per group) were infused with PBS or 3 mpk of specific siRNA-LNPs (Slc27a5, nt-control and apoB) on day 0 and re- dosed on day 14 (A, black arrows). Analysis of liver Slc27a5 and apoB gene expression, conjugated and unconjugated BAs in bile, and animal body weights on days 7, 14, 21 and 28 was performed. (A) Administration of siRNA-LNPs specifically reduced Slc27a5 or ApoB mRNA expression in liver. Slc27a5 mRNA expression levels was specifically reduced ~95% at 7 days, and ~87% at 14 days, after the first dose, and ~95% at 7 days, and ~90% at 14 days, after the second dose. PBS, .; nt-control siRNA-LNP, •; apoB siRNA-LNP, ¦; and Slc27a5 siRNA-LNP. The apoB data (¦) depicts the level of apoB mRNA KD, not that of Slc27a5, since no change in Slc27a5 mRNA occurred with apoB KD. (B) Conjugated and

unconjugated BAs levels in bile were quantified by high- resolution LC/MS. While nt-control siRNA-LNP treated mice had ~30% of BAs in the unconjugated form, Slc27a5 siRNA-LNP treated mice had >90% in the unconjugated form. NT-control conjugated BAs = open bars; nt-control unconjugated BAs = black bars; Slc27a5 conjugated BAs = forward slash bars; Slc27a5 unconjugated BAs = backward slash bars. (C) Animal body weights were measured at day 0 (open bars), 7 (black bars), 14 (stippled bars), 21 (front slash bars), and 28 (backslash bars) after siRNA-LNP dosing. No significant body weight changes were observed for any treatment group. All graphs represent the mean of the group ± standard deviations.

siRNA targeting of hepatic Slc27a5 mRNA significantly reduced non-HDL cholesterol and apoB.

Plasma cholesterol, apoAI and apoB levels in animals treated with one or two doses of siRNA-LNPs were measured on each day of sacrifice and summarized in Table 2. Consistent with the Slc27a5-cKD mice on a high-fat diet, CETP+/-/LDLr+/- hemizygous mice treated with Slc27a5 siRNA-LNP had a significant decrease in plasma non-HDL cholesterol and apoB when compared to nt-control. A significant decrease in non-HDL cholesterol (-12mg/dL; $p<0.021$) resulted at 7 days post-infusion, and a significant decrease in apoB occurred at day 14 (-67 mg/dL; $p<0.002$), suggesting a need for a longer duration of mRNA silencing to yield the apoB phenotype. A re-dose of Slc27a5 siRNA-LNP resulted in a significant decrease in TC (-40 mg/dL; $p<0.001$), non- HDL cholesterol (-30 mg/dL; $p<0.001$) and apoB (-107 mg/dL; $p<0.0004$) at day 21. At day 28, non-HDL cholesterol was significantly reduced (-14 mg/dL; $p<0.013$) but the apoB levels were not significantly changed. ApoB siRNA-LNP significantly lowered both non-HDL cholesterol and apoB at all time points examined. There was an inconsistent effect of Slc27a5 siRNA-LNP on apoAI, where treatment significantly increased apoAI at day 7 but decreased apoAI at day 21, and treatment did not affected HDL cholesterol levels on any day examined. ApoB siRNA treatment significantly reduced apoAI and HDL cholesterol levels at each time point. The lowering of apoAI/HDL by apoB silencing has been previously shown in this mouse model (Tadin-Strapps et al., manuscript in press JLR) and in other mouse models by others (32).

TABLE 2 - Lipid and Apolipoprotein Levels After siRNA Silencing

TC	PBS			nt-con		ApoB			Slc27a5		
mg/dL	avg	SD	p-value	avg	SD	avg	SD	p-value	avg	SD	p-value
day 7	149	14	ns	147	14	20	4	9.9E-08	133	5	0.034
day 14	160	15	ns	157	8	40	44	2.4E-04	164	17	0.391
day 21	174	19	ns	171	16	27	7	1.7E-08	131	9	0.001
day 28	144	15	ns	150	15	36	7	3.2E-08	137	14	0.211
HDL	PBS			nt-con		ApoB			Slc27a5		
mg/dL	avg	SD	p-value	avg	SD	avg	SD	p-value	avg	SD	p-value
day 7	64	6	ns	63	10	16	3	5.7E-06	62	6	0.753
day 14	72	10	ns	74	6	26	18	2.3E-04	81	16	0.256
day 21	84	12	ns	74	15	21	7	2.2E-05	64	4	0.096
day 28	63	12	ns	64	12	30	6	3.9E-05	65	10	0.844
non-HDL	PBS			nt-con		ApoB			Slc27a5		
mg/dL	avg	SD	p-value	avg	SD	avg	SD	p-value	avg	SD	p-value
day 7	85	12	ns	83	10	4	2	1.4E-07	71	7	0.021
day 14	88	10	ns	84	8	14	26	3.2E-04	82	20	0.881
day 21	90	22	ns	97	12	6	3	3.3E-07	67	9	0.001
day 28	81	9	ns	86	10	6	2	4.2E-08	72	8	0.013
apoAI	PBS			nt-con		ApoB			Slc27a5		
mg/dL	avg	SD	p-value	avg	SD	avg	SD	p-value	avg	SD	p-value
day 7	37	6	0.0004	25	4	15	5	2.0E-03	31	8	0.050
day 14	73	43	ns	47	12	14	8	2.0E-05	46	9	0.860
day 21	57	12	ns	53	18	13	3	2.0E-05	33	8	0.010
day 28	46	5	ns	55	30	14	2	2.0E-03	33	6	0.060
apoB	PBS			nt-con		ApoB			Slc27a5		
mg/dL	avg	SD	p-value	avg	SD	avg	SD	p-value	avg	SD	p-value
day 7	190	23	ns	200	52	10	4	1.0E-07	177	27	0.280
day 14	199	40	ns	214	46	30	60	8.0E-06	147	20	0.002
day 21	316	49	ns	313	63	10	4	2.0E-09	206	16	0.0004
day 28	233	44	ns	228	36	7	3	1.0E-10	225	34	0.830

nt-con (non-targeting control siRNA); ApoB (ApoB siRNA); Slc27a5 (Slc27a5 siRNA) treated mice all p-values calculated relative to nt-control

DISCUSSION

The data presented here demonstrates that Slc27a5 plays a key role in non- HDL cholesterol and apoB metabolism in vivo. Silencing gene expression chronically in C57Bl/6 mice (Slc27a5-cKD mice), or acutely in CETP+/-/LDLr+/- hemizygous mice (via siRNA-LNP), resulted in a significant lowering of non-HDL cholesterol and apoB. This effect appears to be linked to a significant change in the BA conjugation state, with a significant increase in unconjugated BAs in plasma and bile, and with a significant increase in BA concentration in the plasma. The effects on non-HDL cholesterol and the BA conjugation levels were independent of the effect of Slc27a5 on body weight since animals sometimes resulted in a significant change in these phenotypes with no significant differences in body weight.

Although the link between lipid and BA metabolism has already been established and is vastly expanding, the mechanism of how Slc27a5 affects non-HDL cholesterol and apoB is currently unknown. Slc27a5 is critical for the reconjugation of BAs during the enterohepatic recirculation of BAs from the intestines (25). In addition, it plays a key role as a free fatty acid (FFA) transporter in the liver. In view of the fact that genetically deficient mice have reduced FFA uptake in liver, a redistribution of FFA to other peripheral tissues (26), and are resistant to diet induced liver steatosis (27), we can speculate that the non-HDL cholesterol and apoB lowering effects observed here are directly linked to a reduction in FFA uptake and VLDL secretion. In fact, Doege et al. showed that Slc27a5 deficient mice on normal chow have less VLDL secretion from the liver in the fasted state and a significant lowering of total cholesterol (26). Though our study cannot support or rule this mechanism out, the Slc27a5 effect on lipids may be more complex than this, as we only observed significant non- HDL cholesterol and apoB lowering in Slc27a5-cKD on a high-fat diet or in CETP+/-/LDLr+/- hemizygous mice after a long duration of acute mRNA silencing. This could suggest that BA flux, composition, and/or local BA concentration is critical for unveiling these phenotypes.

Silencing Slc27a5 gene expression significantly increased BAs concentrations in the plasma (Table 1). This increase could therefore have several potential downstream signaling effects that may alter lipid metabolism. For example, increasing BAs in the plasma could activate the bile acid nuclear receptor FXR. Activation of FXR by synthetic agonists (21, 22) or endogenous BAs (33-35) have been shown to reduce VLDL secretion and to reduce circulating atherogenic lipoprotein particles. In our studies, we measured FXR and FXR-regulated gene expression (Shp, Lxr, Fas, SRBI) in the liver after Slc27a5 silencing and observed no significant differences (see Supplemental data, Table 1). Surprisingly, with such a significant increase in plasma BAs (1.4 to 4.6-fold) in the Slc27a5-cKD mice on a high-fat diet, there was no significant decrease in hepatic Cyp7a1 mRNA, the rate-limiting enzyme for BA synthesis that is known to be down-regulated by FXR under conditions of increased total BAs. Additionally, we did not observe any significant global changes in the Srebp1 or Srebp2 pathway genes, specific genes that have also been shown to be down-regulated after FXR activation (21, 22). Another possible mechanism of affecting plasma non-HDL cholesterol and apoB levels is by inducing hepatic LDLr levels by activating gene expression, protein expression or by reducing levels of PCSK9. In vitro studies have demonstrated that BAs can regulate the expression of PCSK9 or LDLr (10, 11), yet when we analyzed hepatic gene

expression of PCSK9 and LDLr, we observed a significant reduction in LDLr mRNA in male Slc27a5 cKD mice on a high-fat diet compared to WT controls (- 1.8 fold; p<0.0002), and no change in female Slc27a5-cKD mice (1.1 fold; p<0.23). No significant changes were observed in PCSK9 gene expression between the two groups on either diet. Male cKD mice did have a significant reduction in HMGCR (-1.7 fold; p<0.001). Interestingly, male cKD mice on the high-fat diet had similar BA levels in bile as WT mice, and had the most significant and consistent decrease in non-HDL cholesterol and apoB. It is therefore plausible that this phenotype is driven by an increase in primary BA synthesis, which could utilize and reduce liver synthesized cholesterol, as well as circulating apoB-containing cholesterol. Alternatively, Slc27a5 could have a unique, yet unidentified, effect on cholesterol metabolism. Patients that undergo gastric bypass surgery also have reduced circulating apoB-containing lipoproteins and a significant increase in total plasma BAs, with a trending increase in unconjugated BAs (24).

The Slc27a5-cKD mice and CETP+/-/LDLr+/- hemizygous mice dosed with Slc27a5 siRNA-LNP lend two novel models for studying Slc27a5 function in vivo. Using these models, our studies have shown many similarities with the genetically deficient mice (25-27). For example, Slc27a5-cKD mice are also resistant to diet-induced obesity, have reduced plasma and liver triglycerides (data not shown), and have an increase in unconjugated BAs in plasma and in bile. However, there were several differences observed with the cKD model compared to the genetically deficient mice. The cKD mice had a significant increase in gall bladder volume, approximately 70-99% of BAs in bile being conjugated, no increase in hepatic Cyp7a1 mRNA, an increase in total plasma BA concentrations, and a significant decrease in non-HDL cholesterol and apoB on a high fat diet. Some of these differences may be dependent on the constitutive expression of the shRNA transgene in the cKD mice, since acute silencing of Slc27a5 by specific siRNA-LNP treatment resulted in a similar phenotype as described with genetic deficiency (>90% of BAs in bile being unconjugated and no change in gall bladder volumes to day 28 post KD). We have now created Slc27a5 genetically deficient mice and will directly compare them to the cKD and siRNA-LNP infusion models to better understand these differences. BAs are becoming more recognized as fundamental signaling molecules that can regulate lipid and glucose homeostasis. Silencing of Slc27a5 in mice significantly altered the conjugation state and concentration of BAs in the plasma, which resulted in positive effects on lipid and lipoprotein profiles and diet-induced obesity. Although these data are promising, more studies are required to confirm these findings in a higher species, and eventually in humans. If it holds true, therapeutic inhibition of Slc27a5 could potentially result in an opportunity to lower atherogenic lipids and lipoprotein particles, as well as prevent diet-induced obesity.

REFERENCES

1. Adraktas, D. D., Brasic, N., Furtado, A. D., Cheng, S. C., Ordovas, K., Chun, K., Chien, J. D., Schaeffer, S., and Wintermark, M. *Stroke*.

2. Chumaeva, N., Hintsanen, M., Juonala, M., Raitakari, O. T., and Keltikangas-Jarvinen, L. *BMC Cardiovasc Disord* **10,** 34.

3. Mahe, G., Carsin, M., Zeeny, M., and De Bosschere, J. P. *Public Health Nutr***,** 1-8.

4. Tomkin, G. H. *Expert Rev Cardiovasc Ther* **8,** 1015-29.

5. El Harchaoui, K., Akdim, F., Stroes, E. S., Trip, M. D., and Kastelein, J. J. (2008) *Am J Cardiovasc Drugs* **8,** 233-42.

6. Staels, B., and Fonseca, V. A. (2009) *Diabetes Care* **32 Suppl 2,** S237-45.

7. Hylemon, P. B., Zhou, H., Pandak, W. M., Ren, S., Gil, G., and Dent, P. (2009) *J Lipid Res* **50,** 1509-20.

8. Lefebvre, P., Cariou, B., Lien, F., Kuipers, F., and Staels, B. (2009) *Physiol Rev* **89,** 147-91.

9. Staels, B. (2009) *Postgrad Med* **121,** 25-30.

10. Leblond, F., Seidah, N. G., Precourt, L. P., Delvin, E., Dominguez, M., and Levy, E. (2009) *Am J Physiol Gastrointest Liver Physiol* **296,** G805-15.

11. Langhi, C., Le May, C., Kourimate, S., Caron, S., Staels, B., Krempf, M., Costet, P., and Cariou, B. (2008) *FEBS Lett* **582,** 949-55.

12. Rabelink, A. J., Hene, R. J., Erkelens, D. W., Joles, J. A., and Koomans, H. A. (1988) *Lancet* **2,** 1335-8.

13. Vessby, B., Kostner, G., Lithell, H., and Thomis, J. (1982) *Atherosclerosis* **44,** 61-71.

14. Huff, M. W., Telford, D. E., Woodcroft, K., and Strong, W. L. (1985) *J Lipid Res* **26,** 1175-86.

15. Handelsman, Y., Abby, S. L., Jin, X., Donovan, J. M., and Jones, M. R. (2009) *Postgrad Med* **121,** 62-9.

16. Jialal, I., Abby, S. L., Misir, S., and Nagendran, S. (2009) *Metab Syndr Relat Disord* **7,** 255-8.

17. Bays, H. E., Goldberg, R. B., Truitt, K. E., and Jones, M. R. (2008) *Arch Intern Med* **168,** 1975-83.

18. Fonseca, V. A., Rosenstock, J., Wang, A. C., Truitt, K. E., and Jones, M. R. (2008) *Diabetes Care* **31,** 1479-84.

19. Davidson, M. H., Toth, P., Weiss, S., McKenney, J., Hunninghake, D., Isaacsohn, J., Donovan, J. M., and Burke, S. K. (2001) *Clin Cardiol* **24,** 467-74.

20. Insull, W., Jr., Toth, P., Mullican, W., Hunninghake, D., Burke, S., Donovan, J. M., and Davidson, M. H. (2001) *Mayo Clin Proc* **76,** 971-82.

21. Evans, M. J., Mahaney, P. E., Borges-Marcucci, L., Lai, K., Wang, S., Krueger, J. A., Gardell, S. J., Huard, C., Martinez, R., Vlasuk, G. P., and Harnish, D. C. (2009) *Am J Physiol Gastrointest Liver Physiol* **296,** G543-52.

22. Mencarelli, A., Renga, B., Distrutti, E., and Fiorucci, S. (2009) *Am J Physiol Heart Circ Physiol* **296,** H272-81.

23. Hartman, H. B., Gardell, S. J., Petucci, C. J., Wang, S., Krueger, J. A., and Evans, M. J. (2009) *J Lipid Res* **50,** 1090-100.

24. Patti, M. E., Houten, S. M., Bianco, A. C., Bernier, R., Larsen, P. R., Holst, J. J., Badman, M. K., Maratos-Flier, E., Mun, E. C., Pihlajamaki, J., Auwerx, J., and Goldfine, A. B. (2009) *Obesity (Silver Spring)* **17,** 1671-7.

25. Hubbard, B., Doege, H., Punreddy, S., Wu, H., Huang, X., Kaushik, V. K., Mozell, R. L., Byrnes, J. J., Stricker-Krongrad, A., Chou, C. J., Tartaglia, L. A., Lodish, H. F., Stahl, A., and Gimeno, R. E. (2006) *Gastroenterology* **130,** 1259-69.

26. Doege, H., Baillie, R. A., Ortegon, A. M., Tsang, B., Wu, Q., Punreddy, S., Hirsch, D., Watson, N., Gimeno, R. E., and Stahl, A. (2006) *Gastroenterology* **130,** 1245-58.

27. Doege, H., Grimm, D., Falcon, A., Tsang, B., Storm, T. A., Xu, H., Ortegon, A. M., Kazantzis, M., Kay, M. A., and Stahl, A. (2008) *J Biol Chem* **283,** 22186-92.

28. Seibler, J., Kleinridders, A., Kuter-Luks, B., Niehaves, S., Bruning, J. C., and Schwenk, F. (2007) *Nucleic Acids Res* **35,** e54.

29. Seibler, J., Kuter-Luks, B., Kern, H., Streu, S., Plum, L., Mauer, J., Kuhn, R., Bruning, J. C., and Schwenk, F. (2005) *Nucleic Acids Res* **33,** e67.

30. Majercak, J., Ray, W. J., Espeseth, A., Simon, A., Shi, X. P., Wolffe, C., Getty, K., Marine, S., Stec, E., Ferrer, M., Strulovici, B., Bartz, S., Gates, A., Xu, M., Huang, Q., Ma, L., Shughrue, P., Burchard, J., Colussi, D., Pietrak, B., Kahana, J., Beher, D., Rosahl, T., Shearman, M., Hazuda, D., Sachs, A. B., Koblan, K. S., Seabrook, G. R., and Stone, D. J. (2006) *Proc Natl Acad Sci U S A* **103,** 17967-72.

31. Wincott, F., DiRenzo, A., Shaffer, C., Grimm, S., Tracz, D., Workman, C., Sweedler, D., Gonzalez, C., Scaringe, S., and Usman, N. (1995) *Nucleic Acids Res* **23,** 2677-84.

32. Crooke, R. M., Graham, M. J., Lemonidis, K. M., Whipple, C. P., Koo, S., and Perera, R. J. (2005) *J Lipid Res* **46,** 872-84.

33. Mencarelli, A., Cipriani, S., Renga, B., Francisci, D., Palladino, G., Distrutti, E., Baldelli, F., and Fiorucci, S. *PLoS One* **5,** e13238.

34. Hirokane, H., Nakahara, M., Tachibana, S., Shimizu, M., and Sato, R. (2004) *J Biol Chem* **279,** 45685-92.

35. Nakahara, M., Fujii, H., Maloney, P. R., Shimizu, M., and Sato, R. (2002) *J Biol Chem* **277,** 37229-34.

SUPPLEMENTAL

Supplemental Table 1. Real-time quantitative PCR analysis of select hepatic genes. Slc27a5-cKD and WT mice were fed a high-fat diet for 13 weeks, and then fasted for 4 hours prior to euthanasia. Liver tissues (~20 mg) were quickly removed and snap frozen in liquid nitrogen and stored at -80°C. Liver tissues were homogenized in 600mL RLT lysis buffer (Qiagen, Valencia, CA) containing 0.1% (v/v) ß-mercaptoethanol using a PowerGen 125 homogenizer and 7 x 65 mm disposable plastic generators (Fisher Scientific). Total RNA was extracted from the homogenized tissue using RNeasy Mini Kit (Qiagen, Valencia, CA) following the manufacturer's protocol. cDNA was generated from 2 µg of RNA using RT2 First Strand kit (SA Biosciences). Real-time PCR analysis was performed on the 7900HT PCR System (Applied Biosystems, Foster City, CA) with 2x SYBR PCR Master Mix and mouse-specific PCR primers (SABiosciences). The selected expression levels of the listed genes were normalized to an average of that of mouse beta-actin (Actb), Glyceraldehyde 3-phosphate dehydrogenase (Gapdh), Beta-glucuronidase (Gusb), Hypoxanthine-guanine phosphor-ribosyltransferase (Hprt1), Peptidylprolyl isomerase A(cyclophilin A) (Ppia) and ribosomal protein 113a (Rp113a) in each sample. Expression levels of all genes analyzed were normalized to an average of the housekeeping genes (listed above) to obtain dCt. Average of dCt of each gene in treatment groups were then normalized to the dCt of corresponding genes in control group to obtain ddCt values. Fold regulation is calculated as: ddCt of gene in treatment group/dCt of gene in control group. Significance (p value) was calculated from a two-tailed T-test between WT control mice and Slc27a5-cKD mice.

Gene Symbol	Male slc27a5-cKD vs WT		Female slc27a5-cKD vs WT	
	fold change	p-value	fold change	p-value
18SrRNA	-1.2	0.23434	1.1	0.36612
Aacs	-1.3	0.22719	-1.6	0.02295
Abca1	-1.0	0.89572	-1.1	0.36384
Abca2	1.0	0.56680	1.3	0.12789
Abcg1	-1.0	0.78846	-1.1	0.34669
Abcg5	-1.1	0.28348	1.0	0.99775
Abcg8	-1.3	0.17776	-1.1	0.47549
Acaa2	-1.1	0.41074	-1.0	0.61264
Acaca	-1.2	0.43725	-1.2	0.34018
Acaca	-1.2	0.57904	1.6	0.70428
Acacb	-1.7	0.07388	-1.3	0.28725
Acacb	-1.7	0.12688	-1.4	0.25743
Acadl	-1.3	0.00260	1.0	0.93179
Acadm	-1.1	0.07560	-1.1	0.43104
Acadvl	1.1	0.13230	1.0	0.66678
Acer3	1.2	0.13996	-1.1	0.08251
Acly	-1.1	0.79802	-1.0	0.51800
Acox1	-1.3	0.01457	-1.3	0.04396
Acox2	-1.2	0.06868	-1.1	0.21443
Acox3	1.1	0.23098	1.1	0.31505
Acsf2	1.0	0.61204	1.3	0.00369
Acsf3	1.0	0.98512	1.3	0.00175
Acsl1	-1.1	0.22980	-1.1	0.48783
Acsl3	-1.2	0.10965	1.2	0.38832
Acsl4	1.2	0.11208	-1.3	0.02209
Acsl5	-1.3	0.10201	-1.5	0.04899
Acsm1	-1.1	0.45696	1.1	0.75766
Acsm3	-1.3	0.12668	-1.0	0.89051
Acsm3	-1.1	0.46273	-1.0	0.69602
Acsm5	-1.2	0.03439	1.0	0.90672
Acss2	-1.4	0.00431	-1.1	0.35281
Actb	-1.1	0.27442	1.0	0.92240
Acyp1	1.2	0.19622	-1.1	0.39607
Adfp	-1.5	0.00137	-1.2	0.19114
Adh4	1.3	0.03603	1.4	0.05899
Adh5	-1.0	0.74008	-1.0	0.67452
Adipor1	-1.2	0.00187	1.1	0.46225
Adipor2	1.0	0.79861	1.1	0.29208
Agk	-1.3	0.00353	1.0	0.92794
Agpat1	1.1	0.53205	1.2	0.25691
Agpat2	-1.0	0.95072	1.0	0.42894
Agpat3	-1.2	0.01069	-1.0	0.73872
Agpat4	-1.2	0.16248	-1.3	0.02840
Agpat6	-1.2	0.09817	1.0	0.61354
Agt	1.0	0.86296	-1.2	0.14043
Agtr1a	-1.5	0.00001	-1.1	0.43993
Aifm2	-1.2	0.00762	1.0	0.99745
Akr1a4	-1.2	0.01094	-1.0	0.74276
Akr1d1	-1.4	0.03196	-1.0	0.56069
Akt1	1.2	0.08948	1.1	0.33816
Aldh1a1	-1.0	0.52877	1.0	0.65137
Aldh1b1	-1.3	0.04276	-1.0	0.57666
Aldh2	-1.1	0.38421	1.1	0.26772
Aldh3a2	-1.2	0.02259	1.1	0.36679
Aldoa	-1.0	0.93544	1.1	0.24522
Aldob	-1.0	0.91670	-1.2	0.04913
Aldoc	1.1	0.88470	1.3	0.23353
Angptl3	-1.2	0.28873	-1.1	0.37457
Angptl4	-1.3	0.03368	-1.6	0.00670
Angptl6	-1.2	0.02256	1.1	0.45010
Ankra2	1.1	0.44663	1.0	0.63811
Aox1	1.1	0.13752	1.1	0.62652
Apoa1	-1.1	0.34812	-1.2	0.05157

Gene Symbol	Male slc27a5-cKD vs WT		Female slc27a5-cKD vs WT	
	fold change	p-value	fold change	p-value
Apoa1	-1.1	0.76986	-1.2	0.03476
Apoa2	-1.4	0.00131	1.1	0.65374
Apoa4	-1.7	0.33959	-1.3	0.57898
Apoa5	-1.1	0.52365	1.1	0.59631
Apob	-1.1	0.09615	1.0	0.62817
Apob	-1.1	0.09829	1.1	0.39562
Apoc2	-1.3	0.00789	-1.1	0.62657
Apoc3	-1.1	0.23425	1.1	0.23003
Apoe	1.1	0.32925	-1.1	0.21634
Apof	-1.5	0.00067	-1.5	0.00469
Ard1a	-1.2	0.02291	1.1	0.28327
Arid5b	-1.1	0.78156	-1.0	0.85991
Arsa	-1.2	0.06156	1.3	0.16974
Asah1	-1.1	0.47114	1.1	0.42925
Atg12	1.3	0.00867	1.2	0.03242
Atg4b	-1.1	0.35786	1.2	0.17482
Atg5	-1.0	0.75216	1.1	0.22288
Atg7	-1.0	0.66305	-1.0	0.76020
B4galt6	-1.0	0.99020	-1.1	0.30462
Baat	-1.1	0.29328	1.1	0.98504
Bace1	1.3	0.01427	1.0	0.48268
Bcat2	-1.2	0.19136	1.2	0.09136
Bcl2	-1.2	0.46788	-1.1	0.43692
Bcl2a1a	-1.0	0.73739	-1.2	0.23950
Bcl2l1	1.3	0.06574	-1.1	0.27728
Becn1	1.1	0.18957	-1.0	0.68116
Bid	-1.1	0.51760	1.1	0.70735
Birc3	1.3	0.02042	1.1	0.56577
Ccl2	1.6	0.06015	-1.0	0.76926
Ccl5	-1.4	0.14413	-1.1	0.44823
Ccr2	1.5	0.16836	1.3	0.38528
Cdh13	-1.2	0.16185	1.1	0.31988
Cds1	1.7	0.42873	-1.3	0.30801
Cel	-1.2	0.16446	1.2	0.21161
Celsr2	-1.1	0.41482	1.1	0.73776
Cerk	-1.2	0.11700	-1.3	0.01168
Cflar	1.0	0.73990	1.1	0.51096
Chka	-1.1	0.28200	-1.1	0.37925
Chpt1	-1.0	0.78132	1.4	0.04256
Cnbp	1.1	0.24633	-1.0	0.51312
Colec12	-1.2	0.01465	1.1	0.33611
Cpe	1.1	0.75227	-1.5	0.29903
Cpt1a	-1.1	0.23975	1.0	0.74639
Cpt1b	-1.3	0.21197	1.1	0.71401
Cpt2	-1.1	0.13237	1.0	0.91832
Crebbp	-1.2	0.12525	1.0	0.83485
Crot	-1.1	0.12265	1.2	0.15041
Crp	-1.0	0.76266	1.0	0.79653
Cxcl1	1.1	0.65668	1.2	0.83269
Cxcl16	1.4	0.00669	-1.2	0.11993
Cyb5r3	1.2	0.23990	-1.4	0.07494
Cyp27a1	-1.2	0.09566	-1.1	0.22304
Cyp39a1	-1.4	0.06112	-1.2	0.14783
Cyp46a1	-1.4	0.14781	-1.3	0.18487
Cyp51	1.0	0.74809	1.1	0.33699
Cyp7a1	-1.4	0.32220	-1.1	0.43345
Cyp7b1	2.4	0.02040	1.4	0.07894
Cyp8b1	-1.1	0.78167	-1.1	0.31268
Degs1	-1.2	0.00436	-1.1	0.33573
Dgat1	-1.1	0.17760	1.0	0.70780
Dgat2	1.1	0.49922	-1.1	0.23240
Dhcr24	-1.5	0.00002	1.1	0.64847
Dhcr7	-1.5	0.02435	-1.0	0.97078
Dlat	-1.3	0.000002	-1.1	0.34327

Gene Symbol	Male slc27a5-cKD vs WT		Female slc27a5-cKD vs WT	
	fold change	p-value	fold change	p-value
Dld	1.0	0.87546	-1.1	0.32469
E030002G19Rik	-1.4	0.02957	1.0	0.83704
E2f1	1.0	0.52282	1.1	0.30720
Ebp	-1.2	0.02209	1.0	0.72554
Echs1	-1.0	0.54252	1.0	0.77127
Ehhadh	-1.2	0.06322	-1.1	0.48942
Ei24	-1.3	0.00767	1.0	0.74975
Ela3	-1.7	0.03844	1.3	0.07171
Elovl1	-1.1	0.19118	1.1	0.69077
Elovl2	-1.4	0.00133	1.1	0.52432
Elovl3	1.4	0.01980	1.3	0.70252
Elovl4	-1.3	0.15119	1.2	0.21161
Elovl5	-1.4	0.04026	1.1	0.48880
Elovl6	-1.0	0.92186	-1.3	0.16239
Eno3	1.0	0.73988	-1.3	0.06245
Esr1	1.1	0.43483	1.2	0.33225
Etnk1	-1.0	0.53276	1.1	0.13706
Exoc7	-1.2	0.03890	1.1	0.37471
Fabp2	-1.2	0.00686	-1.0	0.83564
Fabp4	-1.2	0.21675	-1.2	0.05431
Fabp5	-1.1	0.93908	-1.5	0.05376
Fads1	-1.6	0.00110	-1.2	0.14344
Fads2	-1.6	0.00122	-1.5	0.08698
Fads3	-1.5	0.05095	1.3	0.15264
Fas	1.1	0.32920	1.0	0.78494
Fasn	-1.2	0.76907	-1.3	0.32868
Fasn	-1.4	0.97349	-1.4	0.19929
Fbp1	1.1	0.62074	1.1	0.61595
Fbp2	-1.5	0.13564	-1.0	0.90076
Fdft1	-1.4	0.00405	1.2	0.17882
Fdps	-1.4	0.09381	1.1	0.89692
Fgf21	-1.2	0.75507	-1.3	0.64145
Flot1	-1.2	0.03263	1.1	0.56922
Flot2	-1.2	0.12608	-1.1	0.54918
Foxa1	1.4	0.01882	-1.1	0.95061
Foxa2	1.3	0.02072	-1.3	0.03803
Foxa3	1.3	0.13766	-1.2	0.10993
Foxo1	-1.2	0.05585	-1.1	0.07098
Foxo3	-1.2	0.10017	-1.1	0.56133
Foxo4	1.1	0.08473	1.1	0.92164
Fto	-1.2	0.02476	1.2	0.02670
G6pc	-1.4	0.23889	-1.1	0.62877
Gabarap	-1.1	0.30383	1.0	0.91026
Galc	1.0	0.79351	1.2	0.20752
Galm	-1.3	0.00791	1.0	0.85982
Gapdh	-1.1	0.45535	-1.0	0.91087
Gba	1.1	0.56058	-1.2	0.26853
Gcgr	-1.2	0.12154	1.0	0.96563
Gck	-1.2	0.15139	-1.2	0.16127
Gla	-1.3	0.09353	-1.1	0.71820
Glb1	-1.3	0.03426	-1.1	0.19790
Glyat	1.1	0.18021	-1.0	0.69504
Glyctk	-1.2	0.16592	1.2	0.14128
Gnpat	-1.1	0.09178	1.1	0.38915
Gpam	-1.2	0.32005	1.0	0.68836
Gpd1	-1.0	0.82194	1.0	0.66280
Gpd2	-1.1	0.09153	-1.0	0.86870
Gpi1	1.1	0.43648	-1.2	0.17919
Gpld1	-1.0	0.95085	1.1	0.22697
Gpsn2	-1.3	0.01278	1.2	0.06541
Gsk3a	1.1	0.20109	1.0	0.52127
Gsk3b	1.0	0.71979	1.3	0.07591
Gusb	1.2	0.35831	-1.4	0.27085

	Male		Female	
	slc27a5-cKD vs WT		slc27a5-cKD vs WT	
Gene Symbol	fold change	p-value	fold change	p-value
Gyk	1.1	0.10955	-1.2	0.11253
Gys2	-1.1	0.37860	-1.2	0.19558
Hacl1	1.3	0.03980	-1.1	0.51990
Hadh	-1.1	0.27513	-1.0	0.68315
Hdlbp	-1.0	0.80696	1.1	0.26930
Hk1	1.0	0.86619	1.1	0.28059
Hk2	-2.1	0.00422	1.1	0.50077
Hmgcr	-1.7	0.00116	1.0	0.98840
Hmgcs1	-1.3	0.16976	1.6	0.00682
Hmgcs2	-1.2	0.00045	1.2	0.08847
Hnf1a	-1.1	0.31673	1.1	0.13439
Hprt1	-1.1	0.11511	1.1	0.14065
Hsd17b12	-1.0	0.63054	1.2	0.03603
Hsd17b4	-1.1	0.05545	1.0	0.55944
Hsd3b7	1.1	0.23368	1.0	0.88423
Hsp90aa1	1.1	0.17785	1.0	0.93588
Hsp90ab1	-1.3	0.00472	1.0	0.98324
Hspa1a	1.2	0.28531	-1.4	0.13171
Hspa1b	1.2	0.32057	-1.4	0.07084
Iars	1.2	0.23886	-1.1	0.60638
Iars2	1.0	0.91282	-1.2	0.07085
Idi1	-1.1	0.51221	1.3	0.33337
Ifng	-1.3	0.20105	1.5	0.09545
Igf1	1.0	0.54384	1.3	0.15823
Igf1r	-1.1	0.41279	-1.4	0.09058
Igf2	-1.1	0.66278	1.1	0.66926
Igfbp1	-1.7	0.11437	-1.1	0.55688
Igfbp3	-1.7	0.00087	-1.2	0.11249
Il1a	-1.0	0.63267	-1.1	0.57290
Il1b	1.6	0.03474	1.3	0.25468
Il4	-1.3	0.13667	1.2	0.20034
Il6ra	-1.4	0.08872	-1.1	0.57849
Ilvbl	-1.2	0.00510	1.1	0.55598
Insig1	-1.4	0.01342	1.2	0.45566
Insig2	-1.1	0.39888	-1.1	0.77644
Insr	-1.2	0.18509	1.1	0.18818
Irs1	1.1	0.22127	1.3	0.08366
Irs2	-1.2	0.33708	-1.2	0.32528
Irs4	-1.3	0.13667	1.2	0.21161
Itgb2	-1.1	0.85113	-1.2	0.14106
Kdsr	-1.3	0.00432	1.1	0.04372
Lars	-1.1	0.08866	-1.1	0.34873
Lcat	-1.0	0.74374	1.0	0.72837
Lclat1	-1.2	0.05980	1.3	0.00968
Lct	-1.3	0.13667	1.2	0.21161
Ldlr	-1.8	0.00015	1.1	0.53013
Ldlr	-1.8	0.00017	1.1	0.23190
Ldlrap1	-1.1	0.52255	1.1	0.35962
Lep	-1.3	0.13667	1.2	0.21161
Lipc	-1.0	0.95487	1.1	0.90151
Lipe	1.4	0.01525	1.3	0.07701
Lipg	-2.0	0.00234	-1.3	0.10349
Lpl	-1.0	0.82099	1.0	0.91314
Lrat	-1.0	0.81900	1.0	0.98085
Lrp12	1.0	0.91548	1.1	0.25819
Lrp1b	-1.3	0.13667	1.2	0.21161
Lrp6	-1.1	0.26639	1.1	0.72689
Lrpap1	-1.2	0.01230	1.0	0.66016
Lypla1	-1.2	0.06272	1.2	0.06252
Lypla2	-1.2	0.10601	1.0	0.82139
Map1lc3a	-1.1	0.12321	1.2	0.01360
Map1lc3b	-1.1	0.39712	-1.0	0.67451
Map2k1	-1.1	0.10799	-1.1	0.60414

Gene Symbol	Male slc27a5-cKD vs WT		Female slc27a5-cKD vs WT	
	fold change	p-value	fold change	p-value
Mapk1	1.8	0.93065	1.2	0.03463
Mapk3	-1.0	0.78332	1.3	0.00570
Mapk9	-1.3	0.00566	1.0	0.93551
Mbtps1	1.1	0.42409	1.0	0.86350
Mlxipl	1.2	0.14827	-1.0	0.78558
Mogat1	-1.4	0.08192	1.2	0.41597
Mogat2	-1.6	0.16603	-1.1	0.49162
Msr1	1.1	0.41813	1.1	0.20718
Mttp	1.2	0.06011	-1.0	0.48240
Mvd	-1.1	0.86982	1.6	0.10187
Mvk	-1.0	0.80404	1.3	0.04692
Myc	1.7	0.00963	1.6	0.05810
Myst3	-1.1	0.22808	1.1	0.44955
Naaa	1.0	0.91347	1.0	0.86066
Nampt	1.0	0.71443	1.0	0.95493
Neu1	-1.0	0.86959	1.1	0.31914
Neu2	1.5	0.00947	-1.0	0.84367
Neu3	-1.2	0.21782	1.2	0.49939
Nfkb1	-1.2	0.05014	1.1	0.42106
Nnmt	1.2	0.34978	1.1	0.67331
Npc1l1	-1.3	0.13667	1.2	0.21161
Npy	-1.5	0.17431	1.0	0.91084
Nr0b2	1.1	0.64818	-1.2	0.19204
Nr1h2	-1.5	0.00003	1.1	0.49792
Nr1h2	-1.5	0.00020	1.1	0.48544
Nr1h3	1.2	0.22639	1.4	0.31505
Nr1h3	1.2	0.23907	1.1	0.69544
Nr1h4	1.1	0.56671	-1.2	0.12901
Nras	-1.1	0.23380	1.1	0.26657
Nsdhl	-1.3	0.40123	1.1	0.80623
Osbpl1a	-1.1	0.06041	-1.0	0.75065
Osbpl5	-1.8	0.00006	1.1	0.48066
Osmr	-1.1	0.21804	1.2	0.25531
Pam	-1.2	0.18991	-1.1	0.20031
Pcca	-1.3	0.00207	1.1	0.47436
Pccb	-1.0	0.68524	1.2	0.17317
Pck1	-1.6	0.00103	-1.0	0.96916
Pck2	-1.3	0.11384	-1.2	0.63558
Pcsk9	-1.1	0.73071	1.2	0.30930
Pcsk9	-1.0	0.82963	1.2	0.35108
Pcyt1a	-1.2	0.02872	1.1	0.12747
Pcyt2	-1.3	0.00542	1.0	0.94322
Pdha1	-1.0	0.77214	1.0	0.63595
Pdhb	1.1	0.26710	1.0	0.87725
Pemt	-1.2	0.02037	1.1	0.65389
Pfkl	1.0	0.78805	1.0	0.69670
Pgm1	1.1	0.64371	-1.0	0.99244
Pisd	-1.3	0.00089	1.1	0.14480
Pklr	-1.2	0.38466	-1.0	0.97097
Pla1a	-1.1	0.69624	-1.1	0.34513
Pla2g4a	1.4	0.12459	-1.0	0.89335
Pld1	1.1	0.67750	-1.1	0.54112
Pld2	1.2	0.27663	-1.0	0.70427
Pmvk	-2.7	0.00009	-1.8	0.00085
Ppap2a	-1.2	0.23003	-1.3	0.07256
Ppap2b	-1.0	0.65145	1.1	0.61701
Ppap2c	-1.2	0.12762	1.2	0.36614
Ppara	1.0	0.79691	-1.0	0.72809
Ppard	-1.0	0.93929	1.1	0.72745
Pparg	-1.0	0.98849	-1.3	0.11987
Ppia	1.0	0.72457	1.0	0.97018
Prkaa2	-1.0	0.75097	1.1	0.24802
Prkab1	1.1	0.43352	1.1	0.42544

Gene Symbol	Male		Female	
	slc27a5-cKD vs WT		slc27a5-cKD vs WT	
	fold change	p-value	fold change	p-value
Prkab2	-1.0	0.89853	1.2	0.25341
Prkag2	-1.4	0.00044	-1.1	0.08865
Psrc1	1.2	0.25230	1.6	0.05156
Ptdss1	-1.1	0.12508	1.0	0.79175
Ptdss2	-1.2	0.15838	1.5	0.00634
Ptpn1	1.3	0.01356	-1.1	0.42315
Rara	-1.1	0.20951	1.3	0.03049
Rpl13a	1.3	0.00052	1.1	0.29048
Rpl32	-1.1	0.49030	1.1	0.45301
Rxra	-1.3	0.22312	1.1	0.73279
Rxrb	1.1	0.34122	-1.1	0.74097
Rxrg	-1.3	0.05546	1.2	0.20814
Scap	-1.1	0.32560	-1.0	0.75203
Scarb1	1.1	0.39318	-1.1	0.34812
Scarf1	-1.1	0.86398	1.2	0.21035
Scd1	-1.8	0.03402	-2.7	0.11895
Scd1	-1.8	0.05626	-2.5	0.14251
Scp2	1.2	0.06198	1.1	0.39932
Selp	1.1	0.41004	1.0	0.86929
Sgpl1	-1.2	0.09440	-1.1	0.42970
Sgpp1	1.1	0.28301	1.4	0.01567
Sirt1	1.1	0.36835	-1.0	0.75978
Sirt4	1.4	0.07317	1.2	0.28645
Slc10a1	-1.1	0.78160	-1.2	0.11048
Slc27a2	-1.1	0.58990	-1.1	0.47963
Slc27a4	1.1	0.42676	1.2	0.13539
Slc27a5	-11.8	0.000002	-13.1	0.000002
Slc2a4	-1.6	0.03684	-1.5	0.12584
Slco1b2	-1.1	0.61915	1.1	0.81124
Smpd2	1.0	0.89462	1.1	0.58399
Snx17	-1.1	0.12109	-1.4	0.88361
Soat1	-1.5	0.00344	-1.1	0.98237
Soat2	-1.5	0.00005	1.0	0.93103
Socs1	1.2	0.38342	1.1	0.90595
Sod1	-1.2	0.07424	-1.0	0.63505
Sorbs1	-1.5	0.00337	1.1	0.45139
Sorl1	1.1	0.97667	1.3	0.21361
Sort1	-1.2	0.30314	-1.0	0.67923
Sp1	-1.2	0.05899	1.0	0.98595
Spp1	-1.0	0.92884	1.2	0.36565
Sptlc1	-1.1	0.30660	1.8	0.06493
Srebf1	-1.4	0.08952	1.1	0.57255
Srebf2	-1.3	0.09523	-1.1	0.68231
Stab1	-1.4	0.00075	-1.2	0.08390
Stab2	-1.3	0.01003	1.1	0.67683
Stard3	1.2	0.05862	-1.0	0.82448
Sulf1	1.0	0.47332	-1.0	0.67590
Tgfb1	1.1	0.46413	-1.1	0.48579
Thra	-1.0	0.69541	1.5	0.04009
Thrb	1.1	0.42240	1.4	0.68410
Tm7sf2	1.1	0.56458	1.1	0.51545
Tnf	-1.1	0.67478	1.0	0.86442
Tnfaip3	1.8	0.00291	-1.1	0.45040
Tpi1	-1.1	0.38814	1.1	0.59050
Trerf1	-1.4	0.25658	-1.3	0.72384
Trib3	-1.7	0.03356	1.4	0.37558
Trip10	-1.2	0.04920	1.1	0.29140
Ucp2	-1.1	0.54102	1.1	0.89415
Vegfa	-1.1	0.34205	-1.1	0.54031
Vldlr	-2.4	0.000004	-1.1	0.56969
Yod1	-1.2	0.12252	1.1	0.46503
Zmynd15	-1.1	0.35500	1.3	0.06490

Supplemental Figure 1. The relative response (peak area/deuterated internal standards) of BAs detected by high resolution LC/MS; unconjugated and conjugated bile acids in bile on days 7 (A), 21 (B) and 28 (C) following administration of the nt-control (light bars) and Slc27a5 (dark bars) siRNA-LNPs.

At each day, unconjugated dihydroxylated (DiOH), trihydroxylated (TriOH) and tetrahydroxylated (TetraOH) BAs increased with Slc27a5 KD. Conjugated tetraOH also increased with Slc27a5 KD.

Part III

Stable isotope tracers and metabolic flux analysis by LC/MS

Chapter 7

Stable isotope metabolic tracer to measure bile acid reconjugation *in-vitro* and *in-vivo* by UPLC/TOF-MS

Stable isotope metabolic tracer to measure bile acid reconjugation *in-vitro and in-vivo* by UPLC/TOF-MS

SUMMARY

The purpose of this study was to evaluate the use of metabolomics and D_4-cholic acid (D_4-CA) as a metabolic tracer to measure the metabolism and reconjugation of bile acids (BAs) *in vitro* and *in vivo*. Stable isotope tracers are becoming an increasingly important research tool for many disease areas since it enables the measurement of small but significant biological changes which may not be apparent when monitoring static endogenous concentrations of particular metabolites. One such tracer, D_4-CA has been previously used for measuring BA metabolism in humans and in cell-based systems. Slc27a5, also known as fatty acid transport protein 5 (FATP5), is the hepatic BA-CoA ligase involved in re-conjugating BAs during enterohepatic BA recycling. Here, we show the utility of using D_4-CA as a tracer to measure re-conjugation of BAs *in vitro* and *in vivo*, and describe a comprehensive novel method for high chromatographic and mass spectral resolution in the detection and quantification of D_4-BA metabolites and endogenous BAs. Using Slc27a5-cKD mice, a significant reduction in the re-conjugation of D_4-CA to D_4–taurocholic acid (D_4-TCA) was observed, as well as other conjugated BA metabolites in plasma (p= 0.0031). Further metabolites of D_4-CA, such as taurotetrahydroxy cholanoyl, were also reduced in the Slc27a5-cKD mouse plasma. The method described allowed a rapid measure of many D_4 and endogenous BA. Analysis of bile resulted in the detection of 39 BA metabolites from a 13 min analytical run. Finally, the utilization of a novel high resolution mass spectrometry method in combination with metabolomics and a stable isotope metabolic tracer *in vivo* allowed for the detection of targeted and untargeted BAs following silencing of the Slc27a5 gene in primary hepatocytes and in mice.

INTRODUCTION

BAs have a well-known property of being able to help solubilize fat in the intestines. What make them unique are the physiological detergent-like properties which they possess (1-4). Their amphipathic property which consists of a hydrophobic core in combination with hydroxyl moieties enables them to act as tensioactive biochemicals, making fat absorption a very efficient process. BAs are synthesized in the liver from cholesterol and are actively transported to the gall bladder and intestines where metabolism of BAs can occur (see Chapter 6 for comprehensive description). BAs return to the liver via the enterohepatic recirculation from the intestines by other active transporters (5). Slc27a5 is the critical enzyme that reconjugates unconjugated BAs upon return to the liver. Genetic deficiency or silencing the Slc27A5 gene has been shown to dramatically increase the unconjugated / conjugated BA ratio (6).

Gas-chromatography and liquid-chromatography coupled with mass spectrometry have been extensively used in the past in the analysis of BAs *in vivo* (7, 8). Recently the use of ultra-performance liquid chromatography (UPLC) coupled to time-of-flight (TOF) mass spectrometry (MS) has been utilized to detect BAs in dog and rat biological matrices (9). Even though MS based techniques have been widely explored for static endogenous BA measurements. The dynamic movement of these BAs *in vitro* and *in vivo* is also of important biological relevance, and stable isotope tracers may be used in this context to follow the metabolism of specific BAs.

Metabolic tracers have been extensively used to study energy expenditure, fatty acid oxidation, cholesterol synthesis, as well as BA synthesis and turnover (10-13). The pioneering work of Klein *et al.* (14, 15) with ^{2}H and ^{13}C to measure the kinetic fate of BAs has paved the way for further research in this area. Following this, work by Stellaard *et al.* (16, 17) with gas chromatography coupled with mass spectrometry has shown that it is possible to accurately measure the pool size and fractional turnover rates of BAs in human serum using ^{13}C labeled BAs. One complicating feature of measuring BA metabolism *in vivo* is that the measurement of endogenous BA pools (18) can mask subtle biological changes because the endogenous BA pool size is large. This is further complicated with a slow turnover rate of the BA pool, or by BA recycling following a postprandial state (19).

 Here, a high resolution UPLC/TOF-MS platform was developed to quantitatively measure endogenous BAs, a D_4-CA BA tracer, and its metabolites in plasma and bile. This platform was used to measure the re-conjugation of BAs *in vitro* and *in vivo*.

MATERIALS AND METHODS

Quantitative measure of BAs by UPLC/TOF-MS

BAs in cell supernatants or plasma were quantified by UPLC/TOF-MS. 10μl of 1μM internal standard D_5-Lithocholic acid (LCA) (Sigma-Isotec St. Louis, MO) was added to 50μl of sample. The BA fraction was then extracted from the sample by the addition 450μL ice-cold acetonitrile (Burdick & Jackson, USA). The mixture was vortexed and centrifuged for 10 minutes at 5,000 g. The supernatant was collected and evaporated under vacuum at 10°C. The extracted BA fraction was then reconstituted with 100μL of 50% ACN, 0.1% formic acid (v/v) and 0.1 % formic acid (v/v) in H_2O and aliquoted into 96 well plates and stored at -20°C. BAs were extracted from bile by a simple one step dilution, in which 1uL of bile was diluted 1:100 or 1:1000 in 50% acetonitrile +0.1% formic acid /50 % water +0.1 % formic acid depending on the signal intensity in the MS system. To quantify endogenous and tracer BA metabolites an external calibration buffer was used containing LCA, Glycholic acid (GCA), Taurocholic acid (TCA), Deoxycholic acid (DCA), Cholic acid (CA), Chenodeoxycholic acid (CDCA), Glycochenodeoxycholic acid (GCDCA), and Taurochenodeoxycholic acid (TCDCA), ranging from 0.02 to 4.0 μM to determine absolute concentrations. Previous determination of responses and calibration parameters were determined in plasma using standard addition of above mentioned synthetic calibrants to the plasma (see supplementary figure 1 and supplementary table 1). Plasma recovery of BAs (D_4-CA, D_4-TCA, and D_4-GCA) was in the range of 67-99% across the different concentration ranges.

The UPLC/TOF-MS system comprised of an Acquity Ultra Performance Liquid Chromatography (UPLC) (Waters, Milford, MA, USA). Samples were injected (10μL) onto a 1.8 μm particle 100 x 2.1 mm id Waters Acquity HSS T3 column (Waters, Milford, MA, USA) maintained at 65°C. The flow rate was 0.7 mL/min, using a binary gradient system consisting of water + 0.1% formic acid (eluent A), and acetonitrile + 0.1% formic acid (Burdick & Jackson, USA). A linear gradient (curve 6) was performed over a 13 min total run time; during the initial portion of the gradient, it was held at 80% A and 20% B. For the next 10 min the gradient was ramped in a stepped linear fashion to 35% B (curve 5) in 4 minutes, 45% B in 7.5 minutes and 99% B in 9.5 minutes and held at this composition for 1.6 minutes hereafter the system was switched back to 80% B and 20% A and equilibrated for an additional 2.9 minutes.

The inlet system was directly coupled to a hybrid quadrupole orthogonal time of flight mass spectrometer (SYNAPT G2 HDMS, Waters, MS Technologies, Manchester, UK). Electrospray (ESI) negative ion ionization mode, capillary voltage and cone voltage of -2 kV and -30 V, respectively, was used. The desolvation source conditions were as follows; for the desolvation gas 800 L/hr was used and the desolvation temperature was kept at 500°C. Data were acquired over the mass range of 50-1200 Da in full scan MS mode. The mass spectral resolution was set to 25K full width half mass (FWHM). The system was equipped with an integral LockSpray unit with its own reference sprayer that was controlled automatically by the acquisition software to collect a reference scan every 10 seconds lasting 0.3 seconds. The LockSpray internal reference used for these experiments was Leucine enkephalin (Sigma-Aldrich, St Louis, MO) at a concentration

of 5 ng/μL in 50% acetonitrile/ 50% H_2O + 0.1% formic acid (v/v). The reference internal calibrant was introduced into the lock mass sprayer at a constant flow rate of 50μL/min using an integrated solvent delivery pump. A single lock mass calibration at m/z 554.2615 in negative ion mode was used during analysis.

In vitro D4-CA conjugation using primary mouse hepatocytes

Primary mouse hepatocytes were isolated from wild type C57Bl/6 mice (Taconic Farms, Inc., Germantown, NY) and Slc27a5 constitutive knockdown (Slc27a5 cKD) mice that express a small hairpin RNA (shRNA) sequence targeted against Slc27a5 that have been described previously (see Chapter 6 for comprehensive description) using a two-step re-circulating EGTA/collagenase (type XI, Sigma) perfusion technique (22). Cells were seeded at 3.5x 10^5 cells/well on collagen-I coated 96 well plates (BD Biosciences, San Jose, CA) and incubated for 24 hours in DMEM (Fisher Scientific, Pittsburg, PA) supplemented with 10% FBS, 1mM Na Pyruvate, 100nM Insulin, 100nM dexamethasone at 37°C, 5% CO_2. Next, the cells were washed and switched to serum-free conditions. D_4-CA (2, 2, 4, 4-D_4-CA) (Sigma- Isotec, St Louis, MO) 10μM was added and incubated at 37C, 5% CO_2 overnight. The culture media was harvested for analyzing precursor D_4-CA to products, D_4-TCA and D_4-GCA by UPLC/TOF-MS, and the cell viability was checked by a luminescent cell viability assay.

In vivo D4-CA infusion studies using WT and Slc27a5-cKD mice

All animal protocols were reviewed and approved by the Merck Research Laboratories Institutional Animal Care and Use Committee (Rahway, NJ). Slc27a5-cKD mice were generated and characterized in-house (see chapter 6). Briefly, small hairpin RNA (shRNA) (gagtccaatcggaaacttgTTCAAGAGAcaagtttccgattggactc) was used to construct the Slc27a5-cKD mice. Recombinase-mediated cassette exchange (RMCE) ready C57Bl/6 mouse embryonic stem (ES) cells were transfected with the exchange vector to generate mouse ES clones expressing Slc27a5 shRNA as described previously described (20, 21). In-vivo D_4-CA tracer studies were performed in WT C57Bl/6 mice (Taconic farms, Germantown, NY) or Slc27a5-cKD mice that were maintained on regular breeder chow. Animals (n=6 females (n=3 females per group)) were dosed with 30mg/kg D_4-CA tracer (Sigma-Isotec St. Louis, MO) formulated in 0.5% $NaHCO_3$ in phosphate buffered saline (w/v, pH8.0) via intra-venous via tail vein injection. Blood samples were collected at 0.5, 1, 3, 6 & 24 hr post infusion via tail vein bleeds and plasma collected and analyzed. Animals were euthanized at terminal bleeds post D_4-CA tracer dosing and bile samples were collected.

Data processing and statistical analysis

UPLC/TOF-MS data acquired was processed by the instrument's manufacturer software (MassLynx) and for the quantitation step TargetLynx was utilized. For the statistical analysis; all the data are presented as ± standard error mean (SEM). Differences between groups were computed by student's *t-test* (GraphPad Prism, La Jolla, CA). Post test analysis

for quantifiable variables was conducted using Mann-Whitney U non-parametric test with two-tailed p-values. Values of p <0.05 were considered as being statistically significant.

RESULTS AND DISCUSSION

A selective UPLC/TOF-MS methodology was developed to obtain BA quantity and composition for both *in vitro* and *in vivo* samples. A chromatographic run time of 13 min enabled us to obtain a high resolution UPLC separation of BAs as shown in figure 1. This novel quantitative/qualitative method was employed to obtain a better understanding of the comprehensive BA metabolism with a focus on major CA metabolites as shown in scheme 1, and the re-conjugation of D_4-CA to D_4-TCA and D_4-GCA.
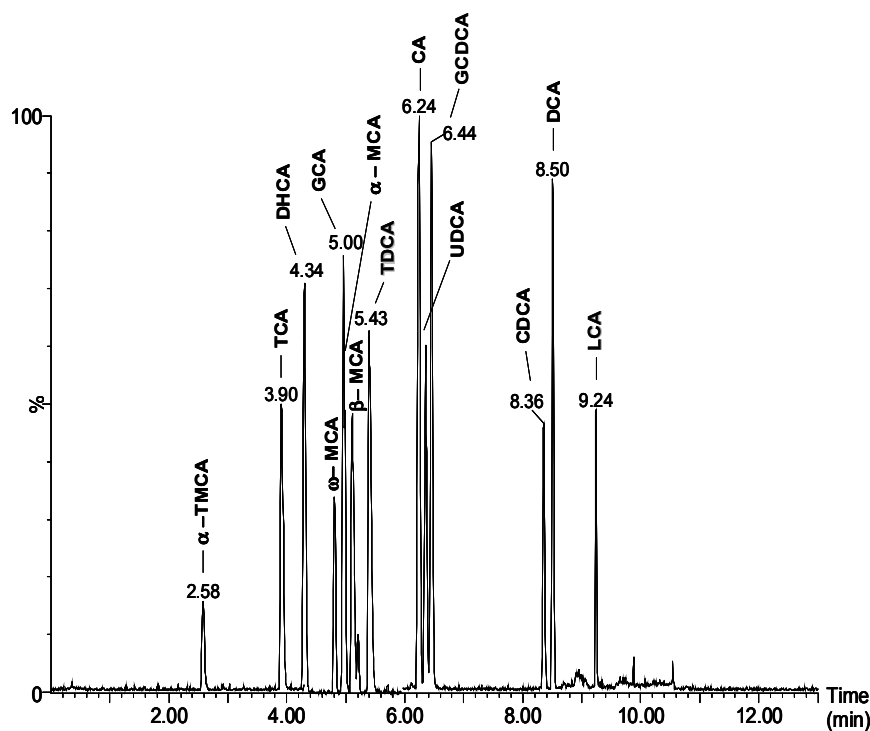
Figure 1. UPLC/TOF-MS analysis for a mixture of BA standards in buffer solution. This chromatogram was generated by using a mixture of chemically synthesized standards (α-TMCA, TCA; DHCA; ω-MCA; GCA; α-MCA; β-MCA; TDCA; GCDCA; UDCA; CDCA ; DCA and LCA) in buffer solution at a final concentration of 1μM.

Abbreviations: α-TMCA (α-Tauromuricholic acid); TCA (Taurocholic acid); DHCA (dehydrocholic acid); ω-MCA (ω-muricholic acid); GCA (Glycocholic acid); α-MCA (α-muricholic acid); β-MCA (β-muricholic acid); TDCA (taurochenodeoxycholic acid); GCDCA (glycochenodeoxycholic acid); UDCA (ursodeoxycholic acid); CDCA (chenodeoxycholic acid); DCA (deoxycholic acid); LCA (lithocholic acid)
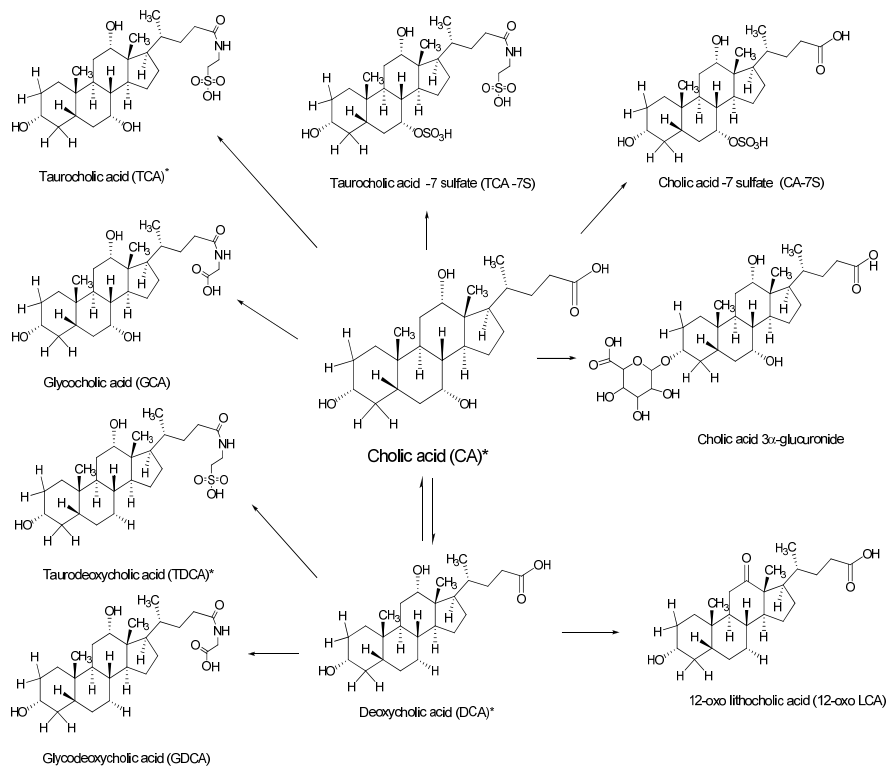
Scheme 1. Major BA metabolic pathway for cholic acid derived metabolites in WT mice

* *Major cholic acid metabolites found in WT mice (plasma and bile)*

In vitro BA conjugation can be quantitated using D$_4$-CA

For the initial *in vitro* experiments, we monitored the BA conjugation step after incubating primary hepatocytes from wild type (WT) C57Bl/6 and Slc25a5-cKD mice with 1µM D$_4$-CA. The metabolic products of D$_4$-CA formed after 24 hr incubation and were quantified by high resolution UPLC/TOF-MS (see scheme 2). The results revealed that taurine and glycine conjugation were significantly elevated in WT hepatocytes, and were significantly attenuated in cells isolated from Slc27a5-cKD animals. Figure 2A shows that the levels of D$_4$-GCA from the Slc25a5-cKD hepatocytes were 4.6 fold lower relative to WT hepatocytes (p = 0.0022). Figure 2B showed a similar effect on D$_4$-TCA, where there was a 3.76 fold lower amount of conjugation in Slc25a5-cKD hepatocytes relative to WT primary hepatocytes (p= 0.0022). At this incubation time point, there were no other D$_4$-BA metabolites identified. These *in vitro* data show that D$_4$-CA can be used to investigate the conjugation and metabolism of CA in a cultured cell system.

Cholic acid 2,2,4,4-D_4

Taurine conjugation

Glycine conjugation

Taurocholic acid 2,2,4,4-D_4

Glycocholic acid 2,2,4,4-D_4
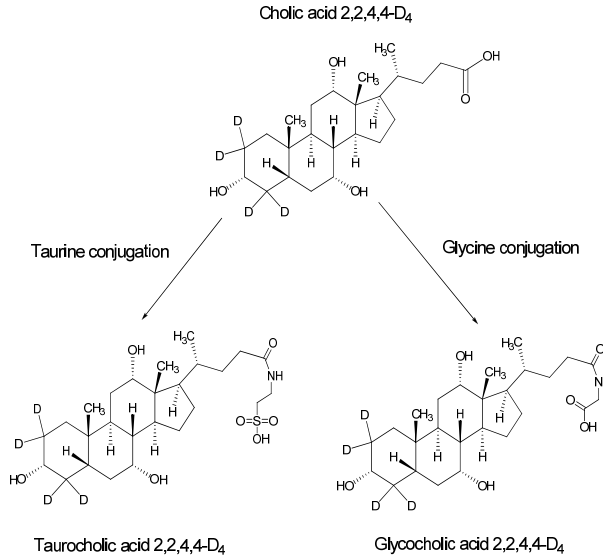
Scheme 2. D_4-CA stable isotope tracer substrate in WT and Slc27a5-cKD mice and the corresponding products D_4-TCA and D_4-GCA monitored to measure reconjugation *in vitro* and *in vivo* by UPLC/TOF-MS

A)

B)
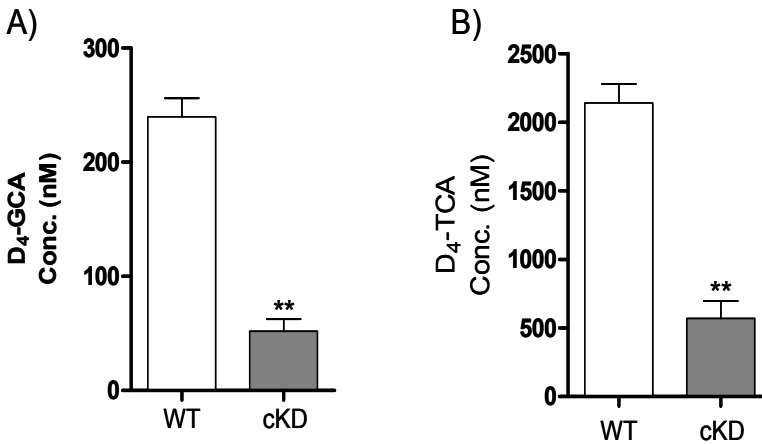
Figure 2. Primary mouse hepatocytes (WT and cKD-Slc27a5) incubated overnight with D_4-CA to measure the reconjugation of CA following silencing of Slc27a5. (A) Conjugation to D_4-GCA decreased in Slc27a5-cKD vs. WT hepatocytes. (B) Conjugation to D_4-TCA decreased in Slc27a5-cKD vs. WT hepatocytes.

** $p < 0.01$

In vivo BA conjugation can be observed using D$_4$-CA

The results from the *in vitro* study prompted the evaluation for the utility of using D$_4$-CA to observe BA reconjugation *in vivo*. Slc27a5-cKD mice were selected as a mouse model that would have less BA reconjugation due to a ~90% loss of Slc27a5 gene expression. Initially, an intravenous dose titration of D$_4$-CA was performed using 3 mg/kg, 10 mg/kg and 30 mg/kg in WT mice to evaluate the optimal dose by identifying the reconjugation detection limit and half-life. These results showed that the D$_4$-CA cleared from the circulation after 3 hrs post-dose and was rapidly converted to D$_4$-TCA (data not shown). The 30 mg/kg dose was selected to monitor BA reconjugation in subsequent experiments, since it offered a large metabolic window and was not at the limit of detection.

We next observed D$_4$-CA reconjugation in WT and cKD mice dosed at 30 mg/kg. Figure 3A shows a 35% (p = 0.1553) increase in the isotope tracer in the plasma of WT mice vs. Slc27a5-cKD mice for all the time points tested. This finding was substantiated by the observation that reconjugation was significantly reduced in the Slc27a5-cKD mice. The levels (AUC) of D$_4$-TCA in the Slc27a5-cKD mice were reduced by 75% (p =0.0031) than in the WT mice (Figure 3B). It is worth noting that D$_4$-GCA levels did not reveal any significant changes between the two mouse models, although the predominant conjugated BA in plasma was D$_4$-TCA (plasma D$_4$-GCA levels accounted for only 0.46% and 1.55% of the levels of D$_4$-TCA in the WT and Slc27a5-cKD, respectively). In addition, the percentage labeling of D$_4$-TCA of the total TCA pool (unlabeled TCA and D$_4$-TCA) was 8.8% in WT mice vs. 6.3 % in Slc27a5-cKD mice and the corresponding values for D$_4$-GCA were 9.3% for WT mice vs. 5.0% for Slc27a5-cKD mice. These data showed that our UPLC/TOF-MS method could detect the *in vivo* reconjugation of D$_4$-CA from mouse plasma.
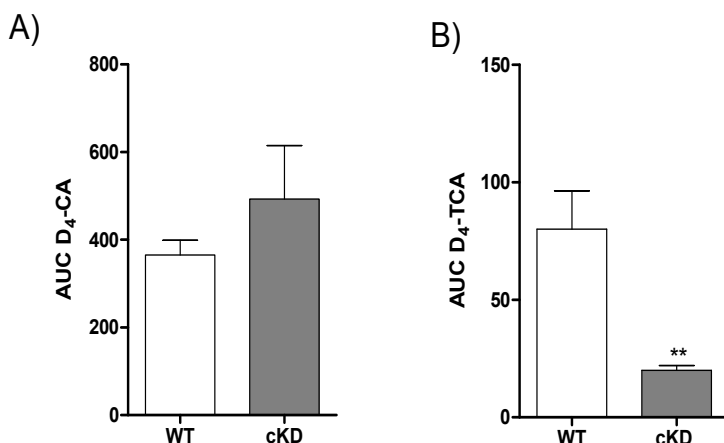
Figure 3. *In vivo* infusion of D$_4$-CA tracer in WT and Slc27a5-cKD mice. Plasma substrate-to-product (D$_4$-CA-to- D$_4$-TCA) measurements by UPLC/TOF-MS are expressed as AUC (all time points). (A) Increment in unconjugated D$_4$-CA BA level in Slc27a5-cKD vs. WT mice. (B) Significantly lower D$_4$-TCA in Slc27a5-cKD mice.

** p<0.0031

Accurate mass and elemental composition analysis confirmed other endogenous BA metabolites in bile

The use of accurate mass measurements allowed for a more detailed profile of all BA metabolites in the bile of WT mice. Table 1 show the accurate mass and elemental composition of 39 BAs (endogenous unlabeled and endogenous D_4-labeled) detected in the bile. As previously shown for WT mice (23), the majority of BAs detected in bile were conjugated to either taurine, glucuronide or sulfated metabolites. Our method also allowed us to detect multiple conjugation BA products such as monohydroxy-sulfate glycine metabolites and taurochenodeoxycholic acid-3β glucuronide.

Table 1. BAs detected in bile by UPLC/TOF-MS using exact mass measurements to determine elemental compositions in WT mice and their corresponding D$_4$-containing BA.

N.B nd = not detected

| BA nomenclature | | Detected endogenous BA in bile | | | | D$_4$-containing BA in bile | | | |
Common name	Type	m/z [M-H]-	elemental composition	ppm	rt (min)	m/z [M-H]-	elemental composition	ppm	rt (min)
Deoxycholic acid	unconjugated	391.2835	$C_{24}H_{39}O_4$	-3.3	8.41	nd	nd	nd	nd
ω-Muricholic acid (3α, 6α,7β)	unconjugated	407.2782	$C_{24}H_{39}O_5$	-3.7	4.75	nd	nd	nd	nd
α-Muricholic acid (3α, 6β,7α)	unconjugated	407.2802	$C_{24}H_{39}O_5$	1.2	4.92	nd	nd	nd	nd
β-Muricholic acid (3α, 6β,7β)	unconjugated	407.2799	$C_{24}H_{39}O_5$	0.5	5.08	nd	nd	nd	nd
Cholic acid (3α, 7α,12α)	unconjugated	407.2797	$C_{24}H_{39}O_5$	0	6.12	411.3045	$C_{24}{}^{1}H_{35}{}^{2}H_4O_5$	-1	6.13
Glycocholic acid	conjugated	464.3017	$C_{26}H_{42}NO_6$	1.1	4.92	468.3271	$C_{26}{}^{1}H_{38}{}^{2}H_4NO_6$	1.7	4.92
Taurochenodeoxycholic acid	conjugated	498.2889	$C_{26}H_{44}NO_6S$	0	5.04	nd	nd	nd	nd
Taurodeoxycholic acid	conjugated	498.2897	$C_{26}H_{44}NO_6S$	1.6	5.35	502.3108	$C_{26}{}^{1}H_{40}{}^{2}H_4NO_6S$	-6.4	5.35
Tauro α-muricholic acid- (3α, 6β,7α)	conjugated	514.2844	$C_{26}H_{44}NO_7S$	1	2.48	nd	nd	nd	nd
Taurocholic acid (3α, 7α,12α)	conjugated	514.2851	$C_{26}H_{44}NO_7S$	2.3	3.7	518.3091	$C_{26}{}^{1}H_{40}{}^{2}H_4NO_7S$	0.2	3.7
Taurohyocholic acid (3α, 6α,7α)	conjugated	514.2852	$C_{26}H_{44}NO_7S$	2.5	2.36	nd	nd	nd	nd
Tetra hydroxy cholanoyl (1)	unconjugated	423.2764	$C_{24}H_{39}O_6$	4	2.79	nd	nd	nd	nd
Tetra hydroxy cholanoyl (2)	unconjugated	423.2735	$C_{24}H_{39}O_6$	-2.8	4.06	nd	nd	nd	nd
Taurine tetra hydroxy cholanoyl (1)	conjugated	530.2776	$C_{26}H_{45}NO_8S$	-2.2	1.35	534.3048	$C_{26}{}^{1}H_{41}{}^{2}H_4NO_8S$	1.7	1.33
Taurine tetra hydroxy cholanoyl (2)	conjugated	530.2789	$C_{26}H_{45}NO_8S$	0.2	1.43	534.3011	$C_{26}{}^{1}H_{41}{}^{2}H_4NO_8S$	-5.2	1.42
Taurine tetra hydroxy cholanoyl (3)	conjugated	530.2793	$C_{26}H_{45}NO_8S$	1	1.63	nd	nd	nd	nd
Taurine tetra hydroxy cholanoyl (4)	conjugated	530.2798	$C_{26}H_{45}NO_8S$	1.9	1.69	nd	nd	nd	nd
Taurine tetra hydroxy cholanoyl (5)	conjugated	530.2803	$C_{26}H_{45}NO_8S$	2.8	1.8	534.3015	$C_{26}{}^{1}H_{41}{}^{2}H_4NO_8S$	-4.5	1.87
Taurine tetra hydroxy cholanoyl (6)	conjugated	530.2786	$C_{26}H_{45}NO_8S$	-0.4	1.86	nd	nd	nd	nd
Taurine tetra hydroxy cholanoyl (7)	conjugated	530.2783	$C_{26}H_{45}NO_8S$	-0.9	1.9	nd	nd	nd	nd
Taurine tetra hydroxy cholanoyl (8)	conjugated	530.2786	$C_{26}H_{45}NO_8S$	-0.4	1.94	nd	nd	nd	nd
Taurine tetra hydroxy cholanoyl (9)	conjugated	530.2802	$C_{26}H_{45}NO_8S$	2.7	2.36	534.3052	$C_{26}{}^{1}H_{41}{}^{2}H_4NO_8S$	2.4	2.36
Taurine tetra hydroxy cholanoyl (10)	conjugated	530.2798	$C_{26}H_{45}NO_8S$	1.9	2.56	534.3054	$C_{26}{}^{1}H_{41}{}^{2}H_4NO_8S$	2.8	2.55
Taurine tetra hydroxy cholanoyl (11)	conjugated	530.28	$C_{26}H_{45}NO_8S$	2.3	2.62	534.3036	$C_{26}{}^{1}H_{41}{}^{2}H_4NO_8S$	-0.6	2.62
Taurine tetra hydroxy cholanoyl (12)	conjugated	530.2795	$C_{26}H_{45}NO_8S$	1.3	2.9	534.3009	$C_{26}{}^{1}H_{41}{}^{2}H_4NO_8S$	-5.6	2.9
Taurine tetra hydroxy cholanoyl (13)	conjugated	530.2798	$C_{26}H_{45}NO_8S$	1.9	2.97	534.3044	$C_{26}{}^{1}H_{41}{}^{2}H_4NO_8S$	0.9	2.97
Glucuronide cholic acid	conjugated	583.3093	$C_{30}H_{47}O_{11}$	-4.3	4.78	nd	nd	nd	nd
Sulfate cholic acid	conjugated	487.2352	$C_{24}H_{40}NO_8S$	-2.8	2.98	nd	nd	nd	nd
Sulfate cholic acid	conjugated	487.2353	$C_{24}H_{40}NO_8S$	-2.6	3.21	nd	nd	nd	nd
Sulfate cholic acid	conjugated	487.2362	$C_{24}H_{40}NO_8S$	-0.8	4.18	491.2657	$C_{24}{}^{1}H_{36}{}^{2}H_4NO_8S$	1.4	4.16
Taurine sulfate cholic acid	conjugated	594.2401	$C_{26}H_{44}NO_{10}S_2$	0.5	2.01	598.2634	$C_{26}{}^{1}H_{40}{}^{2}H_4NO_{10}S_2$	-4	2.01
Monohydroxy sulfate-glycine (1)	conjugated	512.269	$C_{26}H_{43}NO_7S$	1.5	2.69	nd	nd	nd	nd
Monohydroxy sulfate-glycine (2)	conjugated	512.2695	$C_{26}H_{43}NO_7S$	2.5	2.83	516.2921	$C_{26}{}^{1}H_{39}{}^{2}H_4NO_7S$	-2.3	2.83
Monohydroxy sulfate-glycine (3)	conjugated	512.2703	$C_{26}H_{43}NO_7S$	4	2.87	nd	nd	nd	nd
Monohydroxy sulfate-glycine (4)	conjugated	512.2712	$C_{26}H_{43}NO_7S$	5.8	2.95	nd	nd	nd	nd
Monohydroxy sulfate-glycine (5)	conjugated	512.2701	$C_{26}H_{43}NO_7S$	3.7	3.22	nd	nd	nd	nd
Monohydroxy sulfate-glycine (6)	conjugated	512.269	$C_{26}H_{43}NO_7S$	1.5	3.36	nd	nd	nd	nd
Monohydroxy sulfate-glycine (7)	conjugated	512.2703	$C_{26}H_{43}NO_7S$	4	3.49	nd	nd	nd	nd
Monohydroxy sulfate-glycine (8)	conjugated	512.2695	$C_{26}H_{43}NO_7S$	2.5	3.68	nd	nd	nd	nd
Taurochenodeoxycholic acid -3β glucuronide	conjugated	674.3203	$C_{32}H_{52}NO_{12}S$	-1	2.01	nd	nd	nd	nd

Additional metabolites of CA in bile confirmed by using D$_4$-CA stable isotope tracer

Extracted ion chromatograms (XICs) using a narrow 30 millidalton (mDa) window, allowed us to obtain more in-depth information regarding additional metabolites of CA in bile. This narrow chromatogram permits the removal of close m/z endogenous components, enabling a cleaner XIC trace for specific BA metabolites. CA may undergo further hydroxylations to generate tetrahydroxy cholanoyl BA metabolites at different positions. This biotransformation is mediated by the CypP450 enzyme family (24) as shown in figure 4A. Figure 4B shows two hydroxylated metabolites of CA (m/z 423.276) in WT mice that are easily detected and quantitated by our method. In contrast to WT mice, a large number of UPLC/TOF-MS peaks were obtained for the same m/z value in the Slc27a5-cKD mice (figure 4C), highlighting the utility of our detection and quantitative method. Confirmation of some BA metabolites was obtained by the use of the D$_4$-CA tracer, which verified the addition of a hydroxyl group to CA to create tetrahydroxy cholanoyl in both animals (figure 4D and 4E). Overall, accurate mass analysis of both endogenous hydroxylated CA and the D$_4$-labeled cholanoyl showed high-quality mass measurements (figure 5).

A) Cholic acid (CA) — NAPDH + O2 / Cyp P450 — Putative further hydroxylation sites for cholic acid

B) WT Unconjugated Tetra OH BA — 1: TOF MS ES- 423.277 0.0300Da 371

C) cKD Slc27a5 Unconjugated Tetra OH BA — 1: TOF MS ES- 423.277 0.0300Da 1.07e4

D) WT Unconjugated D_4-Tetra OH BA — 1: TOF MS ES- 427.3 0.0300Da 80

E) cKD Slc27a5 Unconjugated D_4-Tetra OH BA — 1: TOF MS ES- 427.3 0.0300Da 938
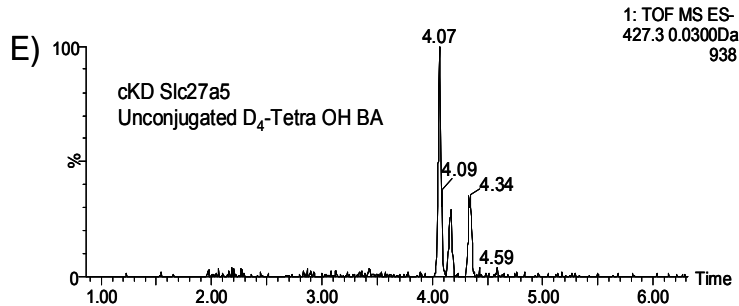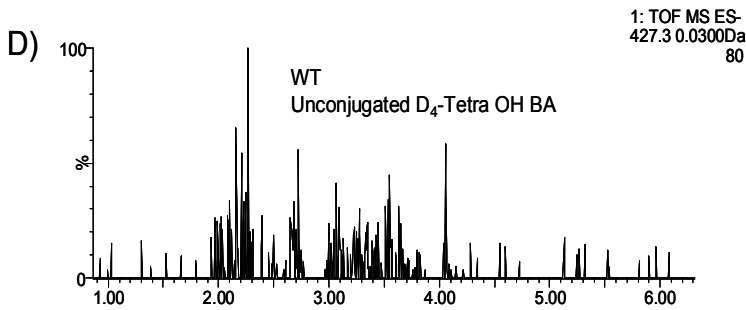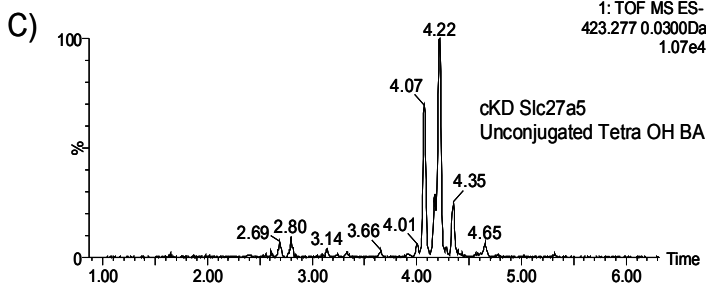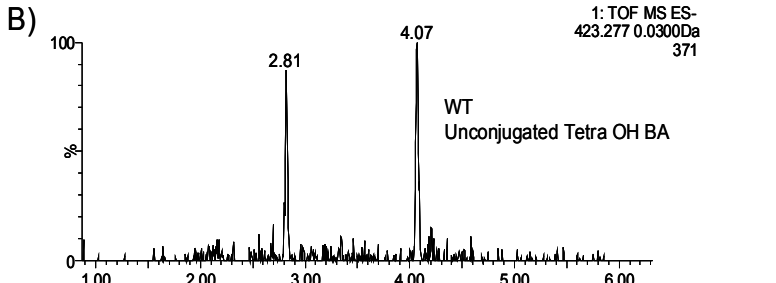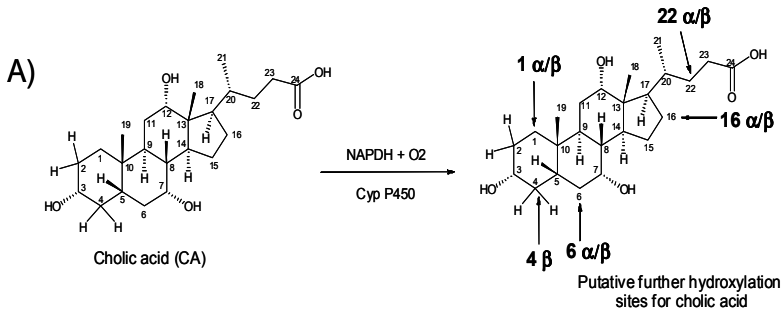
Figure 4. Bile sample analysis by UPLC/TOF-MS in WT and Slc27a5-cKD mice with specific emphasis in unconjugated mono-hydroxylated metabolites of CA. (A) Cholic acid chemical structure showing possible locations for further hydroxylation sites by CypP450 enzymes. (B) Extracted ion chromatogram (30 mDa window) for WT tetrahydroxy cholanoyl BAs in bile. (C) Extracted ion chromatogram (30 mDa window) for Slc27a5-cKD tetrahydroxy cholanoyl BAs in bile. (D) Extracted ion chromatogram (30 mDa window) for WT D_4-tetrahydroxy cholanoyl BAs in bile. (E) Extracted ion chromatogram (30 mDa window) for Slc27a5-cKD D_4-tetrahydroxy cholanoyl BAs in bile.
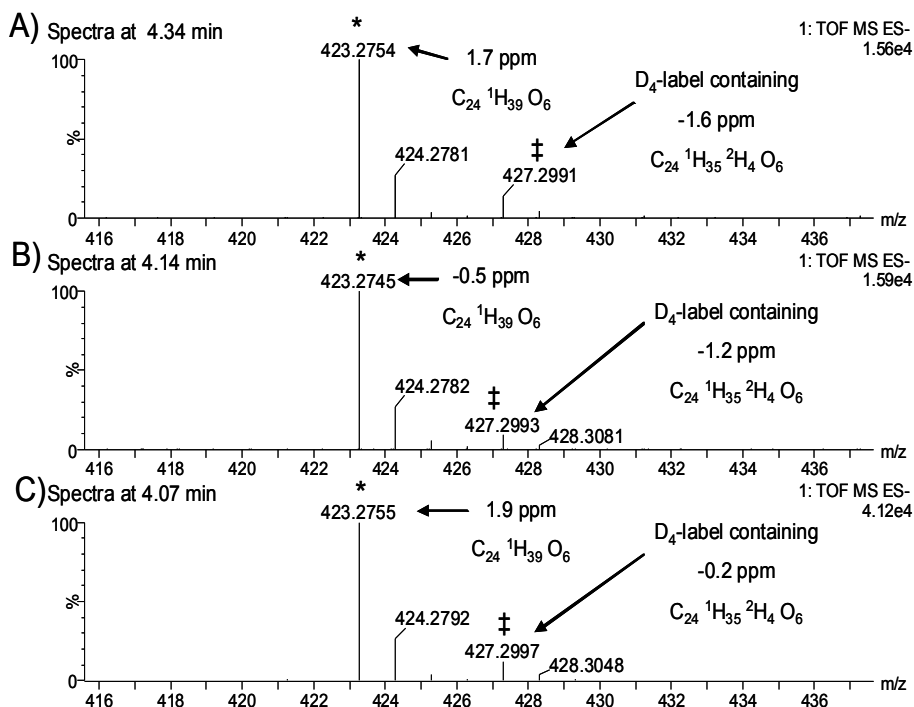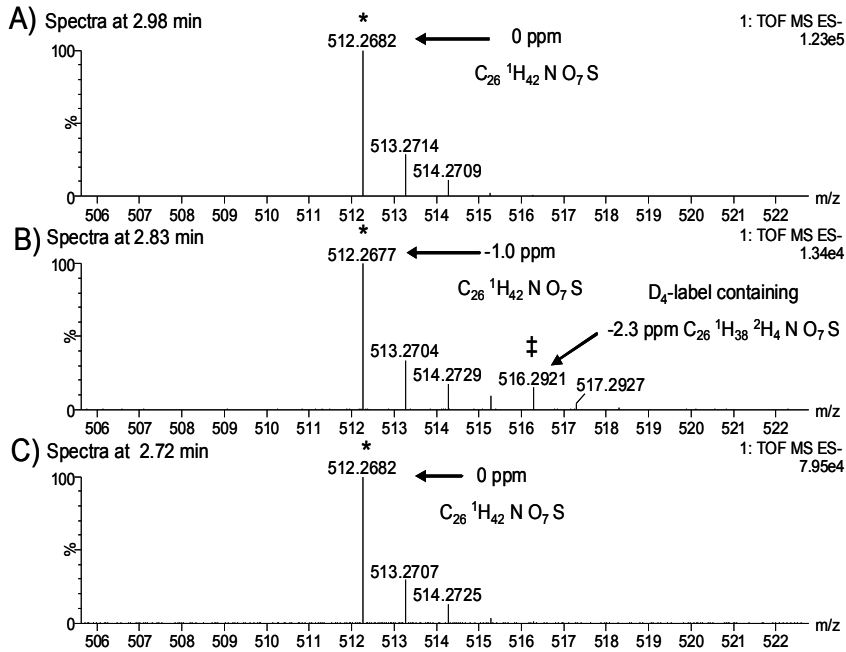

Figure 5. High resolution full scan mass spectra containing endogenous tetrahydroxy cholanoyl BAs and D_4-labeled cholanoyl BAs in bile in Slc27a5-cKD mice. (A) Spectra at 4.34 minutes. (B) Spectra at 4.14 minutes. (C) Spectra at 4.07 minutes

Quantitative differences of the BA metabolites, even those at low levels, were easily obtained. Figure 6 shows that the corresponding tetrahydroxy taurine conjugated BA was detected in the bile of both WT and Slc27a5-cKD mice. Of particular interests, certain metabolites of tetrahydroxy taurine, which were present in one animal cohort, were not observed in the other cohort. For instance, the peak at 2.81 min was present in Slc27a5-cKD mice but not in WT mice, and the peaks at retention times 2.88 min and 2.97 min were present in WT mice but not in Slc27a5-cKD mice. These observations were confirmed with the infusion of D_4-CA where identical results were obtained (figure 6C and D). Furthermore, it was apparent that the levels of the conjugated D_4 label metabolites in the Slc27a5-cKD mice were lower than in WT mice, consistent with BA reconjugation being significantly reduced following silencing of Slc27a5 mRNA (figure 3).
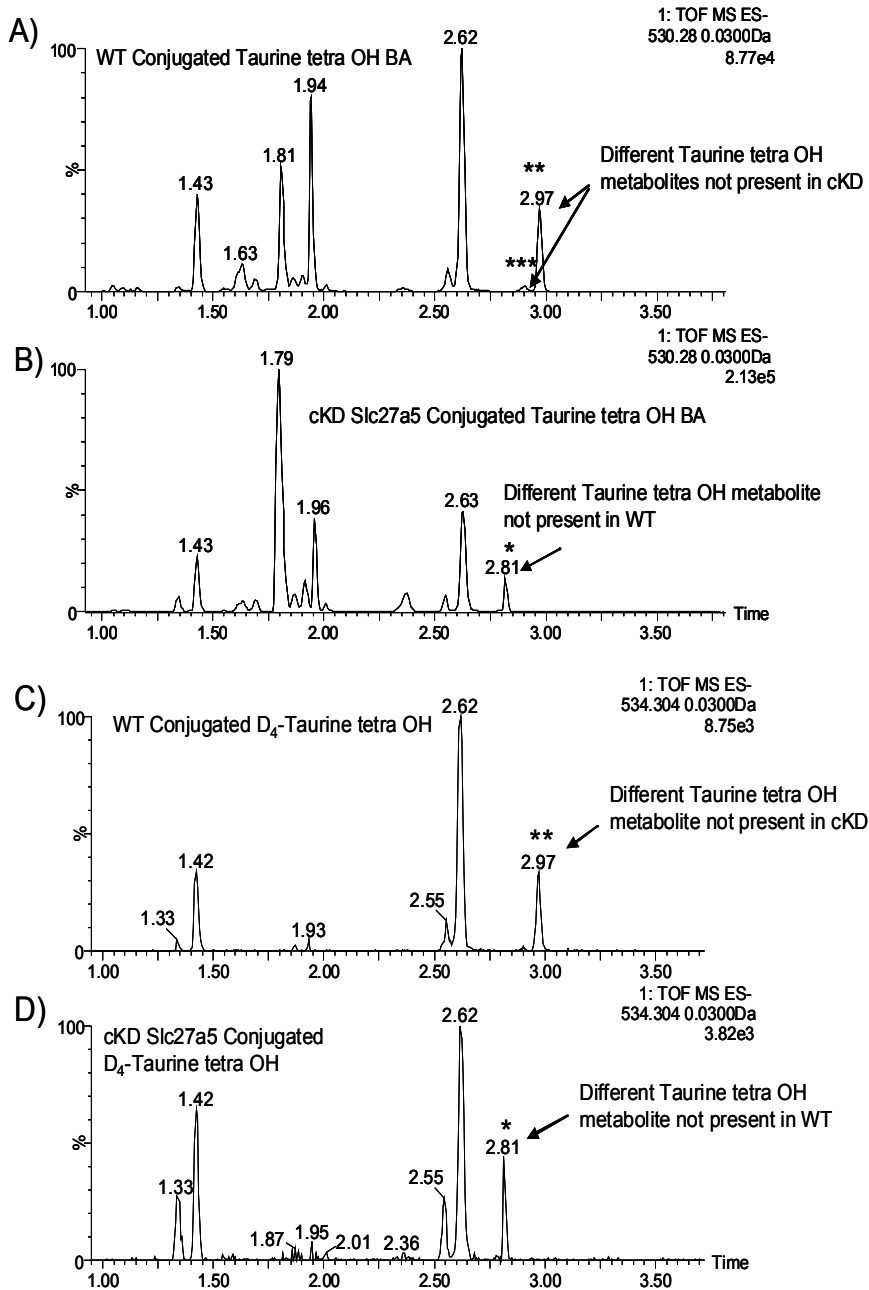
Figure 6. Depicts the detection by UPLC/TOF-MS of conjugated taurotetrahydroxy cholanoyl BA metabolites in bile for WT and Slc27a5-cKD mice. (A) Extracted ion chromatogram (30 mDa window) for WT taurotetrahydroxy cholanoyl BAs. (B) Extracted ion chromatogram (30 mDa window) for Slc27a5-cKD taurotetrahydroxy cholanoyl BAs. (C) Extracted ion chromatogram (30 mDa window) for WT D_4-taurotetrahydroxy cholanoyl BAs. (D) Extracted ion chromatogram (30 mDa window) for Slc27a5-cKD D_4-taurotetrahydroxy cholanoyl BAs.

Endogenous and D_4-labeled taurine conjugated metabolites of tetrahydroxy BA were confirmed by accurate mass measurements (figure 7). Another conjugated metabolite, (m/z 512.2697) monohydroxy sulfate glycine (figure 8), was detected by the use of accurate mass narrow extracted ion chromatograms. Figure 8B shows the biotransformation of this BA in the WT mice, with retention times 2.72, 2.83 and 2.98 min as the major BA metabolites and minor BA metabolites of the same m/z at retention times 3.39, 3.5 and 3.71 min. The elemental compositions of these three peaks (2.72 min (0 ppm), 2.83 min (-1 ppm) and 2.98 min (0 ppm)) were all confirmed by accurate mass in figure 9. Figure 8A depicts the corresponding D_4 – labeled metabolite in the WT mice, but at retention time 2.83 min. The other three peaks (2.41min, 2.61 min and 3.83 min) correspond to the M+2 isotope of taurohyocholic acid (THCA), α-tauromuricholic acid (α-TMCA) and taurocholic acid (TCA) respectively. The single appearance of the D_4-label in the peak of 2.83 min suggests that the other two peaks at retention times 2.72 and 2.98 min may be derived from a different metabolic pathway not related to CA. We consequently compared this profile with that of the Slc27a5-cKD mice. The same endogenous and D_4-labeled metabolites were detected but with significantly lower peak intensities (figures 8C and D), once again showing that reconjugation of all BA metabolites are significantly reduced following Slc27a5 mRNA silencing.
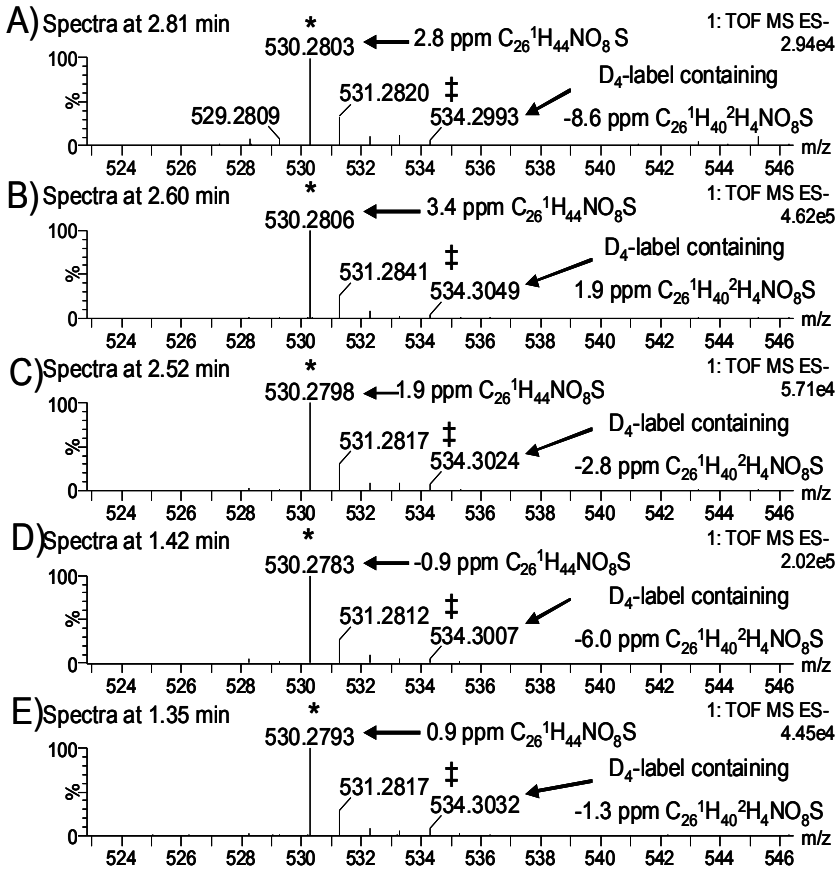
Figure 7. High resolution full scan mass spectra containing endogenous taurotetrahydroxy cholanoyl BAs and D_4-labeled taurotetrahydroxy cholanoyl BAs in bile for Slc27a5-cKD mice. (A) Spectra at 2.81 minutes. (B) Spectra at 2.60 minutes. (C) Spectra at 2.52 minutes. (D) Spectra at 1.42 minutes. (E) Spectra at 1.35 minutes.
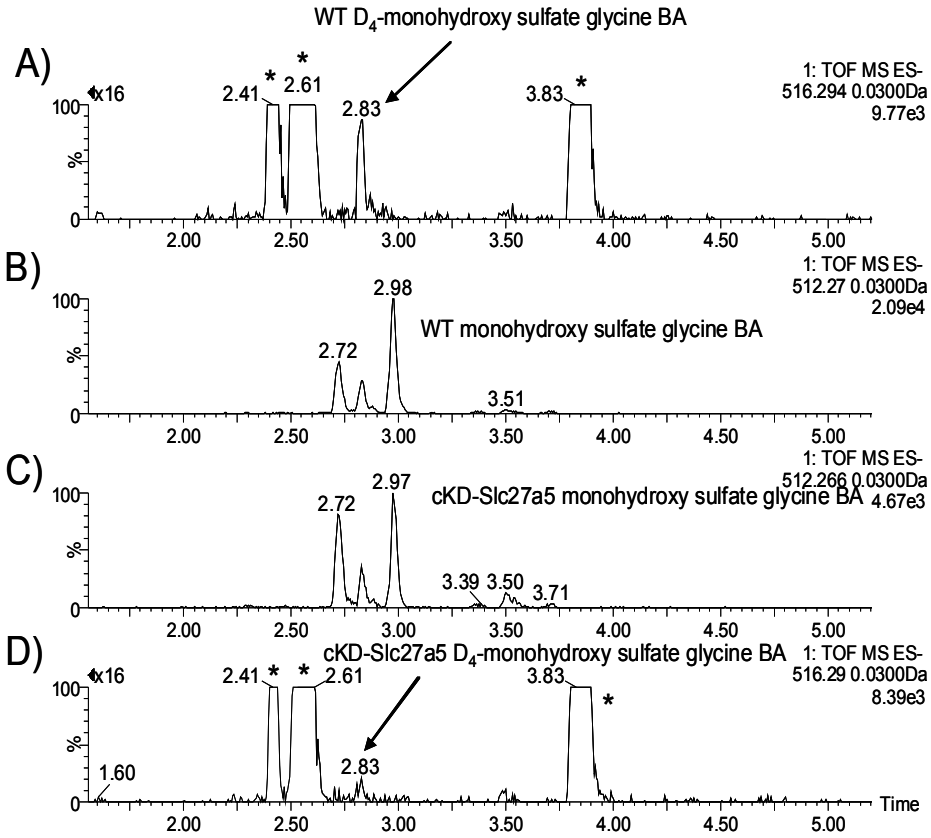
Figure 8. Detection of conjugated monohydroxy-sulfate-glycine BA metabolites in the bile of WT and Slc27a5-cKD mice by UPLC/TOF-MS.(A) Extracted ion chromatogram (30 mDa window) for WT monohydroxy-sulfate-glycine BAs. (B) Extracted ion chromatogram (30 mDa window) for Slc27a5-cKD monohydroxy-sulfate-glycine BAs. (C) Extracted ion chromatogram (30 mDa window) for WT D_4- monohydroxy-sulfate-glycine BAs. (D) Extracted ion chromatogram (30 mDa window) for Slc27a5-cKD D_4- monohydroxy-sulfate-glycine BAs.

Peaks at 2.41min, 2.61 min and 3.83 min correspond to the M+2 isotope of taurohyocholic acid (THCA), α-tauromuricholic acid (α-TMCA) and taurocholic acid (TCA).

Figure 9. High resolution full scan mass spectra containing endogenous conjugated monohydroxy-sulfate-glycine BAs and D_4-labeled conjugated monohydroxy-sulfate-glycine BAs in bile for Slc27a5-cKD mice. (A) Spectra at 2.98 minutes. (B) Spectra at 2.83 minutes. (C) Spectra at 2.72 minutes.

CONCLUSION

We described a novel method to identify and quantitate BAs by high resolution UPLC/TOF-MS, and demonstrated that this method can be used to obtain a full profile of endogenous BA from plasma or bile. This analytical platform was translatable from *in vitro* to an *in vivo* setting, and the use of D_4-CA allowed us to confirm *in vivo* metabolism of many endogenous BAs which were derived from cholic acid (D_4-CA as the substrate). Accurate mass analysis revealed 39 BA metabolites in the bile of WT mice infused with D_4-CA. A key advantage of this method is the use of ultra performance LC coupled with high resolution and accurate mass spectrometry, which enabled *ad-hoc* capability to data mine for BA metabolites from a single injection. Since this metabolomic method does not fully rely on a targeted BA strategy, it can be used with multiple tracers e.g. 'heavy water' to examine several pathways of BA biology and not just confined to cholic acid metabolism derived as described in this research. In comparison to other published protocols (9), the current methodology has the advantage of a rapid sample turn-around time up to 2-fold higher with a simple BA extraction procedure.

The utility of D_4-CA tracer methodology is simple and has a higher throughput than others already published using gas-chromatography coupled with mass spectrometry in which tailored extraction and lengthy chemical derivatization protocols have to be employed (25). Using D_4-CA, we were able to detect and quantify the conjugation to D_4-TCA and D_4-GCA both *in vitro* and *in vivo*. Slc27a5-cKD mice, which are known to have less BA reconjugation (see Chapter 6) served as a good *in vivo* model to observe and confirm D_4-CA reconjugation. Slc27a5-cKD mice had significantly reduced D_4-conjugated BAs in the plasma as compared to WT mice. These data were consistent with data obtained from isolated primary hepatocytes from both WT and Slc27a5-cKD mice. BA profiles from the bile showed that there were an increased number of unconjugated BA metabolites in the Slc27a5-cKD mice, specifically tetrahydroxy cholanoyl metabolites. Although this metabolite of CA has been previously reported (6, 26-28), our analysis detected a larger number of tetrahydroxy cholanoyl metabolites and corresponding taurine conjugated tetrahydroxy cholanoyl metabolites. D_4-CA infusion confirmed these findings and enabled us to track the metabolic fate of CA derived metabolites to all of its conjugated forms, including taurine tetrahydroxy cholanoyl.

Finally in the context of the current research following the silencing of Slc27a5, metabolomics and stable isotope metabolic tracers in combination with high resolution mass spectrometry provided valuable information about BA biology. This combinatory methodology was sensitive to detecting small changes in large endogenous pools, like endogenous BA pools.

References

1.   Williams, C. N. (1976) *Clin Biochem* **9,** 149-52.

2.   Iwamura, K. (1987) *Trop Gastroenterol* **8,** 9-26.

3.   Iwamura, K. (1982) *Tokai J Exp Clin Med* **7,** 7-29.

4.   Ishii, S. *Nippon Yakurigaku Zasshi* **136,** 265-9.

5.   Thomas, C., Pellicciari, R., Pruzanski, M., Auwerx, J., and Schoonjans, K. (2008) *Nat Rev Drug Discov* **7,** 678-93.

6.   Hubbard, B., Doege, H., Punreddy, S., Wu, H., Huang, X., Kaushik, V. K., Mozell, R. L., Byrnes, J. J., Stricker-Krongrad, A., Chou, C. J., Tartaglia, L. A., Lodish, H. F., Stahl, A., and Gimeno, R. E. (2006) *Gastroenterology* **130,** 1259-69.

7.   Griffiths, W. J., and Sjovall, J. (2009) *J Lipid Res*.

8.   Bobeldijk, I., Hekman, M., de Vries-van der Weij, J., Coulier, L., Ramaker, R., Kleemann, R., Kooistra, T., Rubingh, C., Freidig, A., and Verheij, E. (2008) *J Chromatogr B Analyt Technol Biomed Life Sci* **871,** 306-13.

9.   Plumb, R. S., Rainville, P. D., Potts, W. B., 3rd, Johnson, K. A., Gika, E., and Wilson, I. D. (2009) *J Proteome Res* **8,** 2495-500.

10.   Barrett, P. H., and Watts, G. F. (2003) *Curr Opin Lipidol* **14,** 61-8.

11.   Bosje, J. T., Bunch, S. E., van den Brom, W., and Rothuizen, J. (2005) *Vet Rec* **157,** 109-12.

12.   Duane, W. C., Schteingart, C. D., Ton-Nu, H. T., and Hofmann, A. F. (1996) *J Lipid Res* **37,** 431-6.

13.   Svensson, J. O., Jagenburg, R., and Kock, N. G. (1980) *Acta Chir Scand* **146,** 283-9.

14.   Klein, P. D., Haumann, J. R., and Hachey, D. L. (1975) *Clin Chem* **21,** 1253-7.

15.   Klein, P. D., Haumann, J. R., and Eisler, W. J. (1971) *Clin Chem* **17,** 735-9.

16.   Stellaard, F., Schubert, R., and Paumgartner, G. (1983) *Biomed Mass Spectrom* **10,** 187-91.

17.   Stellaard, F., Sackmann, M., Berr, F., and Paumgartner, G. (1987) *Biomed Environ Mass Spectrom* **14,** 609-11.

18.   Engelking, L. R., Barnes, S., Hirschowitz, B. I., Dasher, C. A., Spenney, J. G., and Naftel, D. (1980) *Clin Sci (Lond)* **58,** 485-92.

17.   Stellaard, F., Sackmann, M., Berr, F., and Paumgartner, G. (1987) *Biomed Environ Mass Spectrom* **14,** 609-11.

18.   Engelking, L. R., Barnes, S., Hirschowitz, B. I., Dasher, C. A., Spenney, J. G., and Naftel, D. (1980) *Clin Sci (Lond)* **58,** 485-92.

19.   Collins, B. J., Watt, P. C., O'Reilly, T., McFarland, R. J., and Love, A. H. (1984) *J Clin Pathol* **37,** 313-6.

20.   Seibler, J., Kuter-Luks, B., Kern, H., Streu, S., Plum, L., Mauer, J., Kuhn, R., Bruning, J. C., and Schwenk, F. (2005) *Nucleic Acids Res* **33,** e67.

21.   Seibler, J., Kleinridders, A., Kuter-Luks, B., Niehaves, S., Bruning, J. C., and Schwenk, F. (2007) *Nucleic Acids Res* **35,** e54.

22.   Li AP, R. M., Beck DJ, Kaminski DL (1992) *J. Tissue Cult Meth* **14,** 139-146.

23.   Zhang, Y. K., Guo, G. L., and Klaassen, C. D. *PLoS One* **6,** e16683.

24.   Vore, M., Megaraj, V., Iida, T., Jungsuwadee, P., and Hofmann, A. F. (2010) *Drug Metabolism and Disposition* **38,** 1723-1730.

25.   Tsai, S. J., Zhong, Y. S., Weng, J. F., Huang, H. H., and Hsieh, P. Y. *J Chromatogr A* **1218,** 524-33.

26.   Dumaswala, R., Setchell, K. D., Zimmer-Nechemias, L., Iida, T., Goto, J., and Nambara, T. (1989) *J Lipid Res* **30,** 847-56.

27.   Perwaiz, S., Forrest, D., Mignault, D., Tuchweber, B., Phillip, M. J., Wang, R., Ling, V., and Yousef, I. M. (2003) *J Lipid Res* **44,** 494-502.

28.   Thomassen, P. A. (1979) *Eur J Clin Invest* **9,** 425-32.

SUPPLEMENTARY INFORMATION

Supplementary Figure 1. UPLC/TOF-MS calibration curve for BA mixture of standards in buffer ranging in concentration (0.005-5µM). Showing response (peak area of analyte/corresponding internal standard, see method for specific internal standards used) of different unconjugated and conjugated BA's
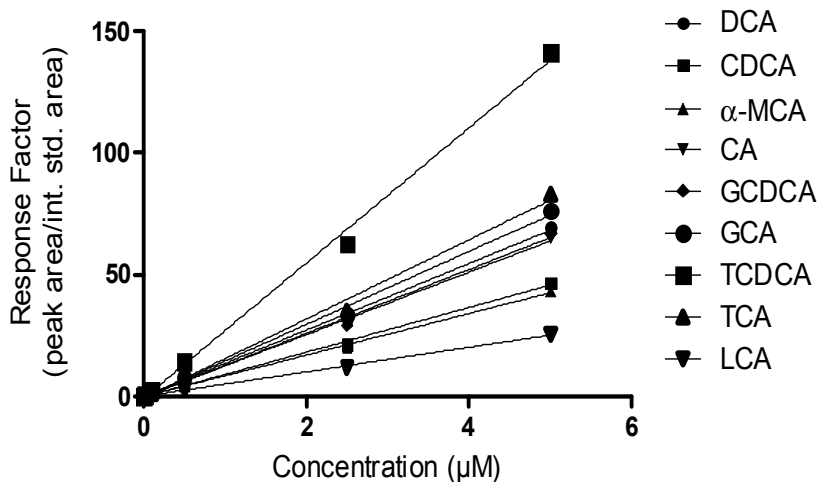
Supplementary Table 1. Calibration curve results summary for BA mixture in buffer solutions

	DCA	CDCA	α-MCA	CA	GCDCA	GCA	TCDCA	TCA	LCA
Best-fit values									
Slope	13.69±0.3102	9.190±0.1779	8.531±0.1477	12.84±0.2276	13.14±0.3980	14.98±0.4498	27.78±0.7778	16.28±0.5972	5.052±0.09151
Y-intercept when X=0.0	-0.1003±0.7109	-0.1051±0.4077	0.02032±0.3384	-0.1976±0.5215	-0.3020±0.9122	-0.3097±1.031	-0.7253±1.782	-0.7084±1.368	0.1109±0.2097
X-intercept when Y=0.0	0.007326	0.01144	-0.002381	0.01539	0.02299	0.02067	0.02611	0.04350	-0.02195
1/slope	0.07303	0.1088	0.1172	0.07788	0.07613	0.06674	0.03599	0.06141	0.1980
95% Confidence Intervals									
Slope	12.83 to 14.55	8.696 to 9.684	8.122 to 8.941	12.21 to 13.47	12.03 to 14.24	13.74 to 16.23	25.63 to 29.94	14.63 to 17.94	4.798 to 5.306
Y-intercept when X=0.0	-2.074 to 1.873	-1.237 to 1.027	-0.9191 to 0.9597	-1.645 to 1.250	-2.834 to 2.230	-3.171 to 2.552	-5.674 to 4.223	-4.507 to 3.091	-0.4713 to 0.6930
X-intercept when Y=0.0	-0.1423 to 0.1462	-0.1155 to 0.1306	-0.1159 to 0.1048	-0.1004 to 0.1246	-0.1791 to 0.2061	-0.1795 to 0.2022	-0.1596 to 0.1957	-0.2025 to 0.2621	-0.1415 to 0.09065
Goodness of Fit									
R square	0.9980	0.9985	0.9988	0.9987	0.9963	0.9964	0.9969	0.9946	0.9987
Sy.x	1.405	0.8057	0.6687	1.031	1.803	2.037	3.522	2.704	0.4144

Chapter 8

In-vivo 'heavy water' labeling in C57Bl/6 mice to quantify static and kinetic changes in free cholesterol and cholesterol esters by LC/MS

In-vivo 'heavy water' labeling in C57Bl/6 mice to quantify static and kinetic changes in free cholesterol and cholesterol esters by LC/MS

SUMMARY

High resolution LC/MS-MS and LC/APPI-MS methods have been established for the quantitation of flux in the turnover of cholesterol and cholesterol ester. Attention was directed towards quantifying the monoisotopic mass (M0) and that of the singly-deuterated labeled (M+1) isotope. A good degree of isotopic dynamic range was achieved by LC/MS-MS ranging from 3-4 orders of magnitude. Correlation between the linearity of GC/MS and LC/APPI-MS are complimentary (r^2 =0.9409). In order to prove the viability of this particular approach, male C57Bl/6 mice on either a high carbohydrate (HC) or a high fat (HF) diet were treated with ^2H_2O for 96 hours. Gene expression analysis showed an increase in the activity of stearoyl-CoA desaturase (Scd1) in the HC diet up to x 69 fold (p <0.0008) in comparison with the HF diet. This result was supported by the quantitative flux measurement of the isotopic incorporation of ^2H into the respective cholesterol and cholesterol ester pools. From these results, it was concluded that it is possible to readily obtain static and dynamic measurement of cholesterol and cholesterol esters *in-vivo* by coupling novel LC/MS methods with stable isotope-based protocols.

INTRODUCTION

The liver plays a vital role in cholesterol metabolism (1-5) and homeostasis. In addition to this, production of bile acids from cholesterol also plays an important role in the secretion and degradation of plasma lipoproteins. A high level of cholesterol in the body circulation is strongly associated with atherosclerosis (6-10). The source of cholesterol comes from different areas; dietary, *de-novo* synthesis and synthesis in extra hepatic tissues. The liver acts as a cross-junction at which cholesterol is incorporated into HDL/LDL, and secreted as free cholesterol in the bile or in the form of bile salts/acids.

Studies of cholesterol metabolism typically require measurements of static concentrations of cholesterol to identify differences between models or to determine the presence or absence of a disease phenotype. The simultaneous use of stable or radio isotope flux analysis can aid in understanding the nature of a metabolic abnormality and yielding information regarding the dynamics that contribute to altered or perturbed homeostasis.

Questions surrounding cholesterol dynamics have been addressed using isotopic labeled water for nearly 70 years, with the pioneering studies of Schoenheimer (11-13) based upon the use of ^2H_2O and the classical work of Dietschy (14-20) and colleagues relied on ^3H_2O. Considering the dose of radiation (typically in mCi) and the advances in mass spectrometry and related instrumentation (e.g. coupling to GC) it is not surprising that many investigators have turned their attention towards the use of the stable isotope, ^2H_2O. The human sterol and fatty acid flux elegant work carried out by Schoeller *et al* (21), Wong *et al* (22, 23), and Jones *et al* (24, 25) has opened up the number of applications for the use of deuterated water in flux lipid experiments.

Although the ability to couple static and dynamic measurements in studies of cholesterol metabolism is of obvious importance, most studies have been done under a relatively low level analytical resolution. For example, investigators typically examine the metabolism of free cholesterol and/or total cholesterol esters. In addition, the classical GC/MS and GC-Isotope Ratio Mass Spectrometry (IRMS) methods are not suitable for routine use in high-throughput analyses since cholesterol esters are generally separated off-line as a single pool (e.g. using TLC), and then subjected to saponification, extraction, derivatization and finally mass spectrometry analysis, this supposes a more time consuming and laborious process in which in today's new demands specially in the discovery arena time is of the essence to make decisions in a faster manner than ever before.

Recent advances in high resolution LC-MS/MS have enabled the rapid high-throughput analyses of complex mixtures, which therein can be used to obtain information regarding different lipid classes and sub-classes. These instruments are able to analyze complex biological mixtures with minimal sample preparation.

A variety of different ionization techniques were utilized for the experiments described herein. For example cholesterol is particularly difficult to ionize by electrospray (ESI) mass spectrometry as its proton affinity is relatively low, but on the other hand ESI is suitable for measuring the ammoniated adduct of cholesterol ester (CE) with good sensitivity. This

finding is highlighted by a comparison of equimolar concentrations (1μg/mL) of CE 16:0 and CE 18:0 analyzed by ESI and APCI (supplementary figure 1). For both saturated CE's the ESI technique proved to have a better signal intensity than in APCI mode (~7-13 x fold better). Having said that, other researchers in this field Butovich *et al* (26, 27) have shown the application of atmospheric pressure chemical ionization (APCI) to measure in one analytical run free cholesterol and cholesterol esters coupled to a reversed phase column. But in their research they were not measuring metabolic flux of free cholesterol and cholesterol esters in plasma. In this research article it was essential to obtain the best sensitivity to measure the M1/M0 isotopomer ratio for free cholesterol and cholesterol esters. One ionization mode such as APcI was not sensitive enough to measure both analytes (free cholesterol and cholesterol esters) in one analytical run.

In addition to the measurement of CE's by ESI, we investigated the use of atmospheric pressure photoionization (APPI) for the measurement of free cholesterol. The major advantage of APPI over APCI is that for free cholesterol we have experienced better limits of detection between 3-4 x fold better signal than in APCI mode (supplementary figure 2). This technique has been used in the past to ionize less polar biochemicals such as sterols and steroids (28-34). The ionization mechanism is somewhat different from electrospray because in most cases a dopant is utilized to provide the proton to complete the ionization process. Typical dopants which may be used are either acetone or toluene. The ionization is initiated by 10-eV photons emitted by a krypton discharge lamp. The mechanism of ionization by APPI involves the absorption of photons by the molecule(s) to be analyzed; this is then followed by the ejection of an electron resulting in a molecular cation M^+. This reaction only occurs if the ionization energy of the dopant is lower than the ionization energy of the photons. The dopant provides the proton, and the radical cation previously mentioned will react with the dopant to form a stable $[M+H]^+$ cation.

In this research a simple method(s) for dissecting cholesterol metabolism via LC-MS/MS is reported, attention was aimed at determining if we could simultaneously quantify the abundance and the isotopic labeling following ^2H_2O administration (35, 36) of different cholesterol ester species in the presence of a high carbohydrate and high fat diets.

MATERIALS AND METHODS

Biological

Male C57Bl/6 mice from Taconic were acclimated in the animal facility for one week. At an age of 10 weeks old, mice were randomized into two groups (n = 26 per group) and the diet was switched to either a high carbohydrate (HC) diet (D12450, 10% fat, 70% carbohydrate, and 20% protein, Research Diets, NJ) or a carbohydrate-free (CF) diet (D12369B, 90% fat, 0% carbohydrate, and 10% protein, Research Diets, NJ). The diet intervention proceeded for 13 days; all mice were then given an intraperitoneal injection of labeled water (20ml/kg of body weight, 99% ^2H_2O). After injection, mice were returned to their cages (n = 6 mice per cage) and maintained on 5% ^2H -labeled drinking water for the remainder of the study; this design is sufficient to maintain a steady-state ^2H labeling of body water. Mice in each group were fed the respective diets *ad libitum*, and were sedated on various days after injection (n = 6 per day per group), blood and tissue samples (liver tissue was used for gene expression analysis only) were then collected and quick-frozen in liquid nitrogen. Samples were stored at -80 °C until analyzed. All animal protocols were reviewed and approved by the Merck Research Laboratories Institutional Animal Care and Use Committee (Rahway, NJ).

Water labeling

The ^2H-labeling of plasma water was determined as described by Shah *et al* (37). Briefly, ^2H present in water is exchanged with hydrogen bound to acetone by incubating samples (e.g. 10 µl of plasma or known standards) in a 2 ml glass screw-top GC vial at room temperature for 4 hours with 2 µl 10N NaOH and 5 µl of acetone. The instrument is programmed to inject 5 µl of headspace gas from the GC vial in a splitless mode. Samples were analyzed using a 0.8 min isothermal run (Agilent 5973 MS coupled to a 6890 GC oven fitted with a DB-17 MS column, 15m x 250µm x 0.15µm, the oven was set at 170 ^0C and helium carrier flow was set at 1.0 ml x min^{-1}), acetone elutes at ~ 0.4 min, the mass spectrometer was set to perform selected ion monitoring of m/z 58 and 59 (10 ms dwell time per ion) in the electron impact ionization mode.

GC/MS of total plasma palmitate and cholesterol

Plasma samples for GC/MS analysis were processed in 1.5 ml eppendorff tubes: To 50 µL of plasma 25 µL internal standard was added (FA 17:0, 0.5 mg/ml $CHCl_3$) and 100 µL 1N KOH in 80% ethanol. The samples were heated at 65°C for 1 hour. Samples were acidified with 25 µL 6N HCl and extracted in 125 µL chloroform followed by vigorous vortexing for 20 sec. The samples were centrifuged at 3000 rpm for 5 min, 100 µL of chloroform (lower layer) was collected and evaporated to dryness under N_2.

Samples were derivatized using Bis Trimethyl Silyl Trifluoroacetamide (BSTFA) + 10% Trimethylchlorosilane (TMCS), 50 µL was added to the sample and then incubated at 75°C for 1 hour. Excess BSTFA was evaporated to dryness in N_2. The TMS-derivative was re-constituted in 50 µL ethyl acetate for analysis by GC/MS.

Samples were analyzed by GC/MS using the Agilent 6890 gas chromatograph linked to an Agilent 5973 mass selective detector (MSD) (Agilent, Palo alto, CA) operated at 70 eV. Gas chromatography was performed using an Agilent J&W DB-5MS capillary column 30.0 m x 250 um x 0.25 µm. 2 µL was injected in a 20:1 split. The inlet temperature was set at 250°C and the helium gas carrier flow was set at 1 ml/min[-1]. The oven temperature was started at 150°C, raised at 20°C /min to 310°C and held at this temperature for 6 min.

The MSD was set for selected ion monitoring (SIM) of m/z 313, 314 for the palmitate TMS derivative; 327, 328, 329 for heptadecanoic acid TMS derivative and 368, 369 for cholesterol TMS derivative with 10 ms dwell time per ion. Concentrations of fatty acids/ cholesterol were corrected for by a standard curve with varying combinations of fatty acid or cholesterol with their respective D1-derivatives.

LC/MS of lipids

Plasma samples from each animal (20µL) were extracted for lipid analysis by LC/MS-MS using a dichloromethane (DCM) /methanol mixture (2:1, v/v) in accordance with the method described by Bligh and Dyer (38, 39) . During the extraction procedure the samples were spiked with a final concentration of 2 µg/mL with non-naturally occurring and deuterated lipids internal standards [(17:0 containing CE and D_6-Cholesterol, (Sigma Aldrich, St Louis, MO))].

The inlet system was comprised of an Acquity UPLC (Waters, Milford, MA, USA). Mouse plasma lipid extracts were injected (10µL) onto a 1.8 µm particle 100 x 2.1 mm id Waters Acquity HSS T3 column (Waters, Milford, MA, USA); the column was maintained at 55 °C. The flow rate used for these experiments was 0.4 mL/min. A binary gradient system consisting of acetonitrile (Burdick & Jackson, USA) and water with 10 mM ammonium formate (Sigma-Aldrich, St Louis, MO) (40:60, v/v) was used as eluent A. Eluent B, consisted of acetonitrile and isopropanol (Burdick & Jackson, USA) both containing 10 mM ammonium formate (10:90, v/v). The sample analysis was performed by using a linear gradient (curve 6) over a 15 min total run time; during the initial portion of the gradient, it was held at 60% A and 40% B. For the next 10 min the gradient was ramped in a linear fashion to 100% B and held at this composition for 2 min hereafter the system was switched back to 60% B and 40% A and equilibrated for an additional 3 min. For the free cholesterol measurements by LC/APPI-MS the gradient conditions were identical apart from the fact that no ammonium formate was used as the additive.

The inlet system was directly coupled to a hybrid quadrupole orthogonal time of flight mass spectrometer (SYNAPT G2 HDMS, Waters, MS Technologies, Manchester, UK). Electrospray (ESI) positive and APPI positive ionization modes were used. In ESI mode a capillary voltage and cone voltage of +2 kV and +30 V respectively was used. The desolvation

source conditions were as follows; for the desolvation gas 700 L/hr was used and the desolvation temperature was kept at 450°C. APPI was utilized using a krypton discharge lamp (10-eV photons) set with a repeller voltage of +3.5 kV. The dopant utilized for the APPI experiments was acetone (Fisher scientific, Pittsburgh, PA) which was infused at a continuous flow rate of 100µL/min post column. The desolvation source conditions for APPI were as follows; for the desolvation gas 900 L/hr was used and the desolvation temperature was kept at 600°C. Data were acquired over the mass range of 50-1200 Da for both MS and MS^E modes (40-43). The mass spectral resolution was set to 25K full width half mass (FWHM) and typical mass accuracies were in the order of 0-2 ppm. The system was equipped with an integral LockSpray unit with its own reference sprayer that was controlled automatically by the acquisition software to collect a reference scan every 10 seconds lasting 0.3 seconds. The LockSpray internal reference used for these experiments was Leucine enkephalin (Sigma-Aldrich, St Louis, MO) at a concentration of 5 ng/µL in 50% acetonitrile/ 50% H$_2$O + 0.1% formic acid (v/v). The reference internal calibrant was introduced into the lock mass sprayer at a constant flow rate of 50µL/min using an integrated solvent delivery pump. A single lock mass calibration at m/z 556.2771 in positive ion mode was used during analysis. The mass spectrometer was operated in the MS^E mode of acquisition. During this acquisition method, the first quadrupole Q1 is operated in a wide band RF mode only, allowing all ions to enter the T-wave collision cell. Two discrete and independent interleaved acquisitions functions are automatically created. The first function, typically set at 5 eV, collects low energy or unfragmented data while the second function collects high energy or fragmented data typically set by using a collision energy ramp from 25-35 eV. In both instances, argon gas is used for collision induced dissociation (CID). This mode of operation allows for fragmentation ions to be generated *ad-hoc*, and the use of the software data mining tool it allowed for the alignment of the low and high energy data. This mode of acquisition proved to be adequate for high throughput screening, but there are some cases where complete ion co-elution occurs between the low and high energy acquisitions. When this takes place, then more rigorous fragmentation experiments MS/MS CID was utilized.

Data processing and statistical analysis

For the LC/MS and GC/MS analysis of the isotopic dilution of cholesterol, a set of standards were prepared in chloroform (1mg/ml), ranging from 0% excess ^{2}H- labeling up to 2.5% excess ^{2}H-labeling (0%, 0.15%, 0.3%, 0.6%, 1.25%, 2.5%) by mixing with cholesterol and its D1- derivative. Labeled palmitate was prepared in the same fashion as cholesterol for the GC/MS analysis only, and heptadecanoic acid was used as the internal standard. All the samples were diluted 10 fold with (65:5:30 v/v/v) IPA: MeOH: H$_2$O to achieve a final concentration of 0.1 mg/ml. For GC/MS analysis 10 µL of each standard was derivatized with BSTFA as described above. For the quantitation of the contribution of cholesterol synthesis the data was processed using a precursor: product labeling ratio to the general equation: % newly made material = product labeling / (water labeling x *n*) x 100 where *n* is the number of exchangeable hydrogens, assumed to equal 26, and where the product labeling is determined from the ratio of M1/M0 isotopomers (44).

The GC/MS and LC/MS data acquired were processed by the instrument's manufacturer software (ChemStation & MassLynx respectively). Gene expression data were processed using Ingenuity software (Ingenuity systems, Redwood City, CA) .For the statistical analysis; all the data are presented as ± standard error mean (SEM). Differences between groups were computed by student's *t-test* statistical analysis (GraphPad Prism, La Jolla, CA). Post test analysis for quantifiable variables was conducted using Mann-Whitney U non-parametric test with two-tailed *p*-values. Values of *p* <0.05 was considered as being statistically significant for all the data derived from the experiments herein.

RNA isolation and Real-time quantitative PCR analysis

Liver tissue (~20 mg) was snap frozen in liquid nitrogen and stored at -80 °C. The tissues were homogenized in 600 µL RLT lysis buffer (Qiagen, Valencia, CA) containing 0.1% (v/v) β-mercaptoethanol using a PowerGen 125 homogenizer and 7 x 65 mm disposable plastic generators (Fisher Scientific). Total RNA was extracted from the homogenized tissue using RNeasy Mini Kit (Qiagen, Valencia, CA) following the manufacturer's protocol. cDNA was generated from 2 µg of RNA using RT^2 First Strand kit (SA Biosciences). Real-time PCR analysis was performed on the 7900HT PCR System (Applied Biosystems, Foster City, CA) with 2x SYBR PCR Master Mix and mouse-specific PCR primers for mouse Scd1, (SABioscienses). Expression levels of stearoyl-CoA desaturase (Scd1) mRNA were normalized to an average of that of mouse beta-actin (Actb), Glyceraldehyde 3-phosphate dehydrogenase (Gapdh), Beta-glucuronidase (Gusb), Hypoxanthine-guanine phosphoribosyltransferase (Hprt1), Peptidylprolyl isomerase A (cyclophilin A) (Ppia) and ribosomal protein 113a (Rp113a) in each sample.

RESULTS

The water labeling after 3 hours was kept constant for both diets for the duration of the study at ~2.5% (Figure 1).
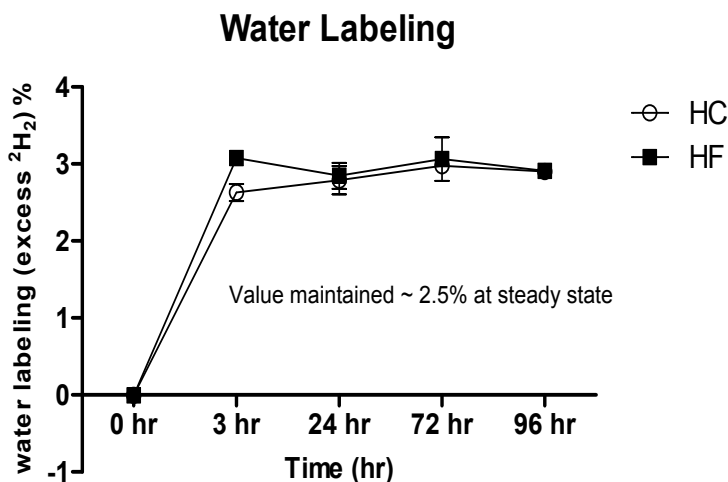
Figure 1. Steady-state labeling of plasma water in mice fed with a HF and HC diets.

Gene expression results from the HC diet revealed an up-regulation in the expression of SREBP1c pathway which contain enzymes involved in *de-novo* lipogenesis, including stearoyl-CoA desaturase (Scd1). In contrast, the SREBP2 pathway was down-regulated. Expression of Scd1 was 69x fold higher ($p < 0.0008$) on the HC diet compared to the HF diet. There is substantial evidence in the literature (45-49) linking over intake of carbohydrates to *de-novo* lipogenesis (DNL). This is accompanied by the synthesis of fatty acids (FA) and the corresponding incorporation into the different phospholipid (PL), triglyceride (TG) and cholesterol ester (CE) pools. When Scd1 is induced, it results in increased desaturation rate of palmitate (FA 16:0) and stearate (FA 18:0) at the 7Z and 9Z position of the fatty acyl chain respectively to give rise to FA 16:1 7Z and FA 18:1 9Z. These newly desaturated fatty acids serve as substrates for other enzymes to promote the synthesis of PL, TG and CE. The lipogenic cholesterol ester index was calculated as the ratio of palmitic acid (FA16:0) containing CE and linoleic acid (FA 18:2 9Z, 12Z) containing CE. This index was increased x 2.7 times ($p = 0.0011$) in the HC diet versus the HF diet. External calibrations were used for the calculation of the CE 16:0 and CE 18:2 ratio as the mass spectral responses were different (see supplementary figure 3a). Scd1 activity was derived by measuring the desaturation index (DI) between the ratio of palmitoleic acid (FA16:1 7Z)-containing CE and palmitic acid (FA 16:0)-containing CE, for this measurement external calibrations were also utilized for CE 16:0 and CE 16:1 (see supplementary

figure 3b). As a result of this analysis, DI increased considerably in the HC diet (~ 3.6 fold, p = 0.0011). In this study the main focus was placed on the information which can be provided by LC-MS/MS in comparison with GC/MS for the quantifiable flux of both free cholesterol and cholesterol ester measurements using an *in-vivo* preclinical murine animal model. A rapid and robust analytical method was developed by LC/ESI-MS and LC/APPI-MS for CE and free cholesterol analysis. This LC/MS lipid method was not exclusively limited to free cholesterol and CE's but to other lipids such as FFA's, LysoPL's, PL's, DG's, SM's, Cer's and TG's. By the use of this LC/MS methodology the following cholesterol esters in positive ion electrospray mode were detected as ammonium adducts $[M+NH_4]^+$ (Figure 2A and B) in both HC and HF diets; CE 16:0, CE 16:1, CE 18:1, CE 18:2, CE 18:3, CE 20:4 and CE 22:6. Free cholesterol was detected in APPI positive ion mode. In order to prove the robustness of the analytical platform developed, different concentrations (0.01, 0.1, 1, 10 and 100µM of unlabeled cholesterol esters were analyzed (n=3 for each concentration). The goal behind this experiment was to determine at which point in the titration curve the ratio between M1/M0 will become imprecise especially at low concentrations when ion statistics may be lower than at the top spectrum of the titration curve. As can be observed in table 1, there was a good level of precision of measurements throughout all different concentrations for the CE's utilized in this experiment. For the vast majority of cases three orders of isotopic dynamic range was shown (0.1-100 µM) , and only in one instance for CE 18:2 four orders of isotopic dynamic range (0.01-100 µM) was achieved. The low concentration of the titration curve showed a higher degree of inaccuracy but as previously mentioned this is not an abnormal finding since the level of ion statistics is lower than at higher concentrations. Nevertheless, it was found to be acceptable for the type of measurements conducted in this study. When all concentrations belonging to the 18 and 16 FA acyl containing cholesterol esters were combined together (figure 3), coefficients of variation of 1.33 % (n=38) and 1.54% (n=22) were achieved respectively. Therefore, irrespective of the concentration of the analyte in the biological matrix good levels of precision are observed at a wide isotopic dynamic range between 3-4 orders as described here. This level of dynamic range was not previously achievable with time of flight mass spectrometers but new developments in the ion detection (analogue to digital converter - ADC) has allowed for the application of this tool for flux analysis. This is a relevant observation as the levels of endogenous cholesterol esters and/or free cholesterol will vary throughout different samples and studies.
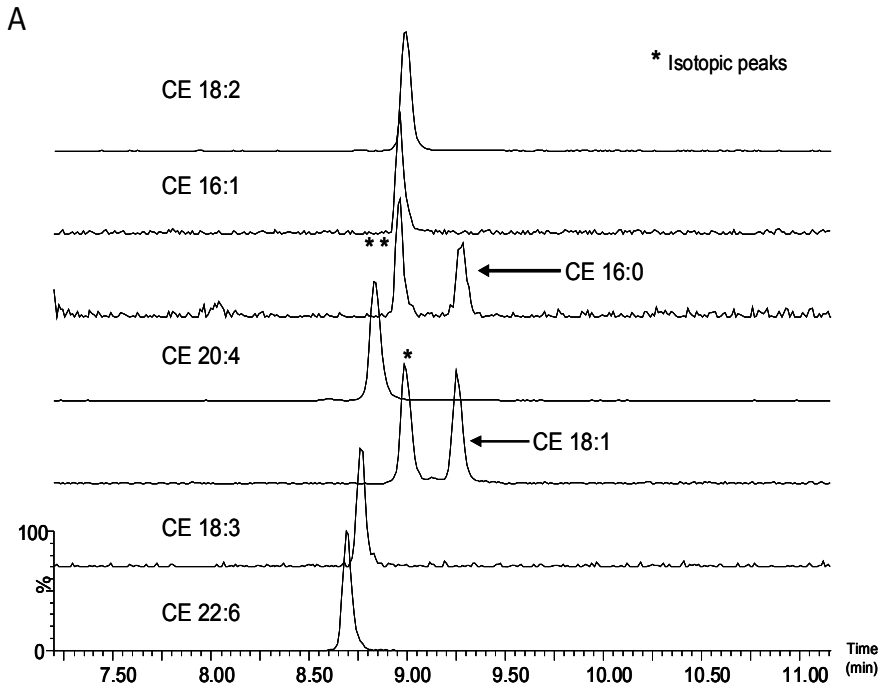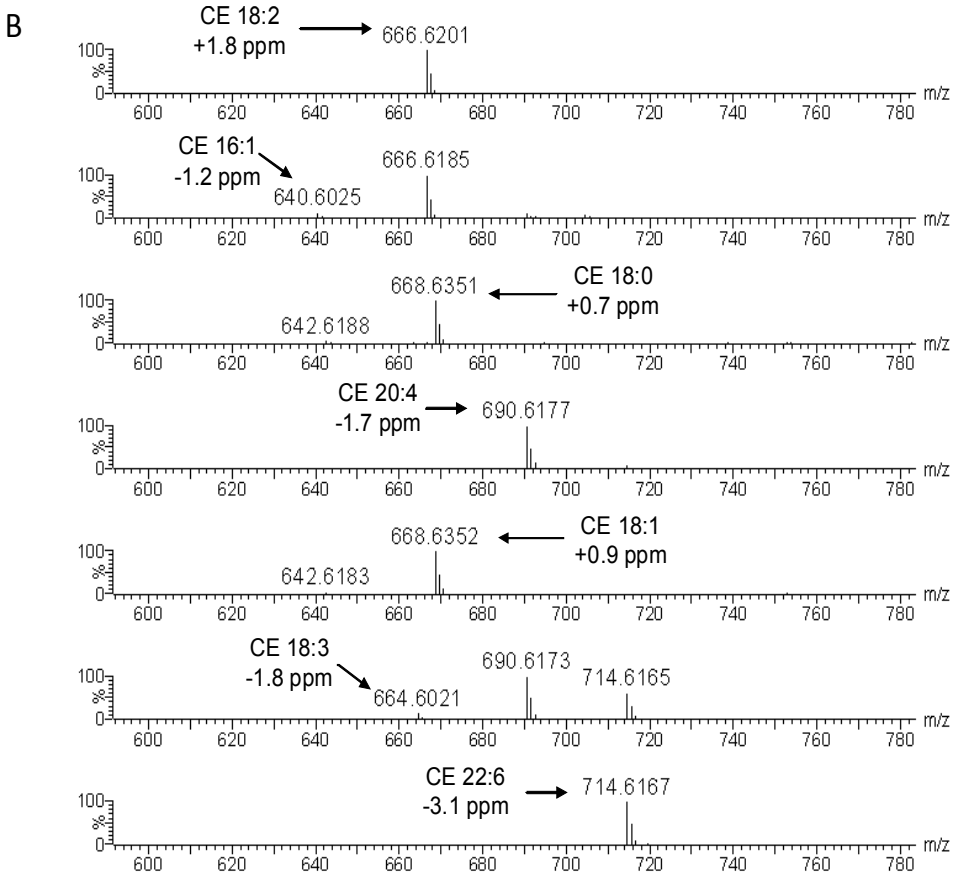
Figure 2: (A) LC/MS profiles of plasma cholesterol esters. Data are shown as the extracted ion chromatogram for each ester, note that the symbols * and ** refer to the M+2 isotopes of cholesterol ester 18:2 and cholesterol ester 16:1, respectively. (B) Full scan MS spectra with accurate mass for the corresponding cholesterol esters.

†*Cholesterol esters detected in electrospray positive ion mode as ammonium adducts*
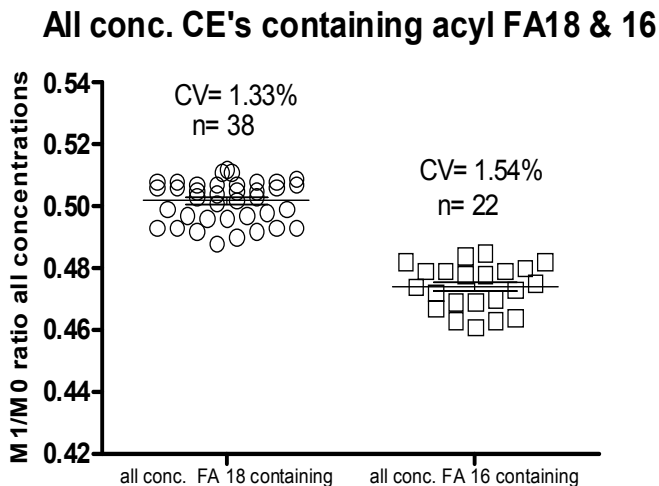
Figure 3: Describes the M1/M0 ratio for all concentrations which contain an acyl FA 18 or 16 for the CE's analyzed in this test. The combination of all concentrations (0.01μM – 100 μM) for the acyl FA 18 containing CE's showed a good coefficient of variation 1.33% (n = 38). With respect to the combination of all concentrations (0.1 μM – 100 μM) for the acyl FA 16 containing CE's showed a good coefficient of variation 1.54% (n=22)

Table1. Isotopic dynamic range measurements for a range of different CE's standards (CE 16:0, CE 16:1, CE 18:0, CE 18:1 & CE 18:2) by LC/ESI-TOF-MS. In all cases a good level of precision was shown. The isotopic dynamic range was between 3-4 orders of magnitude.

| Lipid claass | Cholesterol Ester Concentration (μM) | | | | | | | | | |
| | 0.01 | | 0.1 | | 1 | | 10 | | 100 | |
	M1/M0 ratio	cv (%)	M1/M0 ratio	cv (%)	M1/M0 ratio	cv (%)	M1/M0 ratio	cv (%)	M1/M0 ratio	cv (%)
CE 16:0	nd*	nd*	0.488 ± 0.011	2.18	0.469 ± 0.003	0.54	0.479 ± 0.006	1.15	0.467 ± 0.004	0.81
CE 16:1	nd*	nd*	0.475 ± 0.01	2.03	0.473 ± 0.009	1.89	0.473 ± 0.012	2.43	0.478 ± 0.004	0.73
CE 18:0	nd*	nd*	0.493 ± 0.003	0.61	0.503 ± 0.007	1.43	0.499 ± 0.007	1.34	0.495 ± 0.006	1.28
CE 18:1	nd*	nd*	0.499 ± 0.011	2.14	0.499 ± 0.007	1.42	0.506 ± 0.001	0.2	0.506 ± 0.002	0.3
CE 18:2	0.502 ± 0.008	1.55	0.501 ± 0.009	1.72	0.508 ± 0.004	0.79	0.506 ± 0.003	0.64	0.506 ± 0.003	0.5

*cholesterol esters that were not detected at this concentration

Historically GC/MS and GC/IRMS has been the analytical platform of choice for many years and it has shown a good linearity when isotopic dilutions are conducted. In fact, the use of isotopic dilution is very important because the titration curve is used to read –off the isotopic enhancement from a particular ^2H_2O *in-vitro* or *in-vivo* experiment. Therefore, for the current study it was important to examine the correlation between the two analytical platforms for isotopic dilution titration curves. A range of different isotopic dilutions ranging from 0% excess ^2H- labeling up to 2.4% excess ^2H-labeling of cholesterol was prepared by mixing with unlabeled cholesterol and [^2H] cholesterol. Figure 4a describes very clearly the correlation between LC/APPI-MS and GC/MS measurements for the deuterium isotopic enrichment of free cholesterol (LC/APPI-MS) and total cholesterol (GC/MS) respectively from the different diets. The plot contains all of the data in the study, a very good correlation factor was achieved r^2= 0.9409 with best –fit values of slope and intercept y= 0.9908 x + 0.0317. It is important to note the fact that for the GC/MS measurements the isotopic enrichment in a normal setting would represent the total cholesterol measurement while for the LC/APPI-MS measurements more specificity can be achieved by this latter analytical platform without further sample preparation steps in which the samples do not need to be saponified and free cholesterol can be differentiated from cholesterol esters. Even though we achieved a good level of linearity between the two measurements by the different analytical techniques, Bland-Altman *et al* (50) suggested in their research that a more statistically relevant approach to measure this correlation is by the measurement of the agreement between the two techniques. This method of measuring agreement is based upon the computation of the mean differences between the two techniques and the likelihood that the data agrees with the 95% confidence limits set by the mean +2SD and the mean -2SD. This measurement can be observed in figure 4b, a good degree of agreement was shown between the two methods as most of the results apart from one outlier fell outside the mean +2SD and mean -2SD confidence limits.

Measurement of ^{2}H enhancement can be realized by using this technique but there are certain limitations which need to be noted, if the level of enrichment is below 0.3% then other techniques such as isotope ratio mass spectrometry (IRMS), would be more appropriate. Nonetheless, by the use of IRMS the qualitative information based of the particular lipid class where the label is incorporated and the actual amount is lost as it only measures total incorporation.

A

Correlation between LC/APPI-MS & GC/MS

$$y = 0.9908x - 0.0317$$

$$r^2 = 0.9409$$
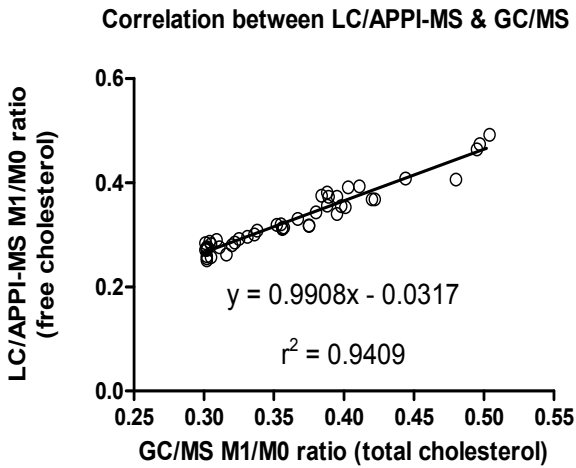
B
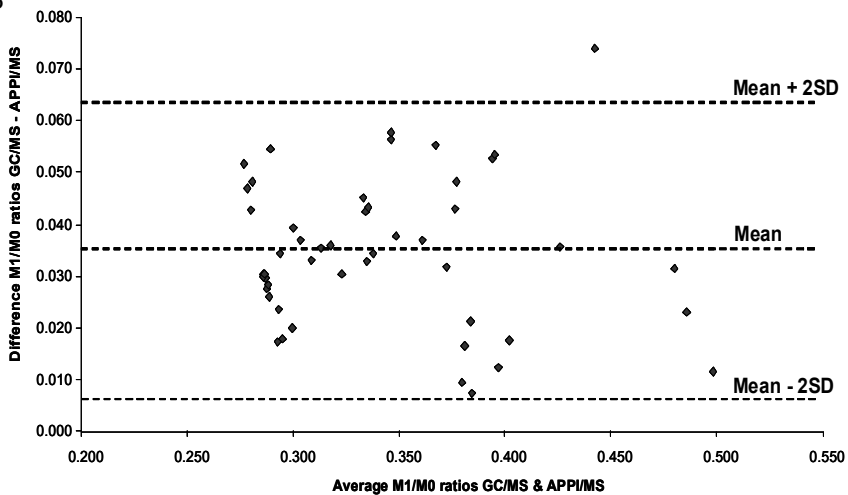
Figure 4. Correlation and isotopic enrichment by ^{2}H between GC/MS (total cholesterol) and LC/APPI-MS (free cholesterol) in the presence of HC/HF diets. (A) Shows the linearity of the isotopic enrichment by GC/MS and LC/APPI-MS for both techniques. (B) Illustrates the differences between GC/MS and LC/APPI-MS against the mean of the two measurements for each individual data set, showing the mean difference and upper and lower 95% limits of agreement (Mean +2 SD and Mean -2SD)

Having proved the ruggedness and the linearity of this new analytical platform, it was necessary to test this approach in the context of biology and with the use of ^{2}H$_2$O for an *in-vivo* study. The first point of interest was to determine whether it was possible to achieve a level of correlation from the biological samples already described in detail in the experimental section between the two techniques. Therefore, the first step was to analyze the samples for free cholesterol content. It is clear that GC/MS (figure 5A) will only provide information about the total cholesterol labeling in contrast to LC/APPI-MS which is more selective (figure 5B), providing information about the free cholesterol labeling measurement. The important point to note here is the fact that the isotopic enhancement detected by either analytical platform is identical. Therefore, validating the results when compared to the widely adopted analytical techniques such as; GC/MS and GC/IRMS for lower levels of isotopic enrichment. Next, total palmitate was reported by GC/MS (Figure 6A) and when compared to the CE 16:0 LC/MS method (Figure 6B) it showed a very similar trend in both cases, mainly the deuterium label incorporation increased by the HC diet instead of the HF diet. In the case of the measurements made by LC/MS now we have the capability to monitor individual lipid pools rather than observing/measuring incorporation in the total FA pools.
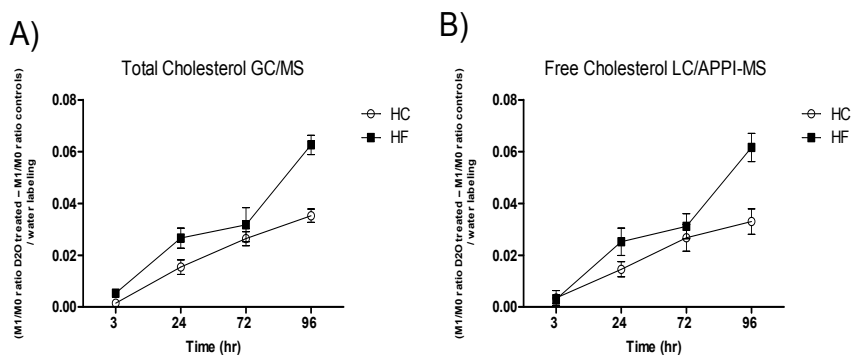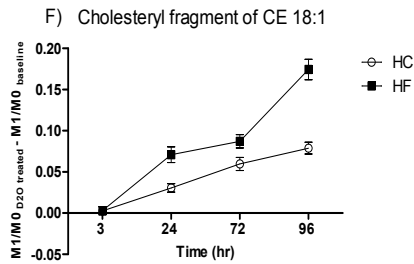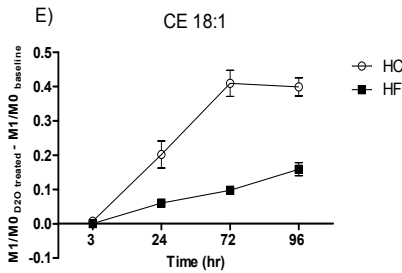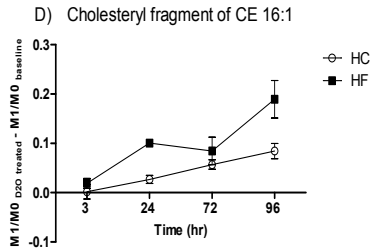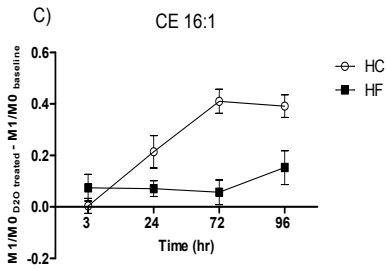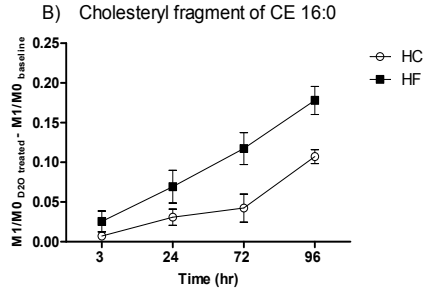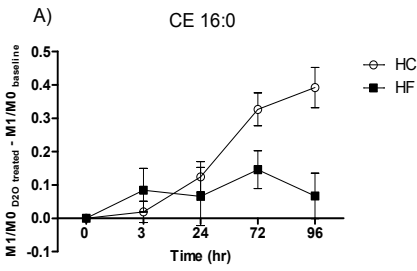

Figure 5. Describes the linearity and correlation of both techniques when used in the context of a biological study. Plot (A) shows the *total* cholesterol ^{2}H incorporation measurement for both diets. Plot (B) shows the *free* cholesterol ^{2}H incorporation measurement for both diets. In both scenarios it shows clearly how there is a higher incorporation of the ^{2}H label in the HF diet vs. the HC diet.
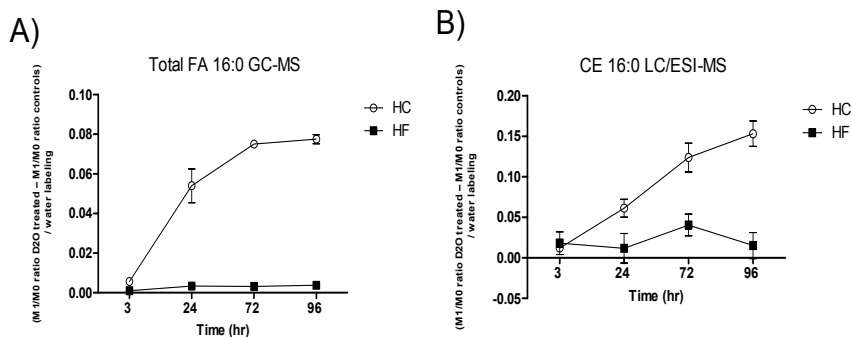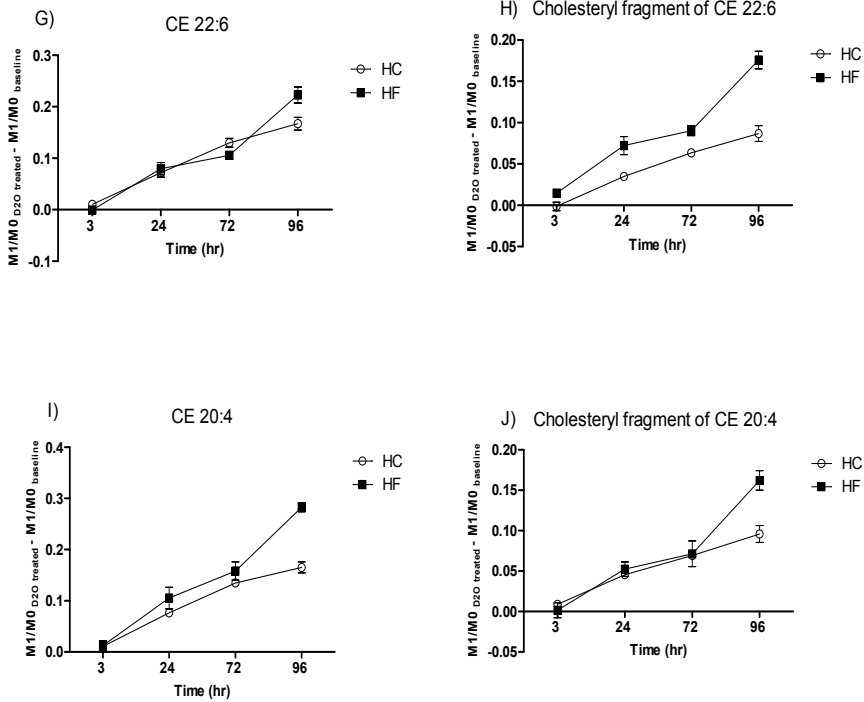
Figure 6. Shows the isotopic labeling correlation in the measurement of total palmitate in plasma by GC/MS vs. the measurement of CE 16:0 in plasma by LC/ESI-MS. Plot (A) provides indication that the palmitate *de-novo* synthesis in the HC diet is very substantial. Plot (B) describes a more selective and complimentary tools in which it is possible to measure the level of incorporation of the labeled palmitate in the CE pool.

In order to achieve an even higher degree of selectivity, the CE's found by this method were further subjected to CID experiments to obtain the cholesteryl motif fragment ion by electrospray mass spectrometry. This was necessary to determine whether the level of FA synthesis or cholesterol synthesis was responsible for the ^{2}H label incorporation in the CE in question. For both diets the following CE's were detected ; CE 16:0, CE 16:1, CE 18:1, CE 18:2, CE 18:3, CE 20:4 and CE 22:6. The data in Table 2 show that the newly synthesize cholesterol in the HF diet (0.051 % newly synthesized cholesterol per hour ± 0.003 SD) was higher than in the HC diet (0.031 % newly synthesized cholesterol per hour ± 0.004 SD). In figure 7, it can be divided in several portions. Figure 7A shows how the palmitate is actually driving the incorporation of ^{2}H in CE 16:0 for the HC diet. This is not an unusual finding to observe because this particular diet contains a high degree of palmitate and stearate (18.45% and 8.48% by FA individual content – HC diet, analyzed by GC-FID). This is very well correlated with the findings in figure 7C and E, where there is an increment in the level of palmitate and stearate in the HC diet. Scd1 is induced and therefore a similar trend should be expected here for the CE 16:1 and CE 18:1. Interestingly enough, when the CE 16:0, CE 16:1 and CE 18:1 are all subjected to CID fragmentation to release the cholesteryl motif (supplementary figure 4). It can be noted that the trend is now reversed (figure 7B, D and F) and the cholesterol in the HF diet is driving the level of incorporation of the ^{2}H label in the cholesterol pool either from diet or *de-novo* synthesis. For the PUFA, the cholesterol ester moieties trend was somewhat reversed to what has been observed with the saturated and monounsaturated FA's in the cholesterol ester motif. In Figure 7H & J it can be seen that the cholesterol motif is clearly driving the level of incorporation of the ^{2}H label for CE 20:4 and CE 22:6 for the HF diet. This may point to the fact that the pool of the PUFA available is relatively smaller in the case of the HC diet and therefore the turnover in the FA pool is smaller in comparison with the size of the cholesterol pool in the HF diet.

A) CE 16:0

B) Cholesteryl fragment of CE 16:0

C) CE 16:1

D) Cholesteryl fragment of CE 16:1

E) CE 18:1

F) Cholesteryl fragment of CE 18:1

Figure 7. Measurement of ^{2}H isotope labeling for CE's and cholesteryl motif in plasma by LC/ESI-MS/MS for CE16:0, CE 16:1, CE 18:1, CE 22:6 and CE 20:4. Plot (A) by observing the M1/M0 ratios it shows that the palmitate is driving the synthesis in the HC diet, the opposite is true for plot (B) where the cholesteryl motif shows that the ^{2}H incorporation mainly takes place in the HF diet. This event repeats itself for plots (C-F). In plots (G-J), it is significantly different from the rest because now in both cases for the CE 22:6 and CE 20:4 the cholesterol seems to be driving the incorporation of ^{2}H primarily in the HF diet.

Table 2. Represents the percentage of newly synthesized cholesterol measured in plasma by LC/ESI-TOFMS per hour for the two different diets HC/HF.

Cholesterol Ester[a]	% Newly synthesized cholesterol per hour							
	16:0	16:1	18:1	18:2	18:3	20:4	22:6	average ± SD
HC	0.031	0.03	0.027	0.033	0.038	0.029	0.03	0.031 ± 0.004
HF	0.053	0.045	0.052	0.052	0.056	0.05	0.05	0.051 ± 0.003

[a]The corresponding cholesterol esters were fragmented by LC/MS-MS to provide the cholesteryl motif.

DISCUSSION

In summary, a fast and robust method of analysis for quantifying the flux of cholesterol and cholesterol esters *in-vivo* was demonstrated. By this approach it is possible to obtain quantitative static and dynamic information not only for sterols but also for another lipid classes. The combination of atmospheric pressure ionization CID mass spectrometry with high resolution allowed us to obtain a high degree of specificity following from a diet intervention study (HC/HF diets) to determine the predominant incorporation of the deuterium label present preferably in the cholesteryl motif or the fatty acyl chain. This level of specificity is the major advantage over other techniques such as IRMS which will require a much higher level of sample preparation to obtain this detailed degree of information in a much faster manner.

Even though, IRMS is the technique of choice for isotopic enrichment measurements we have proven that for levels >0.3 atom % excess enrichment deuterium labeling, it is not necessary to obtain the very low levels of isotopic detection and precision offered by IRMS. This is certainly the case for most studies conducted in the preclinical rodent models as higher dosage levels of deuterated water may be utilized per described in this manuscript. In humans and non-human primates the deuterated water administered for flux studies results in a much lower deuterium isotope enrichment ~0.05 atom % excess (25) and therefore it would be more appropriate to utilize IRMS. In our experience this is certainly the case, very informative data can be generated in this way. Measuring dynamic changes not only for sterol biochemistry but also for other lipid metabolites proves to be a very powerful tool for cardiovascular research as it will allow focusing on the rate of *de-novo* lipid synthesis. Another important key aspect for this approach is the fact that the use deuterated water at safe levels does not perturb the metabolic system homeostasis.

A total integrated approach was highlighted in this study, which consisted of detection of genes and enzymes that are up-regulated or down-regulated by a biological insult. These genes will promote or signal a specific enzyme or enzymes to act upon the induction or inhibition of a single or multiple metabolic pathway(s). The measurements of these final biological endpoints by themselves have little significance if there is no traceability to the source(s). In addition to this, static measurements of lipids do not provide the level of specificity that can be generated by this flux analysis. For instance, Scd1 which is an enzyme involved in *de-novo* lipogenesis was markedly up-regulated in the HC diet and as a consequence there was an increase in the amount of the deuterium label incorporated in the palmitate and stearate FA pools, which in turn lead to the conversion to palmitoleic and oleic acid. The administration of stable-isotope tracers *in-vivo* coupled to LC/MS-MS provides a deeper insight regarding the dynamics of specific lipid classes. The advantage of this very selective approach to monitor and quantify individual lipid pools is that in one single experiment an information rich approach in terms of lipid quantitative and qualitative composition may be achieved. In turn, the use of this analytical strategy will allow us to simplify the sample analysis and reporting of analytical and biological data in a drug discovery setting. The combination of a platform that comprises gene expression which can guide us towards which biochemical pathway is perturbed by either genetic or novel pharmacological intervention together with a multiplex platform that

enable us to monitor *de-novo* synthesis and have the capability to measure qualitative and quantitative changes proves to be a unique and very desirable platform specially at the very early stages of drug discovery.

REFERENCES

1.   Howles, P.N. *Methods Mol Biol* **602**:157-179.

2.   Lecker, J.L., Matthan, N.R., Billheimer, J.T., Rader, D.J., and Lichtenstein, A.H. *Metabolism*.

3.   Racette, S.B., Lin, X., Lefevre, M., Spearie, C.A., Most, M.M., Ma, L., and Ostlund, R.E., Jr. *Am J Clin Nutr* **91**:32-38.

4.   Zhong, S., Magnolo, A.L., Sundaram, M., Zhou, H., Yao, E.F., Di Leo, E., Loria, P., Wang, S., Bamji-Mirza, M., Wang, L., et al. *J Biol Chem* **285**:6453-6464.

5.   Zhao, C., and Dahlman-Wright, K. *J Endocrinol* **204**:233-240.

6.   Alwaili, K., Awan, Z., Alshahrani, A., and Genest, J. *Expert Rev Cardiovasc Ther* **8**:413-423.

7.   Caserta, C.A., Pendino, G.M., Amante, A., Vacalebre, C., Fiorillo, M.T., Surace, P., Messineo, A., Surace, M., Alicante, S., Cotichini, R., et al. *Am J Epidemiol* **171**:1195-1202.

8.   Chakraborty, S., Cai, Y., and Tarr, M.A. *Anal Biochem*.

9.   Gooding, H.C., and de Ferranti, S.D. *Curr Opin Pediatr*.

10.   Unverdorben, M., von Holt, K., and Winkelmann, B.R. 2009. *Biomark Med* **3**:617-653.

11.   Schoenheimer, R., and Rittenberg, D. 1935. *Science* **82**:156-157.

12.   Schoenheimer, R. 1937. The Investigation of Intermediary Metabolism with the Aid of Heavy Hydrogen: Harvey Lecture, January 21, 1937. *Bull N Y Acad Med* **13**:272-295.

13.   Schoenheimer, R., and Rittenberg, D. 1938. *Science* **87**:221-226.

14.   Dietschy, J.M., and Spady, D.K. 1984. *J Lipid Res* **25**:1469-1476.

15.   Dietschy, J.M. 1984. *Klin Wochenschr* **62**:338-345.

16.   Dietschy, J.M., and Spady, D.K. 1984. *Agents Actions Suppl* **16**:177-190.

17.   Dietschy, J.M. 1990. *Hosp Pract (Off Ed)* **25**:67-78.

18.   Dietschy, J.M., Turley, S.D., and Spady, D.K. 1993. *J Lipid Res* **34**:1637-1659.

19.   Dietschy, J.M., Woollett, L.A., and Spady, D.K. 1993. *Ann N Y Acad Sci* **676**:11-26.

20.   Dietschy, J.M. 1997. *Am J Clin Nutr* **65**:1581S-1589S.

21.   Schoeller, D.A. 2002. *Food Nutr Bull* **23**:17-20.

22.   Wong, W.W., Hachey, D.L., Clarke, L.L., Zhang, S., Llaurador, M., and Pond, W.G. 1994. *Appl Radiat Isot* **45**:529-533.

23.   Wong, W.W., Hachey, D.L., Feste, A., Leggitt, J., Clarke, L.L., Pond, W.G., and Klein, P.D. 1991. *J Lipid Res* **32**:1049-1056.

24.   Jones, P.J., and Schoeller, D.A. 1990. *J Lipid Res* **31**:667-673.

25.   Jones, P.J., Scanu, A.M., and Schoeller, D.A. 1988. *J Lab Clin Med* **111**:627-633.

26.   Butovich, I.A. 2009. *J Lipid Res* **50**:501-513.

27.   Butovich, I.A., Uchiyama, E., and McCulley, J.P. 2007. *J Lipid Res* **48**:2220-2235.

28.   Zhang, F., Bartels, M.J., Geter, D.R., Carr, M.S., McClymount, L.E., Marino, T.A., and Klecka, G.M. 2009. *Rapid Commun Mass Spectrom* **23**:3637-3646.

29.   Karuna, R., von Eckardstein, A., and Rentsch, K.M. 2009. *J Chromatogr B Analyt Technol Biomed Life Sci* **877**:261-268.

30.   Cai, S.S., Syage, J.A., Hanold, K.A., and Balogh, M.P. 2009. *Anal Chem* **81**:2123-2128.

31.   Cai, Y., McConnell, O., and Bach, A.C., 2nd. 2009. *Rapid Commun Mass Spectrom* **23**:2283-2291.

32.   Borges, N.C., Astigarraga, R.B., Sverdloff, C.E., Galvinas, P.R., da Silva, W.M., Rezende, V.M., and Moreno, R.A. 2009. *J Chromatogr B Analyt Technol Biomed Life Sci* **877**:3601-3609.

33.   Robb, D.B., and Blades, M.W. 2008. *Anal Chim Acta* **627**:34-49.

34.   McCulloch, R.D., Robb, D.B., and Blades, M.W. 2008. *Rapid Commun Mass Spectrom* **22**:3549-3554.

35.   Previs, S.F., Hazey, J.W., Diraison, F., Beylot, M., David, F., and Brunengraber, H. 1996. *J Mass Spectrom* **31**:639-642.

36.   Previs, S.F., Fatica, R., Chandramouli, V., Alexander, J.C., Brunengraber, H., and Landau, B.R. 2004. *Am J Physiol Endocrinol Metab* **286**:E665-672.

37.   Shah, V., Herath, K., Previs, S.F., Hubbard, B.K., and Roddy, T.P. *Anal Biochem*.

38.   Bligh, E.G., and Dyer, W.J. 1959. *Can J Biochem Physiol* **37**:911-917.

39.   Castro-Perez, J.M., Kamphorst, J., DeGroot, J., Lafeber, F., Goshawk, J., Yu, K., Shockcor, J.P., Vreeken, R.J., and Hankemeier, T. *J Proteome Res* **9**:2377-2389.

40.   Wrona, M., Mauriala, T., Bateman, K.P., Mortishire-Smith, R.J., and O'Connor, D. 2005. *Rapid Commun Mass Spectrom* **19**:2597-2602.

41.   Bateman, K.P., Castro-Perez, J., Wrona, M., Shockcor, J.P., Yu, K., Oballa, R., and Nicoll-Griffith, D.A. 2007. *Rapid Commun Mass Spectrom* **21**:1485-1496.

42.   Castro-Perez, J.M. 2007. *Drug Discov Today* **12**:249-256.

43.   Plumb, R.S., Johnson, K.A., Rainville, P., Smith, B.W., Wilson, I.D., Castro-Perez, J.M., and Nicholson, J.K. 2006. *Rapid Commun Mass Spectrom* **20**:1989-1994.

44.   Diraison, F., Pachiaudi, C., and Beylot, M. 1996. *Metabolism* **45**:817-821.

45.   Collins, J.M., Neville, M.J., Hoppa, M.B., and Frayn, K.N. *J Biol Chem* **285**:6044-6052.

46.   Chong, M.F., Fielding, B.A., and Frayn, K.N. 2007. *Proc Nutr Soc* **66**:52-59.

47.   Harada, N., Oda, Z., Hara, Y., Fujinami, K., Okawa, M., Ohbuchi, K., Yonemoto, M., Ikeda, Y., Ohwaki, K., Aragane, K., et al. 2007. *Mol Cell Biol* **27**:1881-1888.

48.   Hoh, R., Pelfini, A., Neese, R.A., Chan, M., Cello, J.P., Cope, F.O., Abbruzese, B.C., Richards, E.W., Courtney, K., and Hellerstein, M.K. 1998. *Am J Clin Nutr* **68**:154-163.

49.   Hellerstein, M.K., Schwarz, J.M., and Neese, R.A. 1996. *Annu Rev Nutr* **16**:523-557.

50.   Bland, J.M., and Altman, D.G. 1986. *Lancet* **1**:307-310.

SUPPLEMENTARY INFORMATION

Supplementary Figure 1. Sensitivity comparison between ESI and APcI for equimolar concentrations (1µg/mL) of CE 16:0 and CE 18:0

†Cholesterol esters are detected as $[M+NH_4]^+$
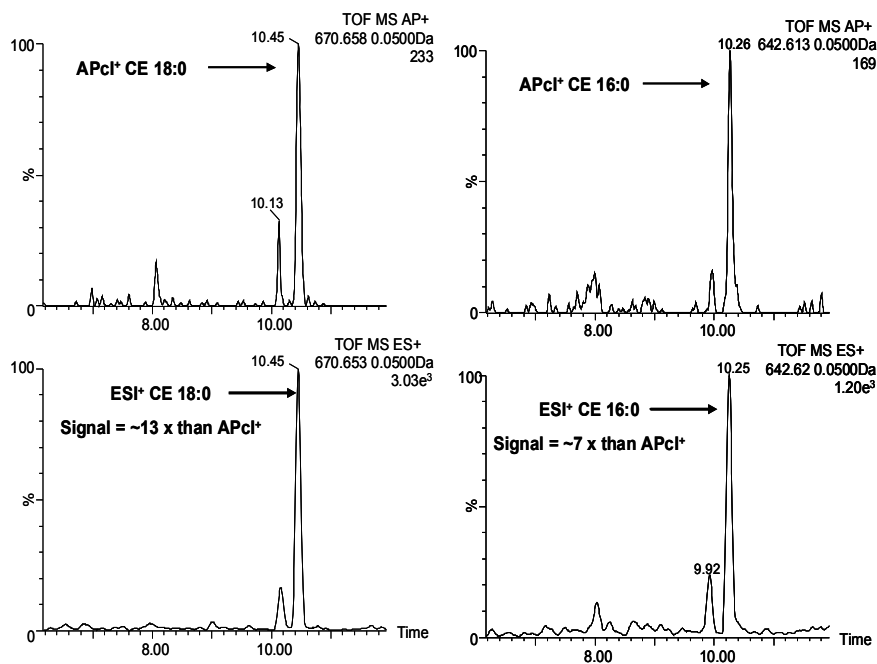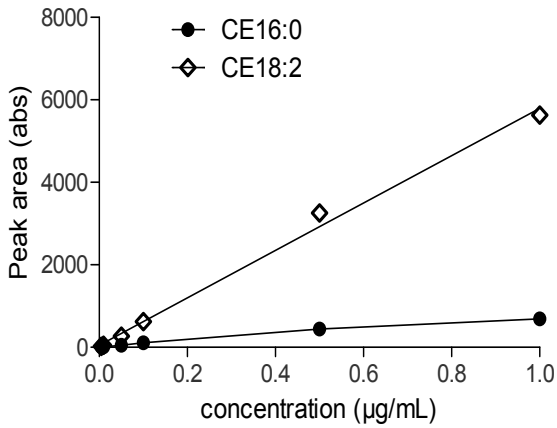
Supplementary Figure 2. (A) Sensitivity comparison between APcI and APPI ionization techniques for cholesterol (standard concentration 1μg/mL). Data was acquired using full scan TOF-MS. (B) Overlay for extracted ion chromatograms ; sensitivity comparison between APcI and APPI ionization with linked axis for cholesterol

††Cholesterol is detected as $[M-H_2O]^+$
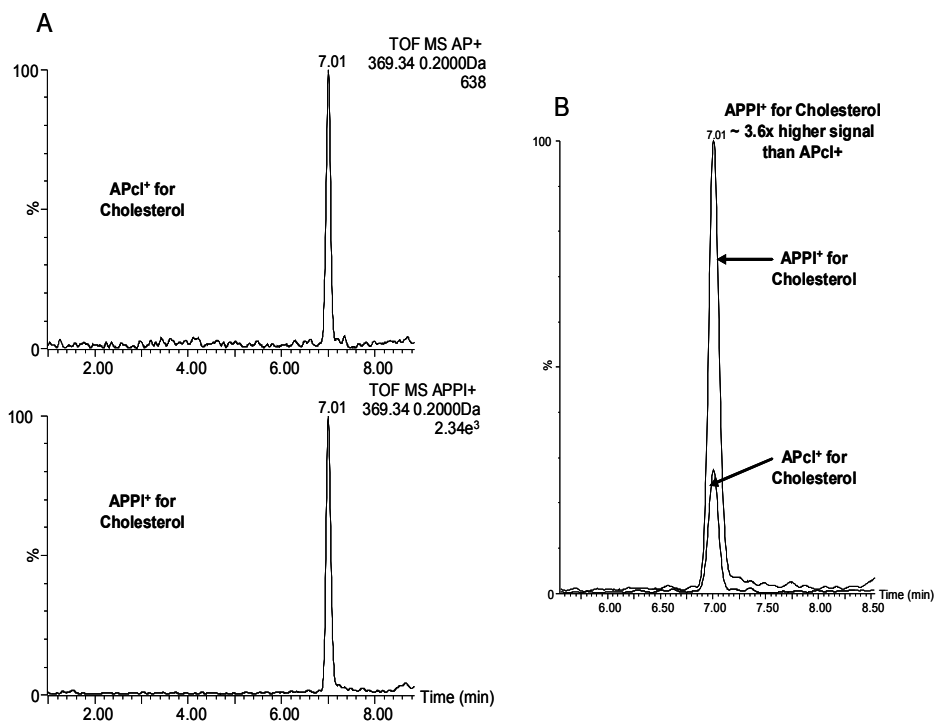
Supplementary Figure 3. (A) Calibration curves for CE 16:0 and CE 18:2 each calibration curve was utilized to calculate the absolute lipogenic index. (B) Calibration curves for CE 16:0 and CE 16:1 each calibration curve was utilized to calculate the absolute desaturation index
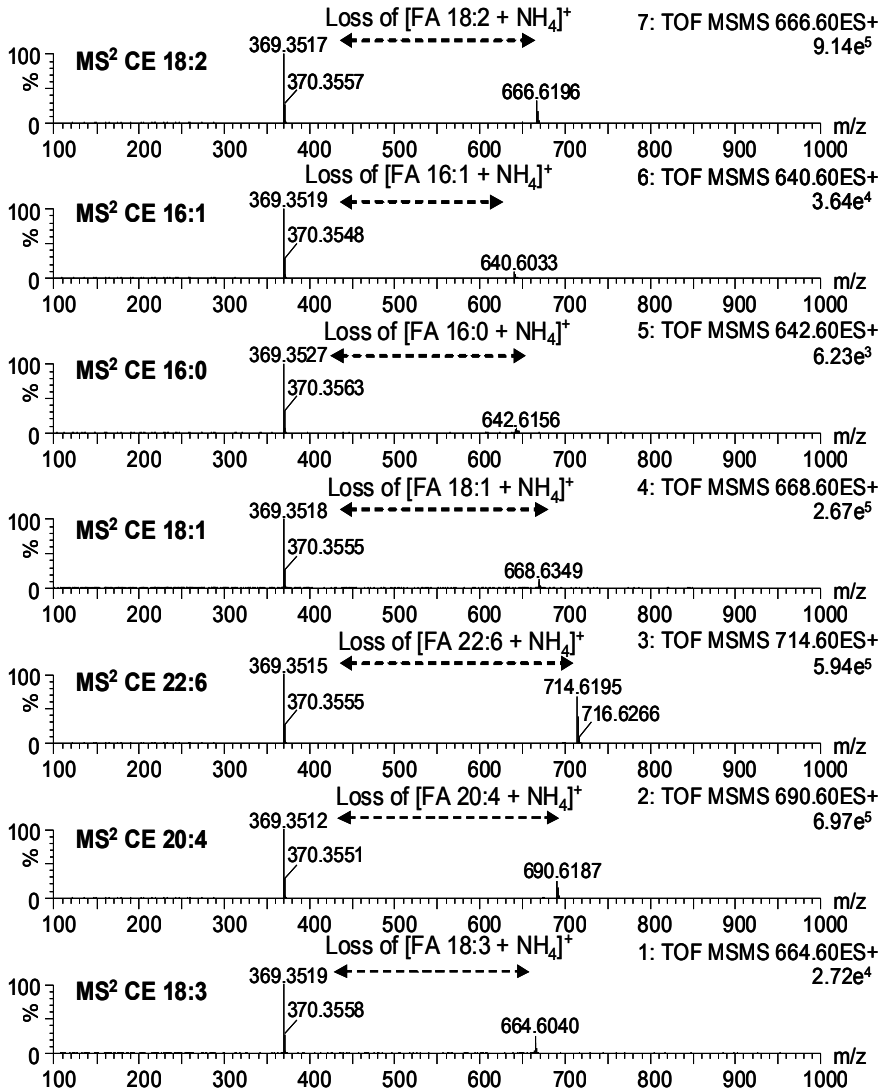
A

B

Supplementary Figure 4. LC/ESI-MS/MS spectra for CE 16:0, CE 16:1, CE 18:1, CE 18:2, CE 18:3, CE 22:6 and CE 20:4 in C57Bl/6 lipid extracted plasma.

Chapter 9

Metabolomics and fluxomics combination to unravel diet-induced changes in lipid homeostasis

Metabolomics and fluxomics combination to unravel diet-induced changes in lipid homeostasis

SUMMARY

A novel method to differentiate diet-induced alterations in plasma lipid phenotypes 'static (concentration of lipid) and kinetic (endogenous production e.g. *de-novo* lipogenesis)' was employed. C57Bl6 mice were randomized into 2 groups and fed either a high-carbohydrate, low-fat (HC) or a carbohydrate-free, high-fat diet (HF) diet for 13 days; D_2O was administered via intra-peritoneal injection and then adding D_2O to the drinking water for 96 hours. Principal component analysis (PCA) revealed differences in the plasma lipid content, for example, triglycerides (TG) 50:2, 50:3, and 52:2 were up-regulated in mice fed the HC diet whereas; TG 52:4, 52:1, 54:5, 54:3, 54:4, and 54:2 were higher in animals fed the HF diet. However, although the fractional contribution of synthesis was ~ 10 fold lower in HF vs. HC fed mice changes in TG concentration were not entirely mediated by altered *de novo* lipogenesis. In addition, the ability to couple isotope labeling measurements with PCA analyses revealed cases where there were no differences in the concentration of a compound but its source was substantially altered. In summary, this strategy determined (i) the presence/absence of differences in concentration and (ii) the contribution of different pathways that could affect lipid biology in a mouse model, respectively.

INTRODUCTION

It is well recognized that dietary carbohydrate and fat intake can affect plasma lipid profiles. For example, fructose-induced triglyceridemia is readily observed in several models, in addition, overfeeding of glucose will up-regulate *de-novo* lipogenesis (DNL) (1, 2). We have recently examined the effect of dietary carbohydrate on modulating triglyceride synthesis in adipose tissue(3). Those studies demonstrated an uncoupling of fatty acid synthesis from glyceride synthesis, i.e. the absence of dietary carbohydrate was associated with a marked reduction in fatty acid synthesis yet there was no effect on total triglyceride synthesis. A follow-up study demonstrated that fatty acid synthesis/secretion into the plasma compartment could be uncoupled from cholesterol synthesis/secretion (4).

In spite of the fact that, novel findings have been obtained showing dietary-influences on lipid biosynthesis (5-8), virtually all studies have been performed under a relatively low level of resolution. For example, investigators typically examine the effects on total triglyceride or phospholipids and do not direct attention to specific species within each class. There are numerous permutations to combine fatty acids when assembling a triglyceride or a phospholipid; modern UPLC/MS instrumentation is capable of resolving many of these analytes by their distinct molecular weight and/or retention time (9-13). The utilization of high resolution mass spectrometry has allowed researchers to obtain a high degree of specificity and accuracy when trying to decipher unknown molecules. For example, it is possible to obtain full scan MS and pseudo MS^2 data (MS^E) from a single chromatographic injection (14, 15) therein improving throughput and streamlining the identification step. In addition to this, the use of stable isotopes and mass spectrometry has been of paramount importance in nutrition and cardiovascular research as it has enabled researchers with a unique analytical tool to monitor lipid synthesis in plasma and tissues (16-19). Mass isotopomer distribution analysis (MIDA) has been employed to investigate rate of synthesis of proteins, lipids and carbohydrates (20-22). This involves measurements of the enrichment (or labeling profile) of an analyte after introduction of a precursor stable isotope label (e.g. ^{13}C or ^{2}H) (23-29). D$_2$O has been used extensively to measure anabolic rates (30-33), the advantages being (i) it does not perturb the biological homeostasis, (ii) it enters tissues/cells evenly and (iii) it is easy to administer. Metabolomics in combination with multivariate statistical analysis (34-43) is an emerging field which provides a powerful insight into underlying molecular mechanism of disease or phenotypic effects to treatment of disease via therapeutic intervention. Differences in treatment or disease groups are attributed to static changes and no information regarding synthesis rates are obtained by this approach. Coupling static and dynamic alterations may prove to be a powerful approach to provide a more significant and in-depth understanding of biological perturbations either by diet, genetic modification or therapeutic intervention.

In this report we have determined whether the presence/absence of dietary glucose would have an effect(s) on individual glyceride species. Attention was directed towards measuring changes in the concentration and the synthesis of circulating triglycerides and phospholipids using the combination of a two-tier metabolomics and fluxomic strategy.

MATERIALS AND METHODS

Biological samples

All animal protocols were reviewed and approved by Merck Research Laboratories Institutional Animal Care and Use Committee (Rahway, NJ). Male C57Bl/6 mice from Taconic were acclimated at the animal facility for one week. At an age of 10 weeks old, mice were randomized into two groups (n = 26 per group) and fed either a high carbohydrate (HC) or a high fat (HF) diet (D12450, 10% fat, 70% carbohydrate, and 20% protein or D12369B, 90% fat, 0% carbohydrate, and 10% protein, respectively, Research Diets, New Brunswick, NJ) for 13 days. All mice were then given an intra-peritoneal injection of D_2O (20ml/kg of body weight, 99% ^{2}H) and returned to their cages (n = 6 mice per cage) where they were maintained on 5% ^{2}H-labeled drinking water for the remainder of the study (96 hr); this design was sufficient to maintain a steady-state ^{2}H-labeling of body water. A separate cohort of male C57Bl/6 mice (n=6 in each group) were fed the same diets as described above but in the absence of D_2O dosing, this control cohort was used for static lipid measurements and to establish baseline labeling of the various lipid analytes. Mice in each group were fed the respective diets *ad libitum*, and were sedated on various days after injection (n = 6 per day per group), blood and liver tissue samples were then collected and quick-frozen in liquid nitrogen. Samples were stored at -80°C until analyzed.

^{2}H-Labeling of plasma water

The ^{2}H-labeling in plasma water was determined as previously described (4). Briefly, ^{2}H present in water was exchanged with hydrogen bound to acetone by incubating samples (e.g. 10 µl of plasma or known standards) in a 2 ml glass screw-top GC vial at room temperature for 4 hours with 2 µl 10N NaOH and 5 µl of acetone. The instrument is programmed to inject 5 µl of headspace gas from the GC vial in a splitless mode. Samples were analyzed using a 0.8 min isothermal run (Agilent 5973 MS coupled to a 6890 GC oven fitted with a DB-17 MS column, 15m x 250µm x 0.15µm, the oven was set at 170°C and helium carrier flow was set at 1.0 ml x min^{-1}), acetone elutes at ~ 0.4 min, the mass spectrometer was set to perform selected ion monitoring of m/z 58 and 59 (10 ms dwell time per ion) in the electron impact ionization mode.

Lipid profiling by UPLC/MS

Plasma (20µL) was extracted for lipid analysis using a dichloromethane (DCM) /methanol mixture (2:1, v/v) as described by Bligh and Dyer (44, 45). The inlet system (Acquity UPLC (Waters, Milford, MA, USA) was coupled to a hybrid quadrupole orthogonal time of flight mass spectrometer (SYNAPT G2 HDMS, Waters, MS Technologies, Manchester, UK). The mass spectrometer was operated in electrospray (ESI) positive ionization mode and a capillary voltage of 2 kV and a cone voltage of 30 V were utilized. The inlet LC flow was nebulized using nitrogen gas (700 L/hr) and the desolvation temperature was kept at 450°C. Data was acquired over the mass range of 50-1200 Da for both MS and MS^E modes (11, 14, 15, 46). The first acquisition function (full scan MS) was set at 5 eV, collected low energy or

unfragmented data while the second acquisition function (MS^E) recorded high energy or fragmented data using a collision energy ramp from 25-35 eV. Argon gas was used for collision induced dissociation (CID). The mass spectral resolution was set to 25K full width half mass (FWHM) and typical mass accuracies were in the order of 0-2 ppm. The system was equipped with an integral LockSpray unit with its own reference sprayer that was controlled automatically by the acquisition software to collect a reference scan every 10 seconds lasting 0.3 seconds. The LockSpray internal reference used for these experiments was Leucine enkephalin (Sigma-Aldrich, St Louis, MO) at a concentration of 5 ng/µL in 50% acetonitrile/ 50% H$_2$O + 0.1% formic acid (v/v). The reference internal calibrant was introduced into the lock mass sprayer at a constant flow rate of 50 µL/min using an integrated solvent delivery system. A single lock mass calibration at m/z 556.2771 in positive ion mode was used during analysis.

RNA isolation and Real-time quantitative PCR analysis

Frozen liver tissue (~20 mg) was homogenized in 600 µL RLT lysis buffer (Qiagen, Valencia, CA) containing 0.1% (v/v) β-mercaptoethanol using a PowerGen 125 homogenizer and 7 x 65 mm disposable plastic generators (Fisher Scientific). Total RNA was extracted from the homogenized tissue using RNeasy Mini Kit (Qiagen, Valencia, CA) following the manufacturer's protocol. cDNA was generated from 2 µg of RNA using RT^2 First Strand kit (SA Biosciences). Real-time PCR analysis was performed on the 7900HT PCR System (Applied Biosystems, Foster City, CA) with 2x SYBR PCR Master Mix and mouse-specific PCR primers for mouse Scd1, (SABiosciences). Expression levels of stearoyl-CoA desaturase (Scd1) mRNA were normalized to an average of that of mouse beta-actin (Actb), Glyceraldehyde 3-phosphate dehydrogenase (Gapdh), Beta-glucuronidase (Gusb), Hypoxanthine-guanine phosphoribosyltransferase (Hprt1), Peptidylprolyl isomerase A (cyclophilin A) (Ppia) and ribosomal protein 113a (Rp113a) in each sample.

Data processing and statistical analysis

GC/MS and UPLC/MS data acquired were processed by the manufacturer software (Chemstation & MassLynx respectively). MarkerlynxXS (Waters Corp, MA, USA) was utilized to deconvolute the UPLC/MS data into a table of variables containing exact mass and retention time pairs (EMRT). Principal component analysis (PCA) and Orthogonal partial least squares- discrimination analysis (OPLS-DA) was computed using Simca-P (Umetrics, Umea, Sweden). The data was scaled using the pareto algorithm and normalization of the variables was conducted utilizing total peak intensities for all the variables detected.

Gene expression data for real-time quantitative PCR was processed using Ingenuity software (Ingenuity systems, Redwood City, CA). For the statistical analysis, all the data are presented as ± standard error mean (SEM). Differences

between groups were computed by student's *t-test* statistical analysis (GraphPad Prism, La Jolla, CA). Post test analysis for quantifiable variables was conducted using Mann-Whitney U non-parametric test with one-tailed p-values. Statistical significance was considered for $p < 0.05$.

Lipid nomenclature

The lipid nomenclature utilized throughout the manuscript is the same as described by Fahy *et al.* (47). For instance, CE 18:1 denotes cholesteryl ester containing 18 carbon atoms and 1 double bond in the fatty acyl substituent, TG 54:3, translates to a triglyceride containing 54 carbon atoms attached to the glycerol back-bone and a total of 3 double bonds in the 3 fatty acyl substituents.

RESULTS AND DISCUSSIONS

Gene expression in HC diet showed increased modulation of de-novo lipogenesis

Liver samples were analyzed in a key expression node array as described in the method section where 384 specific hepatic genes involved in glucose, lipid, apoptosis, autophagy and inflammatory pathways were monitored. Results from the HC diet (figure 1) clearly depicted a strong increase in the expression of genes which were responsible for fatty acid biosynthesis (red color showed up-regulation while green color showed down-regulation); stearoyl-coenzyme A desaturase 1 (Scd1) (x 69 fold, p = 0.0008 vs. HF diet) , Acetyl-CoA carboxylase 1 (Acaca) (x3 fold, p = 0.02 vs. HF diet), Acetyl-CoA carboxylase 2 (Acacb) (x9 fold, p = 0.002 vs. HF diet), Fatty acid synthase (Fasn) (x3 fold, p = 0.09 vs. HF diet) and Fatty acid desaturase (Fads3) (x2 fold, p = 0.05 vs. HF diet). These observations were all consistent with an induction of *de-novo* lipogenesis by the HC diet.
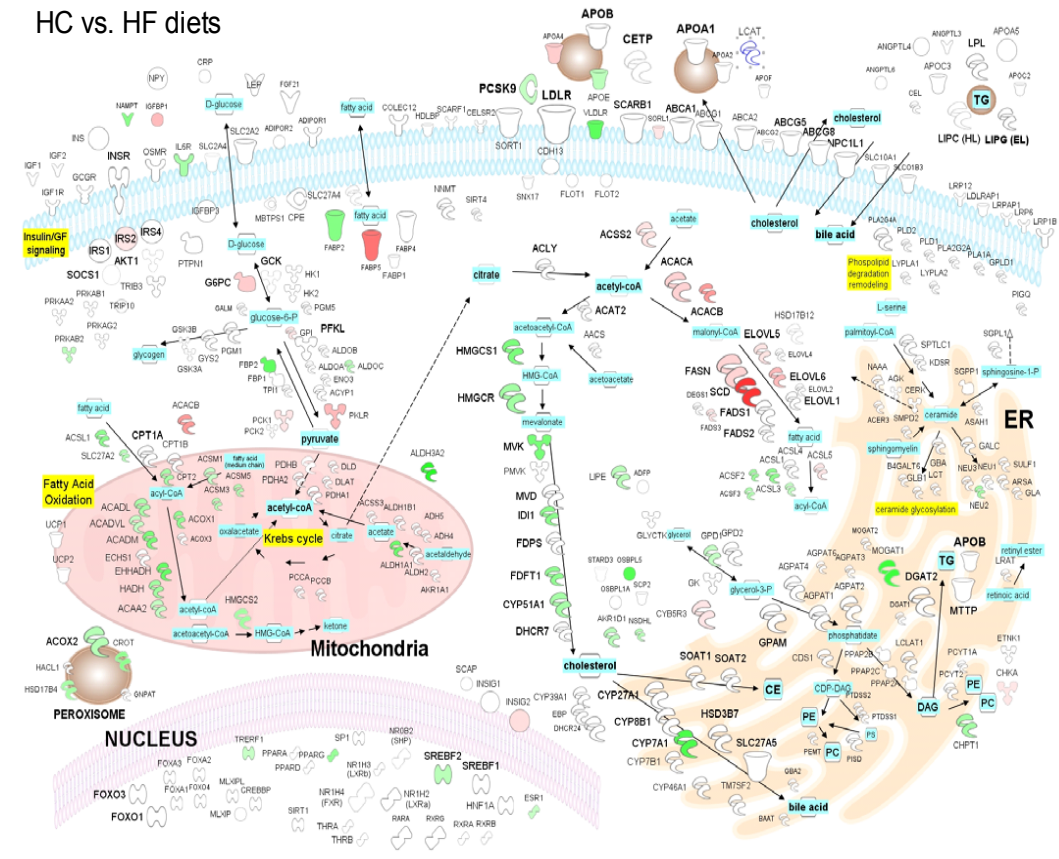

Figure 1. Liver gene expression analysis comparing C57Bl6 mice cohort that were either on a HC or a HF diet. Major genes perturbed in this comparison included; stearoyl-coenzyme A desaturase 1 (Scd1) (x 69 fold, p = 0.0008 vs. HF diet) , Acetyl-CoA carboxylase 1 (Acaca) (x3 fold, p =

0.02 vs. HF diet), Acetyl-CoA carboxylase 2 (Acacb) (x9 fold, p = 0.002 vs. HF diet), Fatty acid synthase (Fasn) (x3 fold, p = 0.09 vs. HF diet) and Fatty acid desaturase (Fads3) (x2 fold, p = 0.05 vs. HF diet).

Red denotes up-regulation and green denotes down-regulation

Multivariate statistical analysis revealed diet-specific lipid alterations

After 13 days on both diets, there was an increment in body weight for mice that were in the HF diet cohort yet energy intake post- treatment remained fairly constant throughout the course of the study (figure 2A and B). A full lipid profile by UPLC/MS was conducted on sample sets obtained from animals which were not dosed with D_2O. A total of 1463 lipid variables were obtained. PCA analysis revealed significant lipid phenotypic differences between the two diets (figure 3A) and OPLS-DA analysis (figure 3B) identified diet-specific lipid alterations (table 1), note that there are a substantial number of TGs with good p values (correlation ranging from 0.84-0.96) that are responsible for the separation between the HF vs. HC diets. However, uniform changes are not observed across the entire TG pool, for example, TG 50:3, TG 50:2, TG 52:2 are decreased in mice fed the HF diet whereas TG 54:4, TG 54:3 and TG 54:2 are increased in mice fed the HF diet. Although these observations demonstrate the ability to obtain specific diet-induced lipid phenotypes these measurements did not provide any specific insight regarding the pathophysiology, e.g. the contribution of newly made lipids.
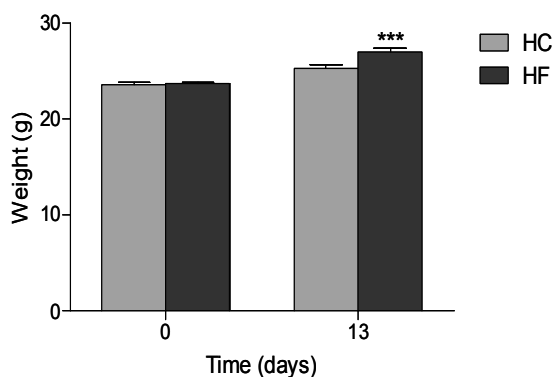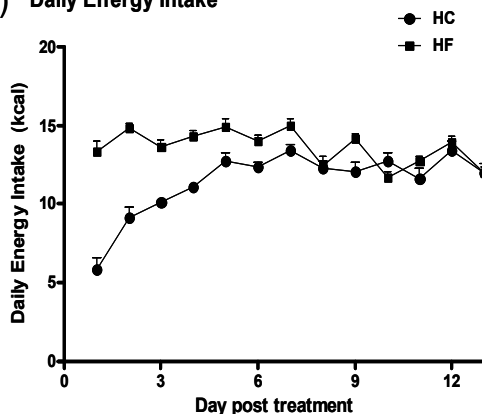

Figure 2. Effects of dietary intervention on body weight and caloric intake. Panel (A) demonstrates a slight increase in body weight in mice fed a HF vs. a HF diet. Panel (B) demonstrates comparable energy intake after ~ 5 days of diet intervention. Data are expressed as mean ± standard error mean (sem), n = 6 per group.

***(p < 0.001, day 13)

A) Scores Plot High Fat Diet Plasma vs. High Carbohydrate diet Lipid Profile
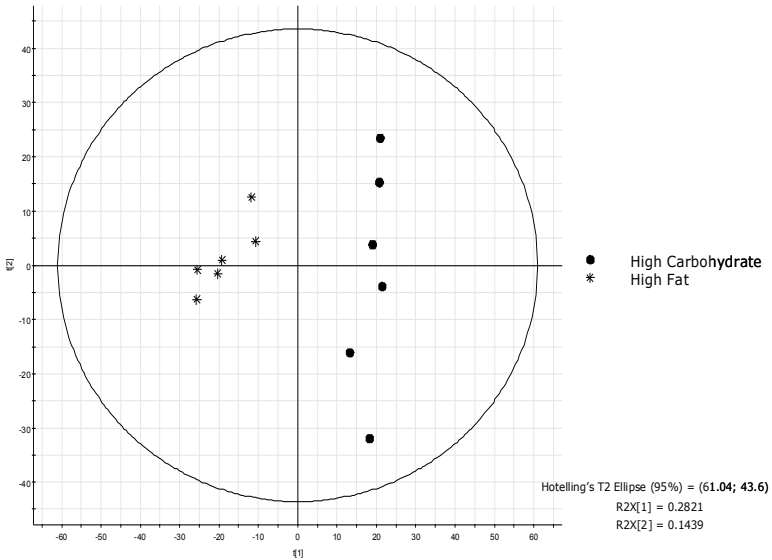
B)   S-Plot High Fat Diet vs. High Carbohydrate Diet
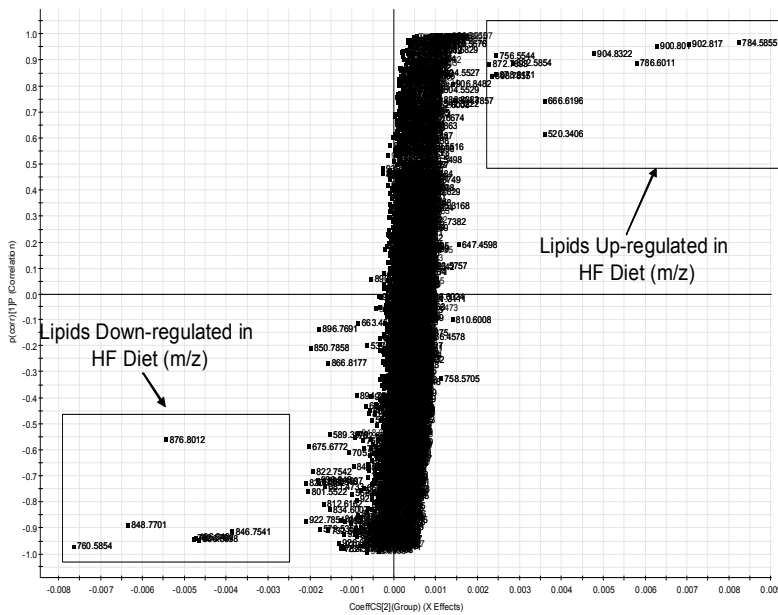
Figure 3. Effect of a HF vs. a HC diet on changes in plasma lipid composition. Multi-variate statistics was used to identify differences in the concentration of circulating lipids, a total of 1463 lipid variables were identified. Panel A presents the data as a PCA scores plot whereas Panel B denotes the S-plot. In panel B, the upper-right box highlights lipids that are up-regulated in mice fed a HF diet vs. HC diet whereas the lower-left box highlights lipids that are down-regulated in mice fed a HF diet vs. HC diet.

Table 1. Identification and quantitation of differences in circulating lipids. The fold-change in concentration is shown as the relative difference in mice fed a HF diet vs. HC diet. A positive sign notes an increase in mice fed a HF diet vs. HC diet. PC = phosphatidylcholines, TG = triglyceride, CE = cholesterol ester, LPC = lysophosphatidyl choline.

Retention Time (min)	m/z	ppm error	p[1]P	p(corr)[1]P	Lipid	Fold Change HF vs. HC diet
1.43	496.3407	0.8	-0.187384	-0.937384	LPC 16:0	-2.0
5.29	760.5854	-0.3	-0.263713	-0.969972	PC 34:1	-2.8
4.71	782.5701	0.1	-0.195263	-0.942795	PC 36:4	-2.0
4.55	806.5698	-0.2	-0.199245	-0.945895	PC 38:6	-2.0
8.35	846.7541	-1.2	-0.121045	-0.916528	TG 50:3	-3.1
8.57	848.7701	-0.7	-0.198257	-0.888712	TG 50:2	-3.3
8.81	876.8012	-0.9	-0.11628	-0.559187	TG 52:2	-1.2
8.98	666.6196	1.1	0.079173	0.743351	CE 18:2	+1.3
4.40	756.5544	0.1	0.066602	0.918485	PC 34:3	+3.1
4.99	784.5855	-0.1	0.245886	0.96919	PC 36:3	+2.7
4.68	832.5854	-0.2	0.076552	0.887637	PC 40:7	+1.9
8.39	872.7693	-1.6	0.135296	0.886215	TG 52:4	+1.6
9.03	878.8171	-0.7	0.148966	0.846114	TG 52:1	+3.2
8.42	898.7855	-1	0.186827	0.837785	TG 54:5	+3.1
8.85	902.817	-0.8	0.324792	0.960438	TG 54:3	+3.8
8.65	900.801	-1.1	0.313566	0.953305	TG 54:4	+4.4
9.05	904.8322	-1.2	0.254099	0.925253	TG 54:2	+4.1

MS^E allowed for further analysis of TG composition and specific FA synthesis

Total body water measurement as described in the material and methods section resulted in ~2.5% labeling at steady-state for the duration of the study.
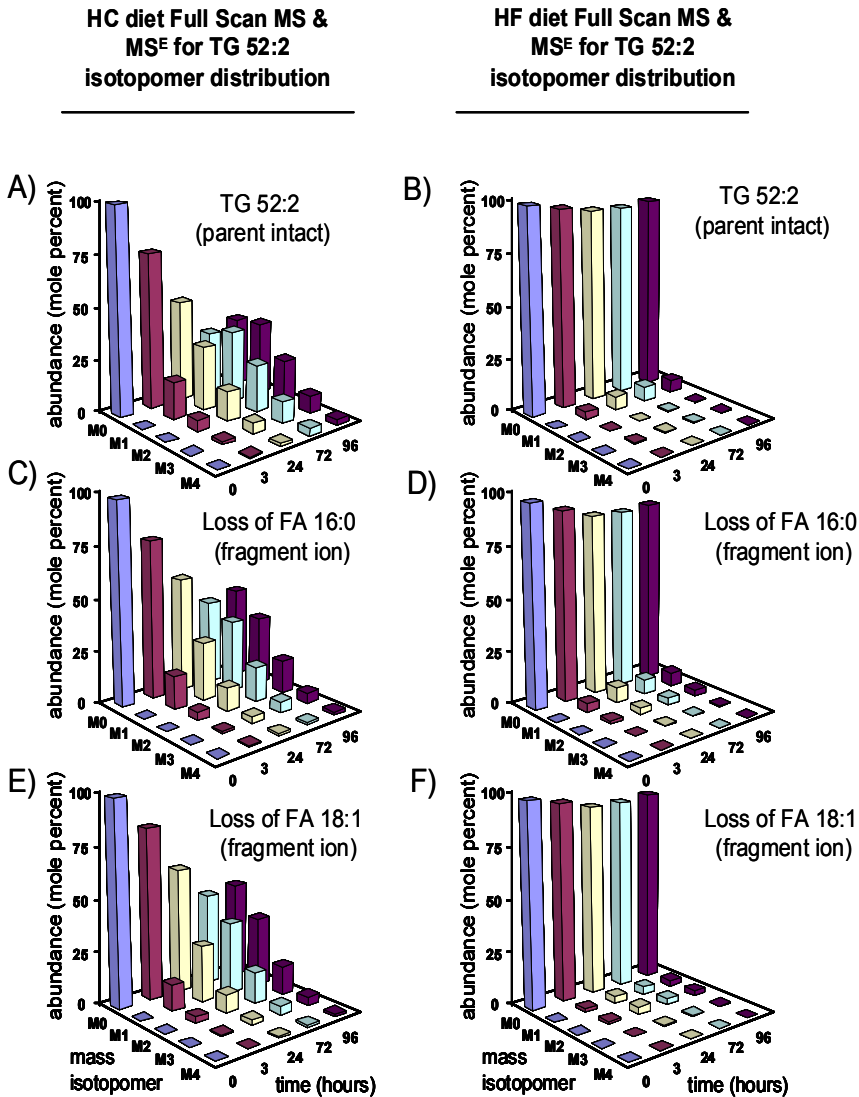
To examine the suitability of UPLC/MS-based analyses for detecting ^{2}H-labeling in various lipids, replicate injections of plasma samples were performed to determine the reproducibility of the isotope ratios. For example, we observed a relatively high degree of reproducibility when measuring the natural background labeling (in the M1 isotopomer / M0 isotopomer) of LPC 16:0, PC 34:1, PC 36:4, TG 52:2 and TG 54:5 (figure 4), the coefficients of variation ranged from ~ 1.2 to 2.6% (LPC 16:0 ~ 1.2%, PC 34:1 ~ 2.6%, PC 36:4 ~ 1.8%, TG 52:2 ~ 1.4% and TG 54:5 ~ 2.1%). Utilization of MS^E increased our ability to quantify the positional labeling. For instance, TG 52:2, which was increased in mice fed the HC diet, can be used as an example to describe the level of structural information obtained in teasing apart the isotopic enrichment. Figure 5 shows discrete differences in the abundance of heavy isotopomers in mice fed HC vs. HF diet. Panel

A and B demonstrate the isotope labeling in the parent (intact) molecule, whereas Panel C and D contain the isotope distribution profile of the fragment ion generated by the high energy acquisition in MS^E mode corresponding to glycerol, 16:0 and 18:1 (i.e. loss of 18:1) and Panel E and F contain the isotope distribution profile of the daughter ion containing glycerol, 18:1 and 18:1 (i.e. loss of 16:0). In all cases, enhanced fatty acid synthesis was observed in mice fed the HC diet. The differences between the labeling in A and E or B and F can be used to estimate the labeling of palmitate. For example, the *de novo* synthesis of palmitate incorporates a set number of hydrogens from water, i.e. ~ 22 (48-50), however, the ^{2}H-labeling in stearate and/or oleate can originate from newly made palmitate or from the elongation of pre-existing/dietary-derived palmitate. In the former case, the labeling of stearate/oleate is markedly different than in the latter, i.e. ~ 25 hydrogens are incorporated when stearate is made from acetyl-CoA whereas only ~ 3 are incorporated when unlabeled palmitate is elongated (51). In addition, the glycerol backbone can incorporate up to 5 hydrogens depending on its source. As we demonstrated (3) that value will be relatively constant ranging between ~ 3.5 and 5, other data in the literature support our observations and suggest that the hydrogen bound to glycerol will readily equilibrate with that in body water (52, 53). Although the interpretation of all glyceride labeling patterns is not immediately obvious, in favorable cases one can determine the positional labeling (figure 5).
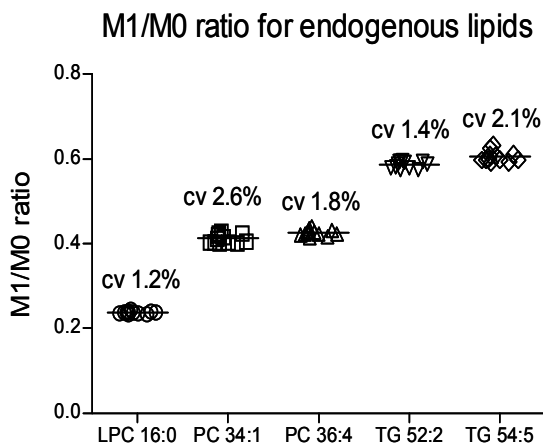
Figure 4. Reproducibility of natural background isotope ratios. The natural isotopic labeling was determined in several lipids detected in control plasma from C57Bl/6 mice; data are expressed as the ratio of the M1 to the M0 isotopomer. PC = phosphatidylcholine, TG = triglyceride, LPC = lysophosphatidylcholine,

cv = coefficient of variation

HC diet Full Scan MS & MS^E for TG 52:2 isotopomer distribution

**HF diet Full Scan MS & MS^E for TG 52:2 isotopomer distribution**

Figure 5. Mass isotopomer distribution profile of triglyceride 52:2 (16:0, 18:1, 18:1). The plasma water labeling remained constant over the course of the study at ~ 2.5% enrichment and there was incorporation of ^{2}H as determined using UPLC/MS. There are distinct differences in the abundance of heavy isotopomers in mice fed a HC vs. a HF diet, Panel (A, C, and E) vs. (B, D and F), respectively. Panel (A and B) demonstrate the isotope labeling in the parent (intact) molecule, whereas Panel (C and D) contain the isotope distribution profile of the daughter ion containing glycerol, 16:0 and 18:1 (i.e. loss of 18:1) and Panel (E and F) contain the isotope distribution profile of the daughter ion containing glycerol, 18:1 and 18:1 (i.e. loss of 16:0). Data are expressed as the average abundance (n = 5) at a given time after correction for natural background labeling.

D₂O Lipid flux analysis resulted in specific subclass glyceride synthesis as a result of de-novo lipogenesis

In an attempt to explain the nature of the different lipid profiles observed in mice fed the HC vs. the HF diet, we examined the ^{2}H-labeling of several lipids that were identified via PCA analyses (Figure 6). The data are plotted as the M1/M0 ratio observed at a given time minus the natural background M1/M0 ratio. Note that there are increases in the other isotopomers, e.g. M2, M3 and M4 (as shown in Figure 5). However, in order to make these figures manageable for the reader we have not plotted those data. The observation of greater incorporation of ^{2}H suggests an enhanced contribution of *de novo* lipogenesis in specific LPCs, PCs and TGs which were determined to be in greater relative concentration via PCA analyses.

In addition to this, it was also of interest to investigate if there was a disconnection between the pool size of specific lipid classes and the contribution of *de novo* lipogenesis. For example, comparable levels of phospholipid PC 34:2 were found in animals fed the different diets. Figure 7A compares the normalized peak areas to total ion intensity of variables detected by PCA for m/z 758.5700 with retention time of 4.81 min (PC 34:2) in both diets which showed no change. However, in contrast with this finding, when the isotopic enrichment was determined there was a clear shift in the abundance of the M1, M2 and M3 isotopomers (figure 7B and 7C). These observations prompted us to quantify the ^{2}H-labeling of certain glycerides which were determined to be higher in mice fed the HF diet. For example, although the abundance of TG 54:4 (m/z 908.8010) was ~ 336 % higher (p <0.0001) in the HF diet than the same triglyceride in the HC diet (figure 7D) the ^{2}H-labeling was much greater in mice for the HC diet (figure 7E and 7F). Hence, showing a clear disconnection between static and kinetic profiles in the different groups. One plausible hypothesis for this finding may be attributed to the fact that in the HC diet *de-novo* lipogenesis is severely up-regulated by specific genes which resulted in increased fatty acid synthesis (figure 1). Increased modulation of fatty acid synthesis leads to an enhancement in overall lipid synthesis, moving these fatty acids to other lipid pools such as phospholipids and triglycerides.
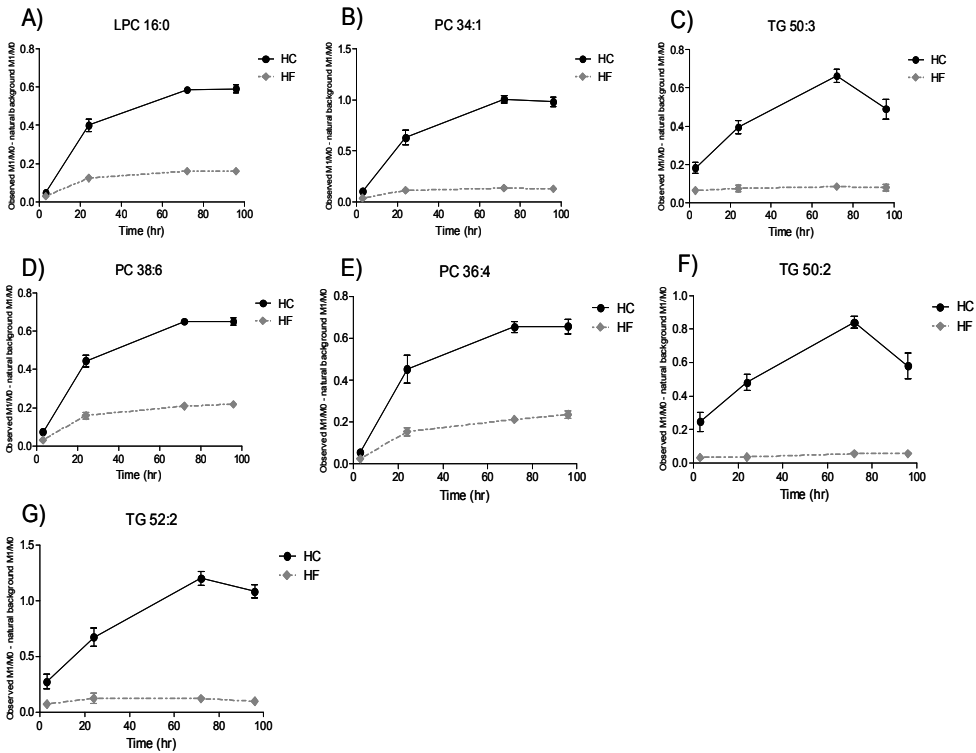
Figure 6. Effect of a HC vs. a HF diet on plasma lipid labeling. The plasma water labeling remained constant over the course of the study at ~ 2.5% enrichment. Consumption of the HC vs. the HF diet led to a greater increase in the isotope labeling, consistent with changes in the contribution of *de-novo* lipogenesis. In all cases there was an increase in the concentration of the noted analytes in mice fed a HC vs. HF diet. Data are expressed as the ratio of M1 to M0 isotopomer for a given analyte; PC = phosphatidylcholine, TG = triglyceride, LPC = lysophosphatidylcholine.
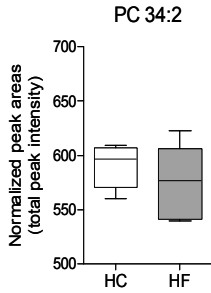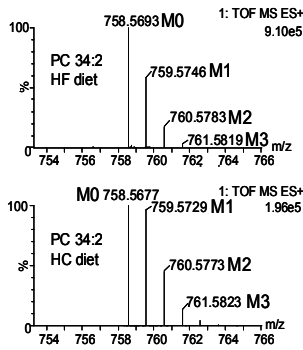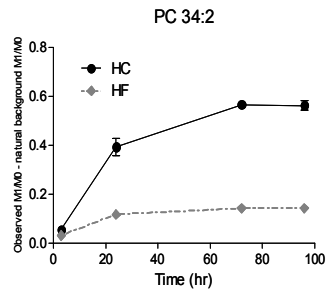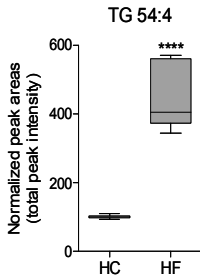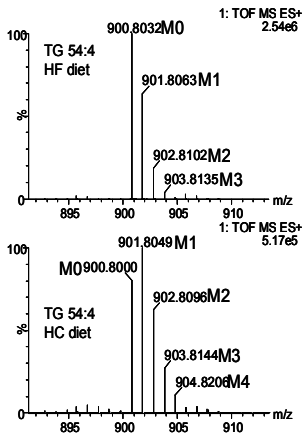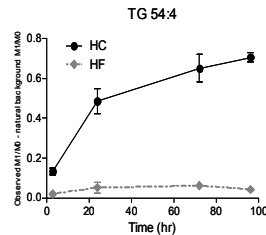
Figure 7. Distinct output from static and kinetic lipid measurements. Panels A and D demonstrate the effect(s) of the respective diets on static concentrations of two lipids, whereas the other panels demonstrate the isotopic labeling. In the case of PC 34:2 (Panel A) there was no change in the concentration between animals fed the different diets yet the HC diet affected the source of the fatty acids, i.e. they mainly come from *de novo* lipogenesis (Panel B and C). In contrast, in the case of TG 54:4 (Panel D) there was a ~4-fold decrease in the concentration in mice fed the HC vs. the HF diet yet the fatty acids mainly come from *de novo* lipogenesis (Panel E and F). Data are expressed as the ratio of M1 to M0 isotopomers for a given analyte; PC = phosphatidylcholine, TG = triglyceride.

*****p < 0.0001*

CONCLUSIONS

The purpose of the work described herein was to determine whether it was possible to improve the identification and interpretation of data sets by combining metabolomics with fluxomics. As expected, the ability to use rather extreme diets served an important role in manipulating the contribution of *de novo* lipogenesis. Our work clearly demonstrates the complexity of alterations in plasma lipid profiles at both the static and kinetic levels. As noted, although we identified 1463 lipid variables using multivariate statistical analysis, a more comprehensive examination was attained when this data output was coupled together with lipid flux measurements. A further advantage of this approach lay in the fact that, it is possible to measure individual synthesis rates for specific lipids and therefore tracking the kinetics of these lipids following dietary intervention.

Finally, the use of gas chromatography-mass spectrometry typically yields information regarding the synthesis of specific fatty acids. While those analyses are highly informative it is not trivial to obtain information regarding fatty acid flux in specific subclasses let alone individual species. We expect that the approach described herein can be used to complement studies of lipid biology yielding information regarding intact lipid class and subclass information with a minimum of sample preparation. This is essential information to have as it will provide a more in-depth understanding of which metabolic lipid pathways undergo modulation and how is it can be combined with the hepatic transcriptome.

REFERENCES

1.   Chong, M.F., Hodson, L., Bickerton, A.S., Roberts, R., Neville, M., Karpe, F., Frayn, K.N., and Fielding, B.A. 2008. *Am J Clin Nutr* 87:817-823.

2.   Guillet-Deniau, I., Pichard, A.L., Kone, A., Esnous, C., Nieruchalski, M., Girard, J., and Prip-Buus, C. 2004. *J Cell Sci* 117:1937-1944.

3.   Bederman, I.R., Foy, S., Chandramouli, V., Alexander, J.C., and Previs, S.F. 2009. *J Biol Chem* 284:6101-6108.

4.   Castro-Perez, J., Previs, S.F., McLaren, D.G., Shah, V., Herath, K., Bhat, G., Johns, D.G., Wang, S.P., Mitnaul, L., Jensen, K., et al. *J Lipid Res* 52:159-169.

5.   Cunnane, S.C., Belza, K., Anderson, M.J., and Ryan, M.A. 1998. *J Lipid Res* 39:2271-2276.

6.   Chascione, C., Elwyn, D.H., Davila, M., Gil, K.M., Askanazi, J., and Kinney, J.M. 1987. *Am J Physiol* 253:E664-669.

7.   Gandemer, G., Pascal, G., and Durand, G. 1980. *C R Seances Acad Sci D* 290:1479-1482.

8.   Hellerstein, M.K. 1999. *Eur J Clin Nutr* 53 Suppl 1:S53-65.

9.   Wilson, I.D., Nicholson, J.K., Castro-Perez, J., Granger, J.H., Johnson, K.A., Smith, B.W., and Plumb, R.S. 2005.. *J Proteome Res* 4:591-598.

10.   Wilson, I.D., Plumb, R., Granger, J., Major, H., Williams, R., and Lenz, E.M. 2005. *J Chromatogr B Analyt Technol Biomed Life Sci* 817:67-76.

11.   Plumb, R.S., Johnson, K.A., Rainville, P., Smith, B.W., Wilson, I.D., Castro-Perez, J.M., and Nicholson, J.K. 2006. *Rapid Commun Mass Spectrom* 20:1989-1994.

12.   Plumb, R., Castro-Perez, J., Granger, J., Beattie, I., Joncour, K., and Wright, A. 2004. *Rapid Commun Mass Spectrom* 18:2331-2337.

13.   Castro-Perez, J., Plumb, R., Granger, J.H., Beattie, I., Joncour, K., and Wright, A. 2005. *Rapid Commun Mass Spectrom* 19:843-848.

14.   Bateman, K.P., Castro-Perez, J., Wrona, M., Shockcor, J.P., Yu, K., Oballa, R., and Nicoll-Griffith, D.A. 2007. *Rapid Commun Mass Spectrom* 21:1485-1496.

15.   Wrona, M., Mauriala, T., Bateman, K.P., Mortishire-Smith, R.J., and O'Connor, D. 2005. *Rapid Commun Mass Spectrom* 19:2597-2602.

16.   Jones, P.J., Dendy, S.M., Frohlich, J.J., Leitch, C.A., and Schoeller, D.A. 1992. *Arterioscler Thromb* 12:106-113.

17.   Schoeller, D.A. 1983. *Am J Clin Nutr* 38:999-1005.

18.   Schoeller, D.A. 2002. *Food Nutr Bull* 23:17-20.

19.   Wong, W.W., Hachey, D.L., Feste, A., Leggitt, J., Clarke, L.L., Pond, W.G., and Klein, P.D. 1991. *J Lipid Res* 32:1049-1056.

20.   Aarsland, A., Chinkes, D., and Wolfe, R.R. 1996. *J Clin Invest* 98:2008-2017.

21.   Chinkes, D.L., Aarsland, A., Rosenblatt, J., and Wolfe, R.R. 1996. *Am J Physiol* 271:E373-383.

22.   Hellerstein, M.K., Christiansen, M., Kaempfer, S., Kletke, C., Wu, K., Reid, J.S., Mulligan, K., Hellerstein, N.S., and Shackleton, C.H. 1991. *J Clin Invest* 87:1841-1852.

23.   Klein, P.D., Haumann, J.R., and Hachey, D.L. 1975. *Clin Chem* 21:1253-1257.

24.   Borel, G.A., and Magnenat, P. 1973. *Helv Med Acta* 37:129-135.

25.   Barrett, P.H., and Watts, G.F. 2003. *Curr Opin Lipidol* 14:61-68.

26.   Chan, D.C., Barrett, P.H., and Watts, G.F. 2004. *Clin Sci (Lond)* 107:221-232.

27.   Gilmore, I.T., and Thompson, R.P. 1980. *Gut* 21:123-127.

28.   Stellaard, F., Schubert, R., and Paumgartner, G. 1983. *Biomed Mass Spectrom* 10:187-191.

29.   Stellaard, F., Sackmann, M., Berr, F., and Paumgartner, G. 1987. *Biomed Environ Mass Spectrom* 14:609-611.

30.   Jones, P.J., Winthrop, A.L., Schoeller, D.A., Swyer, P.R., Smith, J., Filler, R.M., and Heim, T. 1987. *Pediatr Res* 21:242-246.

31.   Schoeller, D.A. 1984. *Hum Nutr Clin Nutr* 38:477-480.

32.   Schoeller, D.A. 2008. *Int J Obes (Lond)* 32 Suppl 7:S72-75.

33.   Schoeller, D.A., and Fjeld, C.R. 1991. *Annu Rev Nutr* 11:355-373.

34.   Wiklund, S., Johansson, E., Sjostrom, L., Mellerowicz, E.J., Edlund, U., Shockcor, J.P., Gottfries, J., Moritz, T., and Trygg, J. 2008. *Anal Chem* 80:115-122.

35.   Lindon, J.C., and Nicholson, J.K. 2008. *Annu Rev Anal Chem (Palo Alto Calif)* 1:45-69.

36.   Major, H.J., Williams, R., Wilson, A.J., and Wilson, I.D. 2006. *Rapid Commun Mass Spectrom* 20:3295-3302.

37.   Nicholson, J.K. 2008. *Annu Rev Nutr*.

38.   Plumb, R.S., Johnson, K.A., Rainville, P., Shockcor, J.P., Williams, R., Granger, J.H., and Wilson, I.D. 2006. *Rapid Commun Mass Spectrom* 20:2800-2806.

39.   Wang, H., Tso, V.K., Slupsky, C.M., and Fedorak, R.N. *Future Oncol* 6:1395-1406.

40.   van der Greef, J., Martin, S., Juhasz, P., Adourian, A., Plasterer, T., Verheij, E.R., and McBurney, R.N. 2007. *J Proteome Res* 6:1540-1559.

41.   van der Greef, J., Hankemeier, T., and McBurney, R.N. 2006. *Pharmacogenomics* 7:1087-1094.

42.   van der Greef, J. 2005. *Syst Biol (Stevenage)* 152:174-178.

43.   Scalbert, A., Brennan, L., Fiehn, O., Hankemeier, T., Kristal, B.S., van Ommen, B., Pujos-Guillot, E., Verheij, E., Wishart, D., and Wopereis, S. 2009. *Metabolomics* 5:435-458.

44.   Bligh, E.G., and Dyer, W.J. 1959. *Can J Biochem Physiol* 37:911-917.

45.   Castro-Perez, J.M., Kamphorst, J., DeGroot, J., Lafeber, F., Goshawk, J., Yu, K., Shockcor, J.P., Vreeken, R.J., and Hankemeier, T. *J Proteome Res* 9:2377-2389.

46.   Castro-Perez, J.M. 2007. *Drug Discov Today* 12:249-256.

47.   Fahy, E., Subramaniam, S., Murphy, R.C., Nishijima, M., Raetz, C.R., Shimizu, T., Spener, F., van Meer, G., Wakelam, M.J., and Dennis, E.A. 2009. *J Lipid Res* 50 Suppl:S9-14.

48.   Diraison, F., Pachiaudi, C., and Beylot, M. 1997. *J Mass Spectrom* 32:81-86.

49.   Lee, W.N., Bassilian, S., Ajie, H.O., Schoeller, D.A., Edmond, J., Bergner, E.A., and Byerley, L.O. 1994. *Am J Physiol* 266:E699-708.

50.   Lee, W.N., Bassilian, S., Guo, Z., Schoeller, D., Edmond, J., Bergner, E.A., and Byerley, L.O. 1994. *Am J Physiol* 266:E372-383.

51.   Ajie, H.O., Connor, M.J., Lee, W.N., Bassilian, S., Bergner, E.A., and Byerley, L.O. 1995. *Am J Physiol* 269:E247-252.

52.   Kalhan, S.C., Bugianesi, E., McCullough, A.J., Hanson, R.W., and Kelley, D.E. 2008. *Metabolism* 57:305-312.

53.   Patterson, B.W., Mittendorfer, B., Elias, N., Satyanarayana, R., and Klein, S. 2002. *J Lipid Res* 43:223-233.

Chapter 10

Summary and future perspectives

Summary and future perspectives

Metabolomics is a very informative and powerful strategy to find phenotypic signatures in complex biological systems. In this thesis, the focus of this 'omics' platform was directed towards the lipidome analysis in cells and in living organisms. The challenge of the work described herein was to build a solid and robust quantitative and qualitative LC/MS platform that could deal with samples from different biological matrices such as whole plasma or serum, feces, tissues, and bile. Of particular interest for lipid profiling experiments was to conduct lipid analysis in the lipoprotein particles, this was accomplished by exploring the utilization of gradient gel electrophoresis in combination with LC/MS by excising the lipoprotein bands and extracting the lipids in each band to obtain a detailed data set for lipids in the VLDL, LDL and HDL fractions. All of the above were static measurements, which are measurements at a certain moment in time. Next, particular attention was also directed towards the kinetic measurements of lipids. This was successfully applied by the use of metabolic tracers which comprised the infusion of deuterated bile acid (D_4-CA) *in-vivo* to measure the reconjugation step of bile acids following silencing of specific genes involved in the reconjugation step of BAs (Slc27a5). Flux analysis was also investigated by the use of 'heavy water' analysis *in-vivo*. The main purpose was to develop and LC/MS platform that could be more informative than current GC/MS strategy and to obtain a better understanding of lipid trackffiicking in an *in-vivo* setting. In order to establish a link between metabolic signatures and perturbations occurring at the mRNA level, gene expression was successfully utilized to provide a more detailed portrait for the coupling of the transcriptome and the metabolome.

In chapter 2, the development of the analytical LC/MS platform that was used throughout the thesis is described. The analytical strategy consisted of a high resolution LC/MS approach using the so called 'MS^E' (alternating low and high energy CID collisions from a single LC injection) which is fully described in chapter 2. This platform was able to obtain in an untargeted manner quantitative and qualitative lipid information from a single injection. The application of this platform allowed the measurement of the perturbation of lipids in osteoarthritis patients suffering from different degrees of severity.

Chapter 3 described the development and application of an ion mobility-TOF platform for the localization of fatty acyl positions and double bonds in PC and LPC. The novelty of this approach resided in the fact that the data was collected without the use of alkali metal adducts ions, which has extensively been used in the past as the only way in electrospray positive ion mode to obtain fatty acyl and double bond information in PCs. The developed method has the advantage to speed up the analysis and simplify the identification process via enhanced fragmentation in combination with accurate mass.

Chapter 4, an investigation in a preclinical dislypidemic golden Syrian hamster was utilized to measure the lipid composition of the lipoprotein particles followed by inhibition of CETP. The results from this investigation resulted in

higher HDL-c levels for animals treated with anacetrapib. Overall it was observed that the changes in HDL lipid composition, taken together with increased fecal sterol excretion and increased HDL cholesterol efflux capacity, may result in promoting cholesterol excretion in this particular animal model, with the hypothesis that this may have been achieved by modulation of reverse cholesterol transport.

Chapter 5 it was investigated whether inhibition of FATP5 (Slc27a5) could offer protection from liver steatosis induced by ApoB siRNA. This study was characterized by the utilization of two siRNAs specifically targeting *Fatp5* and *ApoB* , this study was a proof-of-concept for the combination of two siRNAs *in vivo* using a single siRNA-lipid nanoparticle (LNP) platform. The results from this chapter showed that *Fatp5* knockdown did not influence the size, composition, or zonal distribution of the hepatic triglyceride pool generated by *ApoB* siRNA treatment suggesting that fatty acids are not transported to the liver from dietary uptake or from a store such as adipocytes.

In Chapter 6, was a continuation of the previous chapter in which silencing of the Slc27a5 gene in mice was further explored to obtain a lipid phenotype and proof-of-concept regarding atherosclerosis and possible application to diet-induced obesity. Loss of function of the Slc27a5 gene resulted in altered bile acid (BA) conjugation and concentration in plasma and bile. In turn, this resulted in positive effects on lipid and lipoprotein profiles and diet-induced obesity.

The main aim of chapter 7 was to focus on the use of metabolic tracers. In this chapter an in-depth description was given on how it was possible to measure biomarkers *in vitro* and *in vivo* with the use of a metabolic tracer. The model investigated was the Slc27a5-cKD mice and the tracer D_4-Cholic acid was administered via an intravenous tail injection. It was found that these cKD mice had reduced D_4-conjugated BAs in the plasma as compared to WT mice. BA profiles from the bile showed that there were an increased number of unconjugated BA metabolites in the Slc27a5-cKD mice, specifically tetrahydroxy cholanoyl metabolites. Even though this metabolite of CA has been previously reported, the BA LC/MS method developed specifically for this application provided a greater number of tetrahydroxy cholanoyl metabolites and corresponding taurine conjugated tetrahydroxy cholanoyl metabolites. In summary, stable isotope metabolic tracers in combination with high resolution mass spectrometry provided valuable information about BA biology.

Chapter 8   described the utilization of 'heavy water' or D_2O for the measurement by LC/MS of cholesterol and cholesterol ester synthesis *in-vivo* using C57Bl/6 background mice. *De-novo* lipogenesis was markedly increased in the high carbohydrate diet with a concomitant increase in the expression of Scd1, which resulted in an increment in the enrichment of the deuterium label incorporated in the palmitate and stearate FA pools. Cholesterol synthesis was up-regulated in the high fat diet animal cohort. Without D_2O labeling this finding was not immediately obvious.

Chapter 9 combined a metabolomics and fluxomics approach to measure the static and kinetic effects on lipids on C57Bl/6 background mice as a result of dietary alterations using a high carbohydrate diet and a high fat diet. Lipid flux measurement was conducted by intra-peritoneal injection of D_2O followed by drinking water mixed with D_2O during the

course of the study. Isotopic ratios between detected M0 and M1 minus the natural background were used to gauge the kinetic lipid measurements. The data revealed that it was possible to extract lipid phenotypes based on static measurements with the use of multivariate statistical analysis, but a more comprehensive examination was achieved when this data output was coupled together with lipid flux measurements. A further advantage was that it was possible to measure individual synthesis rates for specific triglycerides and therefore tracking the kinetics of these lipids following dietary perturbations.

In conclusion, this thesis described and demonstrated the development of a comprehensive quantitative and qualitative high resolution LC/MS approach and its application to lipid profiling either in a single compartment or multiple compartment approach in different animal models to study treatment options for atherosclerosis. LC/MS as a front-line analytical platform provided very useful information. Where necessary, coupling with other platforms such as gradient gel electrophoresis, ion mobility, fast protein liquid chromatography and histology analysis offered complimentary data which facilitated the interpretation of the observations. The utilization of metabolic tracers and lipid flux analysis in this thesis has proven to be a very powerful analytical tool which can tease apart modulation of synthesis for specific metabolites involved in a single or multiple metabolic pathways/networks. These kinetic measurements are very complementary to single time points or static metabolite measurements. In addition to this, since most of the research conducted in the thesis targeted genes which were mainly expressed in the liver, mRNA measurements provided vital information which helped to guide the targeted metabolomic/lipidomic approach. Ensuring that perturbations were monitored not just at the transcriptome level but its translatability in the 'omics' cascade with metabolites as the end-points where decisions could be made. Finally, the tools developed in this thesis have already been successfully applied in decision-making in drug research. Therefore, the asset of metabolomics taken together with the other 'omics' will continue to play a pivotal role in systems biology as it will help to provide biological rationale and better understanding of lipid disorders in humans. This benefit offers the potential to develop new and novel therapies in drug research for atherosclerosis.

Appendix

Samenvatting en toekomstige ontwikkelingen

List of publications

Curriculum Vitae

Acknowledgements

Samenvatting en toekomstige ontwikkelingen

Metabolomics is een informatieve en krachtige methodiek om verschillende fenotypen in complexe biologische systemen te karakteriseren. In dit proefschrift wordt beschreven hoe deze nieuwe 'omics'-methode gebruikt kan worden voor de analyse van het 'lipidoom' van cellen en levende organismen. De uitdaging van het hier beschreven werk lag met name bij het ontwikkelen van een robuuste LC/MS methode, die zowel kwalitatieve als kwantitatieve gegevens oplevert en gebruikt kan worden voor de analyse van diverse biologische monsters zoals, plasma, serum, faeces, weefsel en gal. Speciale aandacht ging hierbij uit naar de analyse van lipiden in de diverse lipoproteine fracties. Middels het uitprepareren van de individuele lipiden banden, verkregen dmv gradient gel electroforese en vervolgens de individuele lipiden uit deze bandjes te extraheren en te analyseren mbv LC-MS werden gedetailleerde gegevens verzameld omtrent de samenstelling van de VLDL, LDL en HDL lipoproteine fracties. Al deze metingen zijn zogenoemde statische metingen geweest, dwz metingen op één bepaald moment. Hiernaast is ook specifiek gekeken naar kinetische of dynamische lipiden metingen. Deze werden succesvol toegepast in een *in vivo* studie waar gebruik gemaakt werd van metabole tracers (infusie met gedeutereerd galzuur (D4-CA)) om de reconjugatiestap van galzuren te meten, nadat specifieke genen die betrokken zijn bij deze reconjugatiestap (Slc27a5), waren 'stil gelegd'. De toepassing van de zogenaamde 'flux-analyse' werd onderzocht middels een *in-vivo* studie waarbij 'zwaar water' werd gebruikt. Het primaire doel bij deze studie was om een LC-MS platform te ontwikkelen dat meer informatie verschaft dan het huidige GC-MS platform, en hierdoor een beter begrip te krijgen van het 'lipiden verkeer' in een echte *in-vivo* situatie. Ten einde metabole profielen en veranderingen op mRNA niveau te kunnen koppelen werd gebruik gemaakt van informatie omtrent genetische expressie. Hierdoor kon het transcriptoom en het metaboloom werkelijk worden gekoppeld.

In Hoofdstuk 2 is de ontwikkeling van het stabiele analytische LC/MS platform beschreven dat gedurende het onderzoek, beschreven in dit proefschrift, is gebruikt. De strategie richtte zich op de ontwikkeling van een hoge resolutie LC/MS methodiek gebruik makend van de zogenoemde MS^E techniek (alternerend lage en hoge energetische botsingen tijdens een enkele injectie op het LC/MS systeem). Middels dit platform zijn uit een enkele injectie zowel kwalitatieve als kwantitatieve gegevens verkregen van individuele lipiden. Deze methode werd toegepast om de verandering van de lipiden samenstelling te meten in patienten met diverse gradaties van osteoporose.

Hoofdstuk 3 beschijft in detail de ontwikkeling en toepassing van een LC/MS platform dat gebruik maakt van ionen mobiliteit in combinatie met TOF-MS analyse om de exacte positie van de vetzuurstaarten alsmede de positie van eventuele dubbele bindingen in deze vetzuurstaarten in hetgeval van PC en LPC's te bepalen. Het vernieuwende aan deze aanpak is dat de gegevens zijn verkregen zonder toepassingen van de frequent beschreven alkali metaal-adduct ionen. De

ontwikkelde methode heeft als voordeel dat het identificatie proces, middels verbeterde fragmentatie in combinatie met accurate massa bepaling, aanzienlijk sneller is dan voorheen gerapporteerd.

Hoofdstuk 4 beschrijft de analyse van de lipiden samenstelling van lipoproteine deeltjes, in een pre-klinische model van dislipidemie in een "golden Syrian Hamster", na inhibitie met CETP. De resultaten laten duidelijk zien dat dieren die behandeld zijn met anacetrapib, hogere HDL-c niveau's worden gemeten. De variaties in de lipiden samenstelling van het HDL tesamen met de verhoogde faecale uitscheiding van sterolen alsmede de verhoogde HDL cholesterol efflux capaciteit, suggereert dat de cholesterol excretie in dit model aanzienlijk is verhoogd. Dit is waarschijnlijk veroorzaakt door een modulatie van het 'omgekeerde cholesterol transport'.

Hoofdstuk 5 beschrijft het onderzoek naar de mogelijke bescherming tegen ApoB siRNA geinduceerde lever 'steatosis' middels inhibitie van FATP5(Slc27a5). Hiervoor zijn twee siRNA's gebruikt, welke specifiek gericht waren op *Fatp5* en *ApoB*, respectievelijk. In deze 'proof of concept' studie is de werkzaamheid van de combinatie van twee siRNA's op een enkel siRNA lipide nano-deeltje uitgetest in een *in vivo* situatie. De resultaten laten duidelijk zien dat de *Fatp5* 'knockdown' geen invloed heeft op de grootte, samenstelling of distributie van de hepatische triglyceride voorraad, welke gegenereerd is door de *ApoB* siRNA behandeling. Dit suggereert dat vetzuren afkomstig van opname uit voeding of vanuit een voorraad zoals die aanwezig is in adipocyten, niet naar de lever worden getransporteerd.

In Hoofdstuk 6 wordt het vervolgonderzoek beschreven, waarbij het 'stil leggen' van het Slc27a5-gen in muizen meer in detail werd onderzocht, met als doel een lipiden fenotype, en een proof of concept, voor zowel artherosclerose en mogelijk dieet gerelateerde obesitas, te verkrijgen. Het verlies van functionalitiet van het Slc27a5 gen resulteerde in een veranderd galzuur (BA) profiel (conjugatie en concentratie) in zowel plasma als in gal. Dit had een positief effect op de lipiden- en lipoproteine profielen en de dieet-geinduceerde obesitas.

Het primaire doel van het onderzoek dat in Hoofdstuk 7 is beschreven, is het gebruik maken van metabole 'tracers'. In dit hoofdstuk wordt in detail in gegaan op de mogelijkheid om zowel in *in-vitro* als in *in-vivo* experimenten biomarkers te meten met behulp van metabole tracers. Het bestudeerde model was de Slc27a5-cKD muis waaraan de tracer (D_4-galzuur) werd toegediend via een intraveneuze injectie in de staart. Ten opzichte van de wild type muis heeft deze cKD muis een verlaagd plasma niveau van de D_4-geconjugeerde galzuren. Galzuur profielen vanuit de gal laten duidelijk zien dat er een verhoogd aantal ongeconjugeerde galzuren, met name de tetrahydroxy cholanoyl metabolieten, in deze muis aanwezig is.

Alhoewel deze metabolieten al eerder zijn gerapporteerd, zijn er met deze specifiek ontwikkelde LC/MS methode een aanzienlijk groter aantal tetrahydroxy cholanoyl metabolieten, inclusief de de corresponderende taurine conjugaten, gemeten. Samenvattend kan gesteld worden dat het gebruik van stabiele isotoop gelabelde metabole tracers in combinatie met hoge resolutie massaspectrometrie zeer waardevolle informatie heeft opgeleverd op het gebied van de galzuur biologie.

Hoofdstuk 8 beschrijft de toepassing van 'zwaar water' oftewel D_2O bij de *in-vivo* LC/MS analyse van cholesterol en de producten die bij de cholesterol synthese betrokken zijn in C57B1/6 muizen. Als gevolg van een 'hoog koolhydraten dieet' is de *de novo* lipogenese, en dus ook de expressie van Scd1, aanzienlijk verhoogd. Dit laatste resulteert in een verhoogde verrijking van het deuterium label in zowel de palmitaat en de stearaat voorraad. In de dieren die een 'hoog vet dieet' kregen werd een aanzienlijk verhoogde cholestrol synthese vastgesteld. Zonder gebruik te maken van de hier beschreven deuterium labelling (via D_2O) zou dit niet onmiddelijk duidelijk geworden zijn.

In hoofdstuk 9 worden zowel metabolomics als fluxomics technieken gebruikt om de statische en kinetische/dynamische effect op lipiden te meten (samenstelling en concentratie) in C57Bl/6 'achtergrond' muizen als gevolg van dieet veranderingen zoals 'hoog vet' en 'hoog koolhydraten' dieet. Lipiden flux analyse werd uitgevoerd middels een intra-peritoneale injectie van D_2O gevolgd door het drinken van water gemengd met D_2O gedurende het verdere verloop van de studie. Kinetische lipiden metingen werden gedaan aan de hand van, voor natuurlijke achtergrond gecorrigeerde, isotoop ratio's tussen M0 en M1. De data lieten duidelijk zien dat het, middels statische metingen en gebruik makend van multivariate statische analyse, mogelijk is om lipide gerelateerde phenotypes te definieren. Echter door tevens gebruik te maken van de flux metingen werden aanzienlijk meer gegevens verkregen. Een bijkomend voordeel was dat het nu mogelijk bleek om individuele synthese snelheden voor specifieke triglycerides te bepalen en zodoende de kinetiek van deze lipiden als gevolg van een dieet verandering te bepalen.

Samenvattend beschrijft dit proefschrift de ontwikkeling van een uitgebreide hoge resolutie LC/MS methode voor zowel de kwalitatieve als de kwantitatieve lipide profilering in diverse diermodellen in het kader van artherosclerose onderzoek. Dit onderzoek vindt plaats in zowel enkel kompartiment -, maar ook in meerdere- kompartiment systemen. De toepassing van LC/MS als primaire analytisch platform heeft zeer bruikbare gegevens opgeleverd. Indien nodig is dit platform gekoppeld aan andere technieken zoals: gel electroforese, ionen mobiliteit, snelle eiwit scheiding en histologische technieken. Deze complementaire gegevens hebben bijgedragen aan de interpretatie van de data.

Het gebruik maken van metabole tracers en lipide flux analyse heeft zich, zoals beschreven in dit proefschrift, bewezen als een zeer krachtige analytische techniek, waarmee variaties in de diverse synthese routes voor specifieke metabolieten, betrokken bij één of meerdere metabole routes/netwerken, inzichtelijk gemaakt kunnen worden. Deze kinetische metingen blijken zeer complementair te zijn aan de enkel-tijdspunt metingen. Aangezien het meeste werk dat hier beschreven is zich richtte op specifieke genen, die met name tot expressie komen in de lever , is gebruik gemaakt van de additionele gegevens van mRNA analyse om de metabolomics/ lipidomics metingen te sturen. Hierdoor worden veranderingen niet enkel op het transcriptoom niveau bekeken, maar wordt ervoor gezorgd dat deze informtaie vertaald wordt naar het niveau van metabolieten welke als eindpunt kunnen fungeren waarop beslissingen genomen kunnen worden.

Uiteindelijk zijn deze ontwikkelde technieken al succesvol toegepast in de besluitvorming in geneesmiddelonderzoek. Omdat de brede toepassing van metabolomics tesamen met andere 'omics' technieken de biologische kennis vergroot en een beter begrip omtrent lipide afwijkingen in mensen oplevert, zal deze techniek een cruciale rol blijven spelen in de systeembiologie. Dit voordeel biedt tevens de mogelijkheid om nieuwe en innovatieve behandelingen in geneesmiddelen onderzoek, ten behoeve van artherosclerose, te ontwikkelen.

Publication List

Castro-Perez J.M., Kamphorst J., DeGroot J., Lafeber F., Goshawk J., Yu K., Shockcor J.P., Vreeken R.J., Hankemeier, T. Comprehensive LC-MS E lipidomic analysis using a shotgun approach and its application to biomarker detection and identification in osteoarthritis patients. *J Proteome Res* **9**:2377-2389 (2010)

Castro-Perez J., Previs S.F., McLaren D.G., Shah V., Herath K., Bhat G., Johns D.G., Wang S.P., Mitnaul L., Jensen K., Vreeken R.J., Hankemeier T., Roddy T.P., Hubbard B.K. In vivo D2O labeling to quantify static and dynamic changes in cholesterol and cholesterol esters by high resolution LC/MS. *J Lipid Res* **52**:159-169 (2010)

Castro-Perez J.M., Roddy T.P., Nibbering N.M.M., Shah V., McLaren D.G, Previs S., Attygalle A.B., Herath K., Chen Z., Wang S.P., Mitnaul L., Hubbard B.K., Vreeken R.J., Johns D.G., Hankemeier T. Localization of Fatty Acyl and Double Bond Positions in Phosphatidylcholines using a Dual Stage CID Fragmentation Coupled with Ion Mobility Mass Spectrometry. *(In-press. J. Am. Soc. Mass Spectrom, reprinted with permission)*

Ason B[‡]., **Castro-Perez J.M** [‡].., Tep S., Kang J., Yin W., Ogawa A.K., Dubinina N., Stefanni A., Wong K., Tadin-Strapps M., Roddy T.P., Hankemeier T., Bartz S.R., Hubbard B.K., Sachs A.B., Flanagan W.M., Kuklin N.A., Mitnaul L.J. *ApoB* siRNA induced liver steatosis is resistant to clearance by the loss of fatty acid transport protein 5 (*Fatp5*). *(In-press, Lipid Research, reprinted with permission)*

[‡] *Equal contributing authors*

Castro-Perez J.M., Gagen K., Briand F., Wang S.P., Chen Y., McLaren D.G., Shah V., Vreeken R.J., Hankemeier T., Roddy T.P., Sulpice T., Hubbard B.K., Johns D.G. Evaluation of the dyslipidemic Syrian golden hamster as a model to study cholesteryl ester transfer protein and the novel CETP inhibitor anacetrapib. *(Submitted to the Journal of Lipid Research)*

Castro-Perez J.M., Ouyang X., Tadin-Strapps M., Wang S.P., Gagen K., Rosa R., Mendoza V., Andrews L.E., Robinson M.J., Bartz S.R., Sachs A.B., Yin W., Chen Z., Somers E.P., Wong K., Ogawa A.K., Shah V., Previs S., Johns D.G., Roddy T.P., Wang L., Hubbard B.K., Crook M.F., Mitnaul L.J. Silencing Slc27a5 gene expression and function in vivo results in significant lowering of non-HDL cholesterol and apoB. *(Submitted to Journal of Lipids)*
257

Castro-Perez J.M., Roddy T.P., Shah V., Wang S.P., Ouyang X., Ogawa A.K., McLaren D.G., Tadin-Strapps M., Robinson M.J., Bartz S.R., Ason B., Chen Y., Previs S., Wong K., Vreeken R.J., Johns D.G., Hubbard B.K., Hankemeier T., Mitnaul L.J. Use of a Stable Isotope Metabolic Tracer to measure Bile Acid Reconjugation *in Vitro and in Vivo* by UPLC/TOF-MS. *(Submitted to the Journal of Proteome Research)*

Castro-Perez J.M., Roddy T.P., Shah V., McLaren D.G., Wang S.P., Jensen K., Vreeken R.J., Johns D.G., Hankemeier T., Previs S., Hubbard B.K. Identifying Static and Kinetic Lipid Phenotypes by high resolution UPLC/MS: Unraveling Diet-Induced changes in lipid homeostasis by coupling Metabolomics and Fluxomics. *(In-press, Journal of Proteome Research, reprinted with permission)*

Not in this thesis:

Tadin-Strapps, M., Peterson, L.B., Cumiskey, A.M., Rosa, R.L., Mendoza, V.H., **Castro-Perez, J**., Puig, O., Zhang, L., Strapps, W.R., Yendluri, S., et al. siRNA induced liver ApoB knockdown lowers serum LDL-cholesterol in a mouse model with human-like serum lipids. *J Lipid Res. 2011 (in-press)*

McLaren, D.G., Miller, P.L., Lassman, M.E., **Castro-Perez, J.M**., Hubbard, B.K., and Roddy, T.P. An Ultra Performance Liquid Chromatography Method for the Normal Phase Separation of Lipids. *Anal Biochem*. *2011 (In-press)*

McLaren, D.G., He, T., Wang, S.P., Mendoza, V., Rosa, R., Gagen, K., Bhat, G., Herath, K., Miller, P.L., Stribling, S., Taggart A., Imbriglio J., Liu J., Chen D., Pinto S., Balkovec J.M., DeVita R.J., Marsh D.J., **Castro-Perez J.M.,** Strack A., Johns D.G., Previs S.F, Hubbard B.K., Roddy T.P. The use of stable-isotopically labeled oleic acid to interrogate lipid assembly in vivo: assessing pharmacological effects in preclinical species. *J Lipid Res*. *2011 (in-press)*

Dong, L., Shion, H., Davis, R.G., Terry-Penak, B., **Castro-Perez, J**., and van Breemen, R.B. Collision Cross-Section Determination and Tandem Mass Spectrometric Analysis of Isomeric Carotenoids Using Electrospray Ion Mobility Timeof-Flight Mass Spectrometry. *Anal Chem*. (in-press)

Athersuch, T.J., **Castro-Perez, J**., Rodgers, C., Nicholson, J.K., and Wilson, I.D. UPLC-MS, HPLC-radiometric, and NMR-spectroscopic studies on the metabolic fate of 3-fluoro-[U-14C]-aniline in the bile-cannulated rat. *Xenobiotica* **40**:510-523.

Mortishire-Smith, R.J., **Castro-Perez, J.M**., Yu, K., Shockcor, J.P., Goshawk, J., Hartshorn, M.J., and Hill, A. 2009. Generic dealkylation: a tool for increasing the hit-rate of metabolite rationalization, and automatic customization of mass defect filters. *Rapid Commun Mass Spectrom* **23**:939-948.

Cuyckens, F., Hurkmans, R., **Castro-Perez, J.M**., Leclercq, L., and Mortishire-Smith, R.J. 2009. Extracting metabolite ions out of a matrix background by combined mass defect, neutral loss and isotope filtration. *Rapid Commun Mass Spectrom* **23**:327-332.

Tiller, P.R., Yu, S., **Castro-Perez, J**., Fillgrove, K.L., and Baillie, T.A. 2008. High-throughput, accurate mass liquid chromatography/tandem mass spectrometry on a quadrupole time-of-flight system as a 'first-line' approach for metabolite identification studies. *Rapid Commun Mass Spectrom* **22**:1053-1061.

Tiller, P.R., Yu, S., Bateman, K.P., **Castro-Perez, J**., McIntosh, I.S., Kuo, Y., and Baillie, T.A. 2008. Fractional mass filtering as a means to assess circulating metabolites in early human clinical studies. *Rapid Commun Mass Spectrom* **22**:3510-3516.

Plumb, R.S., Jones, M.D., Rainville, P., and **Castro-Perez, J.M**. 2007. The rapid detection and identification of the impurities of simvastatin using high resolution sub 2 microm particle LC coupled to hybrid quadrupole time of flight MS operating with alternating high-low collision energy. *J Sep Sci* **30**:2666-2675.

Plumb, R.S., Rainville, P.D., Potts, W.B., 3rd, **Castro-Perez, J.M**., Johnson, K.A., and Wilson, I.D. 2007. High temperature ultra-performance liquid chromatography coupled to hybrid quadrupole time-of-flight mass spectrometry applied to ibuprofen metabolites in human urine. *Rapid Commun Mass Spectrom* **21**:4079-4085.

Castro-Perez, J.M. 2007. Current and future trends in the application of HPLC-MS to metabolite-identification studies. *Drug Discov Today* **12**:249-256.

Bateman, K.P., **Castro-Perez, J**., Wrona, M., Shockcor, J.P., Yu, K., Oballa, R., and Nicoll-Griffith, D.A. 2007. MSE with mass defect filtering for in vitro and in vivo metabolite identification. *Rapid Commun Mass Spectrom* **21**:1485-1496.

Athersuch, T.J., Duckett, C.J., **Castro-Perez, J**., Rodgers, C., Nicholson, J.K., and Wilson, I.D. 2007. Metabolism of [14C]-5-chloro-1,3-benzodioxol-4-amine in male Wistar-derived rats following intraperitoneal administration. *Xenobiotica* **37**:44-58.

Plumb, R.S., Johnson, K.A., Rainville, P., Smith, B.W., Wilson, I.D., **Castro-Perez, J.M**., and Nicholson, J.K. 2006. UPLC/MS(E); a new approach for generating molecular fragment information for biomarker structure elucidation. *Rapid Commun Mass Spectrom* **20**:1989-1994.

Plumb, R.S., Rainville, P., Smith, B.W., Johnson, K.A., **Castro-Perez, J**., Wilson, I.D., and Nicholson, J.K. 2006. Generation of ultrahigh peak capacity LC separations via elevated temperatures and high linear mobile-phase velocities. *Anal Chem* **78**:7278-7283.

Yang, J., Song, S.L., **Castro-Perez, J**., Plumb, R.S., and Xu, G.W. 2005. [Metabonomics and its applications]. *Sheng Wu Gong Cheng Xue Bao* **21**:1-5.

Wilson, I.D., Nicholson, J.K., **Castro-Perez, J**., Granger, J.H., Johnson, K.A., Smith, B.W., and Plumb, R.S. 2005. High resolution "ultra performance" liquid chromatography coupled to oa-TOF mass spectrometry as a tool for differential metabolic pathway profiling in functional genomic studies. *J Proteome Res* **4**:591-598.

Plumb, R.S., Granger, J.H., Stumpf, C.L., Johnson, K.A., Smith, B.W., Gaulitz, S., Wilson, I.D., and **Castro-Perez, J**. 2005. A rapid screening approach to metabonomics using UPLC and oa-TOF mass spectrometry: application to age, gender and diurnal variation in normal/Zucker obese rats and black, white and nude mice. *Analyst* **130**:844-849.

Mortishire-Smith, R.J., O'Connor, D., **Castro-Perez, J.M**., and Kirby, J. 2005. Accelerated throughput metabolic route screening in early drug discovery using high-resolution liquid chromatography/quadrupole time-of-flight mass spectrometry and automated data analysis. *Rapid Commun Mass Spectrom* **19**:2659-2670.

Leclercq, L., Delatour, C., Hoes, I., Brunelle, F., Labrique, X., and **Castro-Perez, J.** 2005. Use of a five-channel multiplexed electrospray quadrupole time-of-flight hybrid mass spectrometer for metabolite identification. *Rapid Commun Mass Spectrom* **19**:1611-1618.

Foltz, D.J., **Castro-Perez, J**., Riley, P., Entwisle, J.R., and Baker, T.R. 2005. Narrow-bore sample trapping and chromatography combined with quadrupole/time-of-flight mass spectrometry for ultra-sensitive identification of in vivo and in vitro metabolites. *J Chromatogr B Analyt Technol Biomed Life Sci* **825**:144-151.

Castro-Perez, J., Plumb, R., Liang, L., and Yang, E. 2005. A high-throughput liquid chromatography/tandem mass spectrometry method for screening glutathione conjugates using exact mass neutral loss acquisition. *Rapid Commun Mass Spectrom* **19**:798-804.

Castro-Perez, J., Plumb, R., Granger, J.H., Beattie, I., Joncour, K., and Wright, A. 2005. Increasing throughput and information content for in vitro drug metabolism experiments using ultra-performance liquid chromatography coupled to a quadrupole time-of-flight mass spectrometer. *Rapid Commun Mass Spectrom* **19**:843-848.

Plumb, R., **Castro-Perez, J**., Granger, J., Beattie, I., Joncour, K., and Wright, A. 2004. Ultra-performance liquid chromatography coupled to quadrupole-orthogonal time-of-flight mass spectrometry. *Rapid Commun Mass Spectrom* **18**:2331-2337.

Plumb, R.S., Stumpf, C.L., Granger, J.H., **Castro-Perez, J**., Haselden, J.N., and Dear, G.J. 2003. Use of liquid chromatography/time-of-flight mass spectrometry and multivariate statistical analysis shows promise for the detection of drug metabolites in biological fluids. *Rapid Commun Mass Spectrom* **17**:2632-2638.

Major, H., **Castro-Perez, J**., Nicholson, J.K., and Wilson, I.D. 2003. Characterisation of putative pentose-containing conjugates as minor metabolites of 4-bromoaniline present in the urine of rats following intraperitoneal administration. *Rapid Commun Mass Spectrom* **17**:76-80.

Major, H., **Castro-Perez, J**., Nicholson, J.K., and Wilson, I.D. 2003. Detection of mono- and di-hexoses as metabolites of 4-bromoaniline using HPLC-TOF-MS/MS. *Xenobiotica* **33**:855-869.

Plumb, R.S., Stumpf, C.L., Gorenstein, M.V., **Castro-Perez, J.M**., Dear, G.J., Anthony, M., Sweatman, B.C., Connor, S.C., and Haselden, J.N. 2002. Metabonomics: the use of electrospray mass spectrometry coupled to reversed-phase liquid chromatography shows potential for the screening of rat urine in drug development. *Rapid Commun Mass Spectrom* **16**:1991-1996.

Nicholson, J.K., Lindon, J.C., Scarfe, G.B., Wilson, I.D., Abou-Shakra, F., Sage, A.B., and **Castro-Perez, J.** 2001. High performance liquid chromatography linked to inductively coupled plasma mass spectrometry and orthogonal acceleration time-of-flight mass spectrometry for the simultaneous detection and identification of metabolites of 2-bromo-4-trifluoromethyl. *Anal Chem* **73**:1491-1494.

Nicholson, J.K., Lindon, J.C., Scarfe, G., Wilson, I.D., Abou-Shakra, F., **Castro-Perez, J.,** Eaton, A., and Preece, S. 2000. High-performance liquid chromatography and inductively coupled plasma mass spectrometry (HPLC-ICP-MS) for the analysis of xenobiotic metabolites in rat urine: application to the metabolites of 4-bromoaniline. *Analyst* **125**:235-236.

Corcoran, O., Nicholson, J.K., Lenz, E.M., Abou-Shakra, F., **Castro-Perez, J.**, Sage, A.B., and Wilson, I.D. 2000. Directly coupled liquid chromatography with inductively coupled plasma mass spectrometry and orthogonal acceleration time-of-flight mass spectrometry for the identification of drug metabolites in urine: application to diclofenac using chlorine and sulfur detection. *Rapid Commun Mass Spectrom* **14**:2377-2384.

Curriculum Vitae

José M. Castro Pérez was born on July 23rd 1971 in Las Palmas de Gran Canaria (Canary Islands), Spain. He attained the Bachelor of Science degree (BSc) in 1994 on the subject of Chemistry at King's College London (United Kingdom). Following his BSc degree, he continued further studies to complete his Master of Science degree (MSc) in Clinical Biochemistry and Molecular Biology at the University of Surrey in 1995, Guildford (United Kingdom). In 1995 José M. Castro Pérez started his career as an LC/MS analytical scientist in drug metabolism and pharmacokinetics at Huntingdon Life Sciences (UK). Following this, in 1998 he moved to Micromass UK which is now integrated as part of Waters Corporation where he held the position of Laboratory Manager for the LC/MS Metabolite Profiling group. He started his PhD in 2009 titled "Dynamic System-Wide Mass Spectrometry based Metabolomics Approach for a New Era in Drug Research" at Leiden University under the supervision of Professor Dr. Thomas Hankemeier. Currently José M. Castro Pérez is a Research Fellow in the Atherosclerosis Exploratory Biomarkers analytical group at Merck Research Laboratories in Rahway, New Jersey (USA).

Acknowledgements

I would like to dedicate this thesis to my cousin Carmen who I deeply miss. I lost her last year due to cancer; she was very brave and fought all the way until the very end. During this difficult time I learned to appreciate her wonderful gift to never give up and always try to have a positive frame of mind. She was truly inspirational to me and others around her, and for this I will never forget her. Also, I would like to acknowledge the support given to me throughout my PhD tenure by my wife, my mother and especially my father who would have been very proud of me, I miss him very much. It has been a tough road but a very rewarding one.

Professor Dr. Nico Nibbering has been instrumental in providing his expert advice in Mass Spectrometry related questions. I would like to thank Dr. Lyndon Mitnaul for his guidance in bile acid metabolism related questions; his proficient advice has been priceless. The encouragement and support given to me by Dr. Brian Hubbard has been vital in allowing me to combine this PhD research with my daily responsibilities at Merck. This would have not been possible without his unconditional support and mentorship. Dr. Brandon Ason, has also been very helpful in guiding me throughout siRNA related questions, his advice has been extremely valuable. For questions relating to metabolic flux analysis, Dr Stephen Previs provided me with deep insights in this exciting and powerful analytical tool. Professor Dr. Thomas Hankemeier, Dr. Rob Vreeken and Dr. Thomas Roddy were very inspirational throughout my tenure. I am very grateful to Dr. Douglas Johns for his expert advice in the field of HDL biology and drug research. Finally, I would like to express my gratitude to Loes Beijersbergen she has been extremely helpful in answering all related administrative questions regarding my thesis.